CNWRA®

A center of excellence in earth sciences and engineering®

Geosciences and Engineering Division
6220 Culebra Road • San Antonio, Texas, U.S.A. 78238-5166
(210) 522-5160 • Fax (210) 522-5155

December 16, 2011
Contract NRC–03–10–066

U.S. Nuclear Regulatory Commission
ATTN: Ms. Linda Yee
Division of License Renewal
Office of Nuclear Reactor Regulation
11555 Rockville Pike
Mail Stop: OWFN-11-F1
Rockville, MD 20852

Subject: Final Report on Boric Acid Degradation of Reinforced Concrete
            (Intermediate Milestone 15555.01.001.050)

Dear Ms. Yee:

This letter transmits Intermediate Milestone 15555.01.001.050, Final Report on Boric Acid
Degradation of Reinforced Concrete, associated with the U.S. Nuclear Regulatory Commission
(NRC) Project Technical Assistance for Corrosion/Materials Review of the Effect of Boric Acid
on Concrete Structures and Effect of Moisture on Electrical Cable Materials for License
Renewal. The report is a revision of the draft version that was transmitted to NRC on
August 22, 2011. The revision was made to incorporate the results of a new task on reactive
transport modeling of boric acid leaching of concrete. The subject report presents the results of
a literature review relevant to boric acid degradation of concrete, describes the details and
presents the results of experiments that were conducted to determine the effect of boric acid on
rebar corrosion and concrete degradation, and discusses the results of reactive transport
modeling of boric acid leaching of concrete and their implication to rebar corrosion.

If you have any questions or need additional information, please feel free to contact me at
(210) 522-5282 or Dr. Roberto Pabalan at (210) 522-5304.

Sincerely,

Todd Mintz, Ph.D.
Program Manager
Licensing and Inspection Program

TM/nn
Enclosures

cc: **NRC w/enclosures**   **GED/CNWRA**   **SwRI**
     D. DeMarco, NMSS   W. Patrick   P. Maldonado   Record Copy B, IQS
     R. Jackson, NMSS   B. Sagar   M. Padilla
     J. Schmidt, ADM   GED Directors
     R. Auluck, NRR   GED Managers
     R. Li, NRR   R. Pabalan
     A. Sheikh, NRR   K. Chiang

Washington Office
1801 Rockville Pike, Suite 105 • Rockville, Maryland 20852-1633

BORIC ACID DEGRADATION OF REINFORCED CONCRETE

Prepared for

U.S. Nuclear Regulatory Commission
Contract NRC–03–10–066

Prepared by

Roberto T. Pabalan
Lietai Yang
Kuang-Tsan K. Chiang

Center for Nuclear Waste Regulatory Analyses
San Antonio, Texas

December 2011

CONTENTS

CONTENTS (continued)

FIGURES

FIGURES (continued)

FIGURES (continued)

FIGURES (continued)

TABLES

EXECUTIVE SUMMARY

Spent fuel pools (SFPs) at pressurized water reactors are seismically qualified structures that contain borated water, maintain spent fuel temperatures, and provide radiation shielding. SFPs typically are lined with stainless steel plates on the inner surface of reinforced concrete structures and have leakage collection systems to allow monitoring of SFP leakage and to collect borated SFP water that might leak through the liner. There is a concern that long-term leakage of borated water through SFP liners, reactor cavities, and fuel transfer canals at pressurized water reactors could degrade the concrete support structures and associated reinforcement steel bars (rebars). If the leakage collection system becomes clogged, borated water that leaks through the liners could accumulate, diffuse through pores or seep through cracks in the concrete, expose the rebar in the vicinity of the cracks to mildly acidic solutions, and possibly initiate rebar corrosion. Because the corrosion products have a higher volume than the rebar, the corrosion products could exert pressure on the surrounding concrete and cause cracks to form or to propagate. Cracks could provide a path for more rapid ingress of aggressive substances to the rebar and, thus, accelerate the corrosion process. Over a long period of time, this process could degrade the concrete and rebar and potentially compromise the integrity of the SFP concrete structure or cause unmonitored releases of contaminated water to the environment.

The current U.S. Nuclear Regulatory Commission (NRC) regulatory framework provides sufficient means for licensees and NRC to prevent, detect, and correct SFP leakage conditions that could adversely impact SFP structural integrity over the long term. However, improved understanding of the potential impact of borated water leakage on the service life of SFP reinforced concrete structures is needed for assessing safety for extended periods. NRC tasked the Center for Nuclear Waste Regulatory Analyses to review the published literature and conduct experiments on boric acid degradation of reinforced concrete. This report (i) summarizes the results of a review of literature relevant to boric acid degradation of cement and reinforced concrete and (ii) describes the details and presents the results of experiments conducted to determine the effect of boric acid on rebar corrosion and concrete degradation.

For SFP concrete structures exposed to borated water, the important degradation mechanisms are leaching and rebar corrosion. Published studies indicate that when concrete comes in contact with acid solutions, the hydrated phases (C-S-H, portlandite, monosulfate, ettringite) in the concrete cement matrix dissolve at a rate that depends on the concrete permeability, the concentration and type of acid, and the type of reaction products that form. The quantity of solution that comes into contact with the concrete surface per unit time (i.e., the solution flow rate) also can affect the rate and degree of leaching. Leaching can have several adverse effects on cement and concrete, including increased porosity, decreased compressive strength and modulus of elasticity, increased material ductility, and reduced fracture energy. These effects have been ascribed to portlandite dissolution and, to a lesser degree, decalcification of the C-S-H phase.

Most published studies on cement and concrete leaching have used strong acids such as hydrochloric, nitric, and sulfuric acids. In contrast to those acids, boric acid is a weak acid that does not fully dissociate in aqueous solution. Only a few published studies were found on the effect of boric acid on cement and concrete properties. In those studies, boric acid did not have a significant deleterious effect on cement and concrete properties and affected the properties differently than the strong acids. Concrete immersed in boric acid solutions exhibited an increase in compressive strength, tensile strength, and elastic modulus. Hydrated cement pastes immersed in boric acid solutions showed an increase in weight, bulk density, and

compressive strength, but the porosity decreased due to the formation of poorly soluble calcium borate hydrates in the pore system of the hardened cement paste. Calcium borate formation from boric acid reaction with cement systems was observed in different studies, suggesting its potential importance in reducing the permeability of concrete or to autogenous healing of microcracks in concrete. In one study that flowed boric acid solutions through concrete cracks, the alkaline character of the solids adjacent to the crack was observed to decrease due to dissolution reactions.

The corrosion rate of steel in intact concrete is usually low because of a protective passive oxide film on the steel surface that is stable under the alkaline pH of the cement pore solution. However, corrosion may occur at an accelerated rate when the passive film breaks down, which can be caused by a reduction in the pH of the cement pore solution (e.g., by reaction with boric acid solution) or an ingress of chloride ions. No quantitative data on corrosion rates of carbon steel in concrete in the presence of boric acid were found in published literature, and available data are equivocal on the effect of boric acid on rebar corrosion. Tests that were conducted to support a U.S. patent indicated that boric acid mitigates chloride-induced corrosion of rebar in concrete. Corrosion rates estimated from published weight loss data on rebars immersed in boric acid solutions for 180 days range between 0.032 and 0.039 mm/yr [0.0013 and 0.0015 in/yr], but the data indicated no clear relationship between boric acid concentration and steel bar weight loss. A proprietary report provided a higher corrosion rate of 0.107 mm/yr [0.0042 in/yr] for carbon steel in boric acid solution, but experimental details of that study were not publicly available. Calculations using a commercial code indicated carbon steel corrosion rates increased with increasing boric acid concentration, with values of 0.0083 mm/yr [0.00033 in/yr] in a 2,000 ppm $B(OH)_3$ solution and 0.031 mm/yr [0.0012 in/yr] in a 2.5 wt% $B(OH)_3$ solution. In a study that flowed boric acid solutions through concrete cracks, reinforcement bars in cracks penetrated by boric acid solutions showed considerably more corrosion products than those in cracks penetrated by neutral water, but no significant reduction in rebar cross section was observed after 2 years of testing.

Various methods are available for assessing corrosion of steel embedded in concrete. The corrosion test coupon method is a simple, long-established method and, if used properly, is the most reliable method for corrosion assessment. However, this method is slow when used for corrosion rate measurements, requiring 3-month to 1-year exposure times for applications in industrial process streams and longer timeframes for applications in concrete structures. In contrast, corrosion sensors can provide nearly instantaneous measurements and have been used to assess the corrosion rate of steel in concrete. Corrosion sensor techniques that have been used for corrosion detection or corrosion rate measurements in concrete include (i) electrochemical linear polarization resistance, (ii) electrochemical noise, (iii) coupled multielectrode array sensor, (iv) galvanic coupling, (v) electrical resistance, (vi) eddy current, and (vii) ultrasonic methods. Of these methods, the linear polarization resistance and the coupled multielectrode array sensor methods can give nearly instantaneous indications of corrosion rate and can be used to measure rebar corrosion rate in intact concrete or in concrete cracks filled with aggressive solutions.

The published literature reviewed for this report appears to suggest that boric acid does not significantly degrade concrete properties. However, the published data are mostly based on immersion tests and are applicable to systems involving no flow of the boric acid solution. The one study that flowed boric acid solutions through concrete cracks showed that the concrete alkalinity adjacent to the crack decreased due to dissolution reactions and that reinforcement bars contacted by boric acid solutions showed considerably more corrosion than those contacted by neutral water. Although none of the rebars in that study had significant reductions

in cross section after 2 years of testing, the authors of that study concluded that increased corrosion is expected at longer flow periods, particularly at wider crack widths and lower solution pH.

Given the uncertainty and lack of sufficient published data on the effect of boric acid on rebar corrosion and concrete degradation, experiments were performed to determine this effect. The experiments used several test methods. Rebar corrosion rates at room temperature (~24 °C) [~75 °F], 40 °C [104 °F]; and 55 °C [131 °F] were measured in boric acid (1,200 and 2,400 ppm B) solution, in simulated cement pore solution, and in a mixture of boric acid (2,400 ppm B) solution and simulated cement pore solution. Corrosion rates also were measured at room temperature in boric acid (2,400 ppm B) solution at various pHs. In addition, rebar corrosion rates were measured in boric acid (2,400 ppm B) solution flowing in a simulated concrete crack. Furthermore, the compressive strengths of concrete cylinders reacted with boric acid solution for several months were measured and mineralogical changes due to the reaction were evaluated.

The results indicate that rebar corrosion rates generally increase with temperature and boric acid concentration. The corrosion rate is low (~1 μm/yr or less) [~3.94 $\times 10^{-5}$ in/yr or less] when the solution pH is ~7.1 or higher. Below pH ~7.1, the corrosion rate increases with decreasing pH and can reach ~100 μm/yr [~3.94 $\times 10^{-3}$ in/yr] in solutions with pH less than ~6.7. The threshold pH for carbon steel corrosion in borated solution is between 6.8 and 7.3. The rebar corrosion rates determined in this study agree well with carbon steel corrosion rate data in published literature.

Petrographic examination of concrete cylinders that were immersed in boric acid solutions indicates that the cement paste affected by boric acid leaching is very soft, highly porous, and retains very little inherent strength. The affected paste exhibits a color change from grey to white in some specimens or to yellowish in others. Boric acid crystals also were observed to have deposited in near-surface voids of some specimens. The average depth affected by boric acid leaching increased with time, solution concentration, and temperature. The degradation depths due to boric acid leaching measured in this study are consistent with a square-root-of-time dependence similar to data from an Electric Power Research Institute, Inc. (EPRI) study. However, the boric acid leaching rate determined in the EPRI study is significantly higher than the rates measured in the present study.

The measured compressive strength of concrete cylinders that were reacted with 2,400 ppm B solution for 300 days at room temperature is higher than that of cylinders that were reacted with 1,200 ppm B solution. This observation is consistent with literature data that showed higher compressive strength of concrete that was immersed in 25 wt% boric acid solution compared to concrete that was immersed in 1.2 wt% boric acid solution. Data from this study indicate that solution temperature has a significant effect on compressive strength. The measured compressive strength of concrete cylinders that were immersed in 2,400 ppm B solution at 60 °C [140 °F] is much lower than those of cylinders that were immersed in 2,400 ppm B solution at room temperature. Unfortunately, compressive strength measurements on concrete cylinders that were immersed in tap water or kept in a controlled temperature–relative humidity chamber for 300 days gave unexpectedly low values, which cannot be explained. Because of the unexpected results for the control and tap water samples, there is uncertainty in the measured compressive strengths of the concrete cylinders that were immersed in boric acid solutions.

The experimental data indicate that pH is a critical parameter that determines the corrosion susceptibility of rebar in borated water and the degree of concrete degradation by boric acid leaching. Borated water that leaks through the SFP liner initially will be acidic, but as it diffuses into the concrete pores or flows through the concrete joints or cracks, it will react chemically with the cement matrix, possibly also with the concrete aggregate, and the solution pH will increase. Higher pH will decrease the susceptibility of rebar to corrosion and of concrete to leaching. One-dimensional (1-D) and two-dimensional (2-D) reactive transport simulations were conducted to determine the degree of concrete dissolution and pH change that may occur as boric acid solution diffuses into the matrix or flows in the crack of a reinforced concrete structure. Simulations up to 100 years were performed using different boric acid concentrations, crack apertures, and solution flow rates. The depth of concrete leaching by boric acid solution derived from the 1-D model agree relatively well with the Test 3 leaching depth data. The 1-D simulation results indicate that leaching by boric acid solution diffusing into concrete is mitigated by the acid-neutralizing capacity of the cement minerals such that reinforcement steel with a 5.1-cm [2-in] concrete cover is unlikely to undergo corrosion for at least 77 years. The 2-D simulation results indicate that concrete provides significant chemical reactivity to neutralize the acidic pH of borated water that may leak from an SFP, flow into a crack in the SFP concrete structure, and diffuse into the concrete matrix. However, reinforcement steel close to the crack inlet, whether exposed in the crack or covered by concrete, can become susceptible to corrosion depending on the crack aperture, solution flow rate and duration, and boric acid concentration.

The rebar corrosion rate measurements in this study were performed under aerated conditions. Under deaerated conditions, literature data indicate that carbon steel and low alloy steel corrosion rates in borated water are low. An EPRI study concluded that rebar corrosion in SFP concrete structures due to borated water leakage would be insignificant based on the low corrosion rate in deaerated systems reported in the literature and on the assumption that borated water present in SFP concrete joints or cracks will be deaerated. However, the latter assumption is unsupported by comparison to empirical data. The degree to which borated water in SFP concrete joints or cracks become deaerated will depend on several factors, including the amount of steel material, borated water pH and flow rate, and steel corrosion (oxygen depletion) rate. Because it is impractical to measure the oxygen concentration of borated water in the leakage channels underneath the SFP liner and in the joints or cracks of SFP concrete structures, the reactive transport modeling described in the preceding paragraph could be expanded to include oxygen consumption by carbon steel corrosion. Because even trace amounts of oxygen could significantly increase rebar corrosion rate, additional measurements also would be useful to generate rebar corrosion rates in borated water as a function of oxygen concentration.

Experiments can complement and validate reactive transport modeling results. The experimental design that was used in the present study can be improved to eliminate flow channeling of borated water in the simulated concrete crack. The new design should emplace microflow pH electrodes along the simulated crack, in addition to the coupled multielectrode array sensor and linear polarization resistance probes, such that both solution pH and corrosion rate can be monitored in real time. These experiments would provide information on the correlation between pH and corrosion rate and on the longevity of the alkaline pH buffering by the cementitious material.

The compressive strength measurements of concrete cylinders that have been immersed in boric acid solution should be repeated. To provide data on compressive strength change with time, samples that have been immersed in boric acid solutions for different time periods should be measured.

FINAL

ACKNOWLEDGMENTS

This report was prepared to document work performed by the Center for Nuclear Waste Regulatory Analyses (CNWRA®) for the U.S. Nuclear Regulatory Commission (NRC) under Contract No. NRC–03–10–066. The activities reported here were performed on behalf of the NRC Office of Reactor Regulation, Division of License Renewal. This report is an independent product of CNWRA and does not necessarily reflect the view or regulatory position of NRC.

The authors wish to thank X. He and J. Myers for their technical review, B. Sagar for his programmatic review, L. Mulverhill and E. Pearcy for their editorial reviews, and L. Selvey and L. Naukam for their secretarial support.

QUALITY OF DATA, ANALYSES, AND CODE DEVELOPMENT DATA

DATA: All CNWRA-generated data contained in this report meet quality assurance requirements described in the Geosciences and Engineering Division Quality Assurance Manual. Sources of other data should be consulted for determining the level of quality of those data.

ANALYSES AND CODES: The computer software OLIAnalyzer™ (Gerbino, 2006) and Geochemist's Workbench X1t and X2t (Bethke, 2008) were used in the analyses contained in this report. OLIAnalyzer, X1t, and X2t are commercial software controlled under the CNWRA technical operation procedure (TOP)–18, Development and Control of Scientific and Engineering Software. Documentation for the thermodynamic and corrosion calculations can be found in Scientific Notebook 1034E (Pabalan, 2010). Experimental data on boric acid degradation of concrete and rebar can be found in Scientific Notebooks 1034E and 1042 (Yang, 2010).

REFERENCES:

Bethke, C.M. "Geochemical and Biogeochemical Reaction Modeling." New York City, New York: Cambridge University Press. 2008.

Gerbino, A. "A Guide for Using the OLI Analyzers." Morris Plains, New Jersey: OLI Systems, Inc. 2006. <http://support.olisystems.com/Documents/Manuals/TricksOfTheTrade.pdf>. (25 March 2010).

Pabalan, R. "Boric Acid Degradation of Concrete." Electronic Scientific Notebook 1034E. San Antonio, Texas: CNWRA. 2010.

Yang, L. "Boric Acid Degradation of Reinforced Concrete and Rebar Corrosion." Scientific Notebook 1042. pp. 91–206. San Antonio, Texas: CNWRA. 2010.

1 INTRODUCTION

Spent fuel pools (SFPs) at pressurized water reactors are seismically qualified structures that contain borated water, maintain spent fuel temperatures, and provide radiation shielding. The concrete walls and floor of SFPs are thick {1.2 to 2.7 m [4 to 9 ft]} and heavily reinforced with carbon steel bars (rebars). The concrete cover to the reinforcement is typically 3.8 to 7.6 cm [1.5 to 3 in]. SFPs typically are lined with stainless steel plates, joined by full-penetration welds, on the inner surface of the reinforced concrete structures. Leakage collection systems— channels embedded in concrete at weld seams—generally are present to allow monitoring of SFP leakage and to collect borated SFP water that leaks through the liner. The collected leakage is subsequently directed to the liquid radioactive waste system for processing.   Boric acid [$B(OH)_3$] concentration in SFP water is low and generally less than 2.5 wt%. Boron (B) concentration typically is about 2,000 parts per million [0.2 wt%] (Saling, et al., 2001).

There is a concern that long-term leakage of borated water through the SFP liners, reactor cavities, and fuel transfer canals at pressurized water reactors could degrade the concrete support structures and associated reinforcement steel. If the leakage collection system becomes clogged, borated water that leaks through the liners could accumulate, diffuse through pores or seep through cracks in the concrete, and reach the carbon steel reinforcement bar within the concrete. The borated water could reduce the inherent alkaline environment of the concrete (pore solution pH ≥ 12.5), expose the rebar in the vicinity of the cracks to mildly acidic solutions, and possibly initiate rebar corrosion. Because the corrosion products have a higher volume than the rebar, the corrosion products could exert pressure on the surrounding concrete and cause cracks to form or to propagate (Neville, 1996). Cracks could provide a path for more rapid ingress of aggressive substances to the rebar and, thus, accelerate the corrosion process. Over a long period of time, this process could degrade the concrete and rebar and potentially compromise the integrity of the SFP concrete structure or cause unmonitored releases of contaminated water to the environment. Because these concrete structures are subterranean and inaccessible, damage caused by borated water leakage may not be detected readily or repaired.

The U.S. Nuclear Regulatory Commission (NRC) has issued generic communications to NRC licensees to inform them of the issue regarding borated water leakage and the potential adverse consequences (NRC, 2006, 2004). Current NRC regulatory framework provides sufficient means for licensees and NRC to prevent, detect, and correct SFP leakage conditions that could adversely impact SFP structural integrity over the long term. However, improved understanding of the potential impact of borated water leakage on the service life of SFP reinforced concrete structures is needed for assessing safety for extended periods. NRC tasked the Center for Nuclear Waste Regulatory Analyses to review the published literature, conduct experiments, and perform reactive transport modeling on boric acid degradation of reinforced concrete.

This report presents the results of the literature review, experiments, and modeling that were conducted on boric acid degradation of cement, reinforced concrete, and reinforcement steel. Various chemical degradation mechanisms can compromise the durability of cement-based materials and the service life of concrete structures, including carbonation, sulfate attack, alkali-silica reaction, leaching, and rebar corrosion (Neville, 1996; Pabalan, et al., 2009). For SFP concrete structures exposed to borated water, the important degradation mechanisms are leaching and rebar corrosion, and the literature review focused on these two mechanisms. Section 2 of the report summarizes literature information relevant to leaching of cement and concrete and boric acid effect on cement and concrete. It provides an overview of leaching of

cement-based materials by aqueous, including acidic, solutions, the factors and parameters that affect the degree and rate of leaching, and the effects of leaching on cement and concrete properties. Published studies on boric acid degradation of cement and concrete also are summarized. Section 3 presents literature information relevant to corrosion of steel embedded in cement-based material. It provides an overview of mechanisms and rates of carbon steel corrosion in concrete and discusses techniques for assessing and monitoring steel corrosion in concrete. Literature information on boric acid corrosion of steel, supplemented by corrosion model calculations also is presented in Section 3. Section 4 describes the details and presents the results of experiments conducted to evaluate the effect of boric acid on reinforced concrete. Section 5 discusses the reactive transport simulations that were performed to determine the degree of concrete dissolution and pH change as boric acid solution diffuses into the matrix or flows in the crack of a reinforced concrete structure. Section 6 presents a summary, and Section 7 lists recommendations resulting from the study.

2 LEACHING OF CEMENT AND CONCRETE

2.1 Leaching Mechanism

Leaching is a process by which a liquid dissolves and removes the soluble components of a cement-based material.[1] The solid phases in hydrated cement—portlandite [or calcium hydroxide, $Ca(OH)_2$], calcium silicate hydrate ($CaO–SiO_2–H_2O$, designated C-S-H), ettringite, and monosulfate—are stable under the alkaline pH condition of the cement pore waters, but are susceptible to dissolution when exposed to waters with lower pH. Lower pHs lead to a higher leaching rate; thus acidic solutions can cause a higher degree of concrete degradation. The attack is severe only at a pH below 5.5; below 4.5, the attack is very severe (Neville, 1996). For comparison, the pH of pure water in equilibrium with atmospheric CO_2 gas ($pCO_2 = 10^{-3.5}$ atm) is 5.6 and the pH of a 2.5 wt% $B(OH)_3$ solution is 4.2.

Experimental studies on leaching have shown that when cement is in contact with a reservoir of water having an ionic composition different from (typically lower in concentration than) that of the cement pore solution, diffusion of various ions occurs, driven by the concentration gradient between the pore solution and external water. For example, calcium and hydroxide ions in cement pore water diffuse outward toward the external water. Because the system is in chemical disequilibrium, dissolution also occurs. Typically, portlandite is the first cement phase to dissolve because of its high solubility, followed by the less soluble monosulfate, and then ettringite. Lastly, decalcification of the C-S-H phase, which is the most abundant solid phase in hydrated cement, occurs. Decalcification progressively transforms C-S-H into a silica (SiO_2) gel. Thus, the leached zone is characterized by a succession of dissolution fronts, as represented in Figure 2-1 (Kamali, et al., 2004) and Table 2-1 (Lagerblad, 2001). The silica layer can provide a protective barrier to the transport of aggressive substances to and removal of dissolved constituents from the concrete (Grube and Rechenberg, 1989) and, thus, reduce the concrete leaching rate. During the leaching process, the aggressive substance is transported through this barrier almost entirely by diffusion. Diffusion control makes the leaching rate vary with the square-root of time ($t^{1/2}$) of exposure.
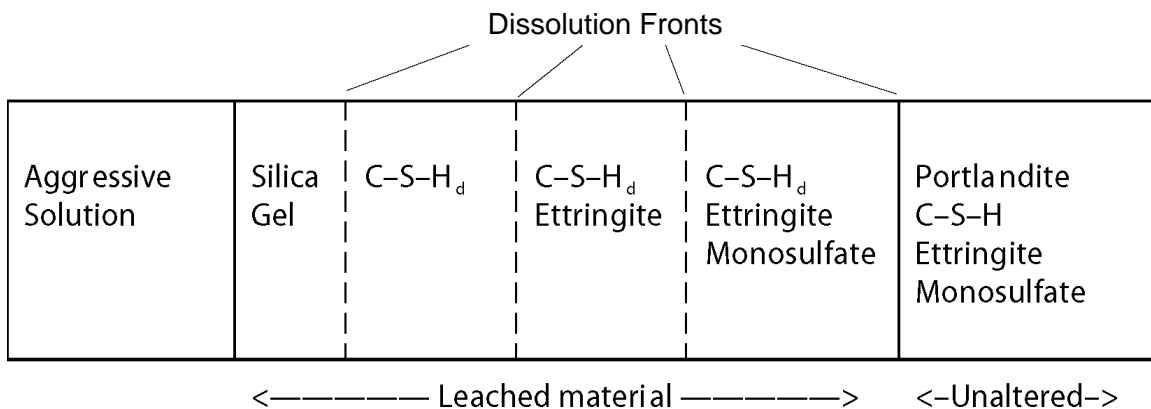
Figure 2-1. Leaching Zones in Hydrated Portland Cement Leached by Pure Water (Kamali, et al., 2004). C-S-H$_d$—Decalcified C-S-H.

---

[1] In some published literature on cement and concrete, the term "corrosion" is used synonymously with "leaching." For the purpose of this report, the term "leaching" is used for the dissolution of cement-based materials and "corrosion" is used for the degradation of the steel reinforcement material.

	Phases Present†					
	Zone 1	Zone 2	Zone 3	Zone 4	Zone 5	Zone 6
Parameter	Calcite Silica Gel Hydroxides	Silica Gel Calcite Hydroxides	Silica Gel C-S-H† Hydroxides	C-S-H(2) Ettringite	C-S-H(1) Ettringite (Cement)	C-S-H Portlandite Ettringite (Cement)
Al_2O_3 content	High	Medium	Low	Low	Low	Low
CaO/SiO_2	<0.1	<0.5	0.5–1.0	~1.0	1.0–1.6	1.6–1.7
Pore solution Ca^{2+} concentration (mmol/kg H_2O)	Low	< 2	< 4	<10	10–20	>20
Pore solution Si^{4+} concentration (mmol/kg H_2O)	1.5	4.2	1.5	1.5	<1	<1
Pore solution pH	7	~10	10.0–10.5	>10.5	10.5–12.4	>12.4
Porosity	Low	Medium	High	Medium	Low	Very Low

Table 2-1. Representation of the Zonal Pattern in Leached Concretes*

*Lagerblad, B. "Leaching Performance of Concrete Based on Studies of Samples from Old Concrete Constructions." TR–01–27. Stockholm, Sweden: Swedish Nuclear Fuel and Waste Management Company. 2001.
†C–S–H(2) has less volume than C–S–H(1).

2.2 Acid Leaching of Cement-Based Materials

As stated in a preceding paragraph, acidic solutions can result in a higher degree of concrete degradation compared to neutral or alkaline solutions. A number of studies have been published on concrete leaching by acid solutions, including sulfuric acid; hydrochloric acid; nitric acid; organic acids, such as acetic and humid acids; and CO_2 solutions.[2] These studies indicate that when concrete comes in contact with acid solutions, the hydrated phases (C-S-H, portlandite, monosulfate, ettringite) in the concrete cement matrix dissolve at a rate that depends on the concrete permeability and the concentration and type of acid. Depending on the mineralogical composition, the acid solutions also can react with the aggregate in the concrete. The rate of leaching of the concrete cement matrix depends on the solubility of salts that are formed as a result of the dissolution reactions; thus, on the nature of the anions involved. The leaching rate is higher when the reaction products formed are soluble than when the products are insoluble. For example, hydrochloric acid leaching of cement forms soluble calcium chloride, whereas sulfuric acid leaching forms a much less soluble calcium sulfate (gypsum). Thus, the leaching rate is higher for the former than the latter acid solution. Oxalic and phosphoric acid reactions with cement result in formation of relatively insoluble calcium oxalate and calcium phosphate salts, respectively; thus the leaching rate for these acids also would be lower than that for hydrochloric acid.

---

[2]Studies pertaining to boric acid effect on cement and concrete are discussed in Section 2.5.

Pavlik (1996) conducted experiments to determine the leaching rate of hydrated cement paste by acetic and nitric acid solutions. The Portland cement pastes were prepared using a range of water/cement ratio from 0.3 to 0.6 and were cured for 28 days in water. The specimens were immersed in 0.2 M solutions of acetic or nitric acid for up to 190 days, and the depth of leaching was measured as a function of time. The results indicate that nitric acid is more aggressive than acetic acid, with the former causing a thicker leached zone than the latter. The results also show that the leaching rate decreases with an increase in cement content per unit volume of hydrated cement paste (a decrease in water/cement ratio). Pavlik (1996) ascribed this result to the increase in neutralization capacity of the hydrated cement paste with an increase in cement content.

Fattuhi and Hughes (1988) also varied the water/cement ratio (and, indirectly, cement content) in their experiments on sulfuric acid leaching of Portland cement paste and concrete. According to Fattuhi and Hughes (1988), published literature often assumed that concrete is more durable if it is made with a low water/cement ratio and a fairly high cement content (hence, higher neutralization capacity), provided it is compacted and cured properly. Previous sulfuric acid leaching tests were done using low sulfuric acid concentration (0.02 wt% or lower), and no data were available at higher concentrations. In the Fattuhi and Hughes (1988) experiments, cubic specimens {102 mm [4 in] on each side} were immersed in 2 wt% sulfuric acid solutions (pH ~1.8) and the changes in weight were determined as a function of time up to 50 days. The results indicated that the mass loss of specimens with lower water/cement ratio (and higher cement content) was higher than those with higher water/cement ratio, in contrast to expected results based on data at low acid concentrations. For example, concrete cubes with a water/cement ratio of 0.40 had three times the weight loss of concrete cubes with a water/cement ratio of 0.70. Fattuhi and Hughes (1988) concluded that the generally accepted requirement of using relatively high cement content to increase concrete durability, which was based on data at low sulfuric acid concentrations, is counterproductive when concrete is exposed to high sulfuric acid concentrations.

2.3 Effects of Leaching on Cement and Concrete Properties

Published literature indicates leaching can have several adverse effects on cement and concrete. It could result in an increased porosity, a decrease in compressive strength and modulus of elasticity, an increase in material ductility, and a reduction in fracture energy (Kamali, et al., 2004). For example, in tests Carde and Francois (1999, 1997) conducted, the compressive strength of hydrated cement pastes decreased and the porosity increased when immersed in concentrated (50 wt%) ammonium nitrate solutions. The results were ascribed to the chemical attack of the hydrated cement paste by ammonium nitrate, which caused total leaching of the calcium hydroxide and a progressive decalcification of C-S-H. Carde and Francois (1999, 1997) ascribed ~92 percent of the strength loss to calcium hydroxide dissolution and ~8 percent to C-S-H decalcification. About two-thirds of the porosity increase was ascribed to calcium hydroxide dissolution and one-third to C-S-H decalcification. Carde and Francois (1999, 1997) concluded that because total leaching of calcium hydroxide crystals creates a macroporosity in the hydrated cement paste, whereas C-S-H decalcification creates microporosity, the decrease in macroporosity is responsible for almost all compressive strength loss observed in their specimens.

Kamali, et al. (2004) evaluated the effect of leaching on the elastic or Young's modulus of hydrated cement pastes. Kamali, et al. (2004) applied the ELAS3D program to compute the Young's modulus of leached and unleached hydrated cement paste microstructure. The results indicated that calcium hydroxide dissolution resulted in a 50 percent reduction in Young's

modulus. Dissolution of the other cement phases (ettringite and monosulfate) caused a much lower decrease in Young's modulus because their initial volume fraction is much lower than that of calcium hydroxide.

Huang, et al. (2005) conducted experiments to determine the effect of hydrochloric acid leaching on the strength and stiffness of concrete. The flexural strength, compressive strength, dynamic modulus of elasticity, and mass loss were measured in the study to determine the leaching resistance of various types of concrete. The experiments used concrete specimens with different strength grades prepared using Type I Portland cement, fine river sand aggregate, and crushed granite coarse aggregate. The specimens, with dimensions of 100 × 100 × 400 mm [3.9 × 3.9 × 15.7 in] and 100 × 100 × 100 mm [3.9 × 3.9 × 3.9 in], were immersed in hydrochloric acid solutions of various concentrations (5, 10, 15, and 20 wt%) for 24 hours. The results showed that the concrete flexural and compressive strengths decreased when reacted with hydrochloric acid solutions. The degree of change in concrete properties depended on both the strength grades of the concrete and the hydrochloric acid concentration. The measured strength loss increased with increasing hydrochloric acid concentration over the range 0 to 20 wt% used in the study. The high-strength concrete exhibited a higher decrease in flexural strength than the normal-strength concrete, but the latter showed a higher decrease in mass and elastic modulus than the former. The decrease in compressive strength with increasing hydrochloric acid concentration was similar in trend for the different concrete types. The higher mass loss observed for normal-strength concrete than for high-strength concrete was ascribed to the higher permeability of the former compared to the latter, which allowed greater penetration of the acid solution.

2.4   Leaching Rates of Cement-Based Materials

The degradation of concrete physical properties due to acid leaching is a gradual process (Zivica and Bajza, 2001). Initially, the concrete surface deteriorates, showing loosened material that easily separates from the concrete. With intensification of acid attack and its progression from the exterior into the interior of the concrete, a gradual degradation of concrete strength occurs. The gradual decrease in mass, compressive strength, and dynamic modulus of elasticity and the increase in porosity are qualitatively illustrated in Figure 2-2. The concrete pore structure decreases in quality, indicated by an increase in total porosity and in the fraction of larger pores. These changes are a direct consequence of the decomposition of the cement hydrates and the leaching away of the decomposition products.

Empirical equations have been published relating the degree of acid leaching of hydrated cement pastes as a function of two factors (Pavlik, 1996): (i) the concentration of the aggressive acid and (ii) the exposure time of the specimens in the aggressive solution, as in the following equation

$$d = k \cdot c^m \cdot t^n \qquad (2\text{-}1)$$

where

d =   thickness of leached layer
c =   acid solution concentration
t =   exposure time
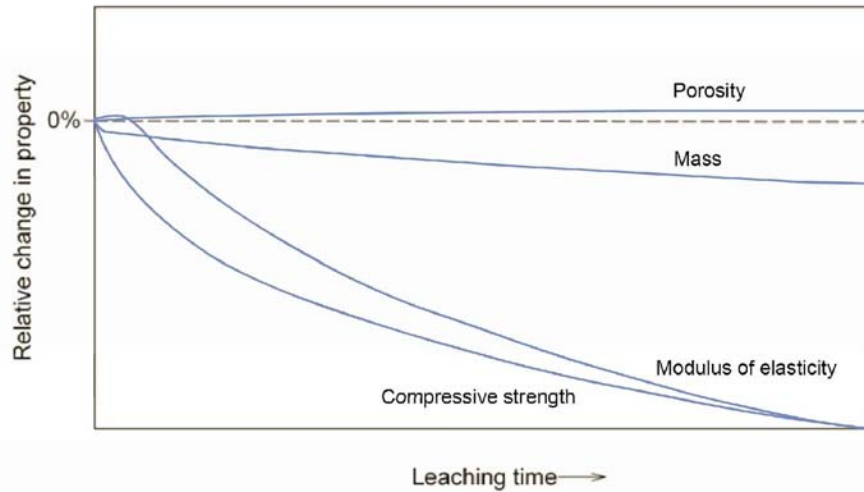
Figure 2-2. Relative Change in Concrete Physical Properties Due to Acid Leaching As a Function of Time (Modified From Zivica and Bajza, 2001)

k =   empirical coefficient that depends on the type of aggressive acid, cement chemical composition, water/cement ratio of the hydrated cement paste, and test conditions

m,n =   empirical exponents, with values ranging usually from 0.5 to 0.7

Pavlik (1996) presented parameters for Eq. (2-1) that apply to acid leaching of hydrated cement paste by nitric acid or acetic acid solutions. Pavlik (1996) also presented modified equations and parameters to account for the effect of water/cement ratio on acid leaching. Zivica (2004) provided other equations relating changes in mass, compressive strength, and modulus of elasticity to acid concentration and time.

An important factor that affects the rate and degree of leaching by acid solutions is the quantity of solution that comes into contact with the surface of the cement or concrete per unit time. Under static conditions in which there is little or no flow of the leaching solution, as in the immersion leaching tests described in preceding paragraphs, the acid concentration is the key factor affecting the rate and degree of leaching of the cement-based material. However, under dynamic conditions in which there is flow of the reacting solution, the flow rate may have a greater influence than the solution concentration (Zivica and Bajza, 2002). If the flow rate is sufficiently high, the leached layer may be disturbed, which will enhance the leaching process by allowing increased transport of the aggressive species to the pore system of the cement-based material.

2.5   Boric Acid Effect on Cement and Concrete

In contrast to acids like hydrochloric acid, nitric acid, and sulfuric acid, which are all strong acids, boric acid [$B(OH)_3$, sometimes also written as H_3BO_3] is a weak acid. Boric acid does not fully dissociate in aqueous solution, but is acidic due to its interaction with water. In an aqueous solution of boric acid, the following equilibrium is established

$$B(OH)_3 + H_2O \leftrightarrow B(OH)_4^- + H^+ \qquad\qquad (2\text{-}2)$$

The dissociation constant, K_a, for the above reaction is given by

$$K_a = \frac{[B(OH)_4^-][H^+]}{[B(OH)_3][H_2O]}$$

(2-3)

and log K_a = −9.25 at 25 °C [77 °F] (Shimada, et al., 2007). Under acidic conditions, $B(OH)_3$ is the dominant species, whereas monoborate ion, $B(OH)_4^-$, is dominant under basic conditions. Polyborate anions are formed at pH 7 to 10 if the boron concentration is higher than about 0.025 M, including $B_2O(OH)_5^-$, $B_3O_3(OH)_4^-$, and $B_4O_5(OH)_4^{2-}$ (Ingri, 1962; Ingri, et al., 1957).

Figure 2-3 is a chemical diagram of boric acid illustrating the dominant aqueous species and solid phases at 25 °C [77 °F] as a function of pH and boric acid concentration. The diagram was calculated using OLIAnalyzer 3.1, a chemical process simulation software developed by OLI Systems, Inc. (Morris Plains, New Jersey). The calculated solubility of boric acid in pure water at 25 °C [77 °F] is 0.948 M.

Because boric acid does not dissociate in aqueous solutions, boric acid solutions are less acidic compared to hydrochloric, nitric, and sulfuric acids. The pH of boric acid solutions as a function of concentration calculated using OLIAnalyzer 3.1 is shown in Figure 2-4.

2.5.1 Literature Information on Boric Acid Effect on Cement and Concrete

A literature search identified only a few published papers relevant to boric acid effects on cement and concrete properties. These papers are summarized in the following sections.

Bajza, et al. (2002)

Bajza, et al. (2002) studied the effect of boric acid solutions on the physical properties and phase composition of concrete and hardened Portland cement paste (HPCP). In the first part of
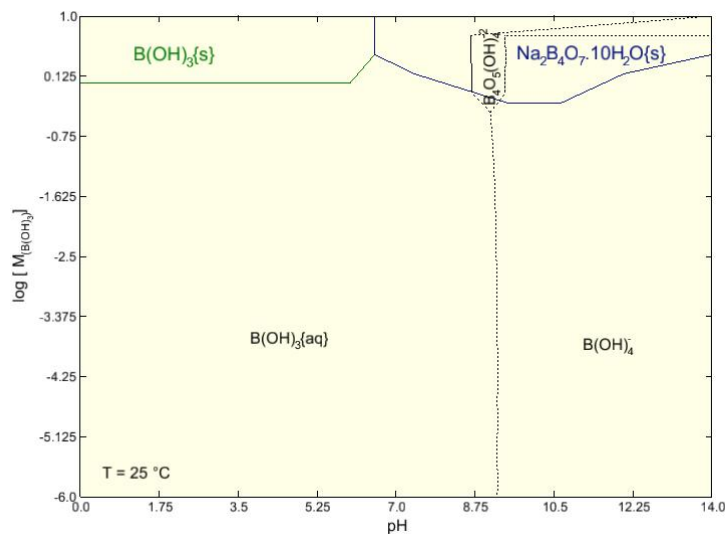
Figure 2-3. Dominant Aqueous Species and Solid Phases in the B(OH)₃–NaOH–H₂O System at 25 °C [77 °F]
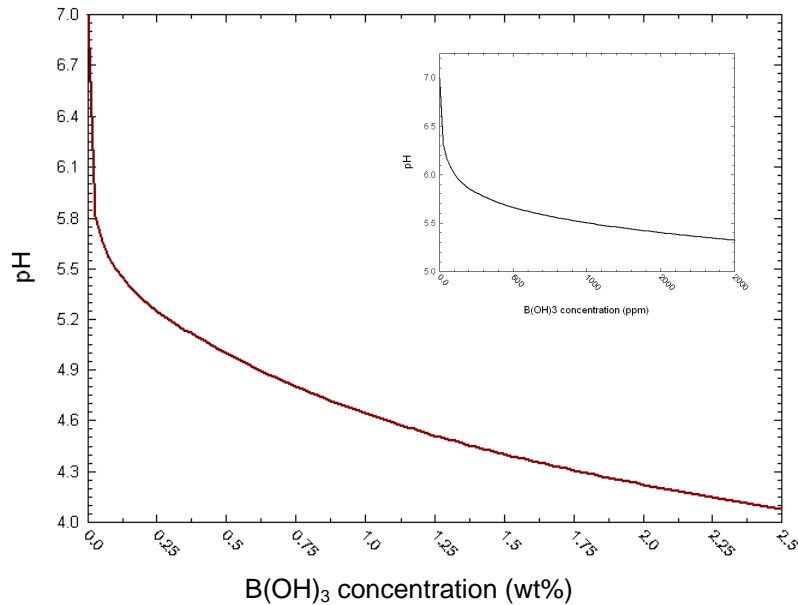
Figure 2-4. Calculated pH of Boric Acid Solutions at 25 °C [77 °F] as a Function of Concentration From 0 to 2.5 wt% B(OH)₃. The Inset Figure Shows the Calculated pH From 0 to 2,000 ppm [0 to 0.2 wt%] B(OH)₃.

the study, samples were taken from the walls of a damaged reinforced concrete tank used for boric acid storage. Using a rotary diamond drill, the samples were cut from areas that exhibited boric acid attack and from areas with no evident boric acid reaction. Nondestructive measurements of the compressive strength of the samples were conducted using a Schmidt hammer. Destructive compressive strength tests also were conducted on some cylindrical cores with a diameter of 100 mm [3.9 in]. In addition, powder samples of the cement matrix were analyzed using X-ray diffraction (XRD) analysis and differential thermal analysis (DTA).

The Schmidt hammer compressive strength of samples unaffected by boric acid ranged from 29 to 45 MPa (n = 16; mean = 36.7 MPa; standard deviation = 4.7 MPa), whereas the values for two samples that exhibited boric acid attack were 40 and 41 MPa. The compressive strength determined from the core cylinders with no evident boric acid attack ranged from 26 to 45 MPa (n = 8; mean = 37.9 MPa; standard deviation = 6.9 MPa), whereas the values for the two samples with evident boric acid reaction were 44 and 48 MPa. From these results, Bajza, et al. (2002) concluded that boric acid attack does not significantly affect the concrete structure. The XRD and DTA results also indicated no significant difference between the samples taken from areas with and areas without boric acid reaction.

In the second part of the Bajza, et al. (2002) study, HPCP cylinders {30-mm [1.2-in] length × 30-mm [1.2-in] diameter} with a water-to-cement ratio of 0.4 were prepared and cured for 27 days in water. Specimens subsequently were immersed in 1.2 or 25 wt% boric acid solutions for 14, 28, 71, and 127 days. Changes in weight, bulk density, total porosity, and compressive strength of the specimens were measured. XRD and DTA analysis of some HPCP samples also were conducted. The test results, which are plotted in Figure 2-5, show that the weight, density, and compressive strength of specimens immersed in boric acid solution increased with time, although total porosity of the specimens decreased with time.
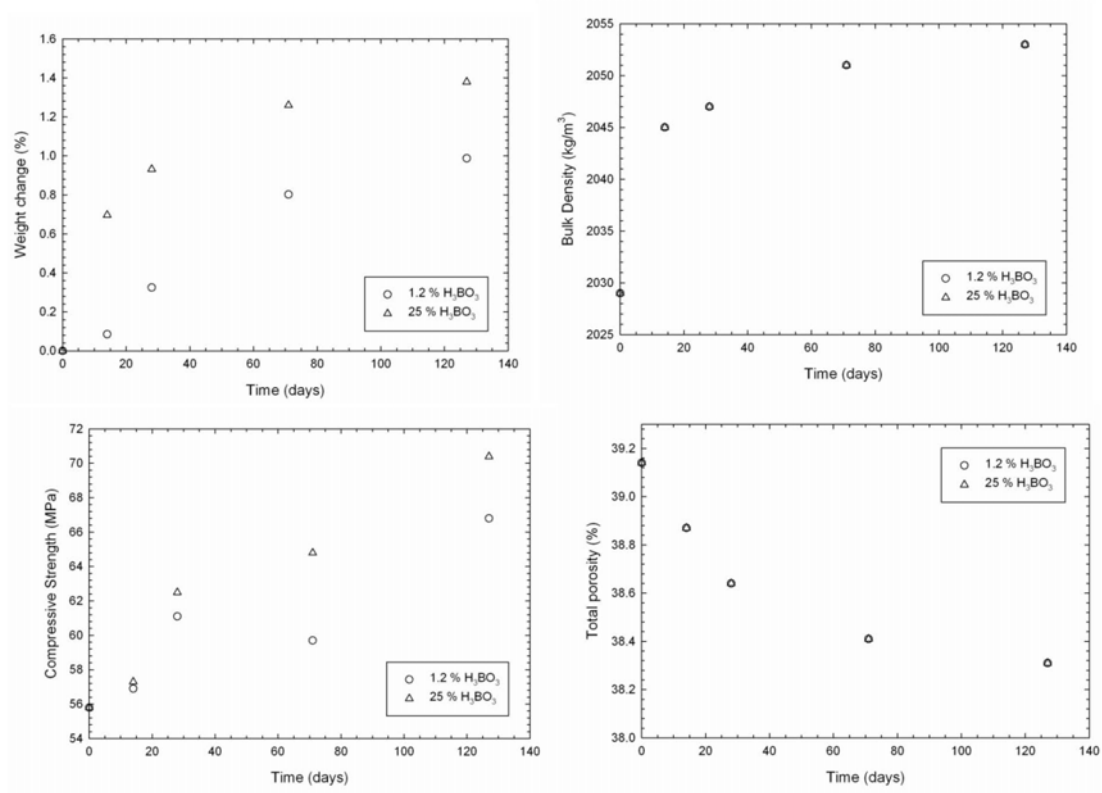
Figure 2-5. Weight Change, Bulk Density, Compressive Strength, and Total Porosity of Hardened Portland Cement Pastes Immersed in Boric Acid Solutions Measured as a Function of Time (Bajza, et al., 2002)

The test results were attributed to the formation of poorly soluble calcium borate hydrates in the pore system of the hardened cement paste. The XRD patterns indicated the presence of $CaB_3O_5(OH)$, $CaB_6O_{10} \cdot 4H_2O$, $Ca_2B_6O_{11} \cdot 5H_2O$, and $Ca_2B_6O_{11} \cdot 13H_2O$. The amount of precipitated calcium borate hydrates was much higher in specimens immersed in the 25 wt% boric acid solution compared to those immersed in the 1.2 wt% boric acid solution. Bajza, et al. (2002) concluded from these results that the reaction of boric acid on HPCP is different from the typical acid leaching. The latter process generally decreases the weight, bulk density, and compressive strength and increases the porosity of the specimen.

Bajza, et al. (2002) also monitored the pH of the boric acid solutions reacting with HPCP. The measured pHs of the 1.2 and 25 wt% boric acid solutions as a function of time are plotted in Figure 2-6. The solution pH increased with time due to the reaction of boric acid with calcium hydroxide in the hydrated cement paste. The most marked pH change occurred during the first week of reaction, and there was little change in pH after about 28 days.

Jin, et al. (2009)

Jin, et al. (2009) investigated the effect of boric acid on the physical properties and performance of reinforced concrete. The basic mechanical properties (compressive strength, splitting tensile strength, and elastic modulus) of concrete reacted with boric acid solutions were compared with
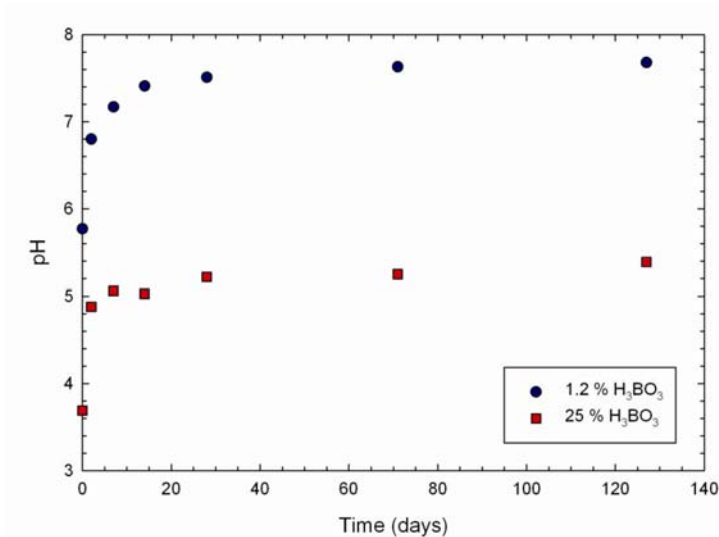
Figure 2-6. Measured pH as a Function of Time of Boric Acid Solutions Reacted With Hydrated Portland Cement Paste (Bajza, et al., 2002)

those exposed to an outdoor natural environment. XRD analysis also was used to examine the chemical reaction products in the concrete.

The study used concrete prepared using Type I Portland cement, fly ash, crushed gravel coarse aggregate, and natural river sand fine aggregate. The water-to-cement ratio was 0.42. The rebar used was hot-rolled ribbed steel bars {16-mm [0.62-in] diameter × 550-mm [22-in] length} or plain bars {10-mm [0.39-in] diameter × 400-mm [15.7-in] length}. The concrete specimens used to determine the basic mechanical properties had dimensions of 100 × 100 × 100 mm [3.9 × 3.9 × 3.9 in] and 100 × 100 × 300 mm [3.9 × 3.9 × 11.8 in]. The bond strength tests used 150 × 150 × 150 mm [5.9 × 5.9 × 5.9 in] concrete specimens reinforced by hot-rolled ribbed steel bars. Three groups of concrete specimens were immersed in boric acid solutions with concentrations of 2,200, 8,000, or 30,000 ppm $B(OH)_3$. A control group of concrete specimens was exposed to an outdoor natural environment. Note that the control group was not immersed in any type of water.

The compressive strength, splitting tensile strength, and elastic modulus of the concrete specimens immersed in boric acid solutions or exposed to the natural environment are plotted as a function of time in Figure 2-7. Compared to specimens that were exposed to a natural environment, those reacted with boric acid had lower compressive strength, splitting tensile strength, and elastic modulus, indicating that boric acid had a negative effect on concrete strength development. However, all the specimens exhibited an increase in mechanical properties with age, such that any effect of boric acid is more than compensated by the increase in concrete strength with age. The results illustrated in Figure 2-7 for the three boric acid concentrations [2,200, 8,000, and 30,000 ppm $B(OH)_3$] are very similar, indicating that boric acid concentration is not a key parameter affecting concrete degradation. The data show that the basic mechanical properties of concrete immersed in boric acid solutions are lower than that of concrete exposed to a natural environment by no more than 1.8 percent at 180 days. Thus, Jin, et al. (2009) concluded that the effect of boric acid on concrete properties is not significant at exposure times up to 180 days.

(a)

(b)

(c)
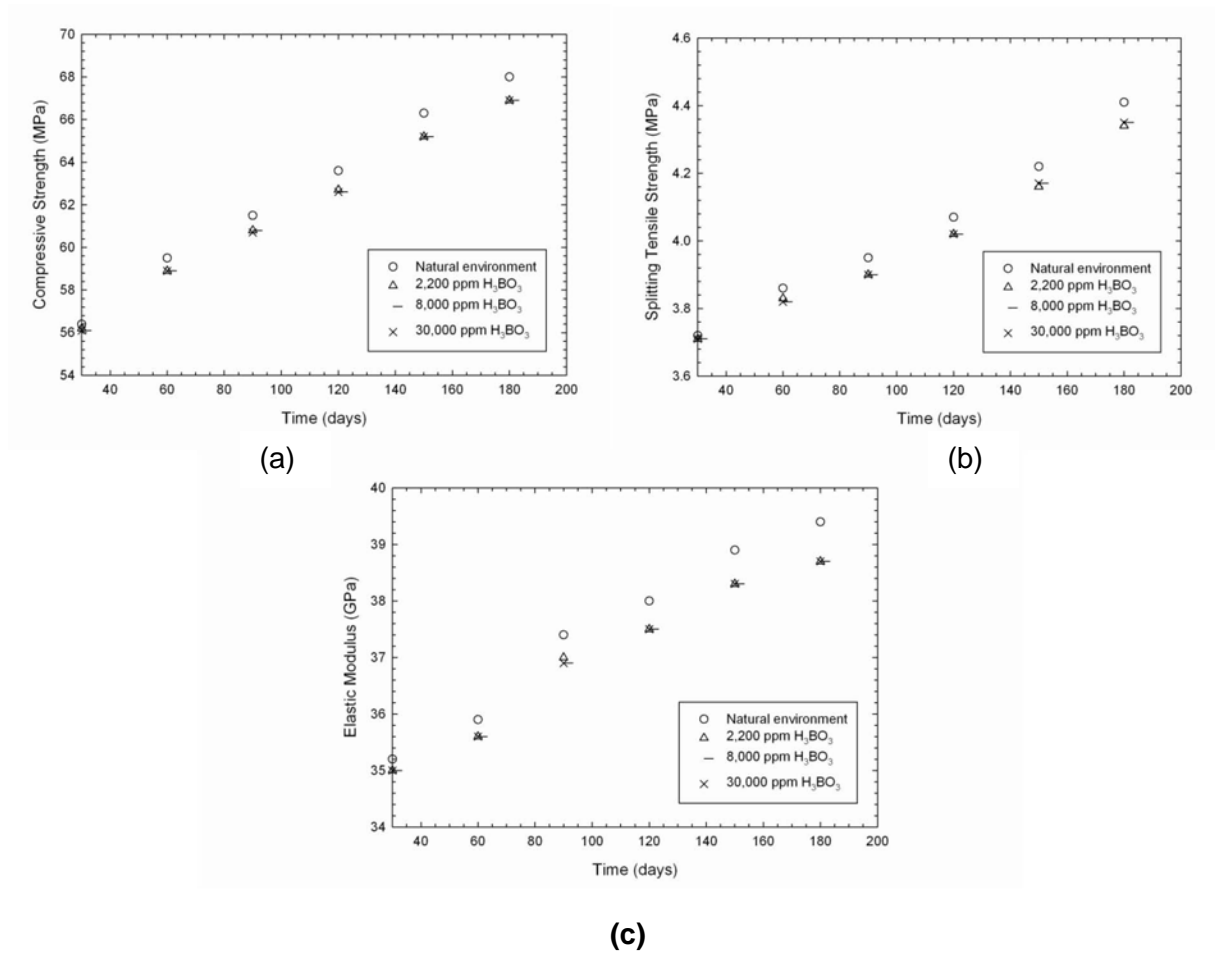
Figure 2-7. (a) Compressive Strength, (b) Splitting Tensile Strength, and (c) Elastic Modulus of Concrete Immersed in Boric Acid Solutions or Exposed to an Outdoor Natural Environment Up to 180 Days (Jin, et al., 2009)

The Jin, et al. (2009) XRD data indicated the presence of three kinds of calcium borate hydrates—$Ca_2B_6O_6(OH)_{10} \cdot 8H_2O$, $Ca_2B_2O_5 \cdot H_2O$, and $CaB_2O_4 \cdot 2H_2O$—in specimens immersed in boric acid solutions from 30 to 180 days. The authors ascribed the presence of these phases to the chemical reaction of boric acid with calcium hydroxide in concrete, as in the following reactions

$$6B(OH)_3 + 2Ca(OH)_2 + 2H_2O \leftrightarrow Ca_2B_6O_6(OH)_{10} \cdot 8H_2O \qquad (2\text{-}4)$$

$$2B(OH)_3 + 2Ca(OH)_2 \leftrightarrow Ca_2B_2O_5 \cdot H_2O + 4H_2O \qquad (2\text{-}5)$$

$$2B(OH)_3 + Ca(OH)_2 \leftrightarrow CaB_2O_4 \cdot 2H_2O + 2H_2O \qquad (2\text{-}6)$$
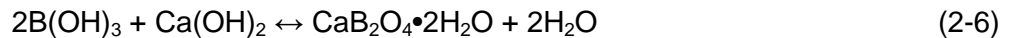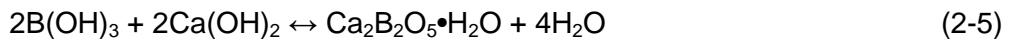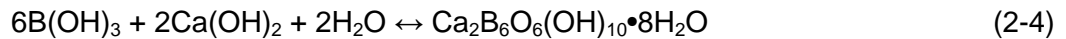
The presence of borate phases in specimens immersed for 30 days suggests the reactions in Eqs. (2-4), (2-5), and (2-6) initiate soon after immersion of the specimens in the boric acid solution. Nevertheless, the observed increase in concrete mechanical properties with time indicates the borate phase formation had no significant effect on concrete strength.

The bond strengths of reinforced concrete immersed in boric acid solutions or exposed to a natural environment are plotted in Figure 2-8. The bond strengths increased with time. Based on the data, Jin, et al. (2009) concluded that boric acid is too weak to affect steel bar–concrete interaction even after 180 days of immersion.

Ramm and Biscoping (1998)

Ramm and Biscoping (1998) conducted a long-term (2-year) investigation of autogenous healing and reinforcement corrosion in water-penetrated cracks in reinforced concrete. Autogenous healing (or self-healing) refers to the ability of cement to heal cracks in fractured concrete (Hearn, 1998). This process, which is largely attributed to the dissolution and reprecipitation of cement phase hydrates or to cement carbonation (i.e., CO_2 reaction with the cement phases and precipitation of $CaCO_3$), can significantly reduce flow in damaged concrete. Thus, autogenous healing could be an important mechanism that could reduce borated water leakage through concrete in a spent fuel pool facility. Calcium borate hydrate precipitation, observed in the Bajza, et al. (2002) and Jin, et al. (2009) studies, is also a possible mechanism for autogenous healing when boric acid solutions penetrate concrete cracks, although literature data are not available to indicate its relative importance.

The objective of the Ramm and Biscoping (1998) study was to clarify the effect of crack width and water chemistry, specifically pH, on the onset and extent of autogenous healing and on reinforcement steel bar corrosion. Tests were conducted using different values of crack width {0.1, 0.2, 0.3, and 0.4 mm [0.004, 0.008, and 0.016 in]}, concrete element thickness {30 and 60 cm [11.8 and 23.6 in]}, and water pressure (0.0245 and 0.123 MPa). Tests also were conducted to determine the extent of reinforcement bar corrosion by measuring the coupling currents between steel bar electrodes located in the cracks of an 18-cm [7.1-in]-thick concrete element and a reinforcement bar embedded in the concrete. Three waters with different degrees of aggressiveness were used: (i) deionized water with pH of 7, (ii) boric acid solution with pH of 6.1, and (iii) boric acid solution with pH of 5.2. All concrete specimens were prepared using Portland cement, aggregates of gravel and hard-coal fly ash, and a water/cement ratio of 0.55, and were reinforced with 16-mm [0.63-in]-diameter steel bars.
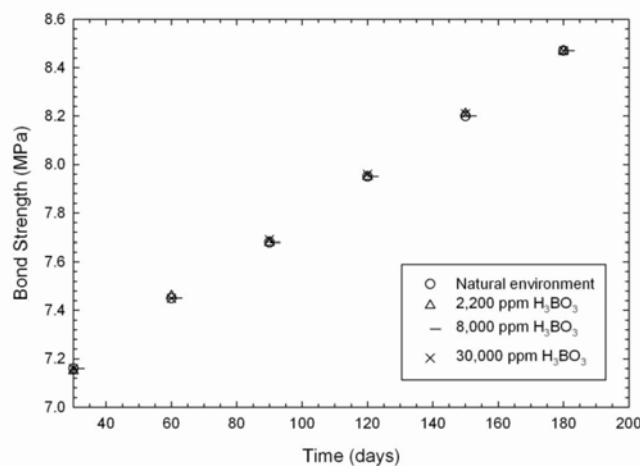
Figure 2-8. Bond Strength of Reinforced Concrete Specimens Immersed in Boric Acid Solutions or Exposed to an Outdoor Natural Environment Up to 180 Days (Jin, et al., 2009)

During the test, the flow rates and coupling currents (also called macrocell currents) were determined at regular intervals. In addition, the initial water pH was kept constant and the dissolved calcium hydroxide concentrations in the effluent were measured. After 2 years, some of the specimens were taken apart to allow visual observation of the crack sides and reinforcement steel bars.

Ramm and Biscoping (1998) made the following observations:

(1)   Flow rates through the concrete elements were higher in specimens with larger crack widths or in tests with lower pH solutions. None of the test specimens were completely sealed by autogenous healing, although the specimens that were reacted with deionized water (pH = 7) had water exiting in the form of individual drops at the end of the 2-year experiment.

(2)   Water flow through cracks in the concrete reduced the alkaline character of the solids adjacent to the crack due to dissolution reactions. The pH 5.2 boric acid solution that flowed through the concrete crack had four to six times higher dissolved calcium hydroxide concentration than the neutral deionized water.

(3)   Reinforcement bars located in cracks penetrated by acidic waters showed considerably higher quantities of corrosion products (rust) than those in cracks penetrated by neutral water. The concrete element thickness and water pressure had little influence on the degree of corrosion.

(4)   The degree of reinforcement steel corrosion increased during the last 28 weeks of the tests due to the lowered cement alkalinity and the decreased pH of water in the cracks.

(5)   A higher degree of corrosion was observed in cracks with wider apertures and/or penetrated by acidic water. The highest corrosion rate was observed in the test with a crack width of 0.4 mm [0.016 in] and a solution pH of 5.2, but the extent of corrosion was limited to the creation of scars in the crack area. For test specimens with a crack width of 0.2 mm [0.008 in], the onset of corrosion depended on the solution pH. Test specimens with a crack width of 0.1 mm [0.004 in] exhibited no reinforcement bar corrosion, even after 2 years.

(6)   None of the reinforcement bars in the test specimens had significant reductions in cross section after 2 years. However, increased corrosion is expected at longer flow periods, particularly for tests using wider crack widths and lower solution pH.

Note that the corrosion rates Ramm and Biscoping (1998) referred to were based on the measured galvanic coupling currents (macrocell currents). Such coupling current can be used to evaluate the effects of solution chemistry and crack width on the degree of corrosion, but may or may not provide a true measure of corrosion rate, depending on the size of the electrodes used in the measurements (see also the discussion in Section 3.3.1).

Other Literature Information

Other published literature provides additional information supporting the possibility of calcium borate hydrate precipitation that could reduce the permeability of cement-based materials or contribute to autogenous healing of cracks in concrete. Tyrer, et al. (2010) evaluated the concept of a novel composite landfill liner, in which a layer of ground borate slag—a byproduct

of silver–zinc refining—is emplaced above a layer of concrete. Tyrer, et al. (2010) hypothesized that borate ions leached from the borate slag will react with calcium ions in the concrete pore solution to produce an insoluble calcium diborate dihydrate, as in the following reaction

$$Ca^{2+} + 2B(OH)_3 + 2OH^- + 2H_2O \leftrightarrow Ca[B(OH)_4]_2 \bullet 2H_2O \qquad (2\text{-}7)$$

Tyrer, et al. (2010) conducted column experiments in which cementitious pore solutions were eluted or diffused into the hydrated borate slag. In all cases, the column permeability markedly decreased as precipitation occurred in the mixing zone between the calcium-rich, cement-conditioned pore solution and that dominated by borate slag. The precipitation product was determined to be $Ca[B(OH)_4]_2 \bullet 2H_2O$.

Bothe and Brown (1999) conducted experiments to understand the mechanism by which soluble borates, such as boric acid, retard the hardening of cement. They reacted $Ca(OH)_2$ solid with 0.27 M $B(OH)_3$ solution at 45 °C [113 °F]. The resulting solid hydration product was characterized and determined to be highly crystalline $CaB_2O_4 \bullet 6H_2O$.

3 CORROSION OF STEEL IN CONCRETE

3.1 Corrosion Mechanism

Corrosion of steel embedded in concrete is an electrochemical process. The corrosion rate of steel in intact concrete is usually negligibly low because of a passive oxide film on the steel surface that is stable under the alkaline pH of the cement pore solution. The protective passive film can break down either by (i) a reduction in the pH of the cement pore solution (e.g., through carbonation or by reaction with acidic solutions) or (ii) an ingress of chloride ions.

Once the passive oxide film on the steel surface is disrupted, the anodic iron reaction

$$Fe \rightarrow Fe^{2+} + 2e^- \tag{3-1}$$

and cathodic oxygen reaction

$$2H_2O + O_2 + 4e^- \rightarrow 4OH^- \tag{3-2}$$

can occur at an accelerated rate. Despite the high alkalinity of the cement-based material, acid production may occur in the vicinity of the anodic sites because of hydrolysis of ferrous ions, as in

$$Fe^{2+} + 2H_2O \rightarrow Fe(OH)_2 + 2H^+ \tag{3-3}$$

The H^+ ion may be reduced to H_2(gas) and, along with O_2 reduction at more remote cathodic sites, further stimulate the anodic process. The following reactions also may occur to form ferrous (hydr)oxides

$$Fe^{2+} + 2OH^- \rightarrow Fe(OH)_2 \tag{3-4}$$
$$Fe^{2+} + 2OH^- \rightarrow FeO + H_2O \tag{3-5}$$

or, if oxygen is available, form ferric or mixed ferrous/ferric (hydr)oxides

$$4Fe(OH)_2 + O_2 + 2H_2O \rightarrow 4Fe(OH)_3 \text{ (red rust)} \tag{3-6}$$
$$6Fe(OH)_2 + O_2 \rightarrow 2Fe_3O_4 + 6H_2O \text{ (black rust)} \tag{3-7}$$
$$4Fe(OH)_2 + O_2 \rightarrow 2Fe_2O_3 \cdot H_2O + 2H_2O \text{ (red rust)} \tag{3-8}$$
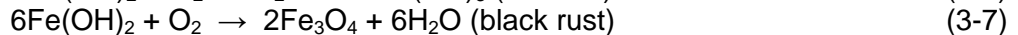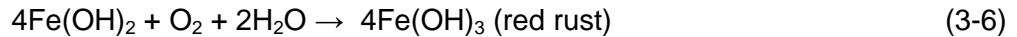
If chloride ions are present in the cement pore water, these ions may act as a catalyst through additional anodic reactions represented by the following equation

$$Fe + nCl^- \rightarrow FeCl_n^{(2-n)} + 2e^- \tag{3-9}$$

where $FeCl_n^{(2-n)}$ are aqueous ferrous chloride complexes (n = 1 to 4), which subsequently react with hydroxyl ions to form various corrosion products, as in the following reaction

$$FeCl_n^{(2-n)} + 2OH^- \rightarrow Fe(OH)_2 + nCl^- \tag{3-10}$$

Equation (3-10) shows that the chloride ions are released and not consumed, such that the process becomes autocatalytic.

The process of steel corrosion in reinforced concrete commonly is modeled as occurring in two stages—initiation and propagation (Figure 3-1). During the initiation period, the metal is passive but certain phenomena can lead to loss of passivity. Carbonation or ingress of acidic solutions can cause the pH of the cement pore water to decrease to a value around 9 where the passive film protecting the steel surface is no longer stable. Chloride ions penetrating into the cement-based material also can locally destroy the protective layer and initiate active corrosion if their concentration at the surface of the metal reaches a critical level. The propagation period begins when the steel is depassivated and ends when a maximum acceptable degree of rebar corrosion is reached.

3.2 Corrosion Rate of Steel in Concrete

Once the passive film on the steel has been disrupted, the corrosion process can initiate and propagate provided that water and oxygen are present on the metal surface. The corrosion rate determines the time it will take to reach the minimally acceptable state of the concrete structure. The corrosion rate is affected by several factors including the (i) permeability of the concrete, (ii) moisture content of the concrete, (iii) temperature, and (iv) availability of oxygen. Typical ranges of corrosion rate of carbon steel in carbonated or chloride-contaminated concrete as a function of relative humidity of the environment are shown in Figure 3-2. The corrosion rate can be considered negligible if it is below 2 µm/yr [7.9×10^{-5} in/yr], low between 2 and 5 µm/yr [7.9×10^{-5} and 2.0×10^{-4} in/yr], moderate between 5 and 10 µm/yr [2.0×10^{-4} and 3.9×10^{-4} in/yr], intermediate between 10 and 50 µm/yr [3.9×10^{-4} and 2.0×10^{-3} in/yr], high between 50 and 100 µm/yr [2.0×10^{-3} and 3.9×10^{-3} in/yr], and very high for values above 100 µm/yr [3.9×10^{-3} in/yr] (Bertolini, et al., 2004).
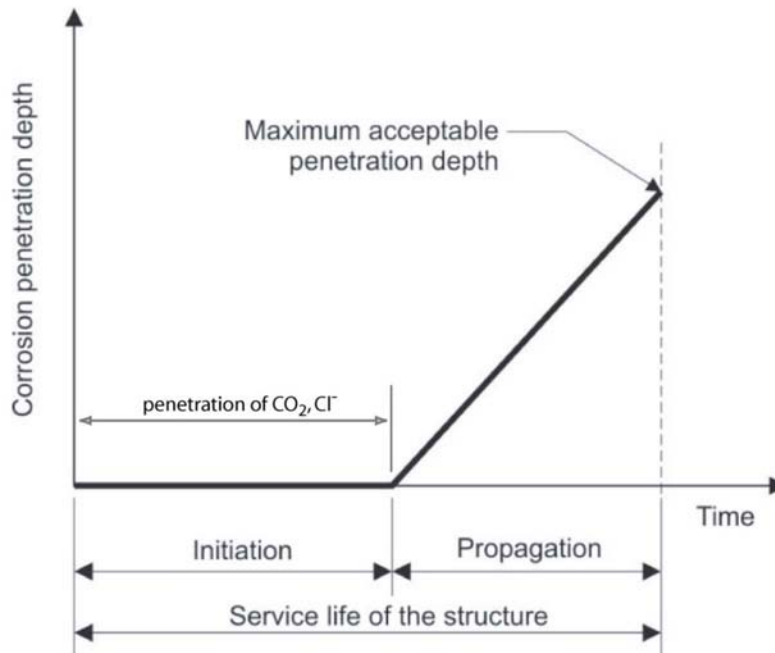
Figure 3-1. Initiation and Propagation Periods for Corrosion in a Reinforced Concrete Structure. [Bertolini, L., B. Elsener, P. Pedeferri, and R. Polder. "Corrosion of Steel in Concrete." Page 72. Copyright© 2004. Wiley-VCH Verlag GmbH & Co. KGaA. Reproduced With Permission.]
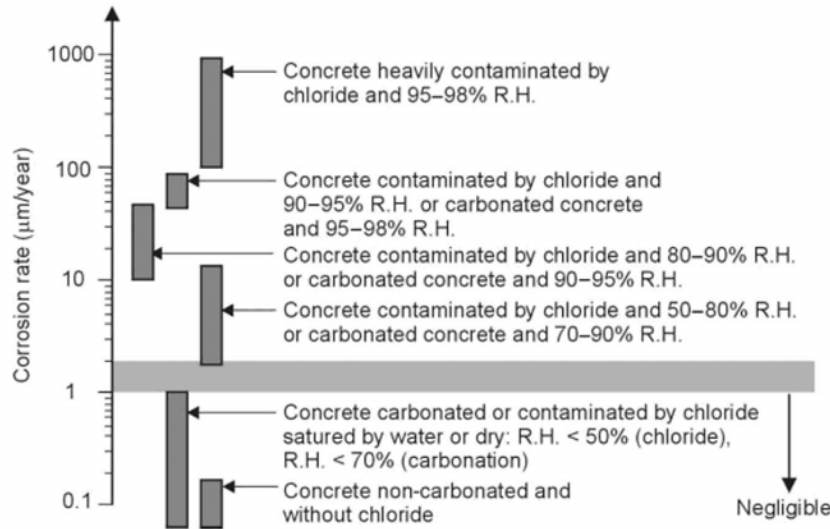
Figure 3-2. Typical Ranges of Corrosion Rate of Carbon Steel in Concrete Exposed to Different Environmental Conditions [Bertolini, L., B. Elsener, P. Pedeferri, and R. Polder. "Corrosion of Steel in Concrete." Page 74. Copyright© 2004. Wiley-VCH Verlag GmbH & Co. KGaA. Reproduced With Permission.]

Numerous researchers have proposed models to predict the rate of reinforcement corrosion [e.g., see review by Raupach (2006)]. Most of these models are based on experiments using laboratory specimens and various parameters, such as properties of the cement-based material (e.g., cement content, water to cement ratio) and exposure conditions (e.g., temperature, relative humidity, chloride concentration).

3.3 Effect of Boric Acid on Corrosion of Steel in Concrete

3.3.1 Literature Information

The following paragraphs summarize information taken from the few studies published in the open literature that evaluated the effect of boric acid on corrosion of steel in concrete. No published data were found that quantified the effect of boric acid on the corrosion rate of steel in concrete.

Dillard and Glanville (1992) were granted a U.S. patent for a method to mitigate chloride-induced corrosion of steel in reinforced concrete structures, such as roadways and bridges, using borate-containing compounds as corrosion inhibitors. As the basis for the patent, Dillard and Glanville (1992) conducted tests in which 1.3-cm [0.5-in]-diameter specimens of rebar were reacted with a synthetic cement pore solution with the following composition: 0.30 M NaOH, 0.60 M KOH, and saturated with $Ca(OH)_2$. Sodium chloride (3.5 wt% NaCl) was added to the synthetic pore solutions to cause chloride-induced corrosion of the rebar. The corrosion inhibitors tested were various boron-containing compounds, including calcium borate, sodium tetraborate, sodium perborate, sodium metaborate, potassium tetraborate, barium metaborate, and boric acid. The test results indicated that the boron-containing compounds, including boric acid, are effective inhibitors of chloride-induced corrosion. For example, Dillard and Glanville (1992) observed by visual examination of the specimens that 26 percent of the rebar surface showed corrosion (rust) after immersion in the simulated cement pore solution

without boron. In the solutions with 0.3 M boric acid, the percentage of rebar samples that exhibited corrosion was lower, ranging from 7 to 11 percent. In the patent, Dillard and Glanville (1992) claimed that the precise concentration of the water-soluble boron compound is not critical, but it stated that useful solution concentrations of borate salts are from ~2 to ~15 percent, preferably ~10 percent by weight of the borate salt.

MPR Associates, Inc. conducted short-term corrosion measurements in a continuously refreshed and aerated boric acid bath and reported a corrosion rate of 106 µm/yr [0.0042 in/yr] for carbon steel (MPR Associates, Inc., 2004). The detailed experimental procedure that was used to derive this corrosion rate is proprietary and was not available for review.

The Jin, et al. (2009) study described in Section 2.5 also included measurements of rebar weight loss due to corrosion in boric acid solutions [2,200, 8,000, and 30,000 ppm $B(OH)_3$]. In Figure 3-3, the weight loss of the steel bars that were immersed in boric acid solutions for a period up to 180 days is compared to that of steel bars exposed to an outdoor natural environment. The measured weight loss increased with time, but the steel bars immersed in boric acid solutions exhibited smaller weight losses than steel bars exposed to the natural environment. After 180 days, the weight loss of specimens immersed in boric acid was between 0.6 and 0.76 percent. The weight loss of specimens exposed to the natural environment for 180 days is 0.85 percent. Although Jin, et al. (2009) did not extract corrosion rate information from their test results, corrosion rates can be approximated from the weight loss data and the reported test specimen dimensions {10-mm [0.39-in] diameter and 400-mm [15.7-in] length}. For specimens immersed in boric acid solutions, the approximate corrosion rates range between 32 and 39 µm/yr [0.0013 and 0.0015 in/yr]. For specimens exposed to the natural environment, the calculated corrosion rate is 43 µm/yr [0.0017 in/yr]. Jin, et al. (2009) concluded from their data that there is no clear relationship between boric acid concentration and weight loss and that boric acid has no significant effect on rebar corrosion.
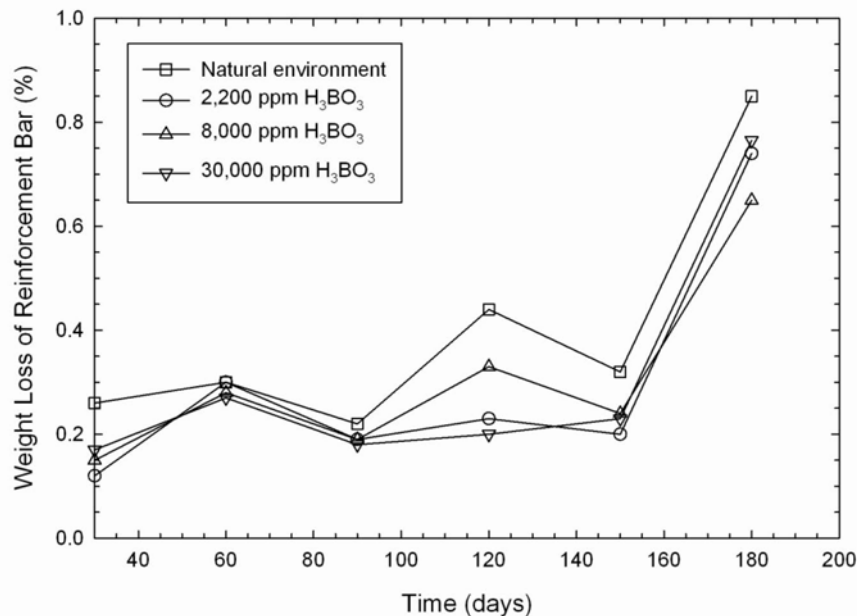
Figure 3-3. Weight Loss of Steel Reinforcement Bars Immersed in Boric Acid Solutions or Exposed to an Outdoor Natural Environment Up to 180 Days (Jin, et al., 2009)

As discussed in Section 2.5.1, Ramm and Biscoping (1998) evaluated the degree of concrete reinforcement steel bar corrosion in cracks penetrated by boric acid solutions. The degree of steel bar corrosion was obtained by measuring the galvanic coupling current (macrocell current) between the steel bar electrodes located in solution-filled concrete cracks and a steel bar embedded in the concrete. If the size of the steel bar electrodes is sufficiently small, the galvanic coupling currents may represent the nonuniform corrosion current, which usually bound the general corrosion rate. However, if the steel bar electrodes are large compared to the steel bar embedded in the concrete, the coupling current may be limited by the polarization of the embedded steel bar. In the latter case, the measured coupling current may not represent the true corrosion current at the steel bar surface (see Section 3.4). Because the detailed dimension of the steel bar electrodes Ramm and Biscoping (1998) used was not given, the galvanic coupling currents cannot be converted to corrosion rate in terms of µm/yr or in/yr.

3.3.2   Modeling of Carbon Steel Corrosion

As stated in Section 3.1, the corrosion rate of steel in intact concrete is negligibly low because the protective passive oxide layer on the steel surface is stable under the alkaline pH of the cement pore solution. Figure 3-4 is a Pourbaix diagram calculated using OLIAnalyzer Version 3.1 showing the stability regions of carbon steel and the passive oxides that form a
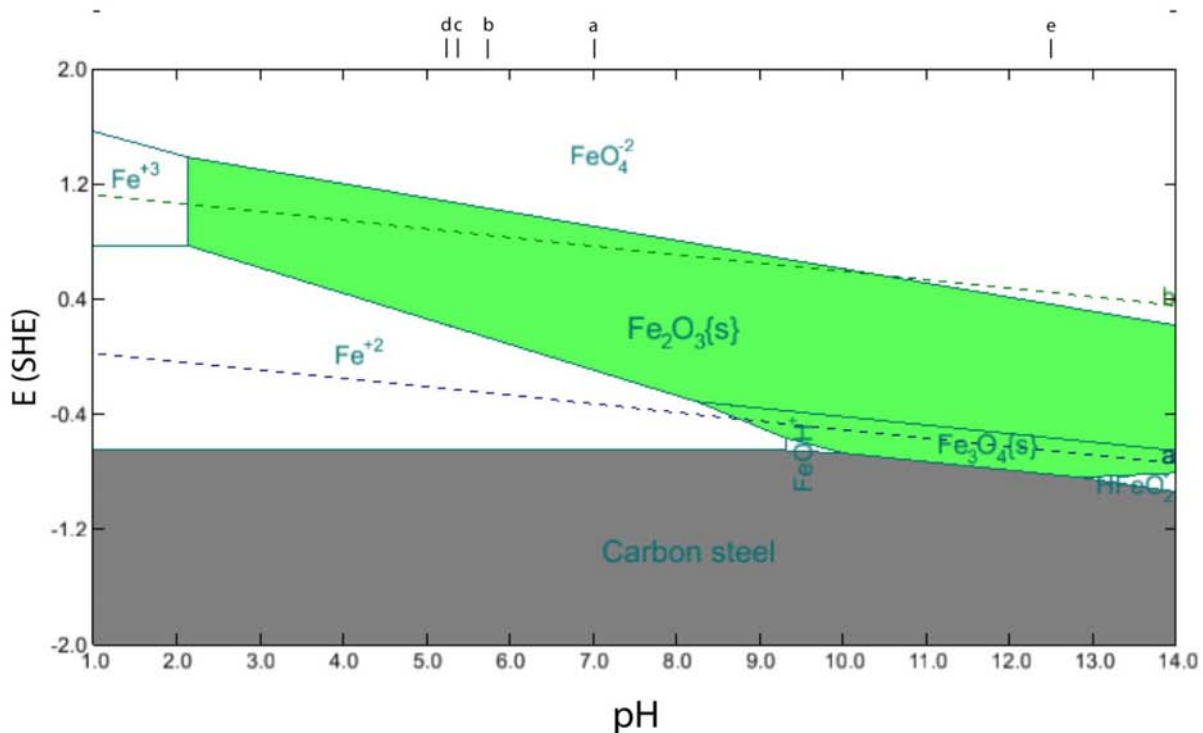
Figure 3-4. Pourbaix Diagram at 25 °C [77 °F] Showing the Stability Regions of Carbon Steel, Iron Oxides, and Iron Aqueous Species as a Function of Solution pH and Redox Potential (E, Versus Standard Hydrogen Electrode). The Vertical Lines (*a,b,c,d,e*) Above the Figure Indicate the Calculated pH for (a) pure water; (b) 500 ppm B(OH)$_3$; (c) 1,500 ppm B(OH)$_3$; (d) 2,500 ppm B(OH)$_3$; and (e) Ca(OH)$_2$-Saturated Cement Pore Solution. Dashed Lines *a* and *b* Delineate the Boundaries of the Water Stability Field.

protective layer on its surface. The diagram shows that the passive oxide, either as Fe_2O_3 or Fe_3O_4, has a very wide range of stability at pHs corresponding to that of cement pore solutions (pH≥12.5, line *e* in Figure 3-4). However, the passive oxide stability region narrows as pH decreases [e.g., as boric acid concentration increases (from line *a* to line *d* in Figure 3-4)], which makes carbon steel more susceptible to corrosion.

Figure 3-5 shows the corrosion rate of carbon steel rebar in deaerated or aerated boric acid solutions calculated using OLIAnalyzer Version 3.1. As indicated in the preceding paragraph, carbon steel becomes more susceptible to corrosion as pH decreases to values less than about 9.0. Under deaerated conditions, the calculated corrosion rate is 7.1 µm/yr [0.00028 in/yr] in pure water (pH = 7) and 8.5 µm/yr [0.00033 in/yr] in a 2,500 ppm $B(OH)_3$ solution. Under aerated conditions, the calculated corrosion rate in pure water (pH = 7) is 129 µm/yr [0.0051 in/yr]. Boric acid addition increases the corrosion rate slightly, to about 131 µm/yr [0.0052 in/yr], in an aerated 2,500 ppm $B(OH)_3$ solution.

Calculations also were conducted to evaluate the Dillard and Glanville (1992) experimental results. The corrosion rate of carbon steel in solutions analogous to those used in the Dillard and Glanville (1992) tests was calculated using OLIAnalyzer. The results are tabulated in Table 3-1. The carbon steel corrosion rate in solutions without boric acid is higher than in solutions with boric acid, which is consistent with Dillard and Glanville's (1992) results.

3.4　　　　Techniques for Assessing Corrosion of Steel in Concrete

Various methods are available for assessing corrosion of steel embedded in concrete. The corrosion test coupon method is a simple and long-established method for evaluating or monitoring corrosion. The general corrosion rate usually is obtained from the measured weight loss or weight gain after a known period of exposure to the environment of interest (ASTM International, 2010). The coupon method is also widely used to evaluate localized corrosion, such as pitting corrosion (ASTM International, 2005). Implemented properly, test coupon methods are the most reliable method for corrosion assessment. However, this method is slow for corrosion rate measurements; it requires a 3-month to 1-year exposure time for applications in industrial process streams and a much longer time for applications in concrete structures. In contrast, corrosion sensors can provide nearly instantaneous measurements and have been used to assess the corrosion rate in concretes (Schiebl and Dauberschmidt, 2008). Techniques that have been used for corrosion rate measurements in concrete are presented in the following sections.

3.4.1　　　　Electrochemical Linear Polarization Resistance Methods

The linear polarization resistance (LPR) method is probably the most commonly used fast-response method for quantitative monitoring of corrosion in concrete. Figure 3-6 is a typical potential–current plot for metal electrodes in activation-controlled systems (Papavinasam, 2008). The potential–current relationship is essentially linear near the corrosion potential, and the corrosion current, I_{corr}, can be calculated using the following equation

$$I_{corr} = \frac{1}{R_P}\left(\frac{\beta_a \cdot \beta_c}{2.303\,(\beta_a + \beta_c)}\right)$$

(3-11)

where R_p is the polarization resistance (shown as the slope in Figure 3-6 and β_a and β_c are anodic and cathodic Tafel constants, respectively. Equation (3-11) is commonly known as the
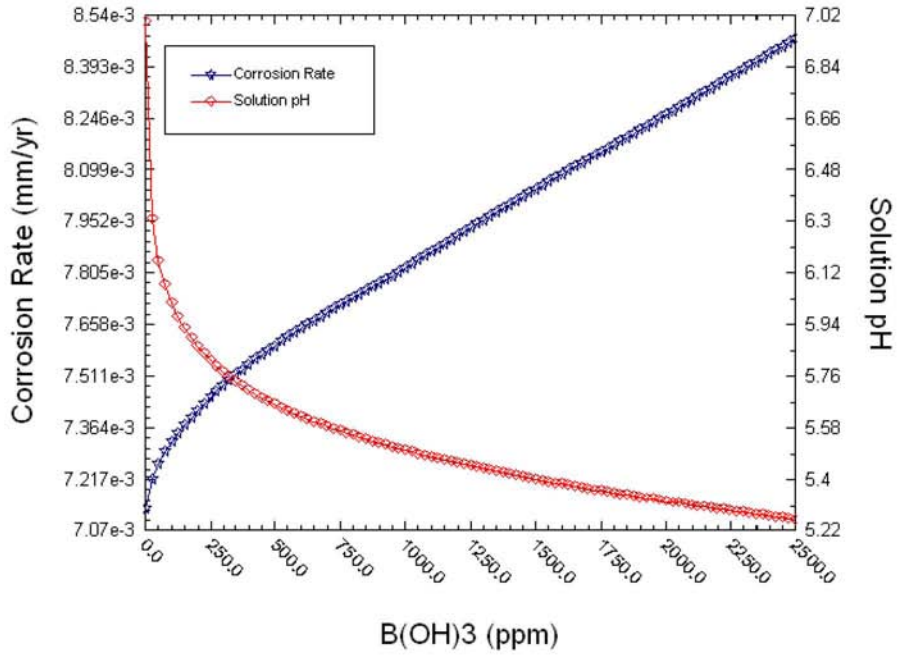
(a)
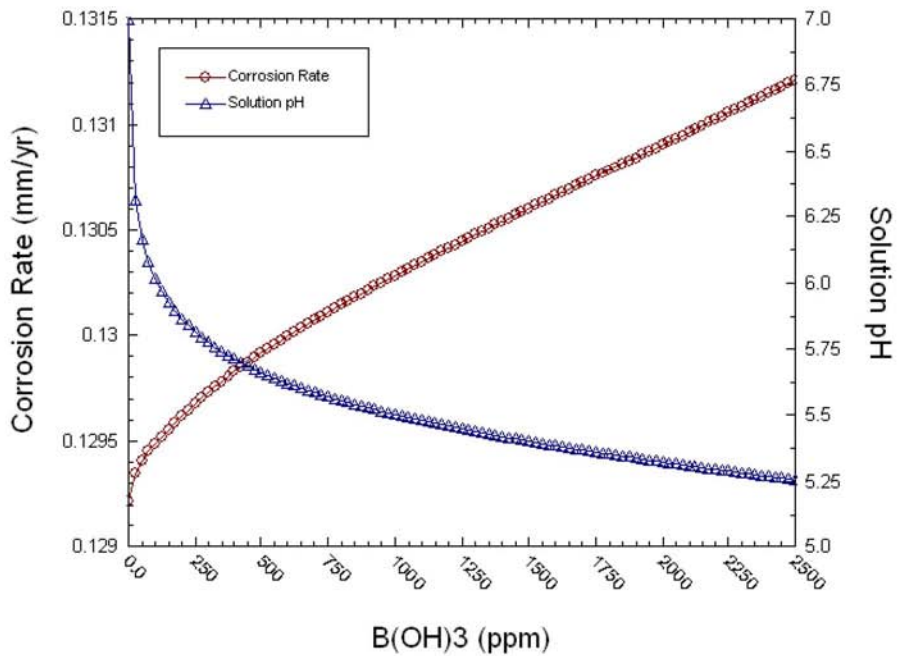
(b)

Figure 3-5. pH and Carbon Steel Corrosion Rates at 25 °C [75 °F] in Boric Acid Solutions With Concentrations to 2,500 ppm [0.25 wt%] B(OH)$_3$ Calculated Using OLIAnalyzer. The Boric Acid Solutions Were Assumed to be Either (a) Deaerated or (b) Aerated (With 8 ppm Dissolved Oxygen, Which is the Solubility of Oxygen in Water).

Table 3-1. pH and Carbon Steel Corrosion Rate at 25 °C [77 °F] in Solutions With or Without Boric Acid* Calculated Using OLIAnalyzer. The Boric Acid Solutions Were Assumed to Have 8 ppm Dissolved Oxygen, Which Is the Solubility of Oxygen in Water.		
Solution Composition	Solution pH	General Corrosion Rate (μm/yr) [in/yr]
0.30 M NaOH + 0.60 M KOH + Ca(OH)$_2$-saturation + 3.5 wt% NaCl (no boric acid)	13.86	2.62 [1.03×10^{-4}]
0.30 M NaOH + 0.60 M KOH + Ca(OH)$_2$-saturation + 3.5 wt% NaCl + 0.3 M B(OH)$_3$	13.68	05.1 [2.01×10^{-5}]
*Ratio of corrosion rate without/with boric acid: 0.00262/0.000510 = 5.1		
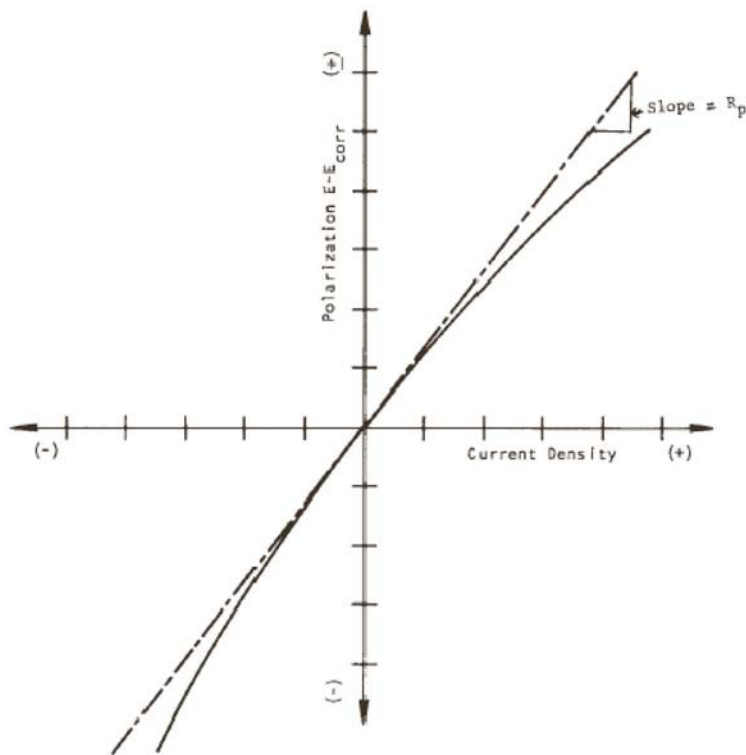
Figure 3-6. Hypothetical Linear Polarization Resistance Plot. Reprinted With Permission From G3–89 Standard Practice for Conventions Applicable to Electrochemical Measurements in Corrosion Testing. Copyright$^{©}$ 2010 ASTM International.

Stern-Geary equation, named for the first investigators to introduce the explicit form of the equation 50 years ago (Stern and Geary, 1957).

Under certain conditions, β_a and β_c in Eq. (3-11) may be treated as constants and combined into a single parameter, B

$$B = \frac{\beta_a \cdot \beta_c}{2.303\,(\beta_a + \beta_c)} \qquad (3\text{-}12)$$

where B is the Stern-Geary coefficient (called B value). Thus, the corrosion current can be related to the polarization resistance by the following simple equation

$$I_{corr} = \frac{B}{R_p} \qquad (3\text{-}13)$$

Therefore, the corrosion current can be determined simply by measuring the potential–current slope near the corrosion potential.

As shown in Figure 3-6, the potential–current relationship is linear only near the corrosion potential. Thus, the measurement should be conducted within ±30 mV, or typically ±10 mV, of the corrosion potential (ASTM International, 2009a). The B value for a metal in a given environment can be obtained experimentally by measuring the Tafel constants, β_a and β_c, usually with a large-scale polarization technique (100 to 500 mV above and below the corrosion potential). This measurement implicitly assumes that β_a and β_c do not change with time. Because of large β_a and β_c variations (usually from 30 mV to infinity) in different metal–liquid systems, B can vary significantly for different systems. Values between 5.5 and 81 mV have been reported (Mansfeld, 1976, Table 2).

In practice, it may not be practical to determine β_a and β_c for a specific metal in different solution compositions or concentrations. It also may not be possible to measure these values because the electrochemical reaction may exhibit Tafel (activation-controlled) behavior only in a narrow region (much less than the 400 mV span). This behavior may be caused by metal surface passivation at potentials slightly above the corrosion potential or by other electrochemical reactions on the working electrode at potentials slightly above or below the corrosion potential. In addition, β_a and β_c values sometimes change significantly with time as corrosion progresses (Mansfeld, 1976, Table 14). In view of these limitations, 26 mV often is used as the nominal B value in laboratory and industrial applications (Papavinasam, 2008).

According to Faraday's Law, corrosion rate (CR) can be calculated from

$$CR = K_1 \left(\frac{I_{corr}}{dA}\right) EW \qquad (3\text{-}14)$$

where CR is given in mm/yr, I_{corr} in µA, K_1 is 3.27×10^{-3} [mm·g/µA·cm·yr], A is the surface area in cm^2, d is the density in g/cm^3, and EW is the equivalent weight, which is defined as the mass

in grams that will be oxidized by the passage of one Faraday (96,489 C) of electric charge. The *EW* for pure elements is given by

$$EW = \frac{W}{n}$$

(3-15)

where *W* is the atomic mass of the element and *n* is the number of electrons involved in the oxidation of an atom of the element in the corrosion process (i.e., the valence of the element).

To calculate the *EW* of an alloy, the following formula may be used

$$EW = \frac{1}{\sum \dfrac{n_i f_i}{w_i}}$$

(3-16)

where n_i, w_i, and f_i are the valence, atomic mass, and mass fraction, respectively, of the ith element of the alloy. Note that valence assignments for elements that exhibit multiple valences under the testing conditions have uncertainties. It is best if an independent technique is used to establish the proper valence for each alloying element. The *EW* values for selected metals can be found in the industrial standard ASTM G102 (ASTM International, 2004).

The LPR method has been used widely in the laboratory to measure the general corrosion rate of steel in concrete and to assess the corrosion rate of actual rebars in the field (Broomfield, 2007). In measuring the corrosion rate of actual rebars in the field, the rebar is used as the testing electrode and a mechanism is required that confines the measured current to a well-defined surface area on the actual rebar. The concept of a guarded-ring electrode (Law, et al., 2000) for measuring rebar corrosion rate in concrete has been used successfully to confine the current from the counter-electrode to a certain area of the rebar embedded in the concrete (Schiebl and Dauberschmidt, 2008). For laboratory applications, the surface area of the testing electrode is not an issue because steel electrodes with well-defined surface areas can be used as testing electrodes (Yang, et. al., 2010a).

In addition to uncertainties in *B* values discussed in a preceding paragraph, strictly speaking the LPR method has a number of restrictions because of certain assumptions associated with the use of the Stern-Geary equation (Oldham and Mansfeld, 1973; Scully, 1998). These restrictions include (i) the corrosion potential should not lie close to the reversible potentials of the metal/metal ion or oxidizing agent/reduction product couples and (ii) no thick film of corrosion product should cover the sensing electrode. Therefore, the accuracy of corrosion rates the LPR method measures may be limited and should be calibrated or verified by other methods, such as weight loss measurements of coupons exposed to the same environment as the LPR probes.

3.4.2 Electrochemical Noise Methods

Electrochemical noise methods measure the fluctuations in potential and current that occur on a corroding metal electrode (Cottis, 2008). Figure 3-7 shows a schematic diagram for electrochemical noise measurement using three electrodes. The fluctuation of currents is measured between two identical sensing electrodes (Sensing Electrodes #1 and #2). The voltage fluctuation is measured between the two sensing electrodes and a reference electrode. The electrochemical noise method has been used to measure the general corrosion rate based on noise resistance, R_n, which is defined as

$$R_n = \sigma_V / \sigma_I$$

(3-17)
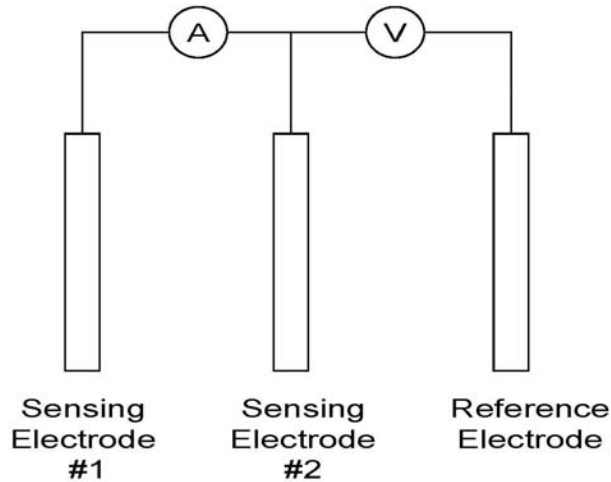
Figure 3-7. Schematic Diagram for Electrochemical Noise Measurement Using Three Electrodes

where σ_V and σ_I are the standard deviations of voltage and current values, respectively, measured during a given time period and are defined as

$$\sigma_V{}^2 = \sum (V_j - V_m)^2 /(n-1) \tag{3-18}$$

$$\sigma_I{}^2 = \sum (I_j - I_m)^2 /(n-1) \tag{3-19}$$

In Eqs. (3-18) and (3-19), V_j is the voltage measured at the jth time interval, V_m is the mean voltage in the given time period, I_j is the current measured at the jth time interval, I_m is the mean current in the given time period, and n is the number of time intervals.

In deriving the corrosion rate, the noise resistance, R_n, is treated as the polarization resistance, R_p, and Eqs. (3-11) or (3-13) are used to calculate the corrosion current.

The electrochemical noise method also has been tested for detection of localized corrosion, such as pitting corrosion. However, this method showed only limited success in detecting pitting corrosion (Yang, et al., 2005).

3.4.3   Coupled Multielectrode Array Sensor Method

The coupled multielectrode array sensor (CMAS) method is a recently developed technology for monitoring corrosion (Yang, 2008), especially localized corrosion. The coupled multielectrode array was initially introduced by Fei, et al. (1996) for studying the spatial and temporal electrochemical behavior of iron metal in solution. The CMAS probe also has been used to estimate the general corrosion rate (Yang, 2008).

When a metal undergoes nonuniform corrosion in an electrolyte, particularly localized corrosion such as pitting or crevice corrosion, electrons are released from the anodic sites and travel to the cathodic sites to support the cathodic reaction (Figure 3-8). If the metal is separated into small sections, some of the local electrode surfaces have properties that are close to the anodic sites and others have properties that are close to the cathodic sites of the corroding metal.
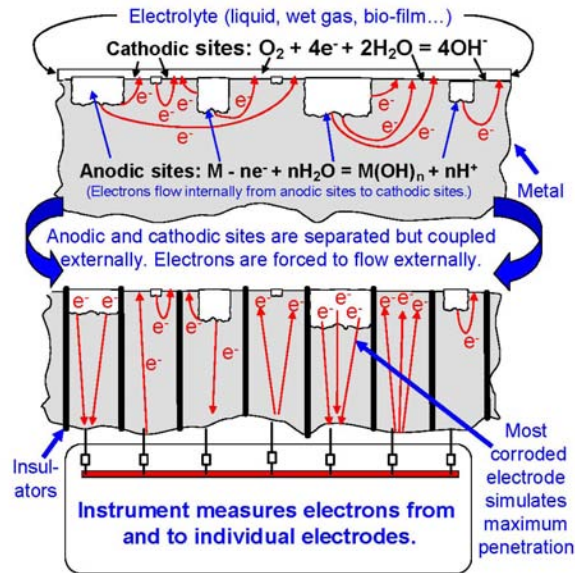
Figure 3-8. Schematic Diagram Showing the Principle of Coupled Multielectrode Array Sensors for Localized Corrosion Monitoring (Sun and Yang, 2006) [Copyright© 2006, With Permission From NACE International]

When these small local electrodes are coupled electrically by being connected to a common contact through an external circuit, the electrode surfaces that exhibit anodic properties simulate the anodic areas and the electrode surfaces that exhibit cathodic properties simulate the cathodic areas of the corroding metal (Figure 3-8). The electrons released from the anodic electrodes are forced to travel through the external circuit to the cathodic electrodes. Thus, there are anodic currents flowing into the more corroding electrodes and cathodic currents flowing out of the less corroding or noncorroding electrodes. The resulting electrical current can be measured, and the localized or nonuniform corrosion rates can be determined quantitatively by the CMAS instrument.

The maximum localized corrosion rate (or maximum localized corrosion penetration rate) is usually derived from the maximum anodic current (Yang, et al., 2002).

$$CR_{max} = I_{max}\, EW\, /\, (F\, \rho\, A) \tag{3-20}$$

where CR_{max} is the calculated maximum penetration rate (mm/s), I_{max} is the maximum anodic current or the most anodic current, F is the Faraday constant (96,485 C/mol), A is the surface area of the electrode (mm^2), ρ is the density of the alloy or electrode (kg/m^3), and EW is the equivalent weight (kg/mol). Equation (3-20) assumes that corrosion on the most corroded electrode is uniform over the entire surface.

Figure 3-9 shows typical responses of the maximum localized corrosion rate of a low carbon steel CMAS probe (Sun, 2004). The CMAS probe has a low detection limit of about 10 nm/yr [3.9×10^{-7} in/yr], which is suitable for measuring corrosion rates in concrete, where the rate usually is less than 5 μm/yr [2×10^{-4} in/yr] (Figure 3-2) and requires high resolution
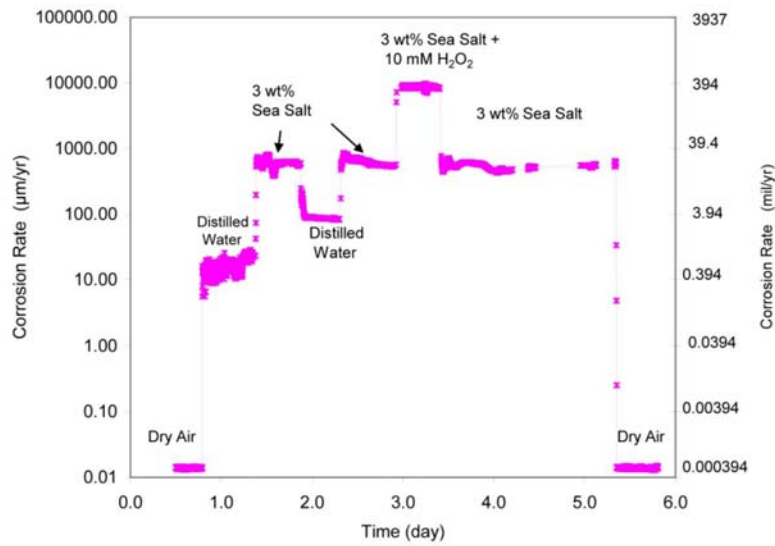
**Figure 3-9. Typical Response of the Maximum Corrosion Rate Measured Using a
16-Electrode Carbon Steel Probe to Changes in Solution Chemistry (Sun, 2004).
[Copyright© 2004, With Permission From NACE International]**

measurements. Figure 3-10 shows maximum nonuniform corrosion rates for carbon steel
(Type 1018) measured using two CMAS probes embedded in a concrete block (Yang, et al.,
2010b). The concrete was prepared using simulated seawater to accelerate the corrosion
process. The stabilized corrosion rates from the two independent CMAS probes were both
about 1 μm/yr [3.9×10^{-5} in/yr].
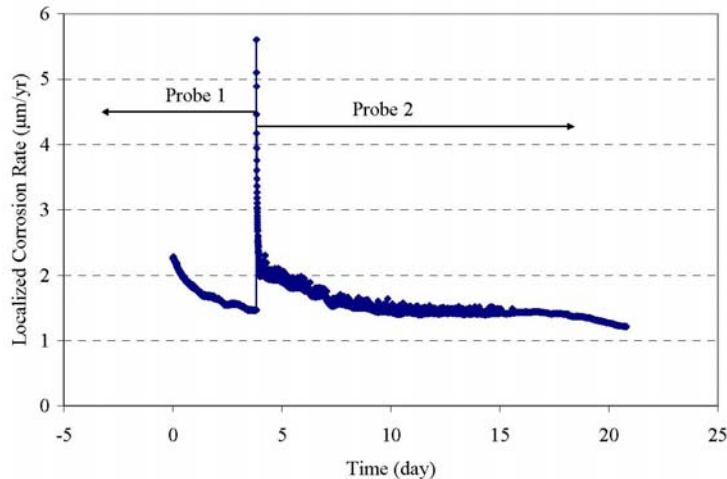
**Figure 3-10. Maximum Nonuniform Corrosion Rates Measured From Two Coupled
Multielectrode Array Sensor Probes Embedded in Concrete. Note: Probe 1 Had
8 Electrodes; Probe 2 Had 16 Electrodes (Yang, et al., 2010b).**

It should be mentioned that the CMAS method measures only nonuniform or localized corrosion. It does not measure uniform or general corrosion. Fortunately, purely uniform corrosion cases are rare. Most of the commonly encountered general corrosion cases, such as carbon steel corrosion in seawater, are better described as nonuniform general corrosion (i.e., a combination of uniform and nonuniform corrosion). In these cases, the CMAS probe measures only the nonuniform portion of the corrosion process. In cases where uniform corrosion is dominant, the CMAS probe would underestimate the corrosion rate. For example, it may underestimate the corrosion rate of aluminum in a 0.2 percent HCl solution by up to 81 percent and of carbon steel in a 0.2 percent HCl solution by up to 44 percent (Yang, et al., 2010b). Corrosion in these systems are known to be dominated by uniform corrosion. On the other hand, the CMAS probe underestimates the corrosion rate only by up to 6 and 7 percent for aluminum and carbon steel, respectively, in simulated seawater (Yang, et al., 2010b). Carbon steel corrosion in seawater is a typical case of nonuniform general corrosion.

3.4.4　　　　Other Methods

Many other methods have been used to measure the corrosion of carbon steel in concrete. The electrical resistance technique is a quantitative monitoring tool for general corrosion based on the metal loss principle. This technique measures the change in electrical resistance of a metallic element exposed to a corrosive environment and converts the electrical resistance into metal loss (Brossia, 2008). This method has been used widely in the process industry, but lacks the sensitivity for monitoring corrosion of metals in concrete.

Ultrasonic techniques have been used widely as nondestructive inspection tools to detect flaws or thinning of metal walls (e.g., in pipes). Increasingly more work has been reported on the use of ultrasonic techniques to monitor wall thinning caused by corrosion (Light, 2008; Rannou, et al., 2010). Ultrasonic thickness measurement is based on the time required for the ultrasonic pulse to travel from the front surface of the component to the back surface then back to the front surface, based on the known ultrasonic velocity in the component.

Eddy current methods have been used to quantitatively measure the metal corrosion. An inductive scanning system that utilizes the phenomenon of eddy current induction has been used to measure corrosion in concrete (Al-Madani, et al., 2010). Similar to the electrical resistance method, both the ultrasonic and eddy current methods do not have the sensitivity to give short-term corrosion rates. However, both methods have been used successfully as inspection tools.

The galvanic sensor is an instantaneous method that has been used to detect rebar corrosion in concrete. In a galvanic sensor, a corroding metal of interest is electrically coupled to a more noble metal (copper, stainless steel, or gold foil if the metal of interest is carbon steel) to raise the electrochemical potential of the metal of interest (Agarwala and Ahmad, 2000). At the elevated potential, corrosion of the metal is accelerated in a corrosive environment. Therefore, the method is a reliable way to detect the corrosivity of the metal in the environment. Because the method only requires two metal electrodes coupled by an ammeter (usually a zero resistance ammeter), a galvanic sensor is simple and low cost. Galvanic probes have been used widely in industry, especially for atmospheric corrosion monitoring. Note that this type of galvanic sensor cannot be used to quantify the corrosion rate, because it operates under accelerated conditions (i.e., at a raised potential).

Strictly speaking, the CMAS system (Section 3.4.3) and the macrocell system Ramm and Biscoping (1998) employed are also galvanic sensors. In this type of sensor, both the anodes and the cathodes are the same type of metal and the coupling current is usually used to indicate nonuniform corrosion. If the anodic electrodes are small and have well defined surface area, this type of galvanic sensor can be used to measure the localized corrosion rate. However, if the anodic electrodes are large, the currents from the anodic electrodes may not represent the corrosion currents on the anodes and this type of system cannot be used to quantitatively measure the corrosion rate.

4 EXPERIMENTAL STUDY OF BORIC ACID DEGRADATION OF CONCRETE AND CORROSION OF REBAR

The published literature reviewed for this report and summarized in Sections 2 and 3 appears to suggest that boric acid does not significantly degrade concrete properties. However, the published data are mostly based on immersion tests and are applicable to systems involving no flow of the boric acid solution. The one study that flowed boric acid solutions through concrete cracks (Ramm and Biscoping, 1998) showed that the concrete alkalinity adjacent to the crack decreased due to dissolution reactions and that reinforcement bars contacted by boric acid solutions showed considerably more corrosion than those contacted by neutral water. Although none of the rebars in that study had significant reductions in cross section after 2 years of testing, the authors of that study concluded that increased corrosion is expected at longer flow periods, particularly at wider crack widths and lower solution pH.

Given the uncertainty and lack of sufficient data on the effect of boric acid on rebar corrosion and concrete degradation, the Center for Nuclear Waste Regulatory Analyses (CNWRA®) conducted experiments to determine this effect.   The experiments initially were planned to be conducted using three methods. In Test Method 1, rebar corrosion rates at room temperature ~24 °C [~75 °F], 40 °C [104 °F]; and 55 °C [131 °F] were measured in borated water, in simulated cement pore solution, and in a mixture of borated water and simulated cement pore solution. In Test Method 2, rebar corrosion rates were measured in borated water flowing in a simulated concrete crack. In Test Method 3, the compressive strength of concrete cylinders reacted with borated water for several months was measured and mineralogical changes due to the reaction were evaluated. Additional experiments were conducted to supplement the data derived from Test Method 2, which was hampered by flow channeling effects.

The experimental details and results are described in the following sections.

4.1   Experimental Methods

4.1.1   Test Method 1—Rebar Corrosion Rate Measurements in Borated Water

Rebar corrosion rates were measured using three techniques: (i) multielectrode array sensor (CMAS) method, (ii) linear polarization resistance (LPR) method, and (iii) rebar coupon weight loss method. As discussed in Section 3, the CMAS method is a recently developed on-line and real-time technology for quantitatively monitoring corrosion, especially localized corrosion (Yang, 2008), whereas the LPR method is the most commonly used fast response method for quantitative monitoring of general corrosion in concrete. The CMAS probes used in the tests were fabricated with nine 1-mm [0.039-in] diameter, carbon steel (Type 1018) electrodes that were embedded in an epoxy insulator (Figure 4-1). The LPR electrodes were made from carbon steel rebar (0.25- to 0.375-in diameter) [6.4- to 9.5-mm diameter], with the electrode side surface coated with epoxy (Figure 4-2). Epoxy coating was applied to the side of the LPR electrode such that the active electrode surface area is restricted to the electrode tip cross sectional area. For both the CMAS and the LPR probes, only the electrode sensing tips were polished and exposed to the solution. Standard calomel electrodes (SCEs) were used as reference electrodes and platinum sheets were used as counter electrodes for the LPR measurements. Standard calomel reference electrodes also were used for the measurement of the corrosion potential of the rebar LPR electrodes. Corrosion potentials of carbon steel LPR electrodes are useful parameters for understanding rebar corrosion.
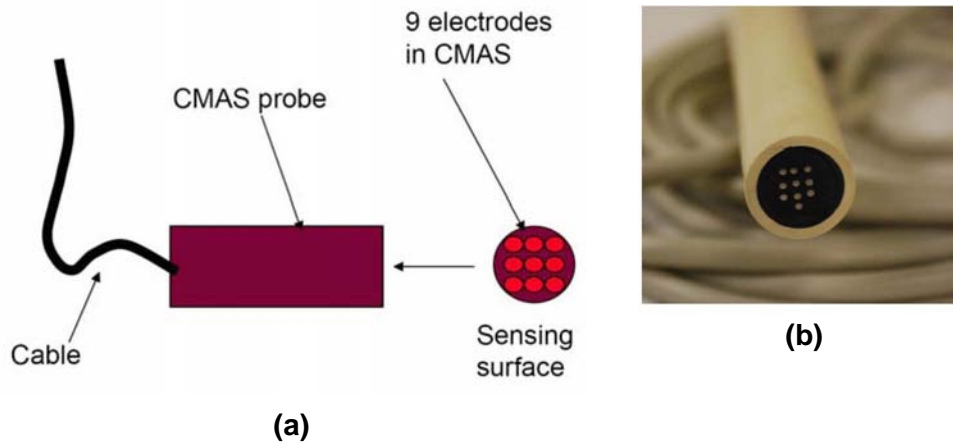
Figure 4-1. (a) Schematic and (b) Picture of Coupled Multielectrode Array Sensor (CMAS) Probe
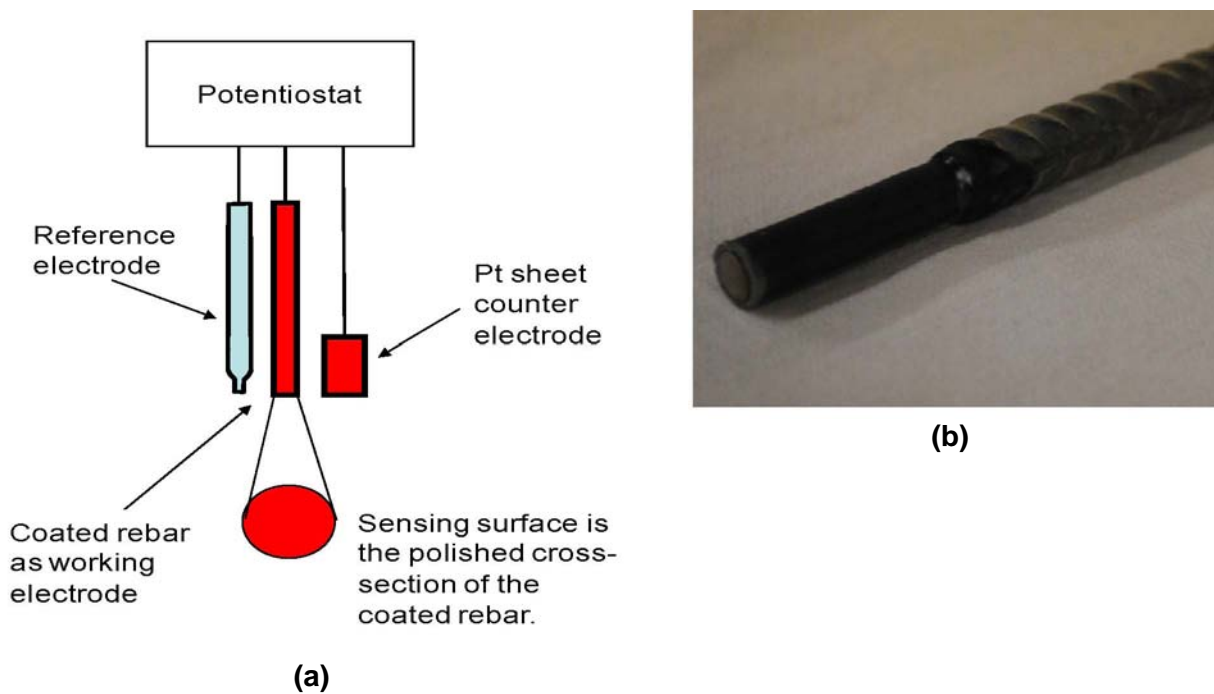
Figure 4-2. (a) Schematic of Linear Polarization Resistance (LPR) Measurement System and (b) Picture of LPR Electrode

A CMAS measuring system described by Yang, et al. (2002) was used with the CMAS probes. This system has four independent channels that allow the simultaneous measurement of up to four CMAS probes. Because the CMAS system has connections for only seven or eight electrodes in some channels, only these numbers of CMAS electrodes were used during the measurements. The sampling rate was set to about 8 minutes per data point. For experiments that required a faster sampling rate, a commercially available nanoCorr® F-20S CMAS system (Corr Instruments, San Antonio, Texas) was used.

A multichannel potentiostat (Solartron MultiStat-1480) was used to automatically conduct the polarization on the LPR electrodes for corrosion rate measurements and to measure the open circuit potential of the electrodes between the polarization measurements. The polarization measurements were conducted every 3 to 6 hours with a three-electrode configuration. The polarization potential range was −15 to +15 mV (versus open circuit potential). The potential scan rate was 0.1667 mV/sec.

A set of CMAS probe, LPR probe, and calomel reference electrode were immersed in each of the following four solutions: (i) 1,200 ppm B, (ii) 2,400 ppm B, (iii) simulated concrete pore solution, and (iv) a 1:1 mixture of 2,400 ppm B solution and simulated concrete pore solution. The first two solutions represent typical boron concentrations of borated water in spent fuel pools. The third represents the pore solution present in concrete, whereas the fourth represents borated water that has reacted with concrete. The composition of simulated concrete pore solution is given in Table 4-1. The same solution composition was used in Poursaee and Hansson's (2007) rebar corrosion experiments. The pHs of the four solutions calculated using OLIAnalyzer are 4.85, 4.46, 13.5, and 12.95, respectively.

The test cells are shown in Figure 4-3. The aqueous solutions, which were contained in 2-L glass vessels, were refreshed continuously from solution reservoirs using a peristaltic pump. During the tests at 40 °C [104 °F] and 55 °C [131 °F], the solution temperatures were controlled to ±2 °C using a heating mantle. Three rebar coupons (1 × 0.27 × 0.125 in) [25.4 × 6.86 × 3.18 mm] also were immersed in each of the solutions. Because of the expected low corrosion rate for carbon steel in borated water or in concrete pore solution, the coupons were made of thin plates to increase their surface-area-to-volume ratio and maximize the weight loss measurement sensitivity. The rebar coupon weights were measured before test initiation and after being cleaned at the termination of each test.

4.1.2   Test Method 2—Rebar Corrosion Rate Measurements in Simulated Concrete Crack

In Test Method 2, rebar corrosion rates in a simulated concrete crack were measured with CMAS and LPR probes and verified with coupon weight loss measurements. A concrete crack was simulated using two blocks of concrete separated by a distance of ~1.0 mm [0.039 in] (Figure 4-4). The two concrete blocks (30 cm × 30 cm × 60 cm) [11.8 in × 11.8 in × 23.6 in] were prepared using the mix design shown in Table 4-2 and were cured for at least 28 days. The sides and bottom of the concrete blocks were lined with plexiglass and a plexiglass box serving as borated (2,400 ppm B) water reservoir was placed over the simulated crack at the top of the two blocks. All surfaces of the concrete in contact with plexiglass were sealed with silicone.

A schematic for the Test Method 2 LPR measurement is shown in Figure 4-5. An LPR electrode similar to those used in Test Method 1 (Figure 4-2b) was used as the working

Table 4-1. Composition of Simulated Cement Pore Solution*	
Component	**Concentration (Molar)**
NaOH	0.131
KOH	0.320
$CaSO_4$	0.0032
$Ca(OH)_2$	0.032
*Poursaee, A. and C. M. Hansson. "Reinforcing Steel Passivation in Mortar and Pore Solution." *Cement and Concrete Research*. Vol. 37. pp. 1,127–1,133. 2007.	
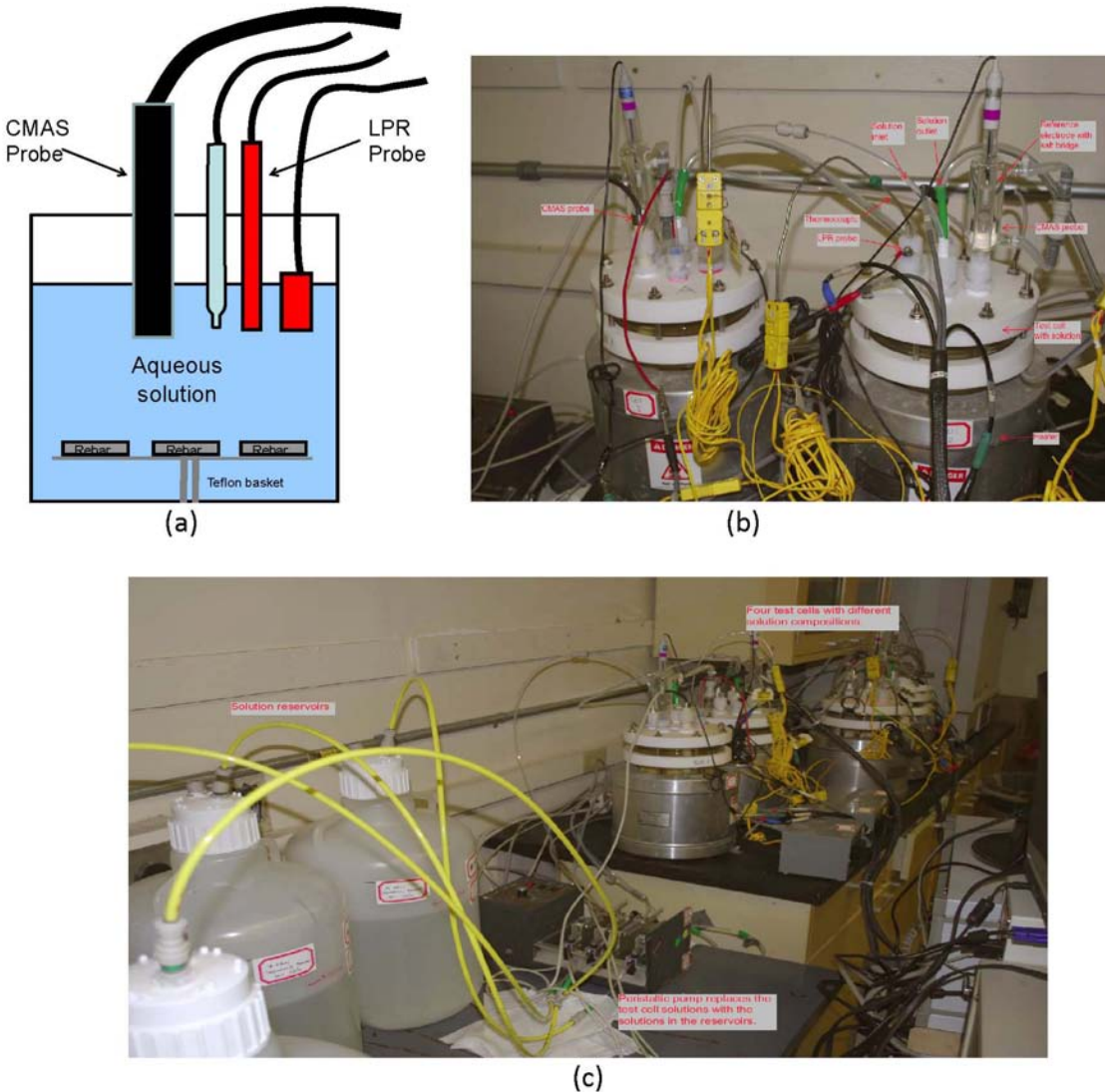
Figure 4-3. Schematic and Pictures of Test Method 1 Experimental Setup. Solutions in the Test Cells Were Continuously Refreshed From Reservoir Tanks Using a Peristaltic Pump (Figure 4-3c). A Closeup of Test Cells (Figure 4-3b) Shows Coupled Multielectrode Array Sensor (CMAS) and Linear Polarization Resistance (LPR) Probes, Reference Electrodes, and Thermocouples. Thin Rebar Coupons Also Were Immersed in the Solutions.

electrode. Identical electrodes were used as the counter and reference electrodes in Test Method 2 instead of the platinum counter electrode and standard calomel reference electrode used in Test Method 1. Using identical metal electrodes is a common practice in LPR field applications (ASTM International, 2008).

Three pairs of CMAS and LPR probes were embedded in the concrete during the pouring stage at the locations shown in Figure 4-4a. Two pairs were arranged such that the sensing electrode surfaces were exposed to borated water in the simulated concrete crack. One of these two pairs of probes was placed high in the concrete block such that the sensing electrode surfaces
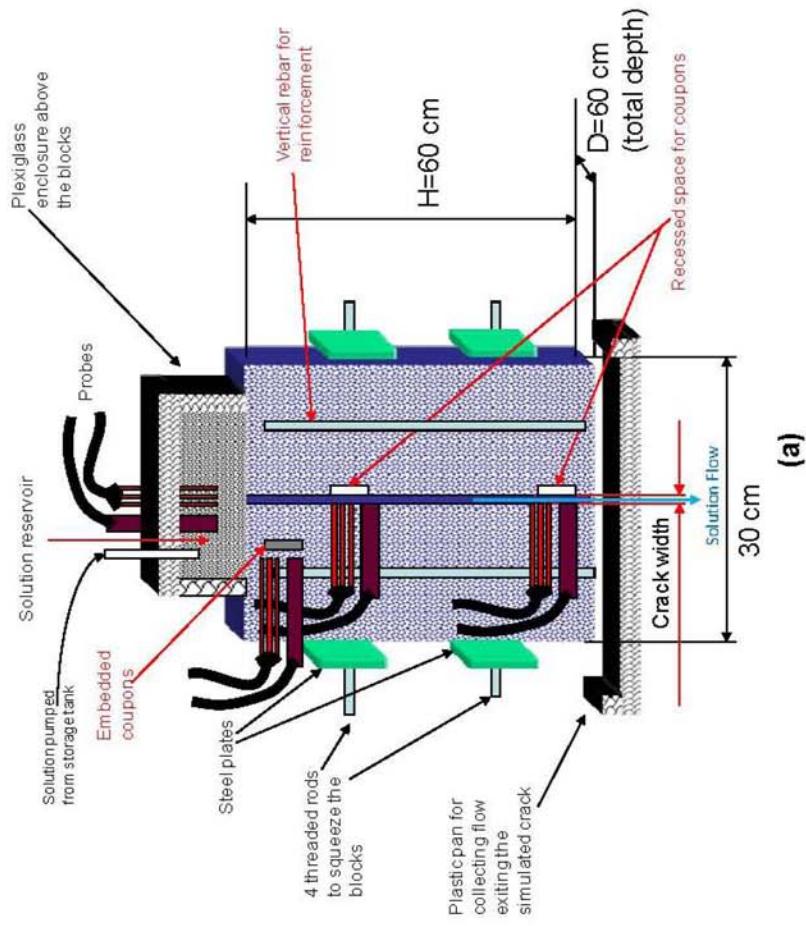
Figure 4-4. (a) Schematic and (b) Picture of Test Method 2 Experimental Setup

Table 4-2. Concrete Mix Design (Batch Weights Per Cubic Yard)		
Material	Weight (lb) [kg]	Reference
CEMEX Type I/II Cement	560 [254]	ASTM C150*
5/8" River Rock	2200 [998]	ASTM C33†
Silica Sand	966 [438]	ASTM C33
Water	258 (31 gal) [117 (117 L)]	
Air Content	1.5±1.5%	
Concrete Properties: Compressive strength at 28 days: 4,000 psi; Water/Cement Ratio: 0.46; and Slump: 3.00±1.0 in [7.62±2.54 cm] *ASTM International. "Standard Specification for Portland Cement." ASTM C150/C150M–09. West Conshohocken, Pennsylvania: ASTM International. 2009. †ASTM International. "Standard Specification for Concrete Aggregates." ASTM C33–03. West Conshohocken, Pennsylvania: ASTM International. 2003.		
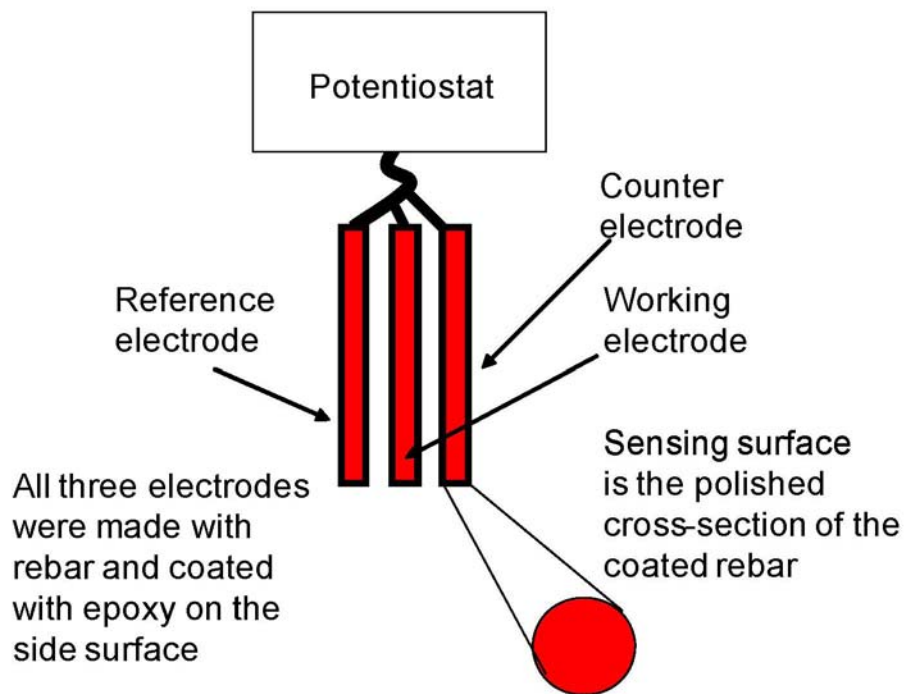
Figure 4-5. Schematic for Linear Polarization Resistance Measurements in Concrete and Concrete Cracks. Identical Rebar Electrodes Were Used as Working, Reference, and Counter Electrodes.

were contacted by relatively fresh borated water and the other pair was placed close to the bottom of the concrete block so that the sensing electrode surfaces were contacted by borated water that has reacted with the concrete. The third pair of the CMAS and LPR probes was placed such that their sensing electrode surfaces are 2 in [5.08 cm] below the concrete surface to provide the baseline corrosion rate for rebars in concrete. The same CMAS measuring systems and potentiostat described in Section 4.1.1 were used in Test Method 2.

For comparison purposes, some of the LPR measurements in the borated water reservoir were conducted using a standard calomel reference electrode immersed in the borated solution above the concrete. No significant difference was observed in the LPR corrosion rates measured with the two types of the reference electrodes (identical rebar electrode and standard calomel electrodes as reference electrodes).

Multiple coupons machined from rebars as discussed for Test Method 1 also were embedded near each pair of corrosion probes. The weight loss data on these coupons were used to verify the general corrosion rates measured by the LPR probes. The coupons were retrieved and their mass measured after termination of the experiment. In addition, the pH of the borated water in the feed tank and of the solution exiting the simulated crack was measured periodically to determine the degree of reaction between the flowing borated water and the concrete.

The borated water flow rate through the simulated crack was adjusted using a control valve at the bottom of the block and the amount of solution in the plexiglass reservoir was maintained as constant as possible by pumping replacement solution from a plastic storage tank. At sufficiently low flow rates (less than ~4 mL/min), continuous solution flow through the simulated crack was allowed and corrosion data was acquired continuously using the data acquisition system.

As discussed later in Section 4.2.2, because the test results indicated solution flow channeling in the simulated concrete crack was occurring, the concrete block assembly was disassembled and three supplementary tests were conducted to measure corrosion rates in borated waters that have reacted with concrete and to determine the borated water threshold pH below which rebar corrosion is negligible. The first involved dripping borated (2,400 ppm B) water at a drip rate of ~20 mL/min over an inclined concrete block that was used in the simulated crack experiment. The nonuniform corrosion rates were measured using the two CMAS probes located along the borated water flow path. Because of the small volume of borated water on the concrete surface, the LPR probes were not useful for measuring the uniform corrosion rate. The pH of the solution that was flowing adjacent to the CMAS probes was measured periodically using a microflow pH electrode (Lazar Research Laboratories, Inc., Los Angeles, California). The pH of the borated water, initially ~4.7, increased as it flowed and reacted with the concrete surface, typically reaching a value of 6.5 to 6.9 near the second CMAS probe. To enable corrosion rate measurement at higher pHs, the initial pH of the 2,400 ppm B solution that was dripped onto the concrete surface was adjusted to higher values by mixing an aliquot of simulated cement pore solution to the feed solution.

In the second supplementary test, nonuniform corrosion rates versus time were measured using CMAS probes immersed in solutions that were collected exiting the concrete block during the simulated concrete crack experiment. The pH of the collected solutions was measured using a Fisher Scientific "accupHast" combination pH electrode and an Orion Model EA940 pH meter.

In the third supplementary test, corrosion rates were measured using CMAS probes immersed in 2,400 ppm B solutions with pH in the range 6.0 to 7.7. The pH of the solutions was adjusted by adding aliquots of simulated cement pore solution to the 2,400 ppm B solutions. The corrosion rates generally were monitored for at least 10 days except in high pH solutions where corrosion rates approached steady state values in two to three days.

The results of the simulated concrete crack test and the supplementary tests are discussed in Sections 4.2.2 and 4.2.3, respectively.

4.1.3 Test Method 3—Compressive Strength Testing and Petrographic Analyses of Concrete Reacted With Borated Water

In Test Method 3, compressive strength tests and petrographic analyses were performed on concrete cylinders that were reacted with borated water for several months. The concrete cylinders (4 in diameter $\times$ 8 in high) [10.2 cm diameter $\times$ 20.3 cm high] were prepared following ASTM C192 (ASTM International, 2007) and the mix design shown in Table 4-2. The concrete cylinders were allowed to cure for at least 28 days prior to testing.

Six concrete cylinders were immersed at room temperature in each of the following solutions: (i) 1,200 ppm B, (ii) 2,400 ppm B, and (iii) tap water. A fourth set of six concrete cylinders was immersed in a 2,400 ppm B solution maintained at 60$\pm$2 °C [140$\pm$4 °F]. All the solutions were refreshed continuously using peristaltic pumps. The experimental setup is shown in Figure 4-6. In addition, a control set of 12 concrete cylinders was kept in a controlled temperature–relative humidity chamber instead of being immersed in solution.

One cylinder was removed from each of the boric acid solutions at 180, 240, and 300 days. Petrographic analyses of these samples were performed by Concrete Research & Testing, LLC (CRT, Columbus, Ohio). At 300 days, the remaining three cylinders from each boric acid solution and three cylinders immersed in tap water were removed and tested for compressive strength following ASTM C39 (ASTM International, 2009b). In addition, at 28, 90, 120, and 300 days, the compressive strengths of three cylinders each from the control set were measured.

(a)

(b)

Figure 4-6. (a) Test Method 3 Experimental Setup. Concrete Cylinders Were Immersed in Test Solutions (1,200 ppm B; 2,400 ppm B; Tap Water), Which Were Refreshed Constantly Using Peristaltic Pumps. A Constant Temperature Bath (Shown in the Background) Maintained the Temperature at 60$\pm$2 °C [140$\pm$4 °F] of a 2,400 ppm B Solution, Which Was Also Constantly Refreshed. (b) Concrete Cylinders Used in Test Method 3.

CRT prepared specimens for petrographic analysis by first coating a portion of the circumference of each concrete cylinder with epoxy to protect and preserve features of the exterior surface during specimen preparation. Sections were then sawcut perpendicular to the long axis of each cylinder. The saw-cut sections were prepared for microscopic examination by lapping on a steel wheel with progressively-finer silicon carbide grit. The lapped sections were then examined under a stereomicroscope at magnifications of 7× to 100× following the guidelines in ASTM C 856 (ASTM International, 2011). The depth of the affected cement paste was measured in each of the concrete specimens at a 10× magnification using a micrometer located in the microscope eyepiece. The average depth of the affected cement paste was determined from 20 random measurements made around the circumference of each cylinder specimen.

The depth of the affected cement paste also was determined by spraying phenolphthalein—a pH indicating solution—on the sawcut, lapped surfaces of the cylinder specimens. Concrete typically has a pH of 13, but acid attack will lower the pH. When phenolphthalein is applied to concrete, the cement paste will turn pink at a pH above 9, but will remain uncolored at pH values below 9. Therefore the depth of the uncolored cement paste will indicate the depth to which the acid has affected the cement paste pH.

4.2　　　Experimental Results

4.2.1　　　Test Method 1—Rebar Corrosion Rate in Borated Water

Rebar Coupon Weight Loss Data

A summary of uniform corrosion rates calculated from the rebar coupon weight loss data is tabulated in Table 4-3 and plotted in Figure 4-7. The data show that rebar uniform corrosion rate increases with increasing temperature and boric acid concentration. Corrosion is negligible in simulated cement pore solution or in the 1:1 mixture of cement pore and boric acid solutions, at least during the short time frame of the tests.

Pictures of rebar coupons after the immersion tests are shown in Figures 4-8. Figure 4-8(a) (left and middle pictures) shows coupons prior to removal of corrosion products. The coupons

Table 4-3. Uniform Corrosion Rates (μm/yr)* Calculated From Measured Weight Loss of Rebar Coupons Immersed in Solutions at Different Temperatures†			
	Temperature		
Solution	24 °C [75 °F]	40 °C [104 °F]	55 °C [131 °F]
1,200 ppm B	154±5	329±28	412±34
2,400 ppm B	213±13	337±49	485±39
Simulated cement pore solution‡	−0.05±0.42	—	—
1:1 mixture of 2,400 ppm B and simulated cement pore solutions§	−0.01±0.02	−0.65±1.01	−0.31±0.11
*1 μm/yr = 3.94 × 10^{-5} in/yr †Average and standard deviations of measurements on three rebar coupons. The coupons were immersed in the solutions at 24, 40, and 55 °C [75, 104, and 131 °F] for a total of 54, 48, and 71 days, respectively. ‡Composition listed in Table 4-2. §Negative values are due to difficulty in cleaning the corrosion products deposited on the rebar coupons.			
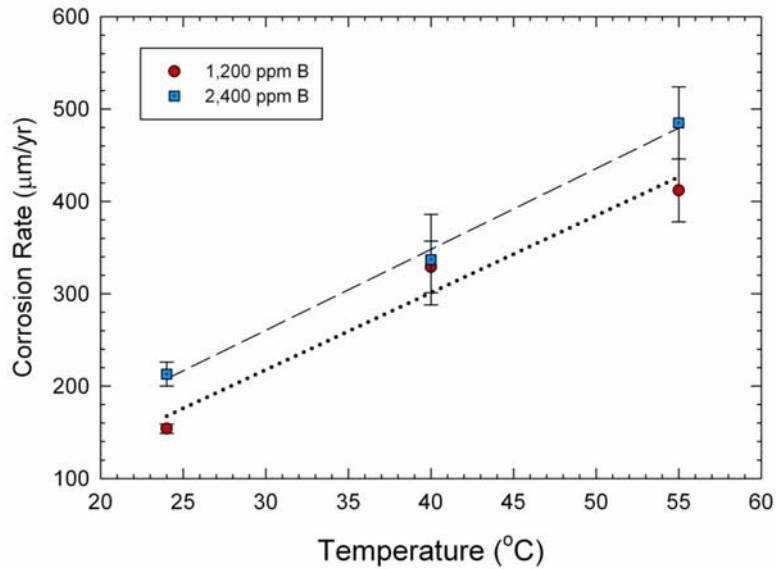
Figure 4-7. Uniform Corrosion Rates in Boric Acid Solutions Versus Temperature Calculated From Rebar Coupon Weight Loss Data. The Dotted and Dashed Lines Are Best Fits to the Rate Data.

| After 67-day exposure at 24 °C in Cell 1; before cleaning | After 71-day exposure at 55 °C in Cell 2; before cleaning | After 54-day exposure at 24 °C in Cell 4; before cleaning | After 71-day exposure at 55 °C in Cell 1; after cleaning | After 71-day exposure at 55 °C in Cell 2; after cleaning | After 54-day exposure at 24 °C in Cell 3; after cleaning | After 71-day exposure at 55 °C in Cell 4; after cleaning |

(a) (b)

Figure 4-8. Weight Loss Coupons After Immersion in 1,200 ppm B Solution (Cell 1), 2,400 ppm B Solution (Cell 2), Simulated Cement Pore Solution (Cell 3), and 1:1 Mixture of 2,400 ppm B Solution and Simulated Cement Pore Solution (Cell 4)

immersed in Cells 1 and 2 (1,200 and 2,400 ppm B solutions) at temperatures of 24 or 55 °C [75 or 131 °F] were all severely corroded and covered by thick layers of corrosion products. The coupons that were immersed in Cells 3 and 4 (high pH solutions) showed no signs of corrosion, with the polishing marks still clearly visible.

Linear Polarization Resistance Data

Figure 4-9 shows typical polarization curves from LPR probes in Cells 1 to 4. Also shown are the corrosion rates and R_p values obtained from data regression. The results indicate that temperature affected the slope of the curves, but not their shape. The LPR curves from Cells 1 and 2 are typical of activation-controlled systems. However, for nearly all data obtained from Cells 3 and 4, only anodic current (or, occasionally, only cathodic current) was observed during the potential scans. The potential was scanned from 15 mV below to 15 mV above the corrosion potential and then back to 15 mV below the corrosion potential. This unusual behavior (i.e., no cathodic current at potentials below the corrosion potential) was probably an indication that the cathodic reaction supporting the measured steady state potential that was established prior to the LPR measurement was due to the cathodic reaction of an extremely small amount of intermediate species adsorbed on the electrode surface. At the start of cathodic scanning, this small amount of reactant likely was quickly consumed before the first data points were recorded. It is also possible that the behavior was due to the fact that the electrode surface property was altered by the small step change (15 mV) of potential and the corrosion potential on the altered surface was no longer the value acquired prior to the step change.

Similar behavior also was observed by Pensado, et al. (2003) during LPR measurements on Alloy 22 specimens in deaerated 0.028 M NaCl at 95 °C [203 °F]. Pensado, et. al. (2003) scanned the potentials between −15 mV and +15 mV with respect to the corrosion potential using a much lower scan rate (0.001 mV/s). No cathodic current was observed in their measurements. The fact that the polarization curve does not cross the zero current line indicates that the criteria for using the LPR probe for corrosion rate measurements as discussed in Section 3.4.1 were not met and that the LPR method may not be applicable to the high pH solutions. Nonetheless, the LPR method was applied to the data from both Cells 3 and 4 and the uniform corrosion rates were calculated.

Figure 4-10 shows the uniform corrosion rates versus time at 24, 40, and 55 °C [75, 104, and 131 °F] from the LPR probes immersed in 1,200 ppm B solution (Cell 1), 2,400 ppm B solution (Cell 2), simulated cement pore solution (Cell 3), and 1:1 mixture of 2,400 ppm B solution and simulated cement pore solution (Cell 4). The measurements in Cell 3 were not conducted at 40 and 55 °C [104 and 131 °F] because of the very low corrosion rates in simulated cement pore solution. At 24 °C [75 °F], the corrosion rates varied in the range ~0.5 to ~10 μm/yr [~1.97 ×10^{-5} to ~3.94 × 10^{-4} in/yr] in the 1,200 ppm B solution and in the range ~15 to ~28 μm/yr [5.91 ×10^{-4} to 1.10 × 10^{-3} in] in the 2,400 ppm B solution. The uniform corrosion rates in the simulated cement pore solution ranged from ~0.2 to ~3.5 μm/yr [~7.87 × 10^{-6} to ~1.38 × 10^{-4} in/yr] and from ~0.2 to ~0.7 μm/yr [~7.87 × 10^{-6} to ~2.76 × 10^{-5} in/yr] in the 1:1 mixture of 2,400 ppm B solution and simulated cement pore solution. At 40 °C [104 °F], the corrosion rates in the 1,200 ppm B solution ranged from ~9 to ~20 μm/yr [~3.54 × 10^{-4} to ~7.87 × 10^{-4} in/yr] and from ~17 to ~ 35 μm/yr [~6.69 × 10^{-4} to ~1.38 × 10^{-3} in/yr] in the 2,400 ppm B solution. The uniform corrosion rate in the 1:1 mixture of cement pore solution and boric acid solution is higher at 40 °C [104 °F] than at 24 °C [75 °F], ranging from ~0.8 to ~2.7 μm/yr [~3.15 × 10^{-5} to ~1.06 × 10^{-4} in/yr]. At 55 °C [131 °F], the uniform corrosion rates in all solutions are higher than at lower temperatures. In the 1,200 ppm B solution, the corrosion rate varied from ~25 to ~ 50 μm/yr [~9.84 × 10^{-4} to ~1.97 × 10^{-3} in/yr] and from ~40 to ~85 μm/yr [~1.57 × 10^{-3} to ~3.35 × 10^{-3} in/yr] in the 2,400 ppm B solution. The uniform corrosion rates at 55 °C [131 °F] in the 1:1 mixture of cement pore solution and boric acid solution ranged from ~2.8 to ~14 μm/yr [~1.10 × 10^{-4} to ~5.51 × 10^{-4} in/yr].
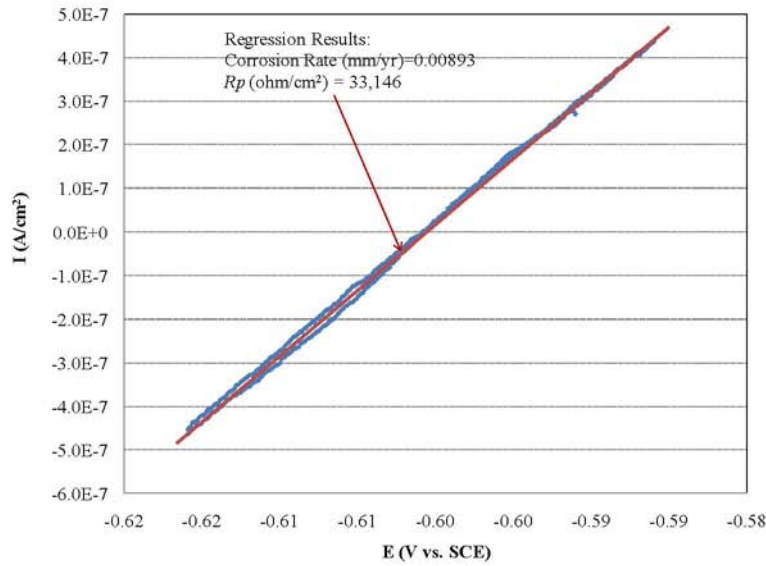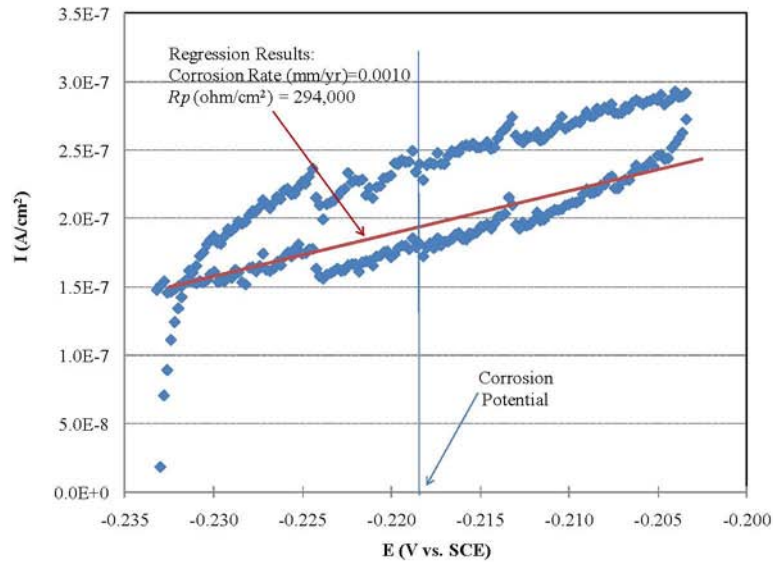
Figure 4-9. Typical Polarization Curves From Linear Polarization Resistance Probes in (a) Cells 1 and 2 and (b) Cells 3 and 4. The Data Shown in (a) Were Measured at 24 °C [131 °F] in Cell 1 (1,200 ppm B Solution) and Those in (b) Were Measured at 40 °C [104 °F] in Cell 4 (1:1 Mixture of 2,400 ppm B Solution and Simulated Cement Pore Solution). In Cell 3 and 4 Measurements, Only Anodic Current (or Occasionally Only Cathodic Current) Was Observed During Potential Scan From 15 mV Above and Below the Corrosion Potential.
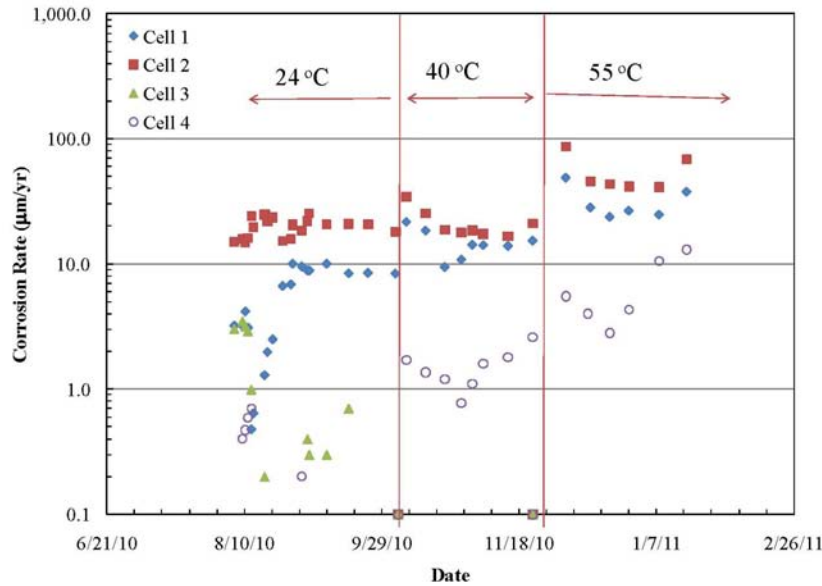
Figure 4-10. Uniform Corrosion Rates Versus Time at 24, 40, and 55 °C [75, 104, and 131 °F] From Linear Polarization Resistance Probes Immersed in 1,200 ppm B Solution (Cell 1), 2,400 ppm B Solution (Cell 2), Simulated Cement Pore Solution (Cell 3), and 1:1 Mixture of 2,400 ppm B Solution and Simulated Cement Pore Solution (Cell 4). Measurements Using Cell 3 Were Not Conducted at 40 and 55 °C [104 and 131 °F] Because of the Very Low Corrosion Rates in Simulated Cement Pore Solution.

The corrosion rates plotted in Figure 4-10 were calculated using Equations 3-13 and 3-14 assuming *B* is equal to 26 mV, which is the nominal *B* value used in laboratory and industrial applications (Papavinasam, 2008). Table 4-4 compares the average corrosion rates in 1,200 and 2,400 ppm B solutions (Cells 1 and 2) derived from the LPR data with those calculated from

Table 4-4. Corrected B Values for the Linear Polarization Resistance Method Based on Corrosion Rates Derived From Coupon Weight Loss Data*									
Temperature	**Average Corrosion Rate Calculated from LPR Probe Data Assuming B = 26 mV (μm/yr)†**		**Average Corrosion Rate Calculated from Coupon Weight Loss (μm/yr)**		**Correction Factor (from B = 26 mV)**			**Corrected B Value (mV)**		
	Cell 1	Cell 2	Cell 1	Cell 2	Cell 1	Cell 2	Average	Cell 1	Cell 2	Average
24 °C [75 °F]	5.79	19.8	154	213	26.6	10.7	18.7	692	280	485.5
40 °C [104 °F]	14.8	21.2	329	337	22.2	15.9	19.0	577	413	494.8
55 °C [131 °F]	31.8	54.6	412	485	13.7	8.9	11.3	357	231	293.7

*Data from Cells 3 and 4 were not used to derive corrected B values because the weight loss data from these cells were close to zero
†1 μm/yr = 3.94×10^{-5} in/yr

the coupon weight loss data (Table 4-3). Also shown in the table are the corrected *B* values (i.e., *B* values that were adjusted to the corrosion rates derived from the weight loss data). The corrected *B* values range from 293 to 486 mV.

Figure 4-11 shows typical large-scale polarization curves in a 1,200 ppm B solution (Cell 1) at 24 °C [131 °F] that were recorded in an effort to determine the appropriate *B* value for the LPR method. Because large-scale polarization tests alter the electrode surface properties, separate LPR electrodes were used for the anodic and cathodic polarizations. All potential scans started from the corrosion potential, after the electrodes have been immersed in the solution overnight, and returned to the corrosion potential after reaching the pre-determined overpotential of +500 or –500 mV. The Tafel constants (β_a and β_c) derived from two polarization regions also are shown in Figure 4-11. The first polarization region is for overpotentials between 50 and 100 mV as suggested by Dean (1977). The second polarization region is for overpotentials between 100 and 500 mV as suggested by Papavinasam (2008). From the data shown in Figure 4-11, the *B* values were calculated and shown in Table 4-5. The *B* values vary from 40.5 mV, obtained in a narrow range near the corrosion potential (50 to 100 mV of overpotential), to 130 mV, obtained over a large potential range (100 to 500 mV of overpotential). These values are significantly lower than the corrected *B* values derived from the weight loss method.
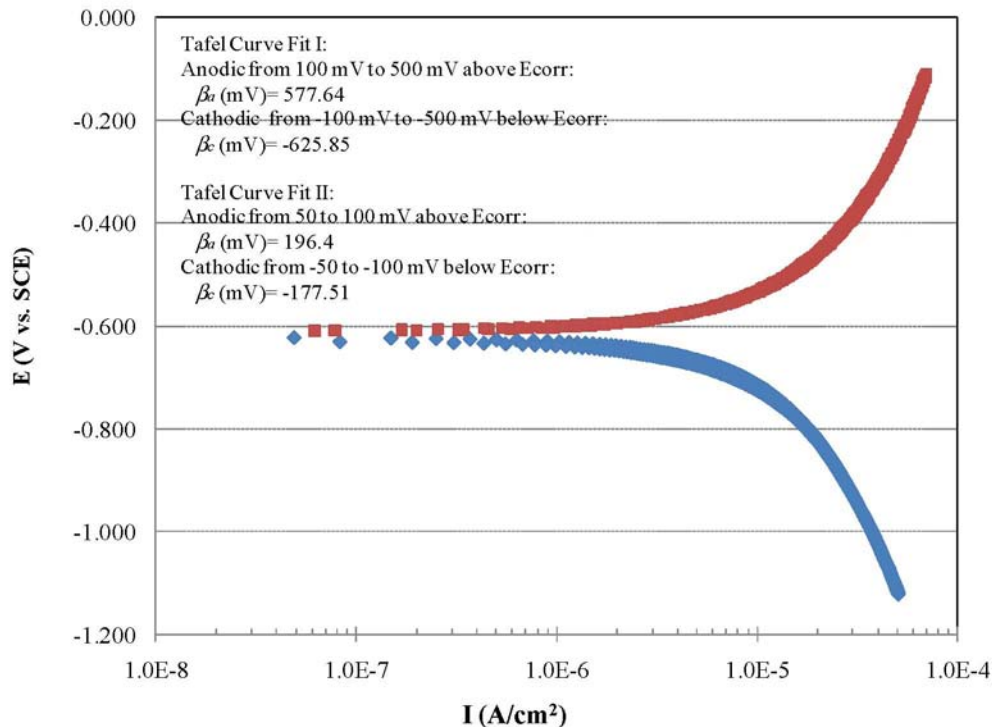
Figure 4-11. Typical Large-Scale Polarization Curves at the End of the Linear Polarization Resistance (LPR) Measurements. Measurements Were Conducted at 24 °C [131 °F] in 1,200 ppm B Solution (Cell 1). Separate LPR Electrodes Were Used During the Anodic and Cathodic Polarization. All Potential Scans Start at and Return to Corrosion Potential After Reaching the Pre-Determined Overpotential of +500 or –500 mV.

Table 4-5. *B* **Values and Tafel Constants Derived from Large-Scale Polarization Curves Measured in 1,200 ppm B Solution at 24 °C [75 °F]**

Range of Potential (mV) Used in Curve Fit	β_a (mV)	β_c (mV)	B (mV)
100 to 500 or −100 to −500	577.6	625.9	130
50 to 100 or −50 to −100	196.4	177.5	40.5

As mentioned in Section 3.4.1, coupon weight loss measurements can be used to calibrate *B* values. The average corrected *B* values derived from weight loss data were used to recalculate the uniform corrosion rates in 1,200 and 2,400 B solutions. The rates are plotted in Figure 4-12. At 24 °C [75 °F], the corrected uniform corrosion rates varied in the range ~9 to ~180 µm/yr [~3.54 × 10^{-4} to ~7.09 × 10^{-3} in/yr] in the 1,200 ppm B solution and in the range ~279 to ~470 µm/yr [~1.10 × 10^{-2} to ~1.85 × 10^{-2} in/yr] in the 2,400 ppm B solution. At 40 °C [104 °F], the uniform corrosion rates in the 1,200 ppm B solution ranged from ~180 to ~415 µm/yr [~7.09 × 10^{-3} to ~1.63 × 10^{-3} in/yr] and from ~315 to ~ 654 µm/yr [~1.24 × 10^{-2} to ~2.57 × 10^{-2} in/yr] in the 2,400 ppm B solution. At 55 °C [131 °F], the uniform corrosion rates in the 1,200 ppm B solution varied from ~269 to ~ 553 µm/yr [~1.06 × 10^{-2} to ~2.18 × 10^{-2} in/yr] and from ~470 to ~980 µm/yr [~1.85 × 10^{-2} to ~3.85 × 10^{-2} in/yr] in the 2,400 ppm B solution.
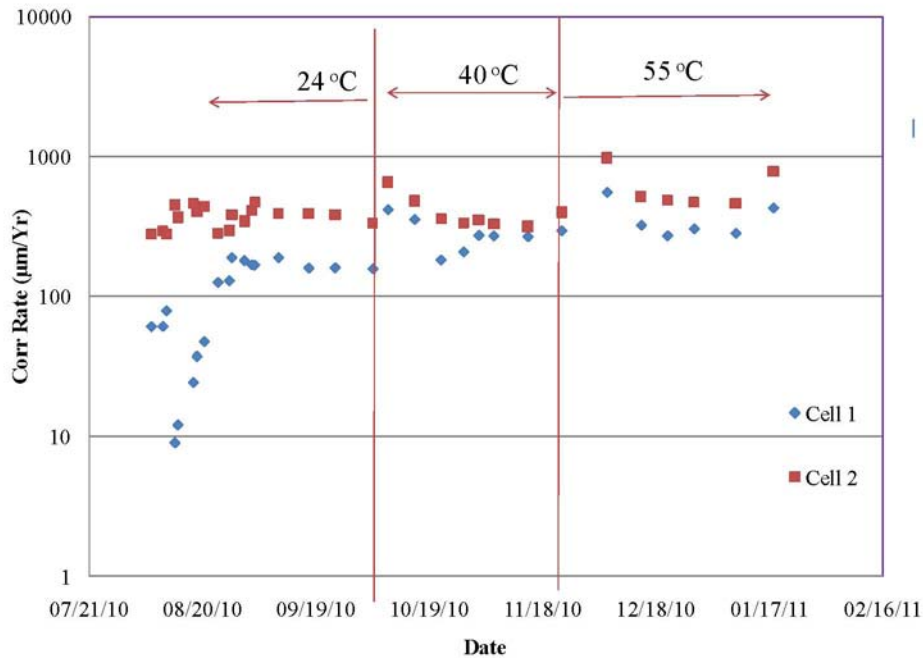
Figure 4-12. Corrected Uniform Corrosion Rates Versus Time at 24, 40, and 55 °C [75, 104, and 131 °F] From Linear Polarization Resistance Probes Immersed in 1,200 ppm B Solution (Cell 1) and 2,400 ppm B Solution (Cell 2). The Corrections Were Based on the Corrosion Rates Obtained From the Coupon Weight Loss Data at the Corresponding Temperature.

Figure 4-13 shows the corrosion potential versus time at 24, 40, and 55 °C [75, 104, and 131 °F] from the LPR probes immersed in 1,200 ppm B solution (Cell 1), 2,400 ppm B solution (Cell 2), simulated cement pore solution (Cell 3), and 1:1 mixture of 2,400 ppm B solution and simulated cement pore solution (Cell 4). The potentials of the LPR probes were active (lower than −0.4 V vs. SCE) in Cells 1 and 2, and relatively noble (mostly above −0.3 V vs. SCE). According to the industry standard for the assessment of carbon steel corrosion in concrete at ambient temperatures (Schiebl and Dauberschmidt, 2008), the probability of corrosion is 90 percent if the potential is lower than −0.291V vs. SCE and only 10 percent if the potential is higher than −0.141V vs. SCE. Based on these criteria, the measured potentials in Cells 1 and 2 indicate that the carbon steel in these cells was undergoing corrosion, which is consistent with the weight loss, LPR, and CMAS data. The corrosion potential data in Cells 3 and 4, especially the Cell 3 data at the start of the experiment (−0.4 V vs. SCE), indicate that the carbon steel also may be corroding. However, the weight loss, LPR, and CMAS data all indicated that there was no corrosion in Cells 3 and 4. The industrial criteria were derived primarily from studies on concrete structures exposed to outdoor rain water, fresh water, or salt water. The criteria may not necessarily apply to solutions containing boric acid, which has been shown to have a corrosion-inhibiting effect (Dillard and Glanville, 1992).

Coupled Multielectrode Array Sensor Data

The nonuniform corrosion rates measured using the CMAS probes are shown as a function of time in Figure 4-14. At 24 °C [75 °F], the corrosion rates in the 1,200 and 2,400 ppm
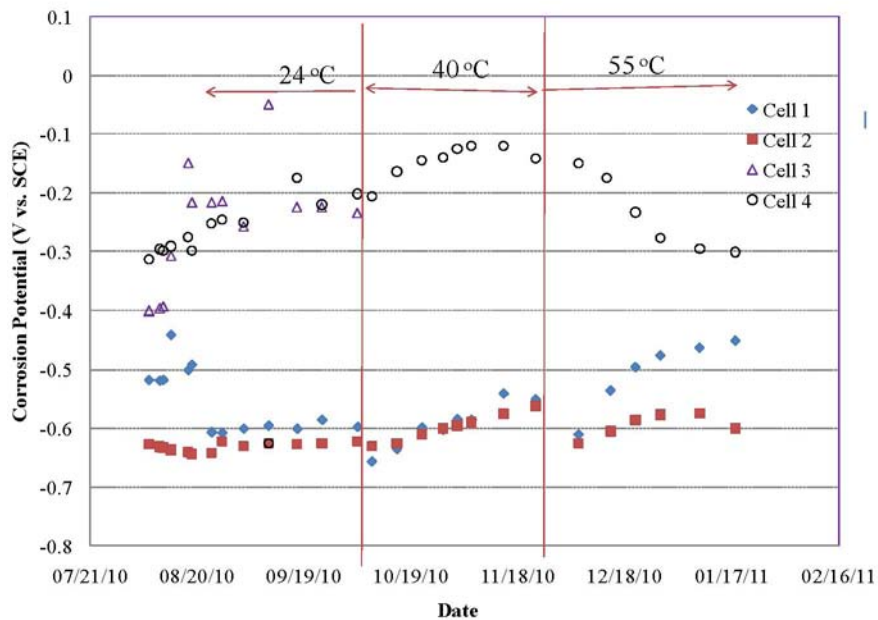
Figure 4-13. Corrosion Potential Versus Time at 24, 40, and 55 °C [75, 104, and 131 °F] From Linear Polarization Resistance Probes Immersed in 1,200 ppm B Solution (Cell 1), 2,400 ppm B Solution (Cell 2), Simulated Cement Pore Solution (Cell 3), and 1:1 Mixture of 2,400 ppm B Solution and Simulated Cement Pore Solution (Cell 4). Measurements Using Cell 3 Were Not Conducted at 40 and 55 °C [104 and 131 °F] Because of the Very Low Corrosion Rates in Simulated Cement Pore Solution.
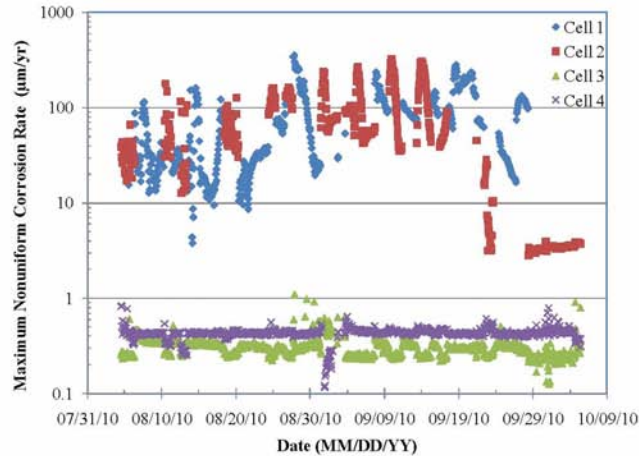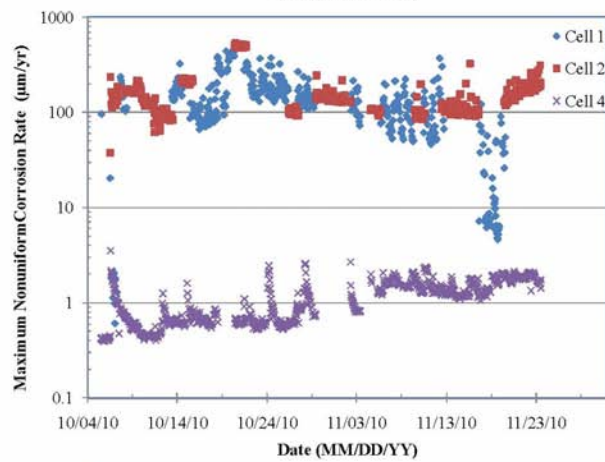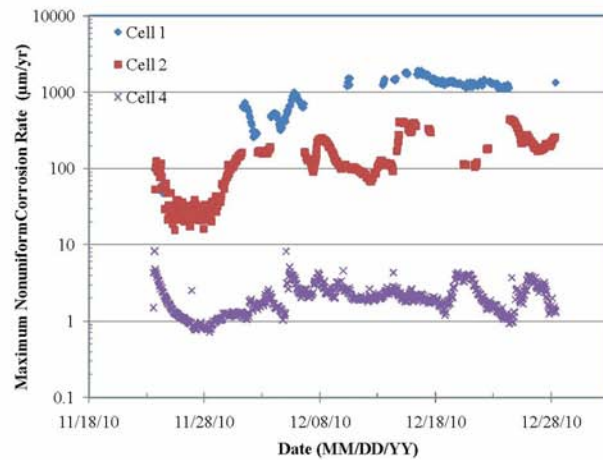
Figure 4-14. Nonuniform Corrosion Rates Versus Time Measured at (a) 24 °C [75 °F], (b) 40 °C [104 °F], and (c) 55 °C [131 °F] Using Coupled Multielectrode Array Sensor Probes Immersed in 1,200 ppm B Solution (Cell 1), 2,400 ppm B Solution (Cell 2), Simulated Cement Pore Solution (Cell 3), and 1:1 Mixture of 2,400 ppm B Solution and Simulated Cement Pore Solution (Cell 4). Measurements Using Cell 3 Were Not Conducted at 40 and 55 °C [104 and 131 °F] Because of the Very Low Corrosion Rates in Simulated Cement Pore Solution.

B solutions are similar, varying with time in the range ~10 to ~300 μm/yr [~3.94 × 10^{-4} to ~1.18 × 10^{-2} in/yr]. The nonuniform corrosion rates in simulated cement pore solution and in the 1:1 mixture of 2,400 ppm B solution and simulated cement pore solution are very low, generally less than 0.5 μm/yr [1.97 × 10^{-5} in/yr], which is the lower detection limit of the CMAS system. At 40 °C [104 °F], the corrosion rates in the 1,200 and 2,400 ppm B solutions also are similar, but are higher than at 24 °C [75 °F], ranging from ~40 to ~500 μm/yr [~1.57 × 10^{-3} to ~1.97 × 10^{-2} in/yr]. The corrosion rate in the 1:1 mixture of cement pore solution and boric acid solution is higher at 40 °C [104 °F] than at 24 °C [75 °F], ranging from ~0.5 to ~2 μm/yr [~1.97 × 10^{-5} to ~7.87 × 10^{-5} in/yr].

At 55 °C [131 °F], the corrosion rates in all solutions are higher than at lower temperatures. However, in contrast to the results at 24 and 40 °C [75 and 104 °F], the corrosion rate measured using the CMAS probe in the 1,200 ppm B solution is higher (~50 to ~2,000 μm/yr) [~1.97 × 10^{-3} to ~7.87 × 10^{-2} in/yr] than in the 2,400 ppm B solution (~15 to ~500 μm/yr) [~5.91 × 10^{-4} to ~1.97 × 10^{-2} in/yr]. Although this result is unexpected, a likely explanation is that uniform, rather than nonuniform, corrosion is more dominant in the 2,400 ppm B solution than in the 1200 ppm B solution because of the lower pH of the former. As discussed in Section 3.4.3, the CMAS sensor measures only the nonuniform portion of the corrosion process. This explanation is consistent with the uniform corrosion rates determined using the LPR probes and the rebar coupon weight loss measurements, which both show higher values in the 2,400 ppm B solution than in the 1,200 ppm B solution.

The nonuniform corrosion rates at 55 °C [131 °F] in the 1:1 mixture of cement pore solution and boric acid solution, which range from ~0.8 to ~5 μm/yr [~3.15 × 10^{-5} to ~1.97 × 10^{-4} in/yr], are higher than at lower temperatures.

4.2.2   Test Method 2— Rebar Corrosion Rate in Simulated Concrete Crack

Linear Polarization Resistance Probe Data

Figure 4-15 shows the uniform corrosion rates versus time measured using LPR probes (i) embedded inside the concrete block, (ii) placed at the simulated crack surface near the top of the concrete block, (iii) placed at the simulated crack surface near the bottom of the concrete block, or (iv) immersed in the reservoir solution. The *B* values used for the calculation of the corrosion rates were 485.5 mV (Table 4-4, corrected from weight loss data) for the data from the reservoir solution and 26 mV for the data obtained under all other conditions. Although the potentiostat is capable of measuring very low current density (<10^{-10} A/cm^2), significant scattering was observed in the slopes of the potential versus current scans when the corrosion rate was less than 1 μm/yr [3.94 × 10^{-5} in/yr]. Some of the slopes had negative values, which correspond to negative corrosion rates and, thus, are unreasonable. For plotting purposes, corrosion rates that are negative or less than 0.001 μm/yr [3.94 × 10^{-8} in/yr] were plotted as 0.001 μm/yr [3.94 × 10^{-8} in/yr] in Figure 4-15.

The uniform corrosion rates from all the probes in the concrete blocks were low (less than 1 μm/yr). The corrosion rates from the probe embedded inside the concrete block appear to be lower than those from the probes installed at the simulated concrete crack. However, because of the scatter in measured corrosion rates less than 1 μm/yr [3.94 × 10^{-5} in/yr], it cannot be determined with confidence if the probes in the simulated cracks were corroding significantly more than the probe embedded in the concrete. No significant corrosion rate
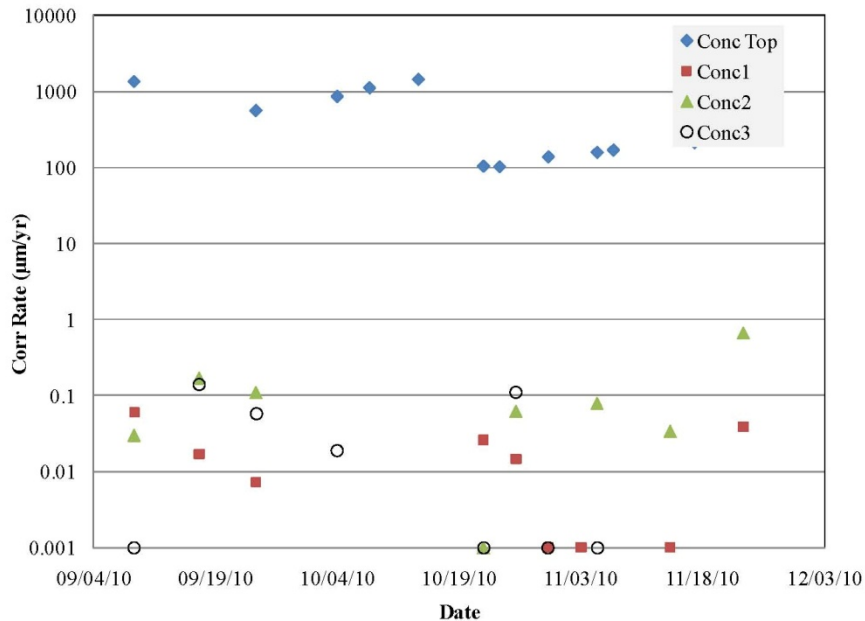
Figure 4-15. Uniform Corrosion Rates Versus Time Measured Using Linear Polarization Resistance With Probe Tips Embedded Two Inches Below the Concrete Surface (Conc1); Placed Along the Simulated Concrete Crack Near the Top of the Concrete Block (Conc2); Placed Along the Simulated Crack Near the Bottom of the Concrete Block (Conc3), or in the Reservoir Solution (Conc Top). The _B_ Values Used to Calculate the Corrosion Rates Were 485.5 mV for the Data From the Reservoir Solution and 26 mV for All Other Data. For Plotting Purposes, Corrosion Rates That Are Negative or Less Than 0.001 μm/yr Are Plotted As 0.001 μm/yr.

dependence with time is evident from Figure 4-15. The corrosion rates measured with the LPR probe immersed in the borated water reservoir were between 100 and 1,437 μm/yr [3.94×10^{-3} and 5.66×10^{-2} in/yr], consistent with the 2,400 ppm B solution data at 24 °C [75 °F] shown in Figure 4-12.

Coupled Multielectrode Array Sensor Data

Figure 4-16 shows the nonuniform corrosion rate data over a three-month period measured with the CMAS probes. The flow rates used and the corresponding pH of borated water exiting the simulated concrete block are tabulated in Table 4-6. Except for four short durations in the figure, the nonuniform corrosion rates were all less than 0.5 μm/yr [~1.97×10^{-5} in/yr], which is the lower detection limit of the CMAS unit. Even at a high flow rate of 65 mL/min (exit pH = 6.66), the corrosion rates measured with the CMAS probes were below 0.5 μm/yr [1.97×10^{-5} in/yr].

The four instances when high nonuniform corrosion rates were observed were (i) at the start of the test during which the flow rate was not well controlled and was higher than planned; (ii) when the flow was raised to a very high rate (1,100 mL/min) for about 20 minutes; (iii) toward the end of the experiment, when the solution reservoir was inadvertently drained; and (iv) at the termination of the test, when the concrete block was disassembled and the probes rinsed with
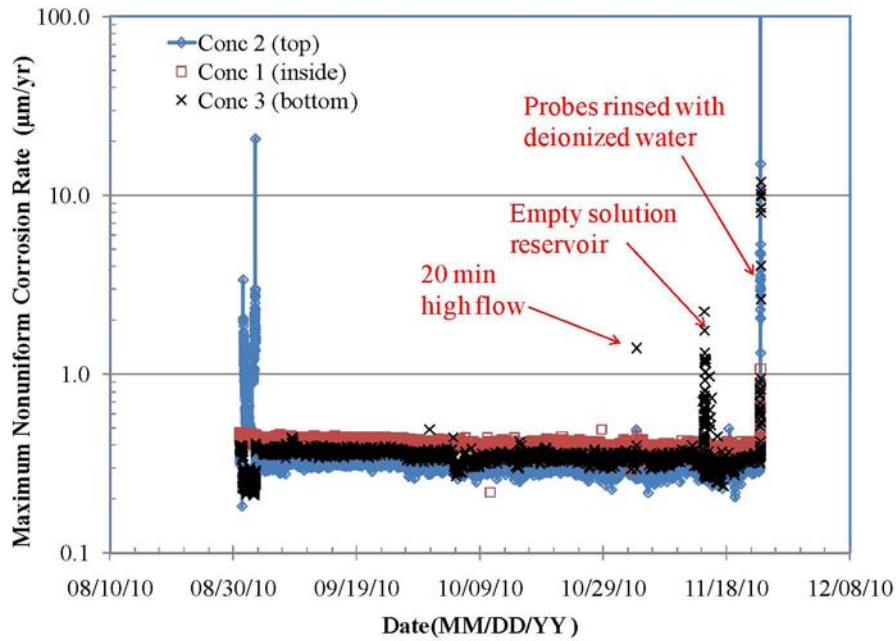
Figure 4-16. Nonuniform Corrosion Rates Versus Time Measured Using Coupled Multielectrode Array Sensor Probes (i) Embedded Two Inches From Concrete Surface (Conc 1), (ii) Placed Near the Top of the Concrete Block (Conc 2), or (iii) Placed Near the Bottom of the Concrete Block (Conc 3).

Table 4-6. Flow Rate and pH of Borated Water Exiting Concrete Block in Test Method 2*	
Flow Rate (mL/min)	**pH of Solution Exiting Concrete Block**
0.75†	8.2
1.90†	7.6
1.60†	7.52
1.33†	7.43
4.20†	7.36
4.10‡	7.32
8.90‡	7.25
18.7‡	6.97
17‡	6.93
65‡	6.66
1,100§	5.92
*Total duration of Test Method 2 test is 82 days †Solution flowed continuously ‡Solution flowed only during the day §Solution flowed only 20 min	

deionized water. Note that the sudden increase in corrosion rate observed at the end of the test is an indication that the probes responded well to changes in environment corrosivity.

The low corrosion rates measured at a high flow rate of 65 mL/min were surprising given that the solution pH at that flow rate was 6.66 (Table 4-6). The second supplementary test described in Section 4.1.2, in which a CMAS probe was immersed in solutions that exited the concrete block, gave corrosion rates (discussed in Section 4.2.3) that were less than 1 μm/yr [3.94 $\times$ 10^{-5} in/yr] when the solution pH was 7.32 or higher, but greater than 30 μm/yr [1.18 $\times$ 10^{-3} in/yr] when the solution pH was 6.96 or lower.

The simulated concrete crack test results suggested that flow channeling was occurring in the simulated crack such that low pH borated water was bypassing the CMAS and LPR probes. To mitigate the effect of flow channeling and allow a more effective contact between the corrosion probes and borated water, the concrete block assembly was disassembled and the experimental design was revised as described in Section 4.1.2.

Posttest Examination and Weight Loss Data

Figure 4-17 shows the disassembled blocks and the rebar coupon and corrosion probe locations on the concrete block surfaces. Close-ups of the CMAS and LPR probe tips (Figure 4-18) show no evidence of significant corrosion on any of the probes. Close-ups of the rebar coupons (Figure 4-19) show no evidence of corrosion on the coupons located near the top of the concrete block. Of the four coupons located near the bottom of the block, two were corroded and the other two showed no evidence of corrosion. These observations are consistent with flow channeling of the borated water inside the simulated concrete crack. The uniform corrosion rates calculated from the weight loss of the two corroded rebar coupons are 5.8 and 0.9 μm/yr [2.28 $\times$ 10^{-4} and 3.54 $\times$ 10^{-5} in/yr].

4.2.3   Test Method 2 Supplementary Test Data

Boric Acid Flowing Over Concrete Surface

As discussed in Section 4.1.2, a supplementary test, shown in Figure 4-20, was conducted in which borated (2,400 ppm B) water was dripped onto the top surface of an inclined concrete block at a drip rate of ~20 mL/min. The short-term data on nonuniform corrosion rates versus time are shown in Figures 4-21 and 4-22. The corrosion rates measured with the upper CMAS probe were higher than those measured with the lower CMAS probe because the solution contacting the former had lower pH than that contacting the latter. Qualitatively, the data indicate that short-term (<3 days) corrosion rates are significant (~10 μm/yr or higher) [~3.94 $\times$ 10^{-4} in/yr or higher] when the solution pH is ~6.8 or lower, whereas the rates are very low (1 μm/yr or lower) [3.94 $\times$ 10^{-5} in/yr or lower] when the solution pH is higher than ~6.8.

Boric Acid Solution Exiting Concrete Block

In the second supplementary test described in Section 4.1.2, a CMAS probe was immersed in solutions that exited the concrete block. Figures 4-23 and 24 show the measured nonuniform corrosion rates versus time. The steady state nonuniform corrosion rates were than less than 0.5 μm/yr [~1.97 $\times$ 10^{-5} in/yr] when the solution pH was 7.32 or higher, but greater than 30 μm/yr [~1.18 $\times$ 10^{-3} in/yr]when the solution pH was 6.96 or lower.

(a)
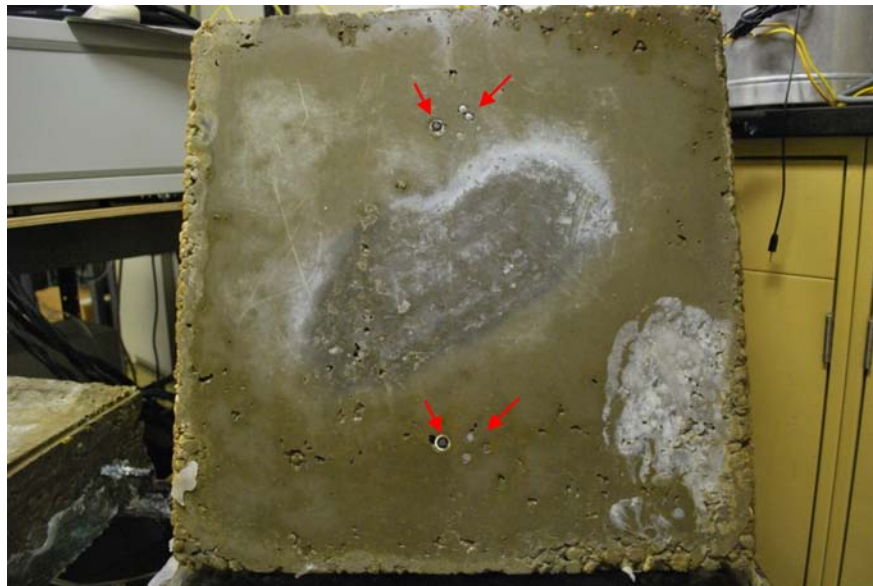
(b)

Figure 4-17. (a) Concrete Block With Rebar Coupons After Disassembly. Left and Right Sides Correspond to Upper and Lower Sections of Concrete Block Assembly. (b) Concrete Block with Coupled Multielectrode Array Sensor and Linear Polarization Resistance Probes (Indicated by Arrows) Near the Upper Section (Top) and Lower Section (Bottom) of the Block.
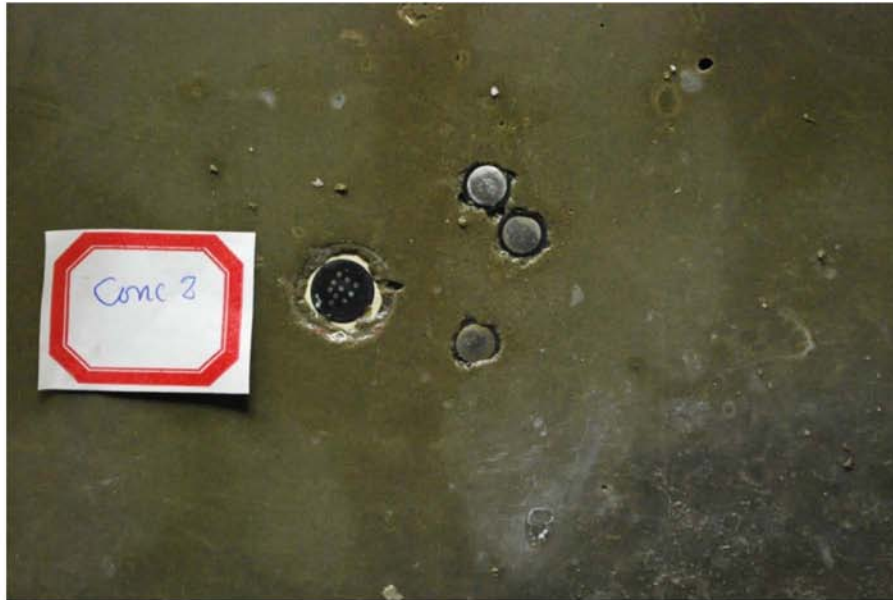
(a)

(b)

Figure 4-18. (a) Upper and (b) Lower Coupled Multielectrode Array Sensor and Linear Polarization Resistance Probes. All Probes Showed No Evidence of Significant Corrosion, Which is Consistent With Real-Time Corrosion Rate Measurements That Indicated Corrosion Rates Less Than 0.5 µm/yr During Most of the Exposure Period.

(a)

(b)

Figure 4-19. (a) Rebar Coupons Near the Top of the Disassembled Concrete Block. The Coupons Show No Evidence of Corrosion. (b) Rebar Coupons Near the Bottom of Disassembled Concrete Block. Two of the Coupons Are More Corroded Than the Other Two, Likely Due to Flow Channeling of Borated Water.
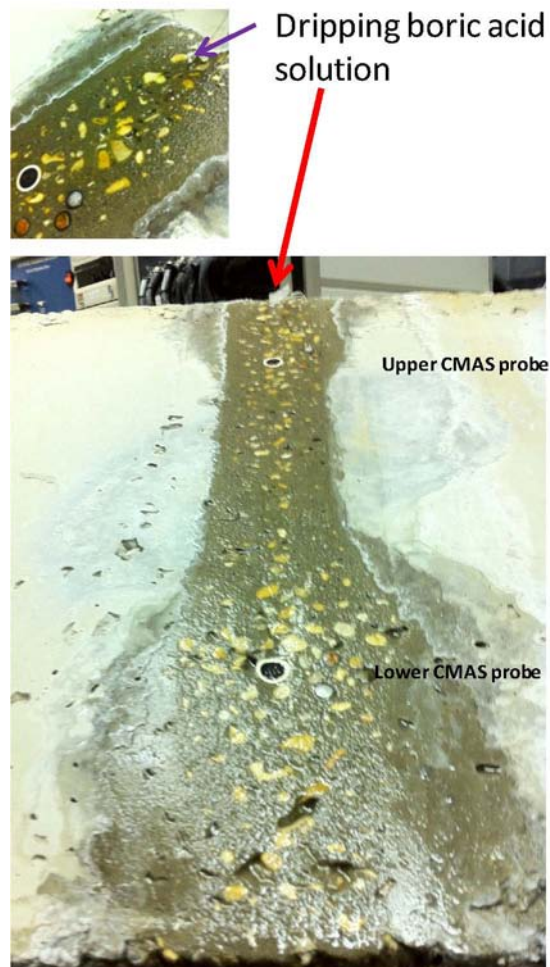
Figure 4-20. The Revised Experimental Procedure Dripped Borated (2,400 ppm B) Water (~20 mL/min) Onto the Top of an Inclined Concrete Block and Measured Nonuniform Corrosion Rates Using Two Coupled Multielectrode Array Sensor (CMAS) Probes. The pH of the Solution Flowing Adjacent to the CMAS Probes Was Measured Using a Microflow pH Electrode.

Boric Acid Solutions Mixed with Simulated Cement Pore Solution

The data for the third supplementary test are shown in Figure 4-25. The data indicate that the steady state nonuniform corrosion (measured after 72-hour immersion) is insignificant (<1 µm/yr) [<3.94 × 10^{-5} in/yr] or nearly so when the pH was 6.8 or higher, whereas at lower pH the corrosion rate was as high as ~300 µm/yr [~1.18 × 10^{-2} in/yr]. Data measured over a two-month period in pH 6.0 and 6.5 solutions, which are shown in Figure 4-26, indicate that the overall nonuniform corrosion rate decreased over time. However, in contrast to solutions with pH higher than 6.8, the nonuniform corrosion rates in pH 6 and 6.5 solutions mostly remained in the 3 and 60 µm/yr [1.18 × 10^{-4} and 2.36 × 10^{-3} in/yr] range, which indicate that the carbon steel in those solutions was not fully passivated even after a 2-month period of immersion in the solutions.
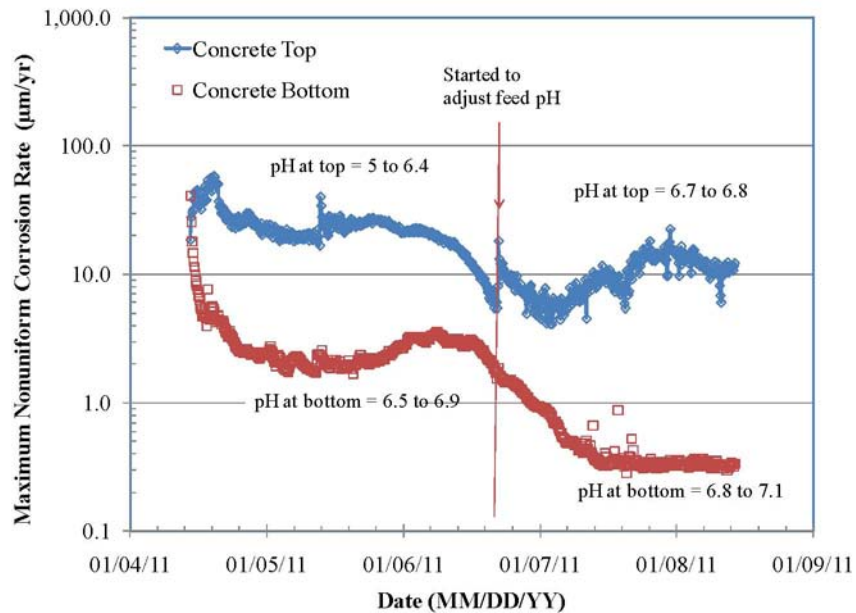
Figure 4-21. Nonuniform Corrosion Rates Versus Time Measured Using a Coupled Multielectrode Array Sensor (CMAS) Probe Near the Top (Diamond Symbols) or Near the Bottom of an Inclined Concrete Block (Square Symbols). The Ranges in Measured pH of Borated Water Flowing Adjacent to the CMAS Probes Also Are Indicated. The Vertical Line Indicates the Time When the Feed Solution pH Was Adjusted Higher By Addition of Simulated Cement Pore Solution to the Boric Acid Solution.
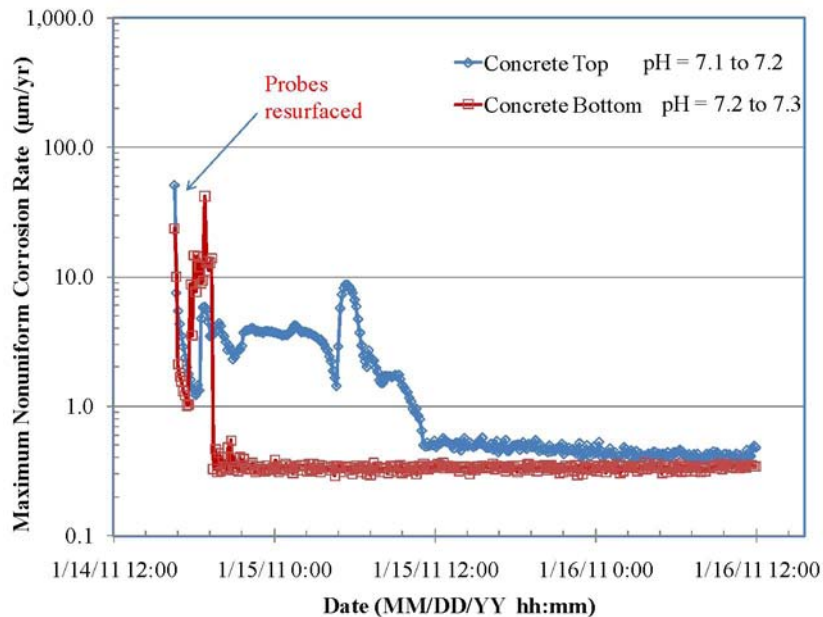
Figure 4-22. Nonuniform Corrosion Rates Versus Time Measured Using a Coupled Multielectrode Array Sensor (CMAS) Probe Near the Top (Diamond Symbols) or Near the Bottom of an Inclined Concrete Block (Square Symbols). The Ranges in Measured pH of Borated Water Flowing Adjacent to the CMAS Probes Also Are Indicated.

4-26
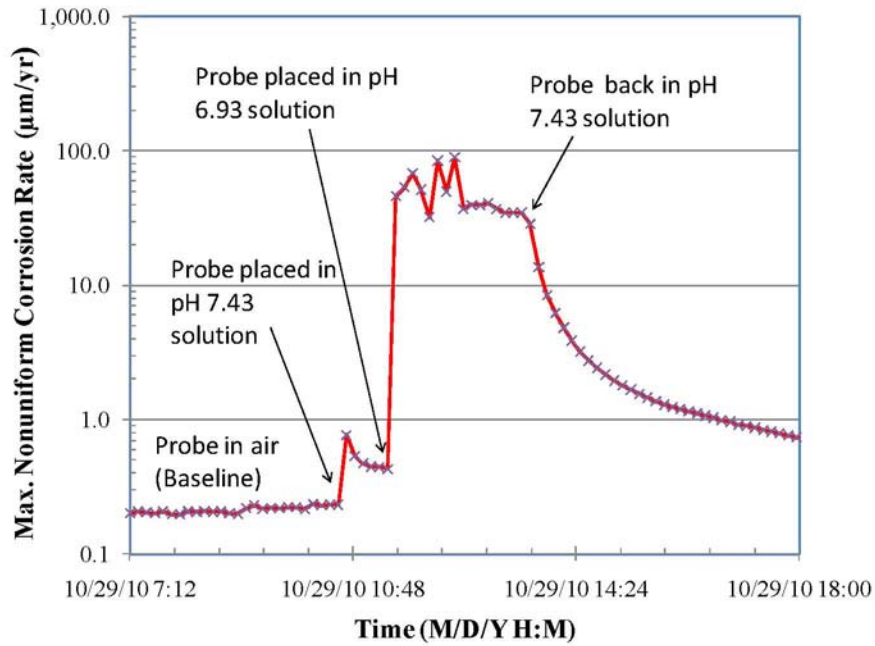
Figure 4-23. Nonuniform Corrosion Rate Measured Using a Coupled Multielectrode Array Sensor Probe Immersed in a Solution That Was Collected Exiting the Concrete Block
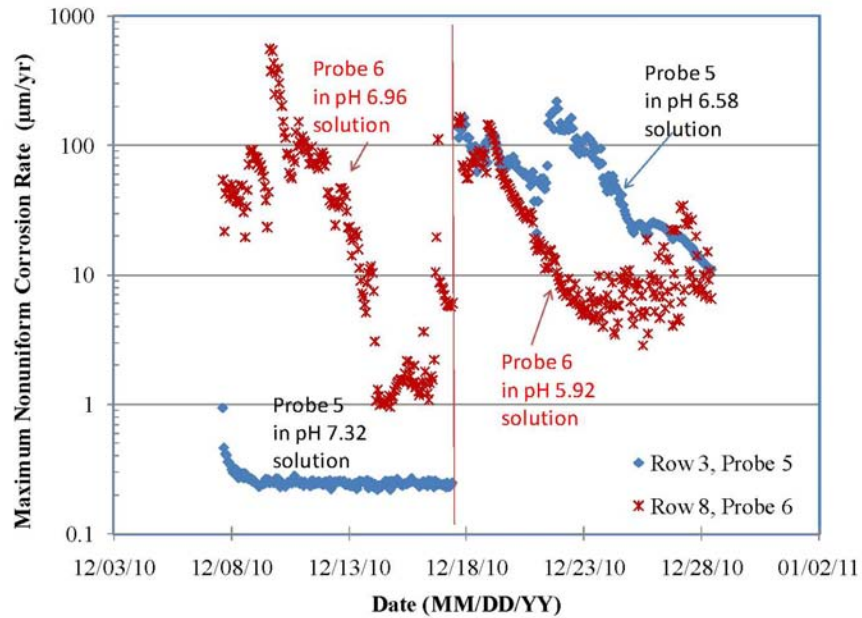
Figure 4-24. Nonuniform Corrosion Rates Versus Time Measured Using a Coupled Multielectrode Array Sensor Probe Immersed in Several Batches of Borated Water Collected Exiting the Concrete Block
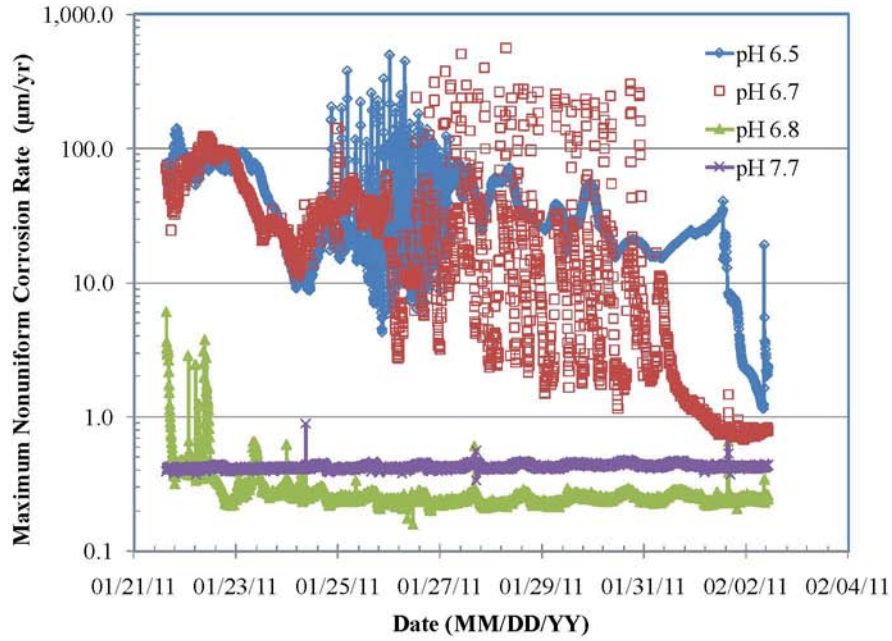
(a)
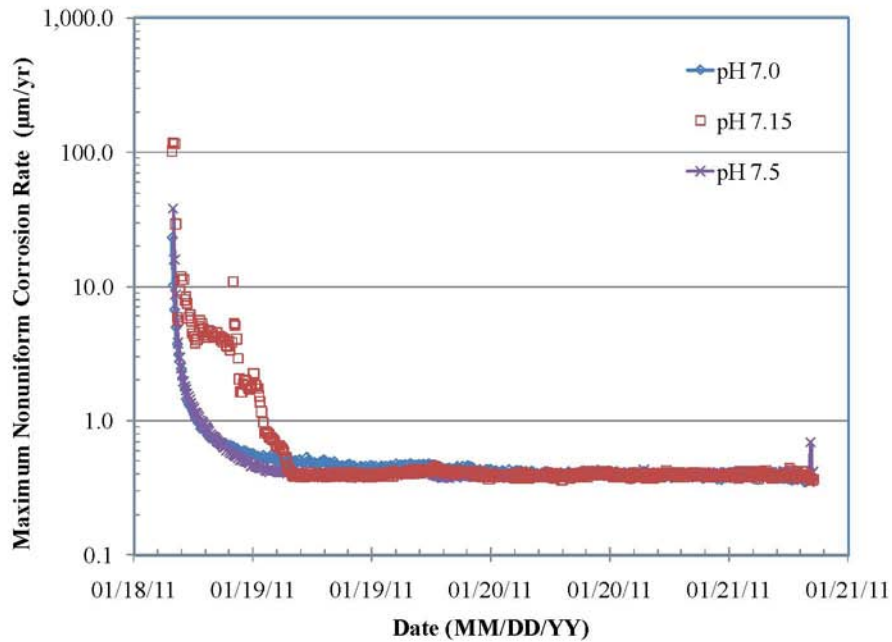
(b)

Figure 4-25. Nonuniform Corrosion Rates Versus Time Measured Using a Coupled Multielectrode Array Sensor Probe Immersed in Borated (2,400 ppm B) Water With pH Adjusted by Adding Simulated Cement Pore Solution
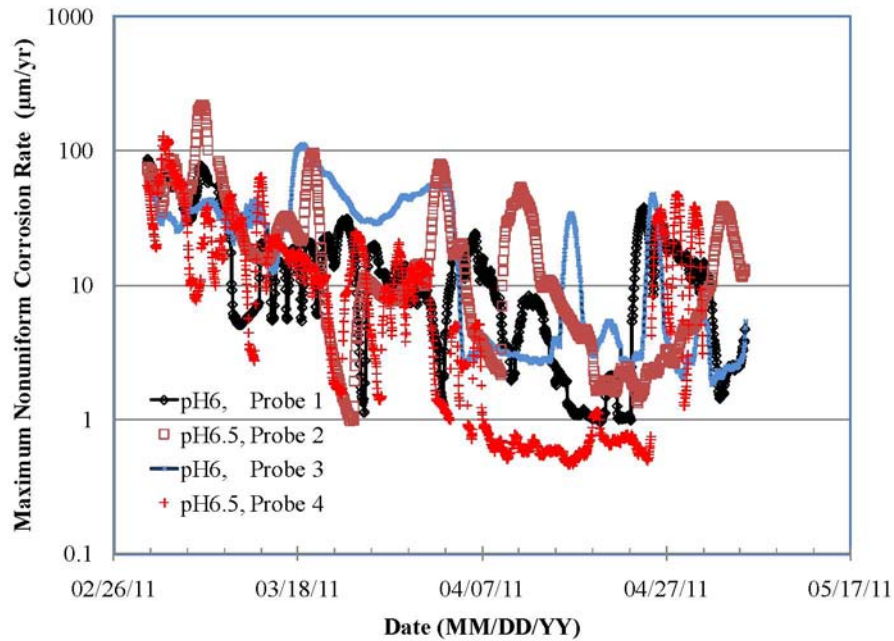
Figure 4-26. Moving Average of Long-Term Nonuniform Corrosion Rates Versus Time Measured Using Coupled Multielectrode Array Sensor Probes Immersed in Borated (2,400 ppm B) Water With pH Adjusted to 6.0 or 6.5 by Adding Simulated Cement Pore Solution

Threshold pH for Rebar Corrosion

Figure 4-27 plots corrosion rate data versus pH measured with CMAS probes either (i) in contact with borated water flowing over an inclined concrete surface, (ii) immersed in borated water that was collected exiting the simulated concrete crack, or (iii) immersed in borated water mixed with simulated cement pore solution. The data in Figure 4-27 were obtained from the nonuniform corrosion rates versus time plots discussed in preceding paragraphs. For better data comparison, the corrosion rates shown in Figure 4-27 are the measured values ~24 hours after the freshly polished probes were contacted with or immersed in the solution. Thus, the data represent short-term corrosion rates. Although some differences are evident in the corrosion rates measured from the three tests, the general trend is the same. The corrosion rate is low (~1 µm/yr or less) [~3.94 × 10^{-5} in/yr or less] when the solution pH is ~7.1 or higher. Below pH ~7.1, the corrosion rate increases with decreasing pH and can reach ~100 µm/yr [~3.94 × 10^{-3} in/yr] in solutions with pH less than ~6.7. The threshold pH for carbon steel corrosion in borated solution is between 6.8 and 7.3.
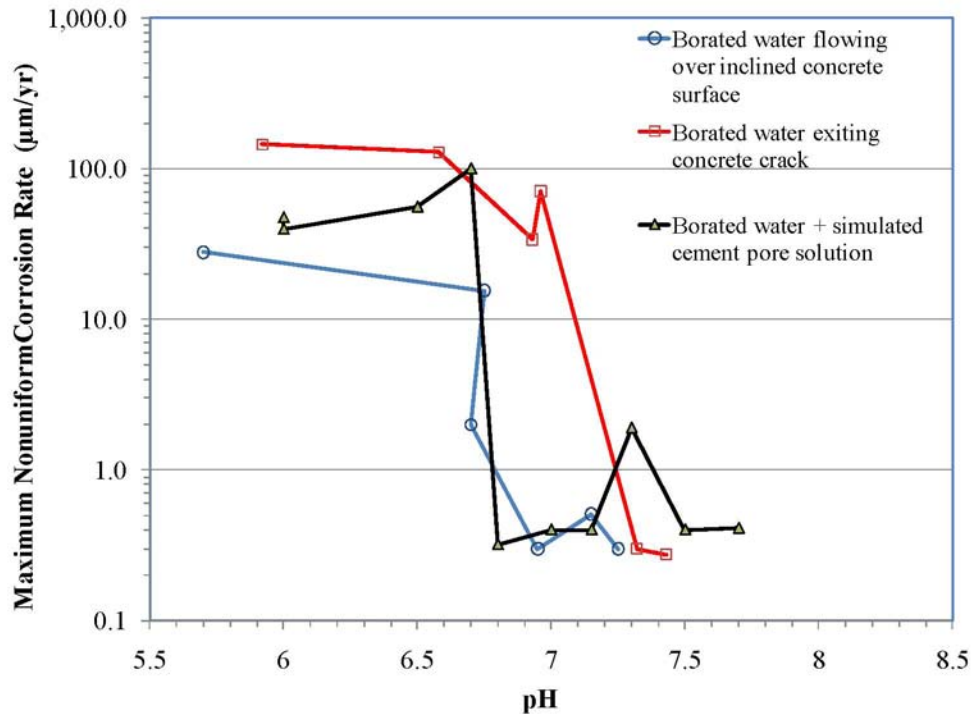
Figure 4-27. Summary of Nonuniform Corrosion Rate Data Measured Using Coupled Multielectrode Array Sensor Probes (i) Contacting Borated (2,400 ppm B) Water Flowing Over Inclined Concrete Surface, (ii) Immersed in Borated (2,400 ppm B) Water Exiting Simulated Concrete Crack, and (iii) Immersed in Borated (2,400 ppm B) Water Mixed with Simulated Cement Pore Solution. The Plotted Data Are the Rates Measured ~24 hours After Test Initiation Using Freshly Polished Probe Surfaces.

4.2.4 Summary of Measured Corrosion Rates and Comparison With Literature Data

A summary of corrosion rates measured in this study using LPR and CMAS probes are plotted in Figure 4-28. The data indicate that corrosion rates generally increase with temperature and boric acid concentration. For comparison, literature data from an Electric Power Research Institute (EPRI) report (EPRI, 2001) on carbon steel corrosion rate in borated water also are plotted in the figure. Because no attempt was made in this study to exclude atmospheric oxygen from the boric acid solutions, only literature corrosion rates measured in aerated borated water are included in Figure 4-28. The literature data agree well with corrosion rates determined in this study.

Note that corrosion rates in aerated systems are higher than in deaerated systems. Literature data EPRI compiled show that corrosion rates for carbon and low-alloy steels in borated solutions are less than 25 μm/yr [.001 in/yr] for conditions where the oxygen concentration is very low throughout the test duration and in the range 150 to 430 μm/yr [0.006 to 0.017 in/yr] for cases where oxygen is present at the start of the test but no new oxygen is added during testing.
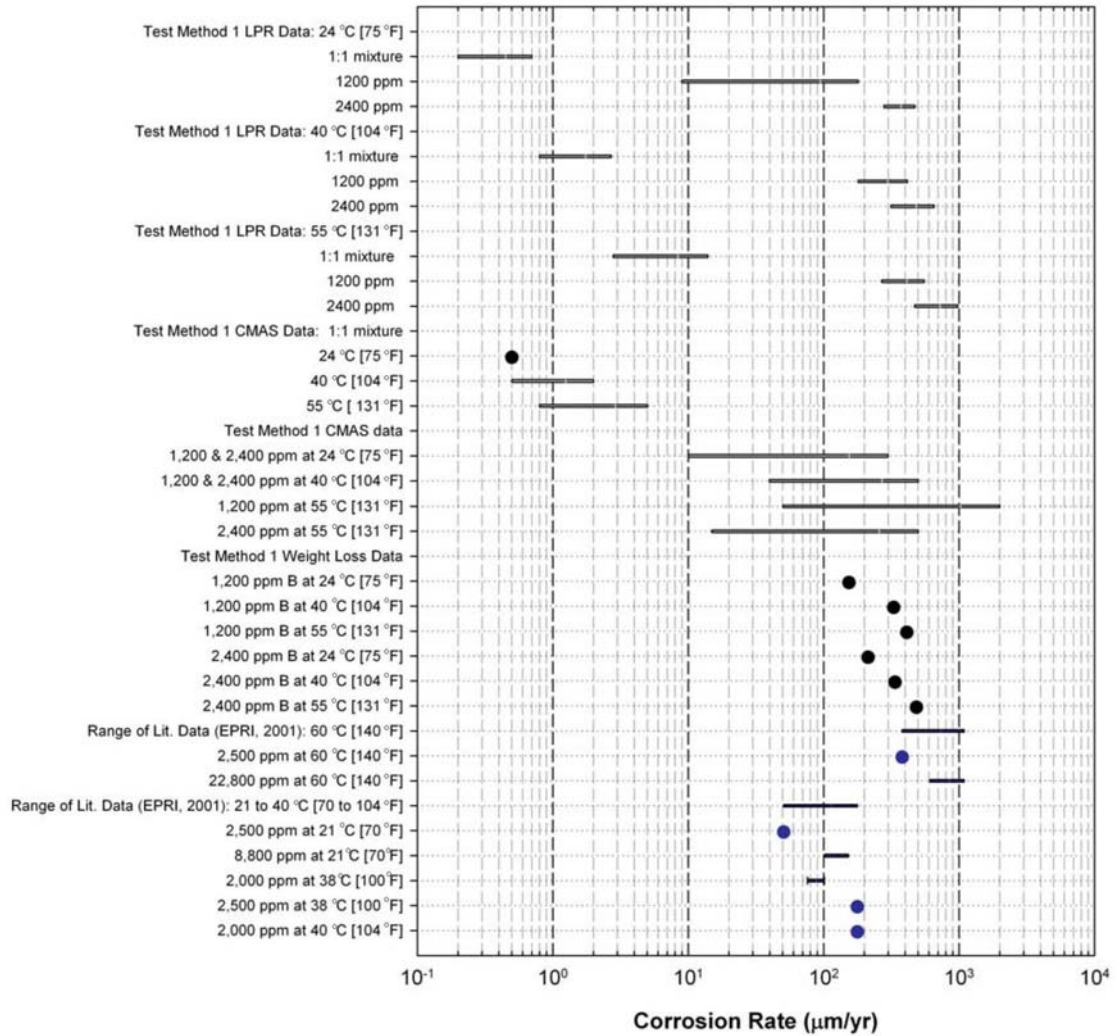
Figure 4-28. Summary of Corrosion Rate Data From This Study. Corrosion Rates in Deaerated Borated Waters Taken From EPRI (2001) Also Are Shown for Comparison.

4.2.5 Test Method 3—Petrographic Analyses and Compressive Strength Testing of Concrete Reacted With Borated Water

Petrographic Analysis

The petrographic examination of concrete cylinders that were immersed in boric acid solutions for 180, 240, and 300 days was conducted by Concrete Research & Testing, LLC (CRT). The results of the CRT examination are summarized in this section. The CRT reports are included in the appendix of this report.

Photographs of some of the concrete cylinders that were immersed in borated water are shown in Figure 4-29. Petrographic examination of the concrete cylinders indicated that the cement paste affected by boric acid leaching is very soft, highly porous, and retains very little inherent
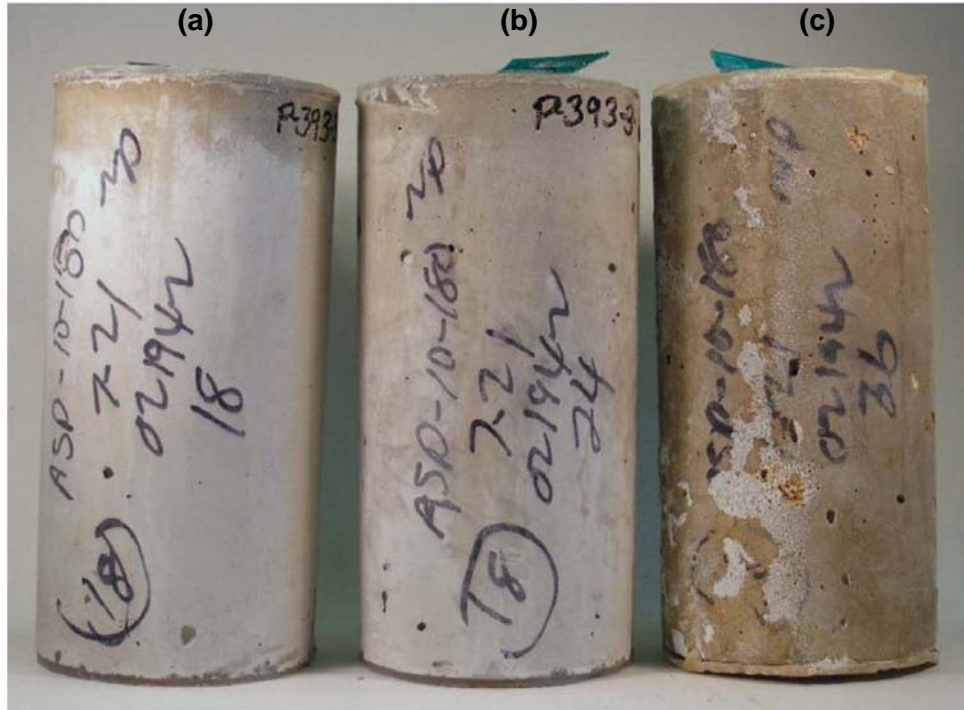
Figures 4-29. Photograph of Concrete Cylinders That Had Been Immersed for 300 Days in (a) 1,200 ppm B Solution at Room Temperature, (b) 2,400 ppm B Solution at Room Temperature, and (c) 2,400 ppm B Solution at 60 °C [140 °F]

strength. The affected paste exhibits a color change from grey to white in some specimens or to yellowish in others. Cross section photomicrographs showing the attacked cement paste are presented in Figure 4-30. Areas of the affected cement paste layer were occasionally lost from the lapped surface during specimen preparation. The depth affected by boric acid leaching for each cylinder specimen is tabulated in Table 4-7 and plotted in Figure 4-31. The results indicate that the affected depths increased with time, solution concentration, and temperature.

In specimens exposed to 1,200 and 2,400 ppm B solutions at room temperature, there is a distinct transition from the weak, porous, affected cement paste to the dense, unaffected cement paste. This transition is less defined in specimens exposed to 2,400 ppm B solution at 60 °C [140 °F]. Also, in some specimens, the severely affected cement paste is underlain by a dark colored, competent cement paste layer, below which is a thin white layer of weak cement paste (Figure 4-32a). Phenolphthalein solution testing showed that the acid attack has affected the cement paste to the depth of the thin, white layer of weakened cement paste (Figure 4-32b).

Voids present on the exterior surface of some specimens are lined with boric acid crystals. Boric acid crystals also were observed in near-surface voids of specimen cross sections. Photomicrographs of the boric acid crystals are shown in Figure 4-33.

Boric Acid Leaching Depth

The rate of boric acid leaching, as with other concrete degradation mechanisms, depends in part on the rate of diffusive transport. A previous EPRI study (Simons, et al., 2009) measured the degradation depth of concrete specimens that were immersed in 2,400 ppm B solutions at

Epoxy layer

(a)

¼ mm

(b)

½ mm

(c)

½ mm
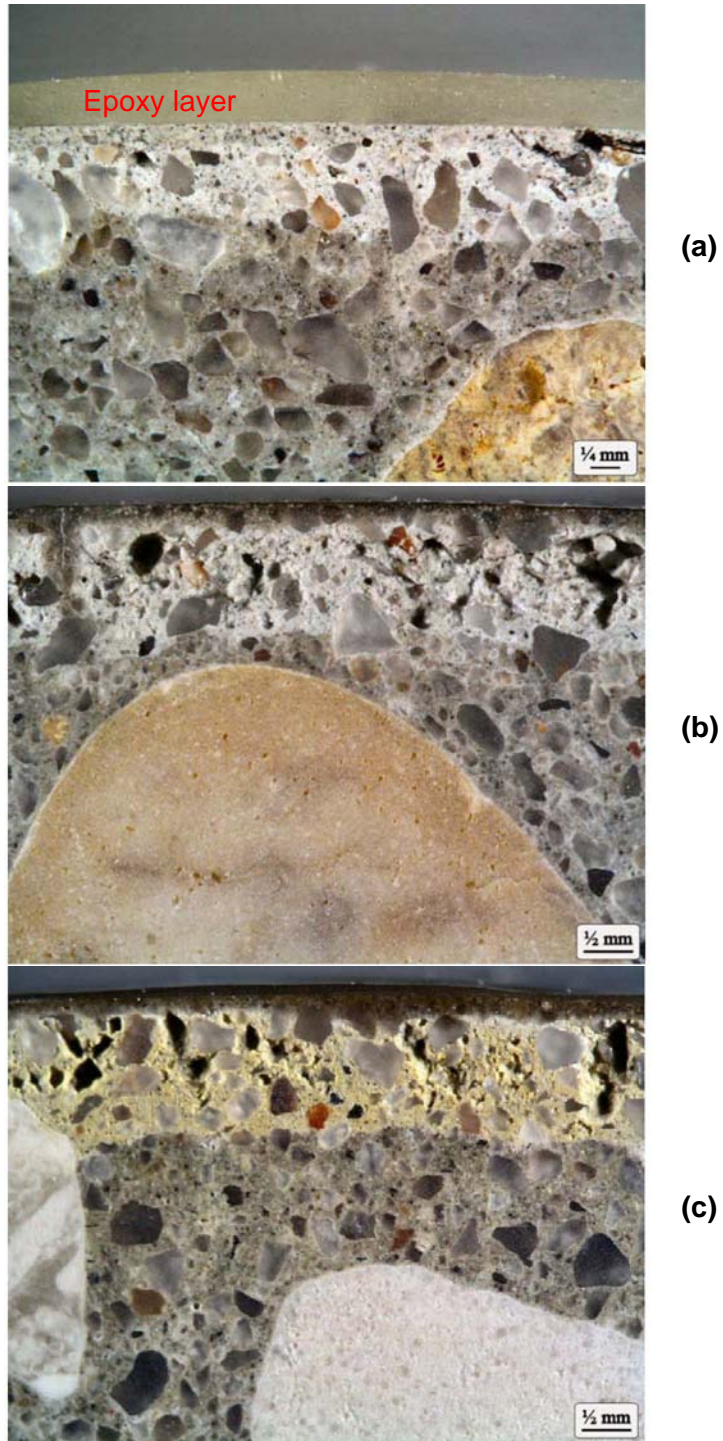
Figure 4-30. Cross Section Photomicrographs of Concrete Specimens That Had Been Immersed in a 1,200 ppm B Solution for (a) 180, (b) 240, and (c) 300 Days. The Epoxy Can Be Seen to Have Penetrated the Cement Paste in (b) and (c).

Table 4-7. Depth of Affected Cement Paste in Test Method 3 Concrete Cylinders Immersed in Boric Acid Solutions

Boric Acid Concentration/ Temperature	Immersion Time		
	180 days	**240 days**	**300 days**
1,200 ppm B/Room Temperature	0.5 to 1.1 mm* (Ave. = 0.75 mm)†	1.0 to 1.5 mm (Ave. = 1.31 mm)	1.4 to 1.8 (Ave. = 1.61 mm)
2,400 ppm B/Room Temperature	0.6 to 1.2 mm (Ave. = 0.85 mm)	1.2 to 1.7 mm (Ave. = 1.42 mm)	1.4 to 1.8 (Ave. = 1.60 mm)
2,400 ppm B/60 °C [140 °F]	0.8 to 2.6 mm (Ave. = 1.27 mm)	2.0 to 2.6 mm (Ave. = 2.17 mm)	2.2 to 4.2 (Ave. = 2.93 mm)
*1 mm = 0.0394 in †Average of 20 measurements			
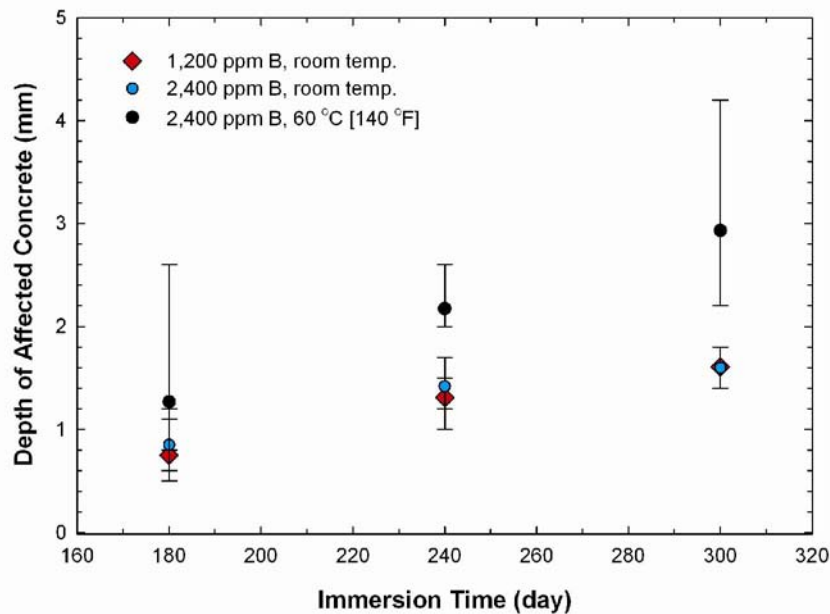
Figure 4-31. Depth of Concrete Specimens Affected by Boric Acid Leaching. Symbols Represent the Average of 20 Measurements. The Error Bars Indicate the Range of Measured Values [1 mm = 0.0394 in]

room temperature for 1, 2, 3, 6, 9, and 39 months. The EPRI data indicated that the degradation depth varied with the square root of time. The EPRI data were best fit by the following diffusion equation:

$$D = kt^{1/2} \tag{4-1}$$

where D is degradation depth (mm), t is time (day), and k equals 0.206248 mm/day$^{1/2}$ [0.008120 in/day$^{1/2}$]. Figure 4-34 shows a plot of Eq. (4-1). Also plotted in the figure are the degradation depths measured in this study and the best-fit lines to those data. Figure 4-34 shows that the boric acid leaching rate determined in the EPRI study is significantly higher than the rates measured in the present study. Because both studies used 2,400 ppm B solutions in the tests, the difference in measured rates is likely due to the different concrete specimen properties.
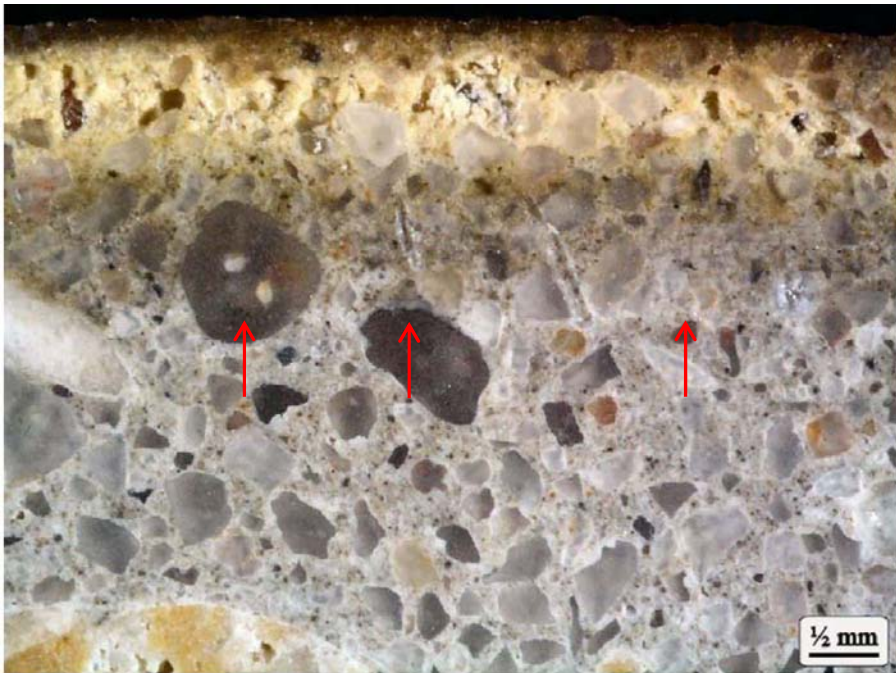
(a)

(b)

Figure 4-32. (a) Cross Section Photomicrographs Showing the Thin Line of Weak Cement Paste (Arrows) Present in Otherwise Unaffected Cement Paste of the Concrete Specimen That Had Been Immersed in a 2,400 ppm B Solution at 60 °C [140 °F] for 240 Days. (b) Photomicrograph of the Same Specimen Following Exposure to Phenolphthalein Solution. The Depth to Which the pH Had Been Lowered by Acid Exposure Is Represented by the Uncolored Cement Paste.
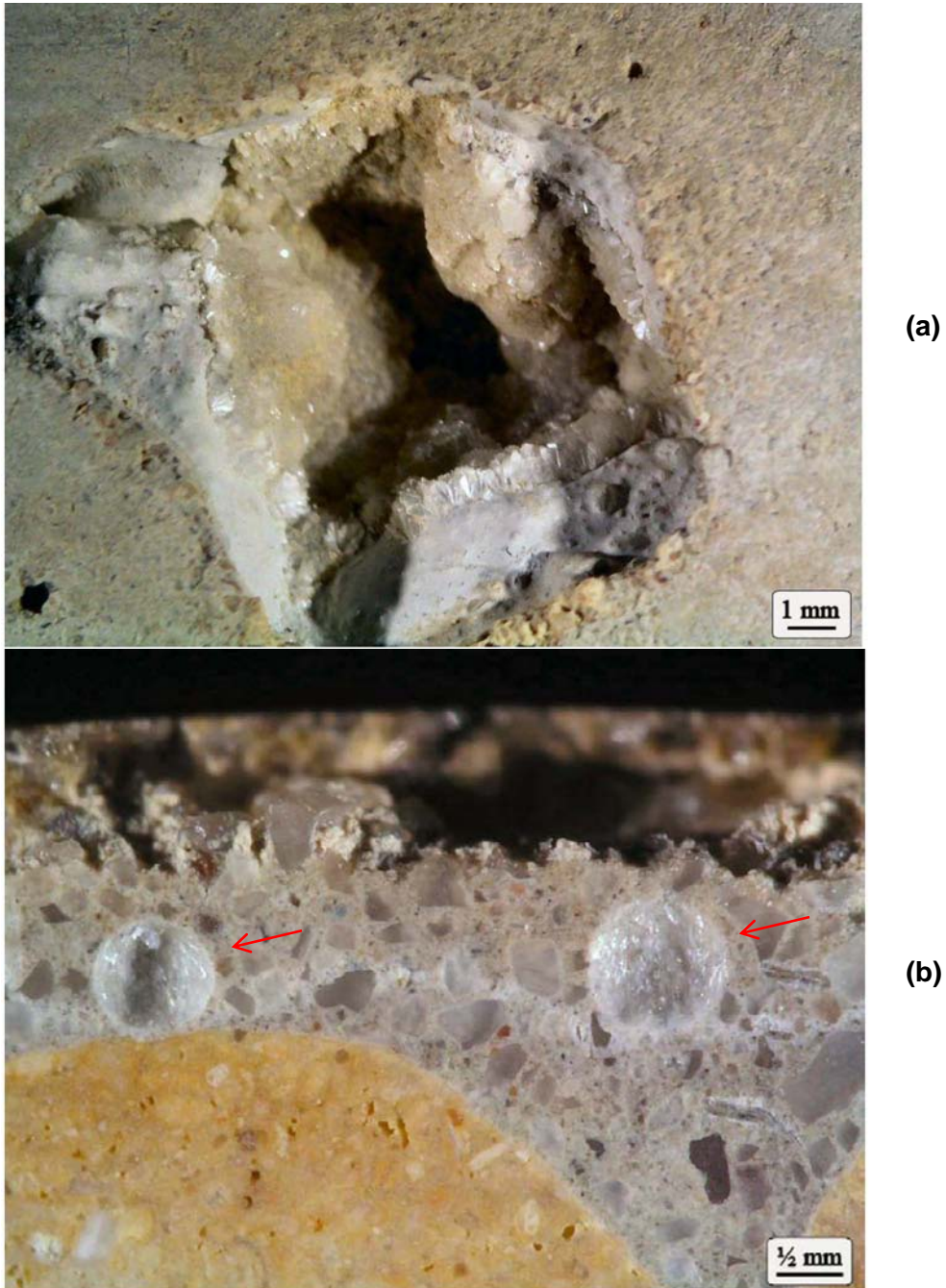
Figure 4-33. Cross Section Photomicrographs Showing the Boric Acid Crystals Present (a) Within a Surface Void or (b) in Near-Surface Voids of a Concrete Specimen That Had Been Immersed in a 2,400 ppm B Solution for 180 Days
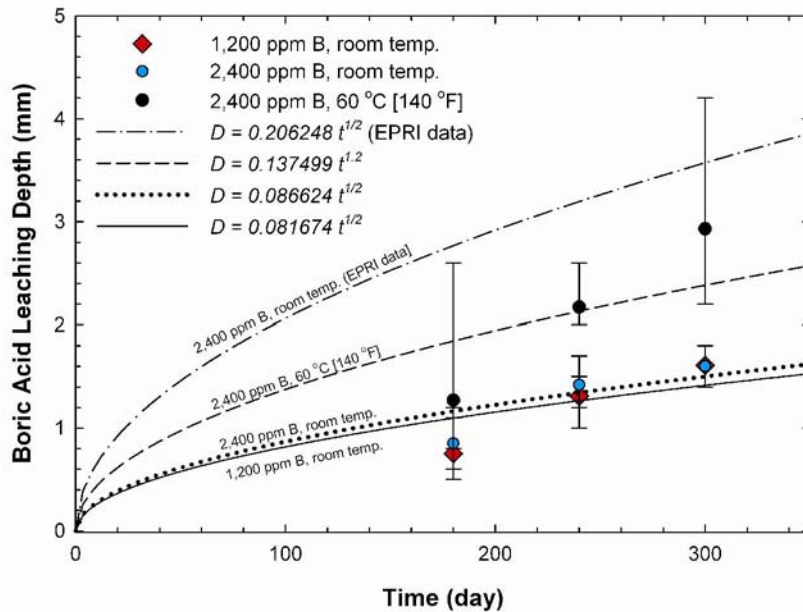
Figure 4-34. Depth of Boric Acid Leaching Calculated Using Diffusion Equations Fit to Experimental Data Shown in Figure 4-31. The Top Curve Shows Calculated Values Using an Equation Fit to EPRI Data (Simons, et al., 2009) [1 mm = 0.0394 in].

Simons, et al. (2009) used Eq. (4-1) to extrapolate the concrete degradation depth to future years. They calculated that the depth of boric acid attack after 70 years of exposure is 33 mm [1.3 in]. Figure 4-35 is a plot of the boric acid degradation depth projected to 100 years using the diffusion equations that were fit to the EPRI data and to data from this study.

Compressive Strength Data

The compressive strengths of concrete cylinders that were immersed in boric acid (1,200 and 2,400 ppm B) solutions for 300 days are listed in Table 4-8. The data show that for concrete cylinders that were immersed at room temperature, the compressive strength of cylinders that were reacted with 2,400 ppm B solution is higher than for those that were reacted with 1,200 ppm B solution. The observed higher compressive strength of samples that were immersed in a higher boric acid concentration is consistent with literature data from Bajza, et al. (2002). As illustrated in Figure 2-5, Bajza, et al. (2002) measured higher compressive strength on samples that were immersed in 25 wt% boric acid solution compared to those that were immersed in 1.2 wt% boric acid solution. The data in Table 4-8 indicate that higher temperature has a significant effect on compressive strength. The compressive strength of concrete cylinders that were immersed in 2,400 ppm B solution at 60 °C [140 °F] is much lower than those of cylinders that were immersed in 2,400 ppm B solution at room temperature.
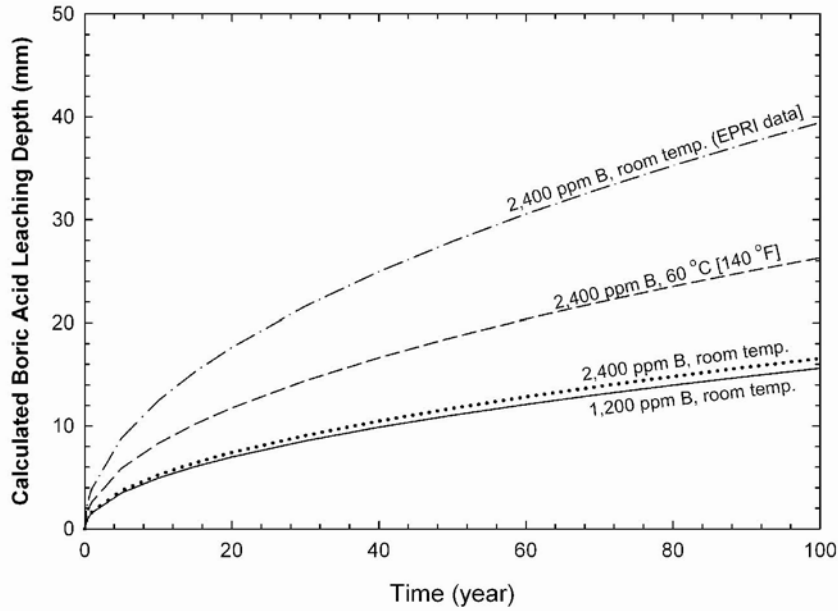
Figure 4-35. Depth of Concrete Leached by Boric Acid Solution As a Function of Time Calculated Using the Diffusion Equations Indicated in Figure 4-34 [1 mm = 0.0394 in]

Table 4-8. Compressive Strength of Test Method 3 Concrete Cylinders Immersed for 300 Days in Boric Acid Solutions or in Tap Water. Also Shown Are Data for Control Samples.*	
Solution Composition/Temperature	**Compressive Strength (psi)†**
1,200 ppm B / Room Temperature	7,970 ± 98
2,400 ppm B / Room Temperature	8,553 ± 38
2,400 ppm B / 60 °C [140 °F]	5,357 ± 102
Tap Water	6,643 ± 163
	8,640 ± 190‡
Control Sample	5,973 ± 35
*Control samples were kept in a controlled temperature–relative humidity chamber.	
†Average and standard deviation of measurements on three samples.	
‡Average and standard deviation of measurements on three additional samples. These samples were tested using the same equipment about two weeks after the first set of samples.	

Also listed in Table 4-8 are compressive strengths of concrete cylinders that were immersed in tap water for 300 days and cylinders that were kept in a controlled temperature–relative humidity chamber for the same period. Both sets of samples gave unexpectedly low values. In particular, the control samples had compressive strengths much below the expected trend based on measurements on control samples at 28, 90, and 120 days (Figure 4-36). The unexpectedly low values cannot be explained. The calibration of the compressive strength test equipment was verified to be current. The compressive strengths of a second set of concrete cylinders that were immersed in tap water for the same period (300 days) were measured. These gave more reasonable values—significantly higher than the first set of samples. Because of the unexpected results for the control and tap water samples, there is uncertainty in the measured compressive strengths of the concrete cylinders that were immersed in boric acid solutions.
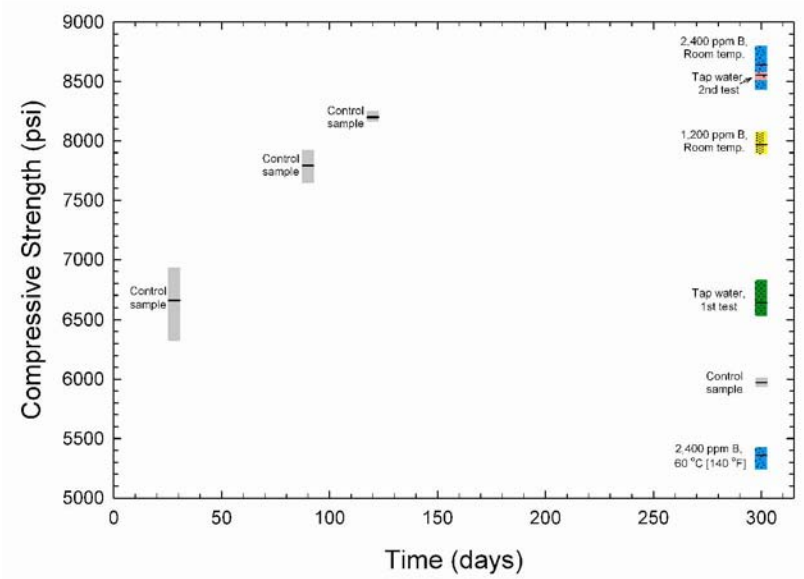
Figure 4-36. Compressive Strength of Concrete Cylinders That Were Immersed for 300 Days in Boric Acid Solutions or in Tap Water.   Also Shown Are Compressive Strength Versus Time of Concrete Cylinders That Were Kept in a Controlled Temperature–Relative Humidity Chamber.

5 REACTIVE TRANSPORT MODELING OF BORIC ACID LEACHING OF CONCRETE

Experimental data presented in the preceding sections indicate that pH is a critical parameter that determines the corrosion susceptibility of rebar in borated water and the degree of concrete degradation by boric acid leaching. Borated water that leaks through the spent fuel pool (SFP) liner initially will be acidic, but as it diffuses into the concrete pores or flows through the concrete joints or cracks, it will react chemically with the cement matrix—possibly also with the concrete aggregate—and the solution pH will increase. Higher pH will decrease the susceptibility of rebar to corrosion and of concrete to leaching. If borated water pH was known at different points along the flow path, an assessment could be performed on the susceptibility to degradation of rebar and concrete at different locations in the SFP concrete structure. However, it is impractical to measure the pH of borated water in the joints or cracks of SFP concrete structures. Although core samples in the vicinity of the construction joint may be taken and the concrete and rebar examined for signs of degradation, as PSEG Nuclear, LLC plans for the Salem Nuclear Generating Station SFP (Davison, 2011), such examination will provide very limited data. Information will not be available on locations that are not sampled, and no data will be available on the time dependence of the concrete and rebar degradation.

To provide information on the pH of borated waters and the degree of concrete degradation at different locations of an SFP concrete structure, reactive transport modeling of concrete leaching by borated water can be performed. Reactive transport models (e.g., Lichtner, et al., 1996; Samson and Marchand, 2007) combine chemical reactions, such as dissolution and precipitation, with hydrodynamic processes, such as water flow, diffusion, and dispersion. These models can account for changes in porosity, permeability, and flow properties of the porous medium due to dissolution and precipitation reactions. Using such models, the boric acid solution pH and concentration as well as the concrete mineralogy can be calculated as a function of time and distance from an SFP leak source. The pH can be correlated to the corrosion susceptibility of rebar that may be located at different locations along the flow path. The changes in concrete mineralogy and porosity as a function of distance and time can indicate the degree of concrete degradation due to leaching.

In this study, reactive transport modeling of boric acid leaching of concrete was conducted using the reactive transport codes X1t and X2t. The X1t and X2t codes are part of the Geochemist's Workbench (GWB) suite of software for simulating groundwater transport and chemical reactions in geochemical systems (Bethke, 2008). X1t can model reactive transport in one linear or radial dimension, whereas X2t can model reactive transport in two dimensions. X1t was used to simulate the chemical reaction of boric acid diffusing into concrete, whereas X2t was used to simulate the interaction between concrete and boric acid solution flowing in a concrete crack.

5.1   Model Assumptions and Parameters

5.1.1   Concrete Mineralogy and Hydraulic Properties

The mineral phases and their relative amounts assumed to be present in the concrete are listed in Table 5-1. The values listed in the table are based on the study by Wang (2009), who used the GWB software to calculate the mineralogy resulting from hydration of Portland cement. Calcium-silicate-hydrate (CSH) is the most dominant cement mineral, followed by portlandite, ettringite, hydrogarnet, and hydrotalcite. Iron oxide was represented by the mineral hematite.

Table 5-1. Solid Phases in 1 m^3 [35.3 ft^3] of Concrete*	
Solids	**Volume %**
Aggregate†	72
Calcium-silicate-hydrate (CSH$_{1.8}$)‡	8.3
Portlandite [Ca(OH)$_2$]	4.7
Ettringite [Ca$_6$Al$_2$(SO$_4$)$_3$(OH)$_{12}$·26H$_2$O]	3.2
Hydrogarnet [Ca$_3$Al$_2$(OH)$_{12}$]	1.67
Hydrotalcite [Mg$_4$Al$_2$(OH)$_{14}$·3H$_2$O]	0.46
Hematite [Fe$_2$O$_3$]	0.33
*Based on Wang, L. "Near-Field Chemistry of a HLW/SF Repository in Boom Clay—Scoping Calculations Relevant to the Supercontainer Design." SCK•CEN–ER–17. Mol, Belgium: SCK•CEN. 2009. Also based on Wang (2009), the concrete pore water was assumed to have dissolved Na and K concentrations of 0.14 and 0.37 molal, respectively, which was necessary to make the initial concrete pore water pH > 13 due to charge balance by OH$^-$ ions. †Wang's (2009) concrete model used calcite aggregate. In this study, aggregate was represented by rutile (TiO$_2$), which is relatively insoluble. ‡Calcium–silicate–hydrate (CSH) in hydrated cement has a variable Ca/Si ratio, which decreases as leaching (decalcification) proceeds. The CSH initially present in the concrete was assumed to be CSH$_{1.8}$ [Ca$_{1.8}$SiO$_{5.6}$H$_{3.6}$], with a Ca/Si ratio of 1.8. Two other CSH phases, CSH$_{1.1}$ [Ca$_{1.1}$SiO$_{4.2}$H$_{2.2}$] and CSH$_{0.8}$ [Ca$_{0.8}$SiO$_{3.6}$H$_{1.6}$], with Ca/Si ratios of 1.1 and 0.8, respectively, were also included in the thermodynamic database.	

Granite initially was assumed to comprise the concrete aggregate. However, granite rock is much less reactive to borated water compared to the minerals present in hydrated cement. Dissolution reactions in concrete and the consequent changes in solution pH are expected to be dominated by the more soluble cement minerals, particularly portlandite and CSH. Thus, to simplify the model, boric acid interaction with aggregate was neglected and aggregate was represented in the model by the relatively insoluble mineral rutile (TiO$_2$). Kosakowski, et al. (2009) employed a similar approach and used SnO$_2$ to represent inert components in their cement model. Values of concrete porosity and pore diffusion coefficient were taken from Wang (2009) and set equal to 0.07 and 1 × 10^{-6} cm^2/s [1.6 × 10^{-7} in^2/s], respectively.

5.1.2   Thermodynamic Database

Chemical reactions in the X1t and X2t simulations used the thermodynamic database *thermo.com.v8.r6+.dat*, which was developed at the Lawrence Livermore National Laboratory and is included in the GWB software package. To enable application of the thermodynamic database to cement-based systems, thermodynamic data on cement minerals were added and data on a few other minerals were revised. The added and revised equilibrium constants are listed in Table 5-2. Because the CSH phase exhibits incongruent solubility behavior, with a reaction stoichiometry that is a function of the Ca/Si ratio, its dissolution could be modeled most accurately using a solid solution model (e.g., Kulik and Kersten, 2001; Sugiyama and Fujita, 2006). However, it is more common to model CSH dissolution as a process involving a series of CSH phases with a different Ca/Si mole ratio, each with its own characteristic thermodynamic properties (e.g., Galindez, et al., 2006; de Windt and Badreddine, 2007; van der Lee, et al, 2008; Barbarulo, 2008; Wang, 2009; Blanc, et al., 2010). The latter approach was used in this study because the GWB software has no option for using solid solution models. Three CSH phases, with Ca/Si mole ratios of 1.8, 1.1, and 0.8, were added to the thermodynamic database. The reaction stoichiometries and equilibrium constants for the CSH phases are listed in Table 5-2. The CSH phase initially present in the concrete was represented in the model by CSH$_{1.8}$. CSH dissolution results in decalcification (i.e., CSH phases with lower Ca/Si ratio), which is represented in the thermodynamic database by CSH$_{1.1}$ and CSH$_{0.8}$.

Table 5-2. Chemical Reactions and Equilibrium Constants for Minerals That Were Revised or Added to the *thermo.com.v8.r6+.dat* Database*		
Mineral	**Reaction**	**log K (25 °C)**
Portlandite	$Ca(OH)_2 + 2H^+ = 2H_2O + Ca^{2+}$	22.8
$CSH_{1.8}$	$Ca_{1.8}SiO_{5.6}H_{3.6} + 3.6H^+ = 1.8Ca^{2+} + 3.6H_2O + SiO_2(aq)$	32.58
$CSH_{1.1}$	$Ca_{1.1}SiO_{4.2}H_{2.2} + 2.2H^+ = 1.1Ca^{2+} + 2.2H_2O + SiO_2(aq)$	16.69
$CSH_{0.8}$	$Ca_{0.8}SiO_{3.6}H_{1.6} + 1.6H^+ = 0.8Ca^{2+} + 1.6H_2O + SiO_2(aq)$	11.07
Ettringite	$Ca_6Al_2(SO_4)_3(OH)_{12}\cdot26H_2O + 12H^+ = 6Ca^{2+} + 38H_2O + 2Al^{3+} + 3SO_4^{2-}$	54.3
Hydrogarnet	$Ca_3Al_2(OH)_{12} + 12H^+ = 3Ca^{2+} + 12H_2O + 2Al^{3+}$	78.0
Hydrotalcite	$Mg_4Al_2(OH)_{14}\cdot3H_2O + 14H^+ = 17H_2O + 2Al^{3+} + 4Mg^{2+}$	75.0
Na_2O	$Na_2O + 2H^+ = 2Na^+ + H_2O$	24.94†
K_2O	$K_2O + 2H^+ = 2K^+ + H_2O$	25.71†
*Log K values taken from Wang, L. "Near-Field Chemistry of a HLW/SF Repository in Boom Clay—Scoping Calculations Relevant to the Supercontainer Design." SCK•CEN–ER–17. Mol, Belgium: SCK•CEN. 2009. †Wang (2009) used these Na_2O and K_2O log K values to impose equilibrium Na^+ and K^+ concentrations equal to 0.14 and 0.37 molal, respectively, in the cement pore water.		

5.2   One-Dimensional Reactive Transport Simulations

One-dimensional (1-D) reactive transport simulations were performed using the X1t code to determine the degree of degradation of intact (uncracked) concrete due to leaching by boric acid solution. The simulations are relevant to situations in which diffusion is the mechanism whereby boric acid solution penetrates a reinforced concrete structure (Figure 5-1). The 1-D model domain is 1 cm [0.39 in] long divided into 50 equal length grids. The concrete mineralogy is listed in Table 5-1. The pore diffusion coefficient and initial concrete porosity were set equal to 1×10^{-6} cm^2/s [1.6×10^{-7} in^2/s] and 0.07, respectively. To determine the effect of boric acid concentration on concrete leaching and to enable a comparison of model results with experimental data discussed in Section 4.2.5, the simulations assumed initial boron concentrations of 1,200 and 2,400 ppm. The reactive transport simulations were conducted for a temperature of 25 °C [77 °F] and time periods up to 100 years. An example X1t input file is given in Appendix D.
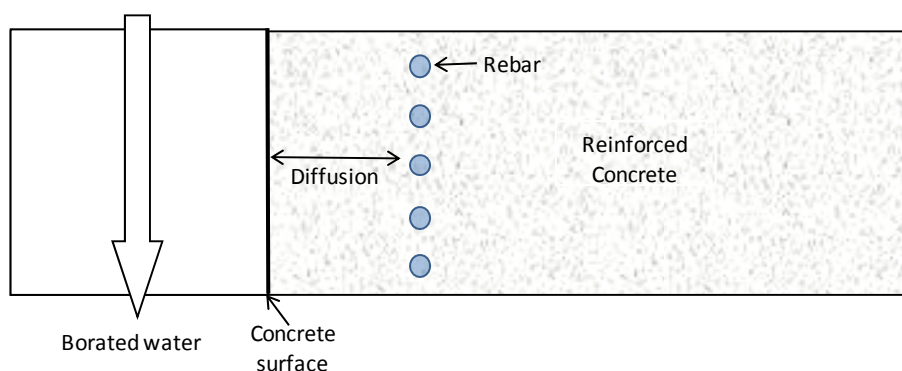
Figure 5-1. Simplified Representation of Reinforced Concrete Exposed to Leaching by Borated Water at One Side. Borated Water Transport Into the Concrete Is Modeled as a Diffusion Process Using X1t.

5.2.1 X1t Simulation Results

The simulation results are shown in Figures 5-2 to 5-4 for time periods up to 1 year. Figure 5-2 illustrates the calculated concrete mineralogy as a function of distance into the concrete matrix after several time periods of reaction with 2,400 ppm B solution. With increasing time, the dissolution front moves deeper into the concrete, resulting in portlandite dissolution, CSH decalcification (indicated by a transition from $CSH_{1.8}$ to $CSH_{1.1}$), and formation of a leached layer dominated by the minerals quartz, hematite, and hydrotalcite. Quartz represents the residual silica remaining after cement minerals have been dissolved (e.g., leached layer illustrated in Figure 2-1.)

Figure 5-3 shows the calculated concrete pore solution pH as function of depth from the concrete surface and time of reaction with the boric acid solution. The pH of the solutions, initially 5.10 and 4.95 for the 1,200 and 2,400 ppm B solutions, respectively, increases quickly to alkaline values as the solution diffuses into and reacts with the cement matrix. Boric acid penetration into the concrete matrix is faster at higher solution concentration due to the higher concentration gradient.

Figure 5-4 plots the calculated concrete porosity as a function of depth from the concrete surface and reaction time. The porosity is high close to the concrete surface due to complete dissolution of the cement minerals. For example, the 44-day porosity profile shown in Figure 5-4 indicates that a 0.03-cm [0.012-in]-thick leached layer has formed with a porosity greater than 0.23. The leached layer is composed of quartz, hematite, and aggregate (Figure 5-2) and is likely to have very little inherent strength. The porosity decreases with increasing depth due to lesser dissolution of cement minerals, eventually attaining the initial porosity of 0.07, but localized increases in porosity occur due to reprecipitation of ettringite and hydrogarnet.

5.2.2 Comparison With Measured Concrete Leaching Depth

The results of the 1-D reactive transport simulations can be compared with the measured depth of concrete leaching reported in Section 4.2.5. As discussed in that section, the depth of concrete leaching was determined by petrographic examination of saw-cut, lapped sections of concrete cylinders that were immersed in boric acid solutions for a maximum of 300 days. In most specimens, the depth of leaching was visually evident in the form of a distinct transition from a weak, porous, affected cement paste to a dense, unaffected cement paste. In the more severely leached specimens, this transition was less defined and determination of leaching depth was aided by a phenolphthalein test method. Using this test method, phenolphthalein solution was sprayed on the saw-cut, lapped surface of the concrete specimens. Concrete pore solution typically has an initial pH of 13, which decreases due to acid attack. Phenolphthalein solutions are pink in color at pHs above ~9 and are colorless at a pH below ~8 (the approximate pH range for color transition is 8.0 to 9.8). When phenolphthalein is applied to concrete, the cement paste will turn pink at a pH above ~9 and will remain uncolored at pH values below ~8. Therefore, the depth of the uncolored cement paste will indicate the depth to which the acid has affected the pH of the cement paste. Figure 5-5 (also shown in Figure 4-32) is a photomicrograph of a specimen sprayed with phenolphthalein solution. The depth to which the pH has been lowered by acid exposure is represented by the uncolored cement paste. The depths of concrete leaching by 1,200 and 2,400 ppm B solutions measured at 180, 240, and 300 days and discussed in Section 4.2.5 are listed in Table 5-3.
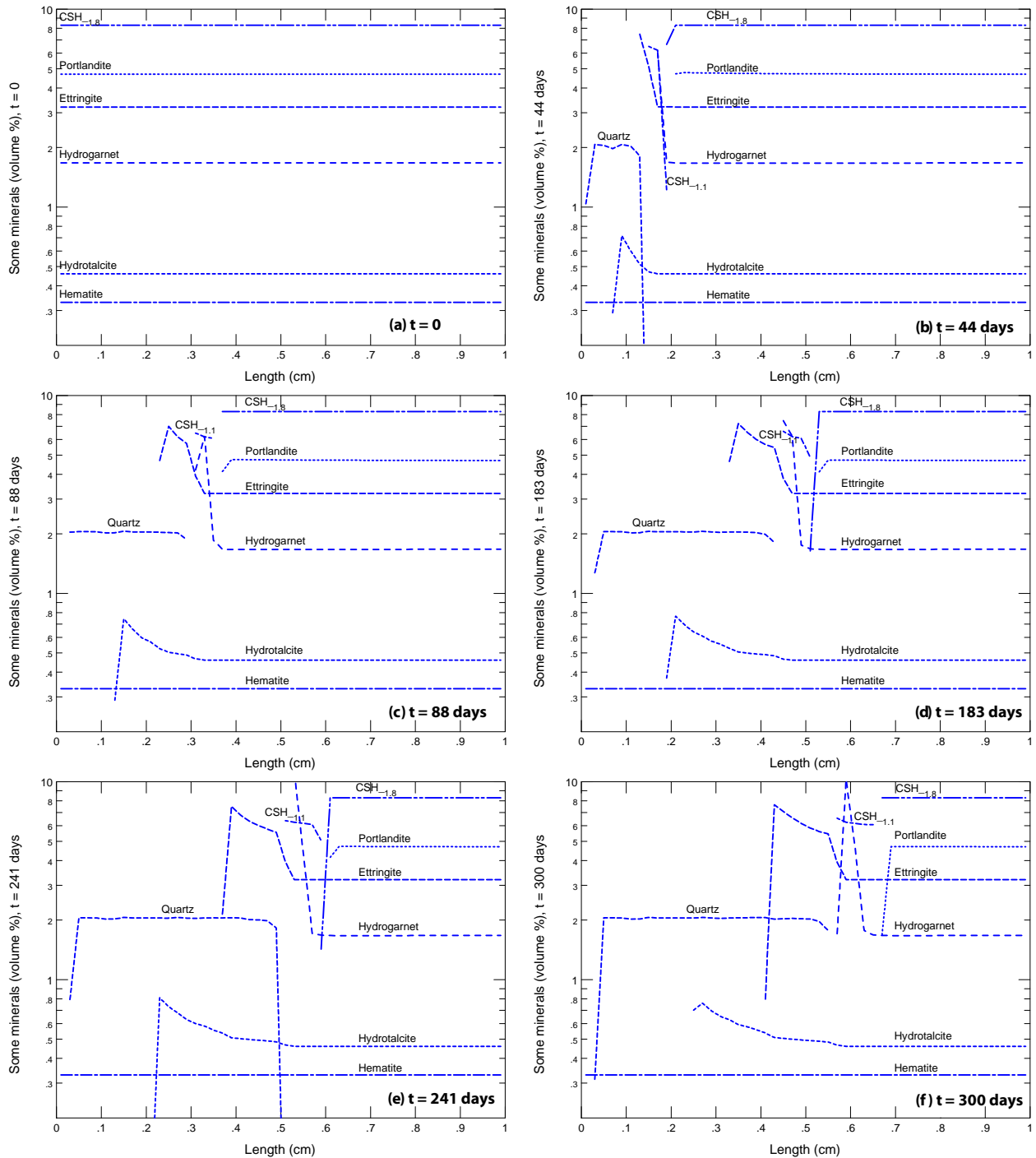
Figure 5-2. Calculated Mineralogy (Volume %) as a Function of Distance Into the Concrete Matrix After 0, 44, 88, 183, 241, and 300 Days of Reaction with 2,400 ppm Boron Solution. The Relative Amount of Aggregate (Represented by Rutile) Remained Constant at 72 Volume % and Is Not Shown. [1 cm = 0.39 in]
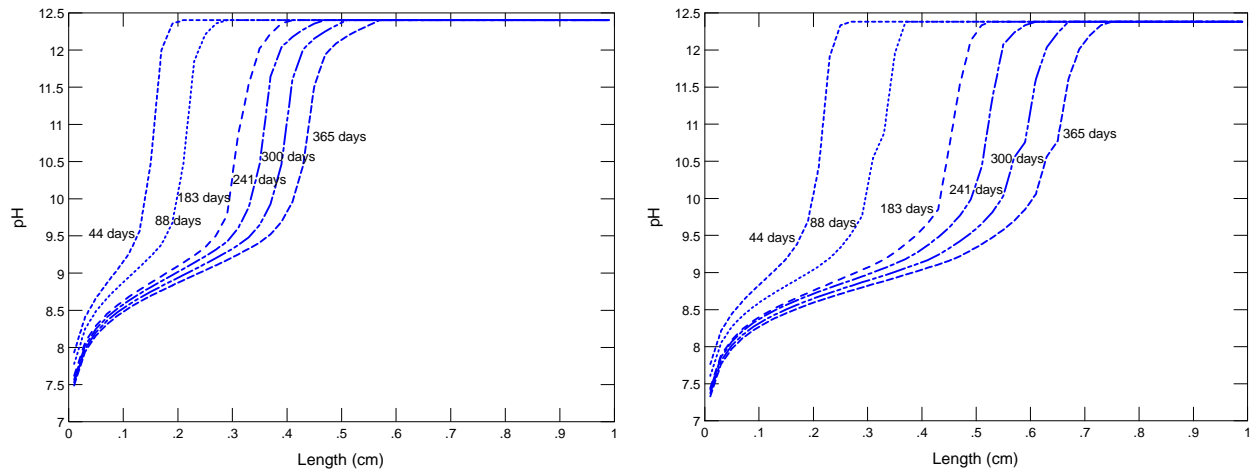
(a)   **(b)**

Figure 5-3. Calculated Pore Solution pH Versus Depth in Concrete After Various Time Periods of Reaction With (a) 1,200 and (b) 2,400 ppm Boron Solutions. The Initial pHs of the 1,200 and 2,400 ppm B Solutions Were 5.10 and 4.95, Respectively. [1 cm = 0.39 in]
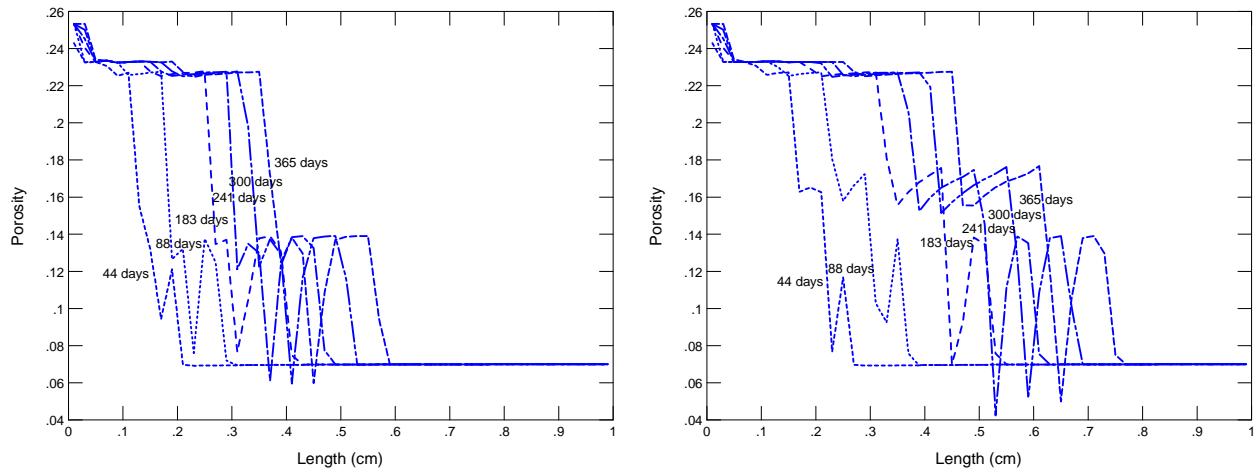
(a)   **(b)**

Figure 5-4. Calculated Concrete Porosity Versus Depth After Various Time Periods of Reaction With (a) 1,200 and (b) 2,400 ppm Boron Solutions. The Initial Concrete Porosity Was 0.07. [1 cm = 0.39 in]

**Figure 5-5. Cross Section Photomicrograph of Saw-Cut, Lapped Concrete Specimen After Exposure to Phenolphthalein Solution. The Depth to Which the pH Has Been Lowered by Acid Exposure Is Represented by the Uncolored Cement Paste.
[1 mm = 0.039 in]**

Table 5-3. Measured Boric Acid Leaching Depth Compared with Calculated Values				
Reaction Time	**Leaching Depth in 1,200 ppm B Solution**		**Leaching Depth in 2,400 ppm B Solution**	
	Measured*	**Calculated†**	**Measured**	**Calculated**
180	0.5 to 1.1 mm‡ (Ave. = 0.75 mm)	0.78 mm	0.6 to 1.2 mm (Ave. = 0.85 mm)	1.24 mm
240	1.0 to 1.5 mm (Ave. = 1.31 mm)	0.86 mm	1.2 to 1.7 mm (Ave. = 1.42 mm)	1.32 mm
300	1.4 to 1.8 (Ave. = 1.61 mm)	0.95 mm	1.4 to 1.8 (Ave. = 1.60 mm)	1.49 mm
*Measurements on concrete specimens that were immersed in boric acid solutions at room temperature. Values taken from Table 4-7. Average values are based on 20 measurements. †Derived from X1t reactive transport simulation results at 183, 241, and 300 days and using pH 8.5 as the criterion for leaching depth. ‡1 mm = 0.039 in				

Figure 5-6 plots the calculated concrete pore solution pH as a function of depth after reaction with 1,200 and 2,400 ppm B solutions. To compare X1t results with measured leaching depths, the concrete depths at which the pore solution pHs are equal to 8.5 were derived from Figure 5-6 and listed in Table 5-3. The X1t model underpredicts the leaching depth in 1,200 ppm B solution at 240 and 300 days and slightly overpredicts the leaching depth in 2,400 ppm B solution at 180 days. However, considering the general uncertainties in the model parameters and in the limited experimental data, the agreement between calculated and measured leaching depths is relatively good.
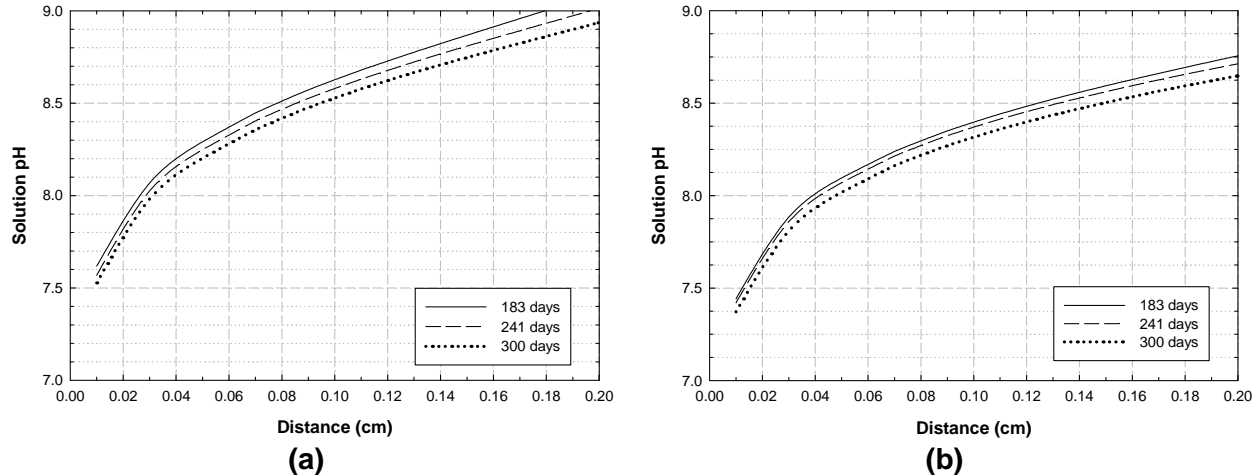
**Figure 5-6. Calculated Concrete Pore Solution pH Versus Concrete Depth After Reaction
With (a) 1,200 and (b) 2,400 ppm Boron Solutions for 183, 241, and 300 Days. A pH Value
of 8.5 Is Used To Estimate the Depth of Leaching of Concrete by Boric Acid Solution.
[1 cm = 0.39 in]**

5.2.3   Comparison With Diffusion Equation

In Section 4.2.5, a diffusion equation was fit to the leaching depth measured using
2,400 ppm B solutions at 180, 240, and 300 days to enable extrapolation to longer time
periods. The leaching depth as a function of time calculated using the diffusion equation to
100 years is plotted in Figure 5-7. For comparison, the leaching depths derived from the X1t
simulations (using pH 8.5 as the leaching depth criterion) are also shown in the figure.[1] There is
good agreement between the values derived from the diffusion equation and those from the
X1t results.

5.2.4   Implication for Rebar Corrosion in Intact Concrete

The results discussed in Section 4 indicate that the threshold pH for carbon steel corrosion
in borated solution is between 6.8 and 7.3. The corrosion rate is low {~1 µm/yr or less
[~3.94 ×10^{-5} in/yr or less]} when the solution pH is ~7.1 or higher. Below pH ~7.1, the corrosion
rate increases with decreasing pH and can reach ~100 µm/yr [~3.94 × 10^{-3} in/yr] in solutions
with pH less than ~6.7. The potential for reinforcement steel corrosion can be evaluated by
comparing the concrete pore solution pH calculated using X1t with the threshold pH for
corrosion. Figure 5-8 shows the calculated pore solution pH in concrete that was reacted with
2,400 ppm B solution. The figure shows that even after 70 years of reaction, the pore solution
pHs are above the threshold pH for rebar corrosion. Thus, the results indicate that the cement
minerals provide sufficient acid neutralizing capacity and that reinforcement steel with a 5.1-cm
[2-in] concrete cover is unlikely to undergo corrosion to time periods of at least 77 years, if
diffusion is the mechanism by which borated water penetrates the concrete.

---

[1]X1t output does not provide values at pH exactly equal to 8.5. The leaching depths at pH 8.5 were
interpolated between the two closest pH values bookending 8.5. Also, the X1t run did not converge at
time periods beyond 77 years.
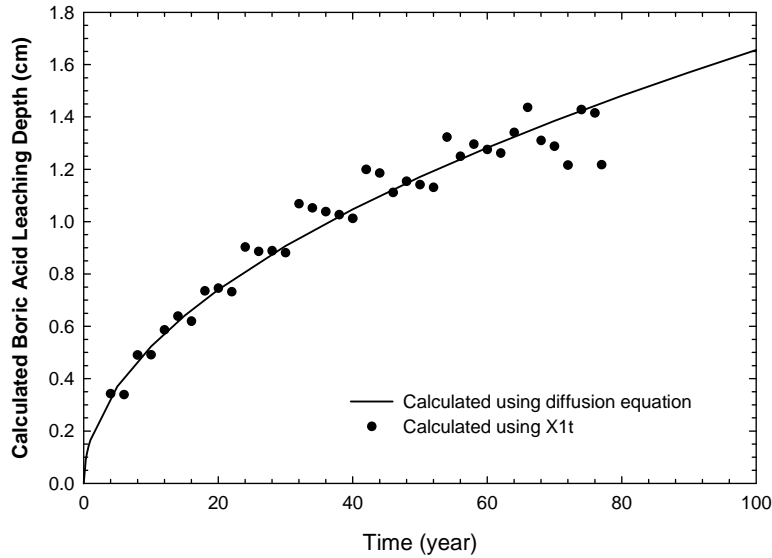
Figure 5-7. Comparison of Leaching Depths Calculated Using a Diffusion Equation Fit to Short-Term Experimental Data (Described in Section 4) and Derived From Reactive Transport Simulations
[1 cm = 0.39 in]
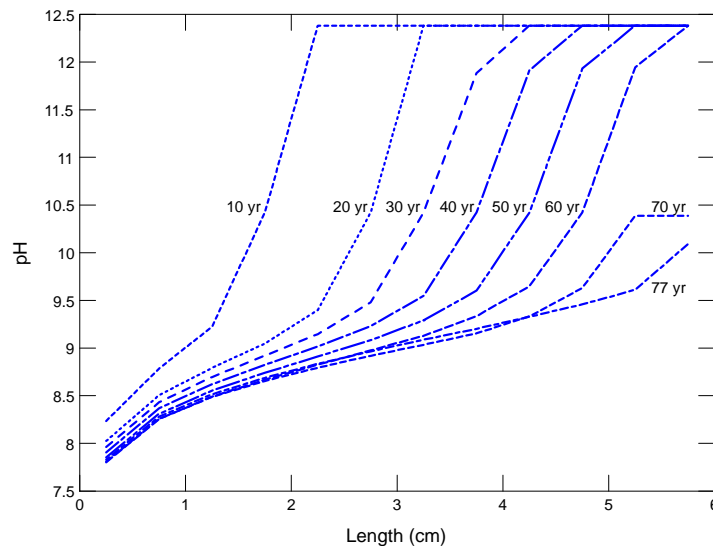
Figure 5-8. Calculated Concrete Pore Solution pH Versus Concrete Depth After Various Reaction Times with 2,400 ppm Boron Solution
[1 cm = 0.39 in]

5.3 Two-Dimensional Reactive Transport Simulations

The X2t code was used to perform two-dimensional (2-D) reactive transport simulations of the interaction between reinforced concrete and boric acid solution that leaks from a spent fuel pool into a crack in a concrete structure. The simulations were conducted to determine the degree of concrete dissolution and pH change as boric acid solution flows in the crack or diffuses into the

concrete matrix (Figure 5-9). The simulation results would allow an evaluation of the corrosion susceptibility of concrete rebar that may be exposed to boric acid solution in the crack or in the concrete matrix.

The cracked concrete was represented by two blocks, 130-cm [51.2-in] long and 7-cm [2.8-in] wide, separated by a crack of uniform aperture. Because of symmetry, only one of the blocks and half of the crack aperture were included in the model. In the x-direction, the block length was divided into 20 nonuniform grids, with a denser grid near the inlet (left) side where more chemical alteration is expected, and a coarser grid farther along the flow path (toward the right) where less alteration is expected (Figure 5-10). Similarly, in the y-direction, the 7-cm [2.8-in] block width was divided into seven nonuniform grids, with a denser grid near the crack and a coarser grid farther away from the crack. The 20 grids in the x-direction were spaced in the following sequence: four 2.5-cm [0.98-in]-wide grids, then six 5-cm [2.0-in]-wide grids, followed by four 7.5-cm [3.0-in]-wide grids, then six 10-cm [3.9-in]-wide grids. The seven y-grids in the concrete block were given 0.25-, 0.5-, 0.75-, 1.0-, 1.25-, 1.5-, and 1.75-cm [0.098-, 0.20-, 0.30-, 0.39-, 0.49-, 0.59-, and 0.69-in] widths. One row of 20 cells along the bottom of the concrete block represented the crack. A total of 160 cells were used in the model, including the 20 cells representing the concrete crack.
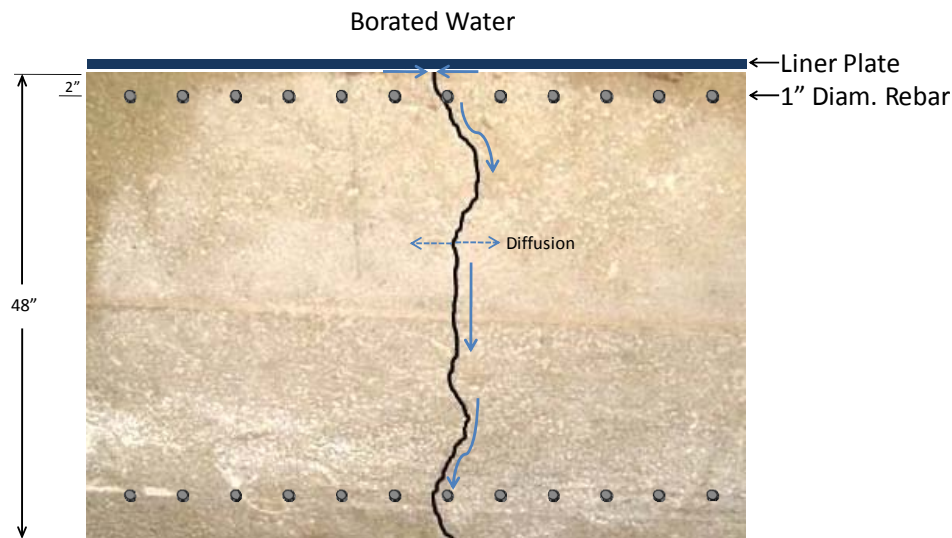
Figure 5-9. Schematic Representation of Borated Water Flow From a Leak in the Spent Fuel Pool Steel Liner Through a Crack in Reinforced Concrete. Not Drawn to Scale.
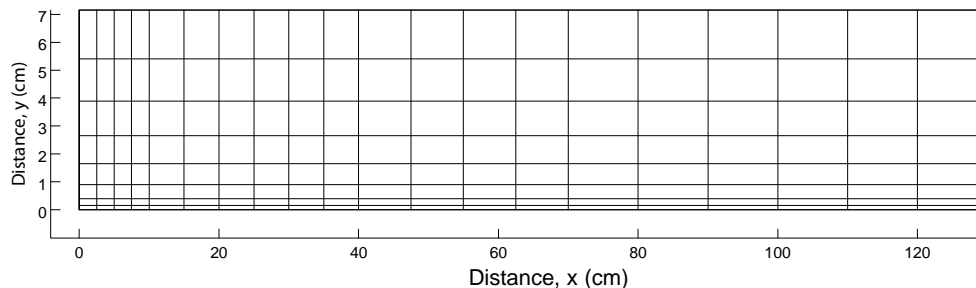
Figure 5-10. Grid Spacing Used in the 2-D Reactive Transport Model
[1 cm = 0.39 in]

For each simulation, 2,400 ppm B solution enters the left side of the domain, flows in the crack at the bottom (and diffuses into the concrete matrix), and exits the right side of the domain. To determine the effect of crack aperture on model results, concrete crack half-apertures of 0.15, 0.25, and 0.5 cm [0.059, 0.098, and 0.20 in] were specified. The solution flow rate also was varied by specifying two values of flow rate (termed specific discharge—the volume of solution flowing per unit time through a unit cross-sectional area of the porous medium) on the inlet side equal to 0.2 and 1.0 $cm^3/cm^2 \cdot day$ [0.079 and 0.39 $in^3/in^2 \cdot day$]. An example X2t input file is given in Appendix E. The model results included solution pH in the crack and in the concrete matrix, concrete porosity, mineralogy, and specific discharge at the crack outlet (volume of solution flowing per unit time through a unit cross-sectional area of the crack).

The volume of solution exiting the crack can be calculated from the values of specific discharge derived from the model, the input crack half-aperture, and an assumed crack length. In the absence of information on crack lengths in an actual SFP concrete structure, a 1-m [3.3-ft] crack length was assumed to calculate the solution volume exiting the crack at various half-apertures and inlet flow rate. The calculated values are tabulated in Table 5-4. When the inlet flow rate is 0.2 $cm^3/cm^2 \cdot day$ [0.079 $in^3/in^2 \cdot day$], ~300 cm^3/day [~0.08 gal/day] is calculated to exit the concrete crack. When the inlet flow rate is increased by a factor of 5, the amount of solution exiting the crack also increased by a factor of 5 {to ~1,500 cm^3/day [~0.4 gal/day]}. To put these calculated values into perspective, the leakage that is still occurring through the east wall of the Fuel Handling Building of the Salem Nuclear Generating Station has been estimated to be 473 cm^3/day [0.125 gal/day] (Davison, 2011). The calculated flow rate of boric acid solution exiting the crack in Simulations 4, 5, and 6 is more than three times that estimated to be leaking from the Salem Fuel Handling Building. Thus, the X2t simulations reasonably approximate the borated water flow rate that has been observed in an SFP concrete structure. To determine the effect of a much higher flow rate, an additional simulation (Simulation 7) was performed with an inlet flow rate four times higher than in Simulations 4 to 6. The calculated solution volume exiting the crack in Simulation 7 is 5,721 cm^3/day [1.51 gal/day], 12 times higher than what has been observed at the Salem Fuel Handling Building.

Table 5-4. Matrix of 2-D Reactive Transport Modeling Simulations and Calculated Volumetric Flow Rate Exiting the Concrete Crack				
Simulation Number	Inlet Specific Discharge ($cm^3/cm^2 \cdot day$)*	Crack Half-Aperture (cm)*	Calculated Specific Discharge at Crack Outlet ($cm^3/cm^2 \cdot day$)	Volumetric Flow Rate for 1-m-Long Crack (cm^3/day) [gal/day]†
1	0.2	0.15	9.54	286 [0.0756]
2	0.2	0.25	5.80	290 [0.0766]
3	0.2	0.5	3.00	300 [0.0793]
4	1.0	0.15	47.7	1,431 [0.378]
5	1.0	0.25	29.0	1,450 [0.383]
6	1.0	0.5	15.0	1,500 [0.396]
7	4.0	0.15	190.7	5,721 [1.51]
*1 $cm^3/cm^2 \cdot day$ = 0.39 $in^3/in^2 \cdot day$; 1 cm = 0.39 in				
†For comparison, the leakage that is still occurring through the east wall of the Fuel Handling Building of the Salem Nuclear Generating Station has been estimated to be 473 cm^3/day [0.125 gal/day] (Davison, P.J. "Update to December 14, 2010 PSEG Nuclear, LLC Response to NRC Request for Additional Information Related to Structures Monitoring Associated with the Salem Nuclear Generating Station, Units 1 and 2 License Renewal Application." Letter (February 25) to U.S. Nuclear Regulatory Commission. Hancocks Bridge, New Jersey: PSEG Nuclear, LLC. 2011)				

5.3.1   X2t Simulation Results

The pH evolution with time of pore solutions in the concrete block is illustrated in Figures 5-11 and 5-12. The results shown in the figures are for simulations using a crack half-aperture of 0.15 cm [0.059 in] and inlet flow rates of 0.2 and 1.0 cm^3/cm^2·day [0.079 and 0.39 in^3/in^2·day]. The figures show that the pH of the concrete pore solutions, initially 13.5, decreases as boric acid flows in the concrete crack and diffuses into the concrete matrix. With increasing time, the decreased pH propagates deeper into the concrete matrix. A comparison of Figures 5-11 and 5-12 shows that the pH decrease is accelerated by an increase in inlet flow rate.

Figures 5-13 and 5-14 show the calculated pH of a boric acid solution flowing in a concrete crack with a half-aperture of 0.15, 0.25, and 0.5 cm [0.059, 0.098, and 0.20 in]. With an inlet flow rate of 0.2 cm^3/cm^2·day [0.079 in^3/in^2·day], the solution pH, initially 4.95, rises to neutral values within a few centimeters of the inlet, at least during the first 30 years. At later times, it takes longer flow distances in the concrete crack before the boric acid solution is neutralized. At distances from the inlet of 20 cm [7.9 in] or more, the solution pH in the crack remains higher than the threshold pH (~7.1) for rebar corrosion at time periods up to 100 years. With a five times higher inlet flow rate of 1.0 cm^3/cm^2·day [0.39 in^3/in^2·day], the solution pH rises to neutral values within 10 cm [3.9 in] of the inlet during the first 30 years, but longer flow distances are needed at later times before the solution attains a neutral pH. At distances from the inlet of 40 cm [7.9 in] or greater, the solution pH in the crack remains higher than the threshold pH for rebar corrosion at time periods up to 100 years.

Figures 5-15 and 5-16 show the calculated solution pH in the concrete matrix as functions of time and distance from the concrete crack. Only pH values in grid cells near the crack inlet {x ≤ 22.5 cm [8.86 in} are shown. With an inlet flow rate of 0.2 cm^3/cm^2·day [0.079 in^3/in^2·day] and close to the crack inlet {x = 3.75 cm [1.48 in]}, the pH in the concrete matrix is maintained above the threshold pH for rebar corrosion up to 30 years. At later times, further diffusion of the boric acid solution reduces the concrete matrix pH to less than the threshold value. Farther away from the crack inlet, boric acid diffusive transport into the concrete matrix is delayed such that at 12.5 cm [4.9 in] from the crack inlet the matrix pH is maintained above the threshold pH for rebar corrosion even after 100 years. With a five times higher inlet flow rate of 1.0 cm^3/cm^2·day [0.39 in^3/in^2·day] (Figure 5-16), boric acid transport into the concrete matrix is faster, causing the pH in the matrix close to the crack inlet to be lower than the threshold pH even at 10 years. It takes a longer distance from the inlet {x ~ 22.5 cm [8.9 in]} before the matrix pH is maintained above the threshold pH at 100 years.

Figure 5-17 shows the calculated solution pH in the crack or in the concrete matrix for the highest simulation flow rate of 4.0 cm^3/cm^2·day [1.6 in^3/in^2·day]. Compared to simulations at lower flow rates, it takes longer distances from the crack inlet for the solution pH to rise above the threshold pH for rebar corrosion. For example, at 100 years, it takes approximately 80 cm [31.5 in] from the inlet for the solution pH in the crack to exceed the threshold pH for rebar corrosion and approximately 27.5 cm [10.8 in] from the inlet for the matrix solution pH to exceed the threshold pH.

Figure 5-18 plots the calculated concrete porosity as functions of distance (y) from the crack, distance (x) from the inlet, and inlet flow rate. Values are plotted for grid cells near the inlet {x = 12.5 cm [4.9 in]}, at the midpoint of the model domain {x = 66.25 cm [26.1 in]}, and near the outlet {x = 125 cm [49.2 in]}. The figure shows that the concrete porosity is high close to the concrete crack due to complete dissolution of the cement minerals and formation of a leached
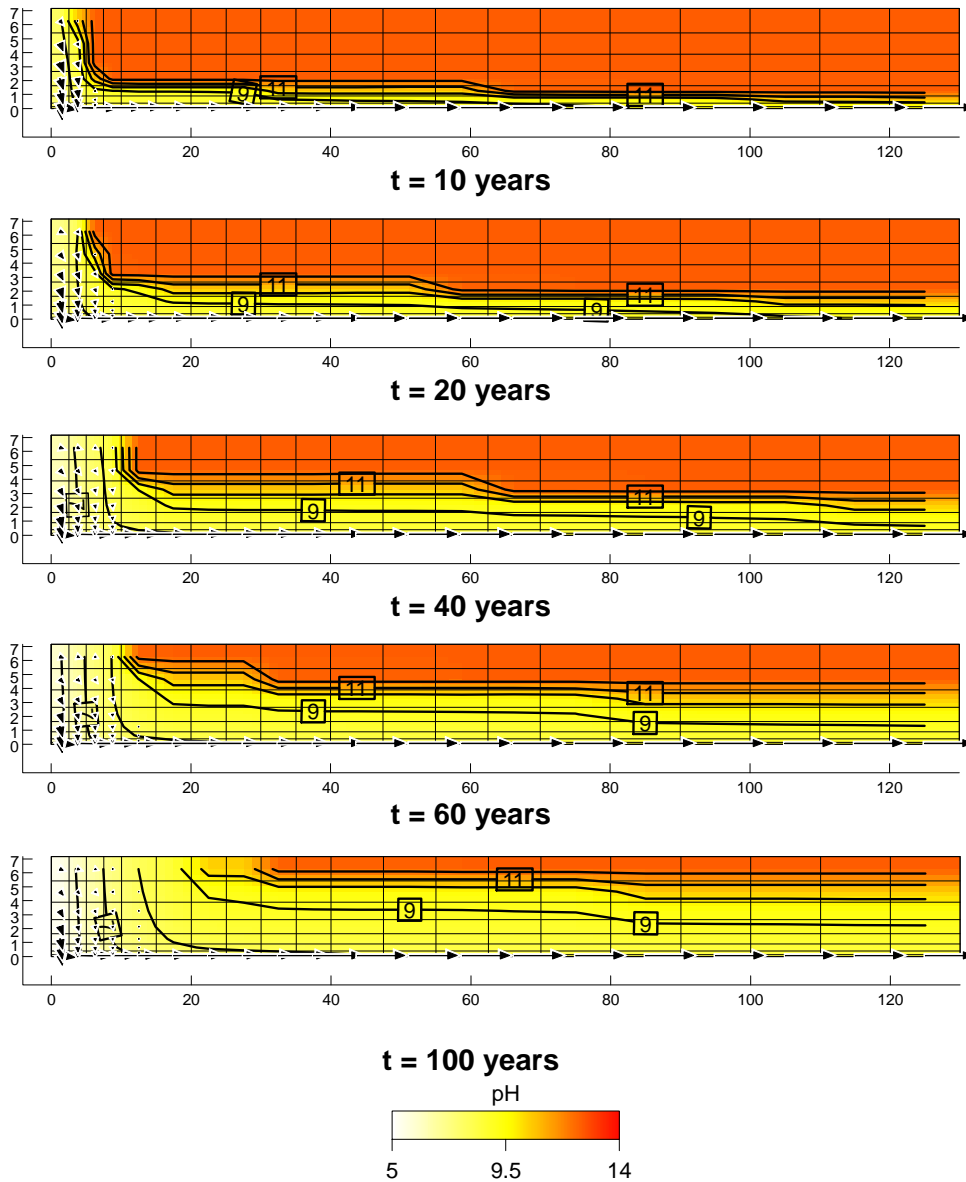
Figure 5-11. 2-D Model Representation of a Concrete Block {130 × 7 cm [51.2 × 2.8 in]} Showing Solution pH at *t* = 10, 20, 40, 60, and 100 years. Boric Acid Solution (2,400 ppm B; Initial pH = 4.95) Enters the Left Side of the Domain, Flows in the Crack {0.15 cm [0.059 in] Half-Aperture} at the Bottom (and Diffuses into the Concrete Matrix), and Exits the Right Side of the Domain. pH Contours Are Shown in the Figure. Inlet Specific Discharge = 0.2 cm³/cm²·day [0.079 in³/in²·day]. Calculated Specific Discharge at Crack Outlet = 9.54 cm³/cm²/day [3.78 in³/in²·day]. [1 cm = 0.39 in]
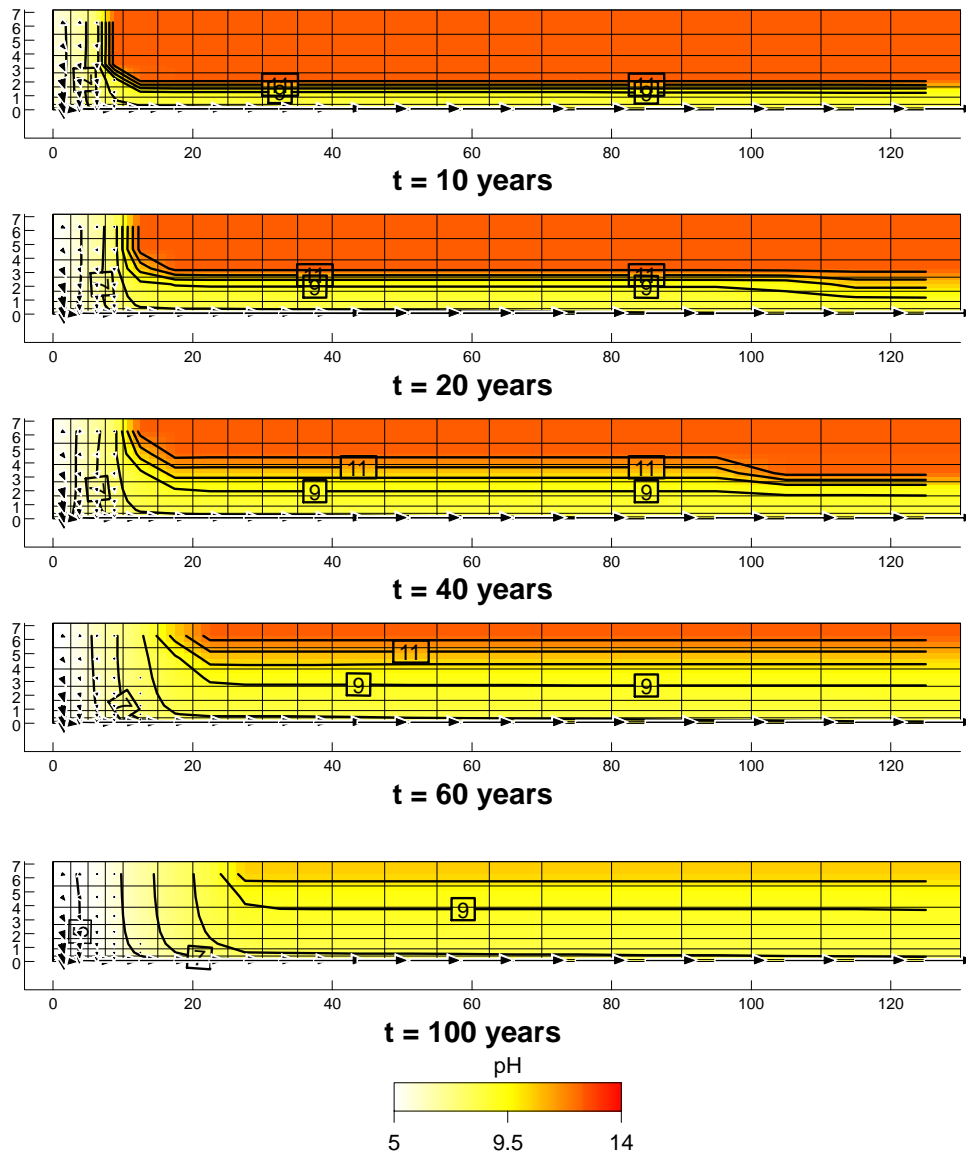
Figure 5-12. 2-D Model Representation of a Concrete Block {130 × 7 cm) [51.2 × 2.8 in]} Showing Solution pH at *t* = 10, 20, 40, 60, and 100 years. Boric Acid Solution (2,400 ppm B; Initial pH = 4.95) Enters the Left Side of the Domain, Flows in the Crack {0.15 cm [0.059 in] Half-Aperture} at the Bottom (and Diffuses into the Concrete Matrix), and Exits the Right Side of the Domain. pH Contours Are Shown in the Figure. Input Specific Discharge = 1.0 cm³/cm²·day [0.39 in³/in²·day]. Calculated Specific Discharge at Crack Outlet = 47.7 cm³/cm²/day [18.8 in³/in²·day].
[1 cm = 0.39 in]
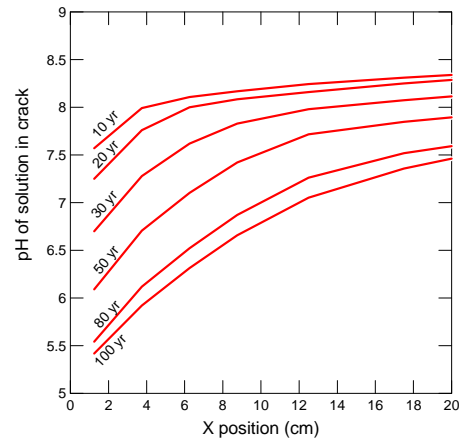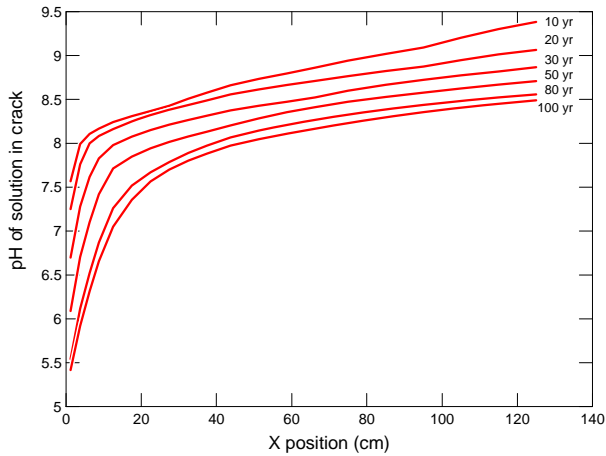
(a) Crack Half-Aperture = 0.15 cm
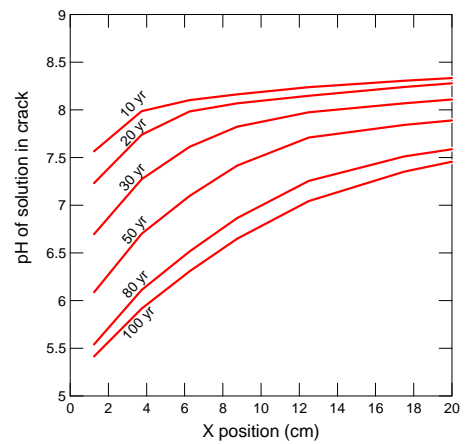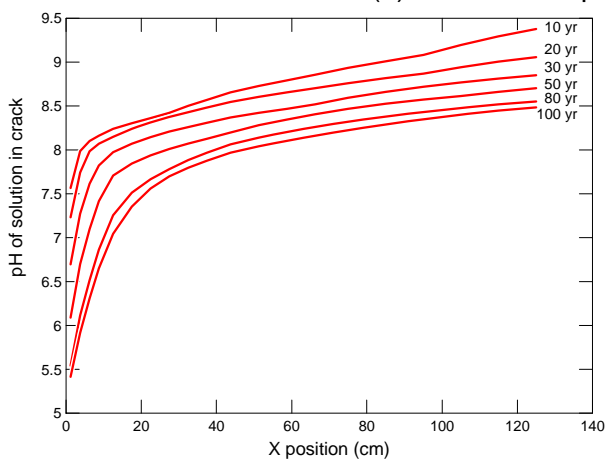
(b) Crack Half-Aperture = 0.25 cm
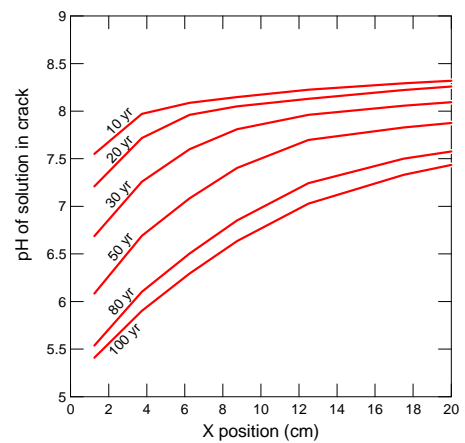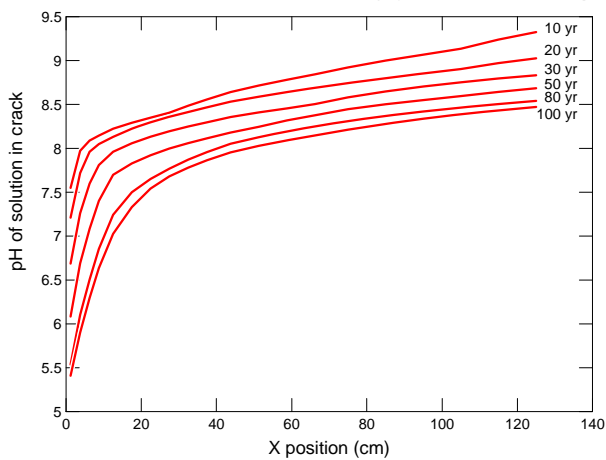
(c) Crack Half-Aperture = 0.50 cm

Figure 5-13. pH of Solution Flowing in the Concrete Crack as a Function of Time and Distance (x) from the Inlet. Values Are Plotted for Crack Half-Apertures of 0.15, 0.25, and 0.50 cm [0.059, 0.098, and 0.20 in]. Inlet Specific Discharge = 0.2 cm^3/cm^2·day [0.079 in^3/in^2·day]. The Figures on the Right Show Solution pHs Within 20 cm [7.9 in] of the Inlet.
[1 cm = 0.39 in]
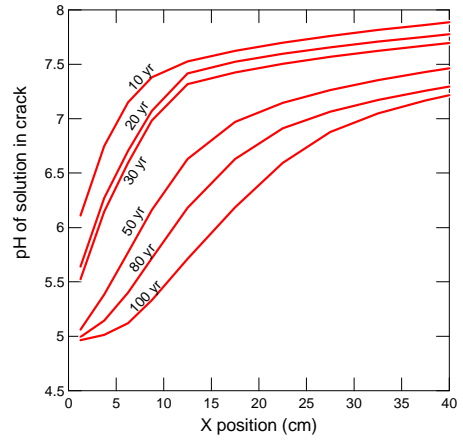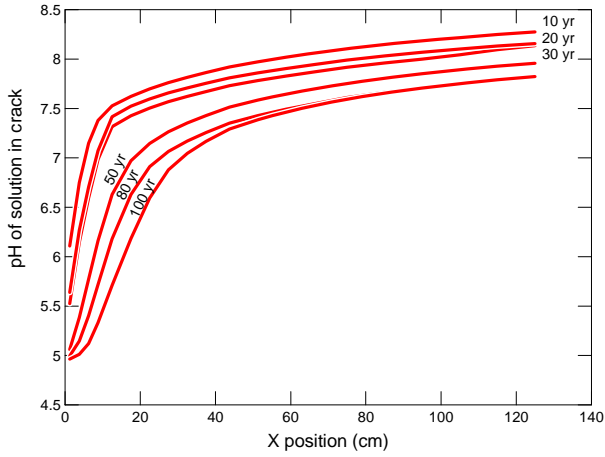
(a) Crack Half-Aperture = 0.15 cm
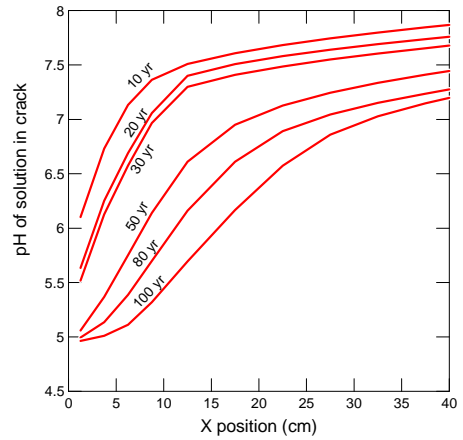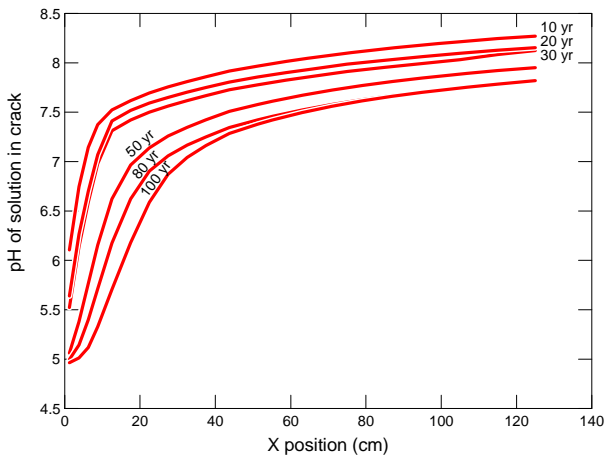
(b) Crack Half-Aperture = 0.25 cm
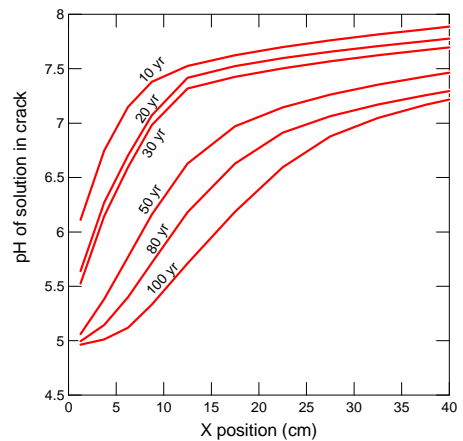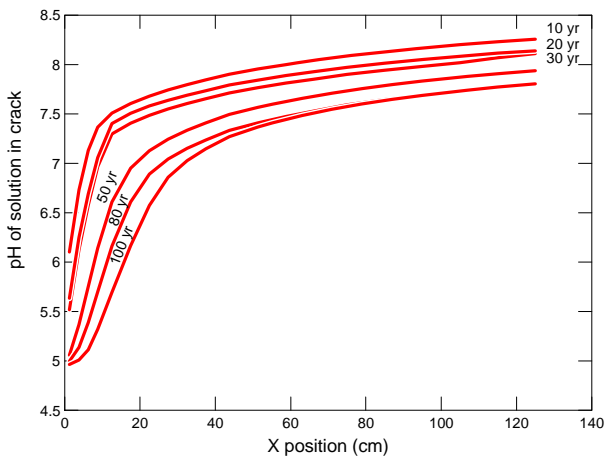
(c) Crack Half-Aperture = 0.50 cm

Figure 5-14. pH of Solution Flowing in the Concrete Crack as a Function of Time and Distance (x) from the Inlet. Values Are Plotted for Crack Half-Apertures of 0.15, 0.25, and 0.50 cm [0.059, 0.098, and 0.20 in]. Inlet Specific Discharge = 1.0 cm^3/cm^2·day [0.39 in^3/in^2·day]. The Figures on the Right Show Solution pHs Within 40 cm [15.7 in] of the Inlet.
[1 cm = 0.39 in]
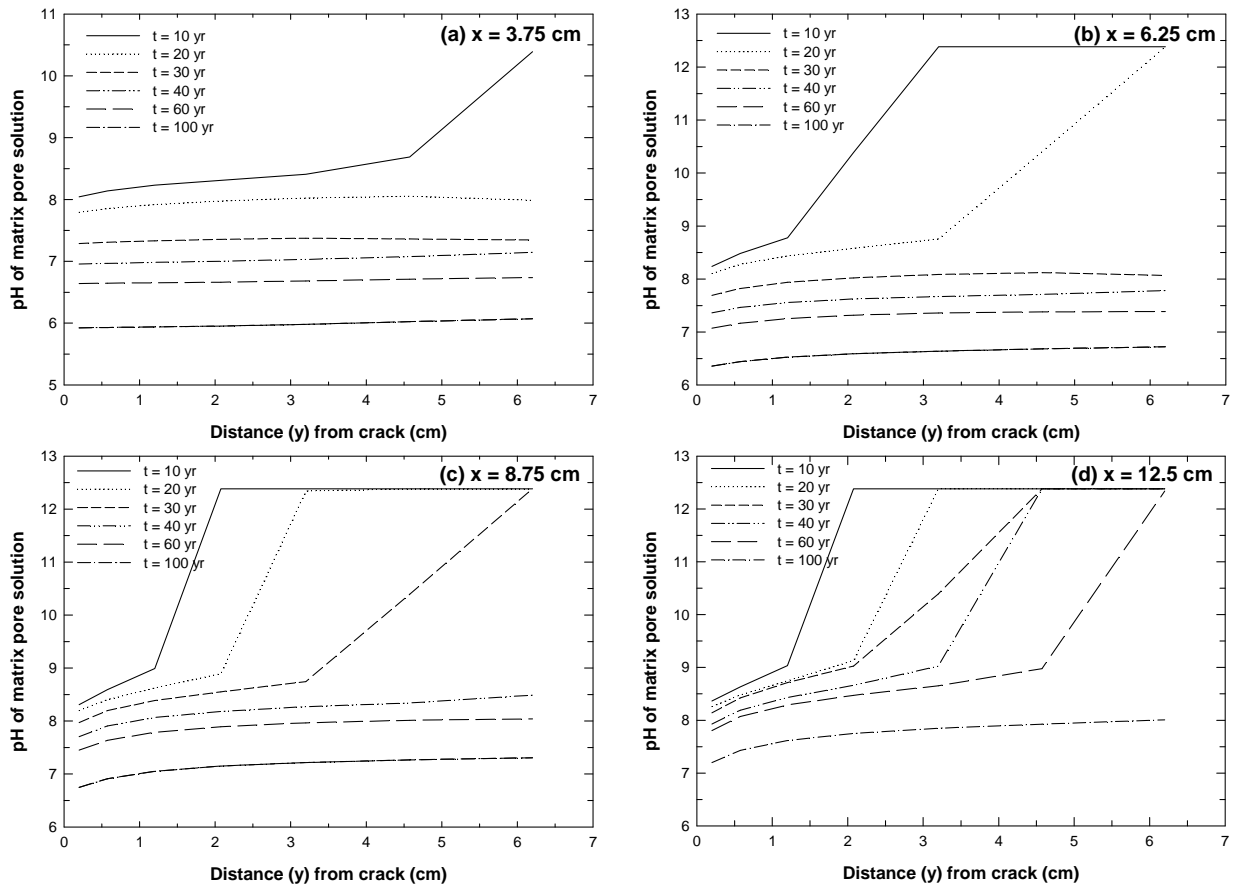
Figure 5-15. Solution pH in Concrete Matrix as a Function of Time, Distance (y) from the Crack, and Distance (x) from the Inlet. Crack Half-Aperture = 0.15 cm [0.059 in]. Inlet Specific Discharge = 0.2 cm^3/cm^2·day [0.079 in^3/in^2·day]. A Typical Thickness of Rebar Concrete Cover Is 5.1 cm [2.0 in].
[1 cm = 0.39 in]
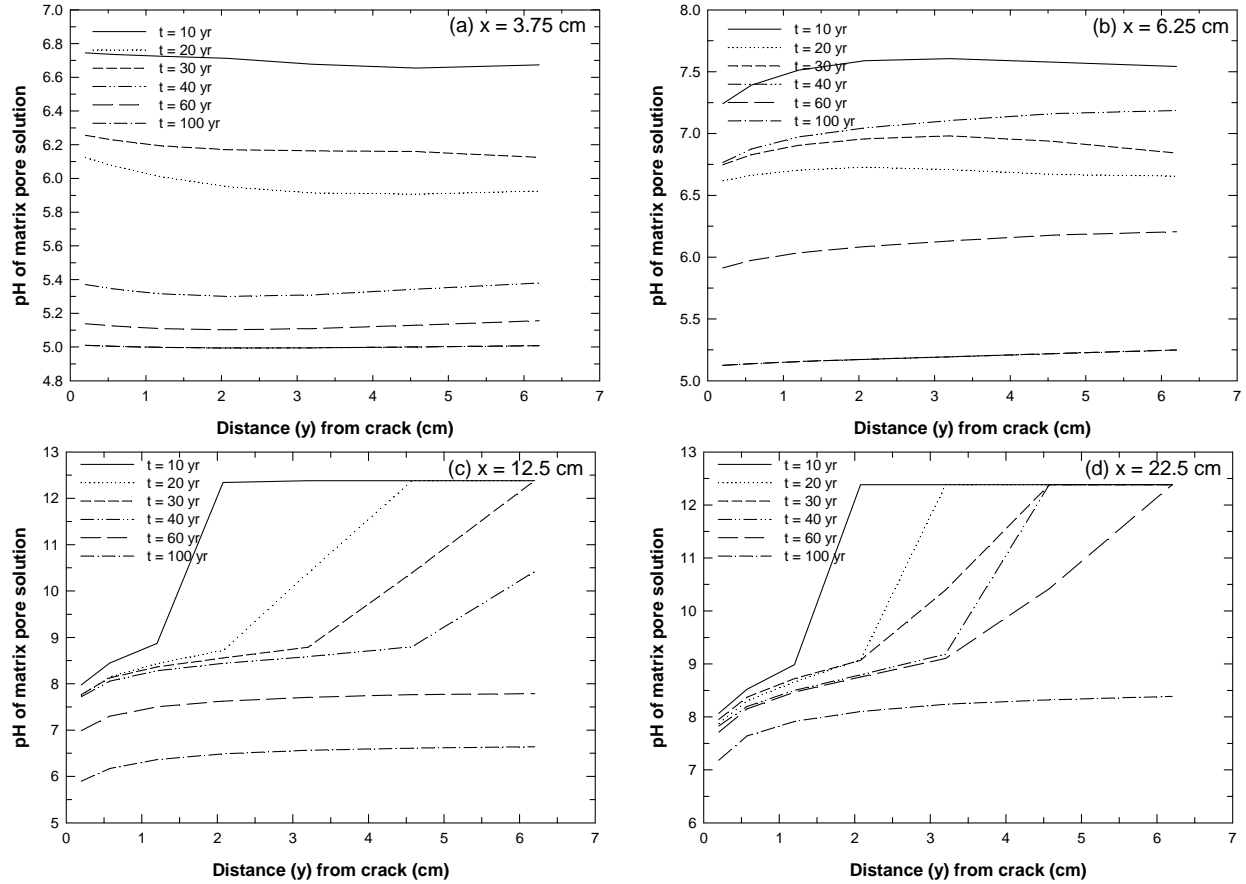
Figure 5-16. Solution pH in Concrete Matrix as a Function of Time, Distance (y) From the Crack, and Distance (x) From the Inlet. Crack Half-Aperture = 0.15 cm [0.059 in]. Inlet Specific Discharge = 1.0 cm³/cm²·day [0.39 in³/in²·day]. A Typical Thickness of Rebar Concrete Cover Is 5.1 cm [2.0 in].
[1 cm = 0.39 in]
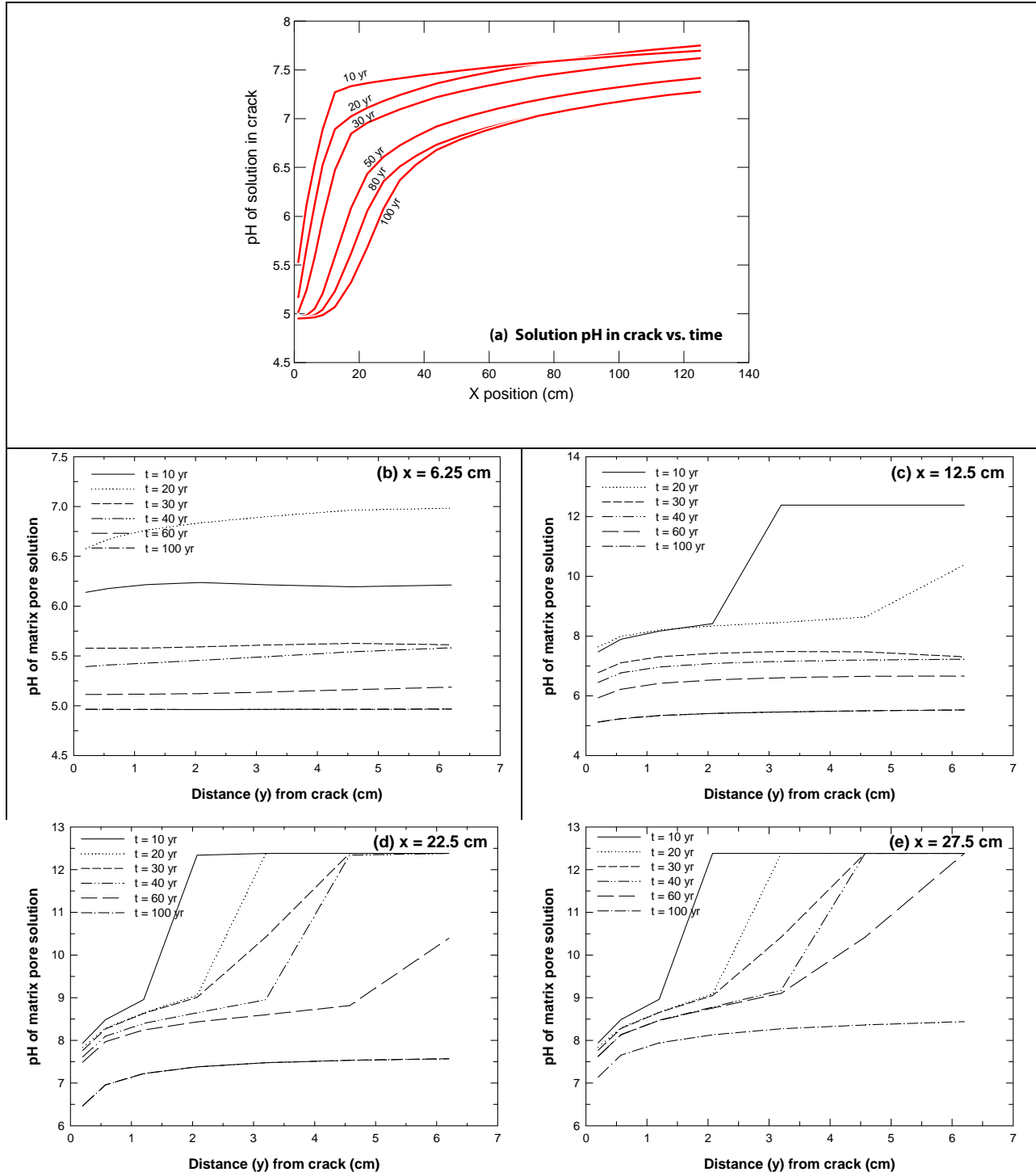
Figure 5-17. Solution pH in Concrete Crack (a) or Matrix (b) to (e) as a Function of Time, Distance (y) From the Crack, and/or Distance (x) From the Inlet.
Crack Half-Aperture = 0.15 cm [0.059 in]. Inlet Specific Discharge = 4.0 cm^3/cm^2·day [1.6 in^3/in^2·day]. A Typical Thickness of Rebar Concrete Cover is 5.1 cm [2.0 in].
[1 cm = 0.39 in]
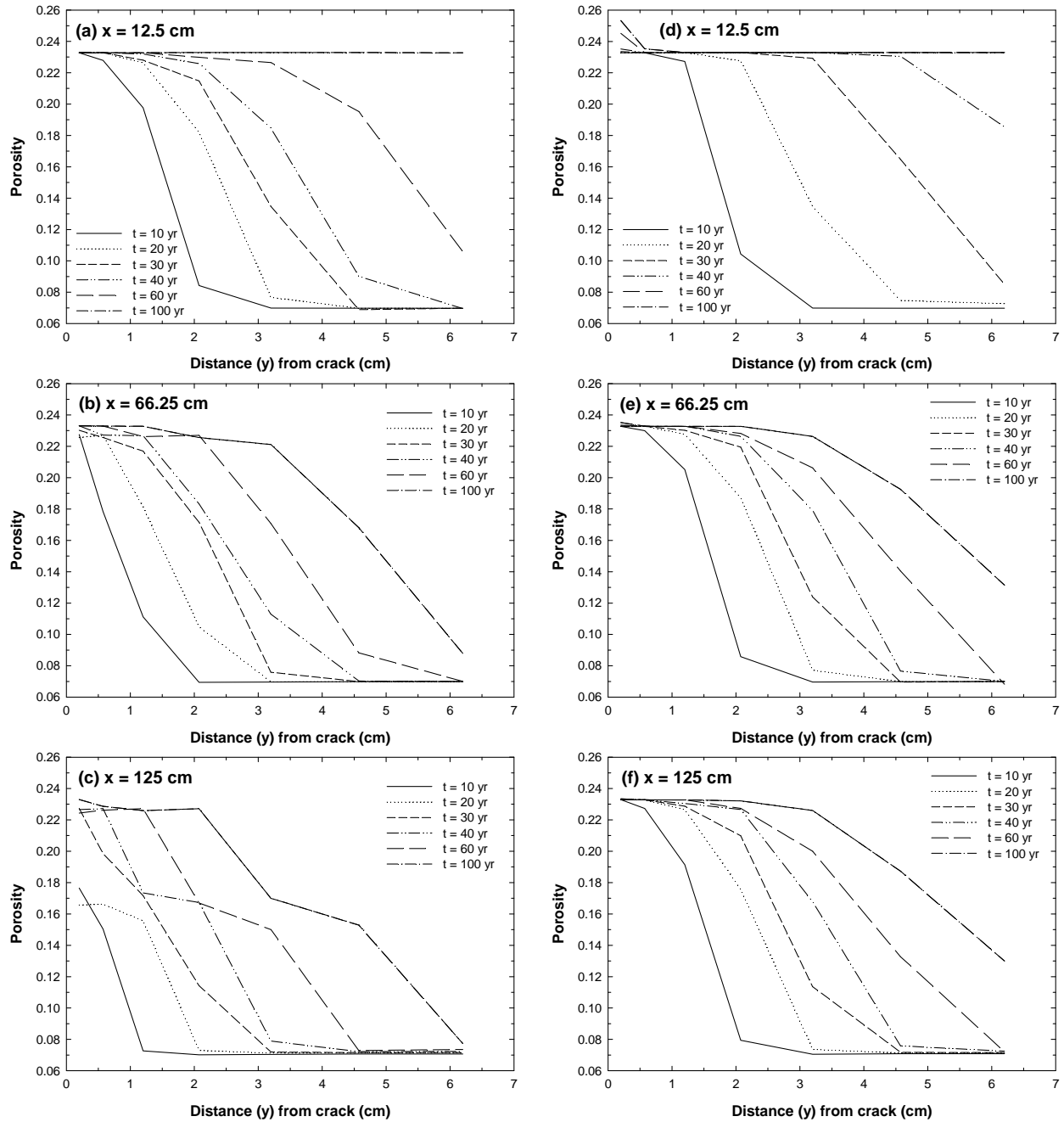
Figure 5-18. Concrete Porosity as a Function of Time, Distance (y) From the Crack, Distance (x) From the Inlet, and Inlet Flow Rate. Figures 5-17(a) to (c) Are Simulation Results for an Inlet Flow Rate of 0.2 cm³/cm²·day [0.079 in³/in²·day], Whereas Figures 5-17(d) to (f) Are for an Inlet Flow Rate of 1.0 cm³/cm²·day [0.39 in³/in²·day]. Initial Concrete Porosity = 0.07. Crack Half-Aperture = 0.15 cm [0.059 in]. [1 cm = 0.39 in]

layer. The porosity decreases with increasing distance from the crack due to lesser dissolution of cement minerals, eventually attaining the initial porosity of 0.07. Concrete porosity is higher at the higher flow rate due to a higher degree of concrete leaching. At 100 years of simulation time, a leached layer thicker than the typical concrete cover of 5.1 cm [2.0 in] has formed near the crack inlet {x = 12.5 cm [4.0 in]}.

The changes in concrete mineralogy due to concrete leaching are illustrated in Figure 5-19 as functions of time and distance from the crack. The plotted results are for a distance of 27.5 cm [10.9 in] from the inlet. With increasing time, a dissolution front propagates into the concrete, resulting in the formation of a leached layer dominated by the hematite, hydrotalcite, and silica (quartz).

5.3.2   Implication for Rebar Corrosion in Cracked Concrete

The 2-D reactive transport simulations indicate that concrete provides significant chemical reactivity to neutralize the acidic pH of borated water that may leak from an SFP, flow into a crack in the SFP concrete structure, and diffuse into the concrete matrix. However, the simulation results indicate that rebar close to the crack inlet, whether exposed in the crack or covered by concrete, can become susceptible to corrosion. This susceptibility will depend on the concrete aperture and solution flow rate, in addition to solution concentration. At the lowest flow rate used in the simulations, the boric acid solution is quickly neutralized, exceeding the threshold pH (~7.1) for rebar corrosion within ~4 cm [~1.6 in] of the inlet even after 30 years of flow. At a higher flow rate approximately similar to that of borated water leakage at the Salem Fuel Handling Building, it takes a longer flow distance {~12 cm [4.7 in]} to increase the solution pH in the crack above the rebar corrosion threshold pH at 30 years. At a flow rate 12 times higher than that observed at the Salem Fuel Handling Building, it takes approximately 30 cm [11.8 in] before the threshold pH is exceeded at 30 years. Thus, rebar exposed in the crack close to the borated water inlet could be susceptible to corrosion. Rebar exposed in the crack farther from the inlet would be less susceptible to corrosion, but would become more susceptible to corrosion with increasing flow duration. Similarly, rebar embedded in the concrete but close to the flow inlet would be the most susceptible to corrosion. At the lowest flow rate used in the simulation, rebar close to the inlet {x = 3.75 cm [1.48 in]} would be protected from corrosion for 30 years, but could be subject to corrosion afterwards. Rebar embedded in concrete and located farther away from the inlet would be less subject to corrosion. However, increases in flow rate and flow period would result in increased dissolution, increased porosity, and decreased solution pH in the concrete. Thus, the concrete cover may provide little protection to rebar embedded in concrete but located near the inlet if the boric acid flow rate is high enough and/or the flow duration is long enough.
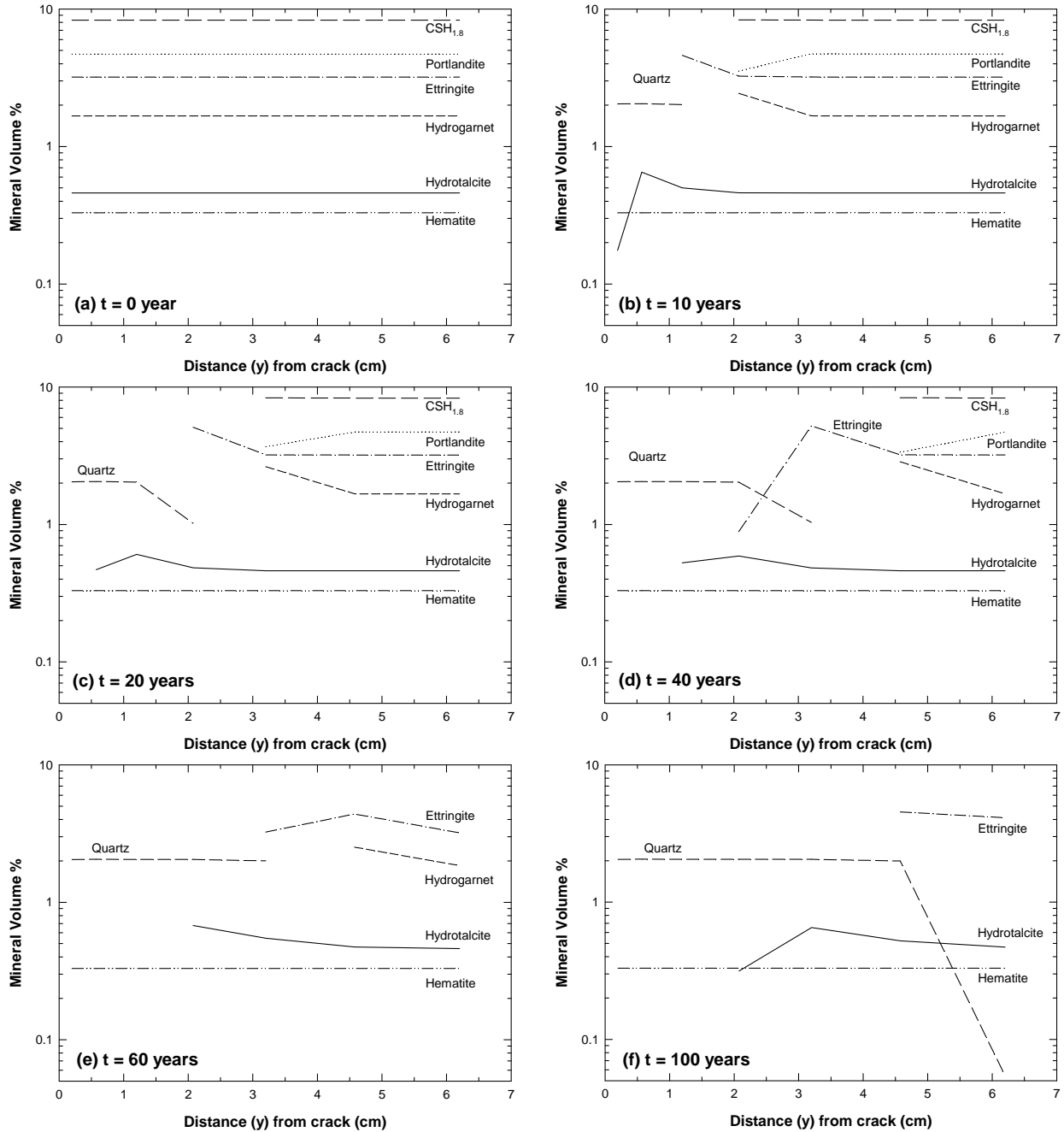
Figure 5-19. Mineral Distribution (Volume%) in the Concrete as a Function of Time and Distance (y) From the Crack. The Results Shown Are for a Distance (x) of 27.5 cm [10.8 in] From the Inlet, a Crack Half-Aperture of 0.15 cm [0.059 in], and an Inlet Specific Discharge of 0.2 $cm^3/cm^2 \cdot day$ [0.079 $in^3/in^2 \cdot day$]. Aggregate (Represented by Rutile) Remained Constant at 72 Volume% and is Not Shown.
[1 cm = 0.39 in]

6 SUMMARY

Spent fuel pool concrete structures exposed to borated water could degrade by leaching of the cement-based material and by corrosion of the reinforcement steel. Published studies indicate that when concrete comes in contact with acid solutions, the hydrated phases (C-S-H, portlandite, monosulfate, ettringite) in the concrete cement matrix dissolve at a rate that depends on the concrete permeability, the concentration and type of acid, and the type of reaction products that form. The quantity of solution that comes into contact with the concrete surface per unit time (i.e., the solution flow rate) also can affect the rate and degree of leaching. Leaching can have several adverse effects on cement and concrete, including increased porosity, decreased compressive strength and modulus of elasticity, increased material ductility, and reduced fracture energy. These effects have been ascribed to portlandite dissolution and, to a lesser degree, decalcification of the C-S-H phase.

Most published studies on cement and concrete leaching have used strong acids such as hydrochloric, nitric, and sulfuric acids. In contrast to those acids, boric acid is a weak acid that does not dissociate in aqueous solution. It is acidic due to its interaction with water to form borate $[B(OH)_4{}^-]$ and hydronium $[H^+]$ ions. Only a few published studies were found on the effect of boric acid on cement and concrete properties. In those studies, boric acid did not have a significant deleterious effect on cement and concrete properties and affected the properties differently than the strong acids. Concrete immersed in boric acid solutions exhibited an increase in compressive strength, tensile strength, and elastic modulus. Hydrated cement pastes immersed in boric acid solutions showed an increase in weight, bulk density, and compressive strength, but the porosity decreased due to the formation of poorly soluble calcium borate hydrates in the pore system of the hardened cement paste. Calcium borate formation from boric acid reaction with cement systems was observed in different studies, suggesting its potential importance in reducing the permeability of concrete or to autogenous healing of microcracks in concrete. In one study that flowed boric acid solutions through concrete cracks, the alkaline character of the solids adjacent to the crack was observed to decrease due to dissolution reactions.

The corrosion rate of steel in intact concrete is usually low because of a protective passive oxide film on the steel surface that is stable under the alkaline pH of the cement pore solution. However, corrosion may occur at an accelerated rate when the passive film breaks down, which can be caused by a reduction in the pH of the cement pore solution (e.g., by reaction with boric acid solution) or an ingress of chloride ions. No quantitative data on corrosion rates of carbon steel in concrete in the presence of boric acid were found in published literature, and available data are equivocal on the effect of boric acid on rebar corrosion.

Various methods are available for assessing corrosion of steel embedded in concrete. The corrosion test coupon method is a simple, long-established method and, if used properly, is the most reliable method for corrosion assessment. However, this method is slow when used for corrosion rate measurements, requiring 3-month to 1-year exposure times for applications in industrial process streams and longer timeframes for applications in concrete structures. In contrast, corrosion sensors can provide nearly instantaneous measurements and have been used to assess the corrosion rate of steel in concrete. Corrosion sensor techniques that have been used for corrosion detection or corrosion rate measurements in concrete include (i) electrochemical linear polarization resistance, (ii) electrochemical noise, (iii) coupled multielectrode array sensor, (iv) galvanic coupling, (v) electrical resistance, (vi) eddy current, and (vii) ultrasonic methods. Of these methods, the linear polarization resistance and the coupled multielectrode array sensor methods can give nearly instantaneous indications of

corrosion rate and can be used to measure rebar corrosion rate in intact concrete or in concrete cracks filled with aggressive solutions.

The published literature reviewed for this report appears to suggest that boric acid does not significantly degrade concrete properties. However, the published data are mostly based on immersion tests and are applicable to systems involving no flow of the boric acid solution. The one study that flowed boric acid solutions through concrete cracks showed that the concrete alkalinity adjacent to the crack decreased due to dissolution reactions and that reinforcement bars contacted by boric acid solutions showed considerably more corrosion than those contacted by neutral water. Although none of the rebars in that study had significant reductions in cross section after 2 years of testing, the authors of that study concluded that increased corrosion is expected at longer flow periods, particularly at wider crack widths and lower solution pH.

Given the uncertainty and lack of sufficient data on the effect of boric acid on rebar corrosion and concrete degradation, experiments were performed to determine this effect. Three test methods initially were used for the experiments. In Test Method 1, rebar corrosion rates at room temperature (~24 °C) [~75 °F], 40 °C [104 °F], and 55 °C [131 °F] were measured in boric acid (1,200 and 2,400 ppm B) solution, in simulated cement pore solution, and in a mixture of boric acid (2,400 ppm B) solution and simulated cement pore solution. In Test Method 2, rebar corrosion rates were measured in boric acid (2,400 ppm B) solution flowing in a simulated concrete crack. In Test Methods 1 and 2, the corrosion rates were measured using CMAS and LPR probes and by a rebar coupon weight loss method. Test Method 2 was supplemented by corrosion measurements using other methods because the initial test was hampered by flow channeling in the simulated crack. In Test Method 3, petrographic examination of concrete cylinders reacted with boric acid (1,200 and 2,400 ppm B) solution for 180, 240, and 300 days was conducted and the depth of concrete degradation due to boric acid leaching was measured. In addition, the compressive strength of the concrete cylinders that were reacted with boric acid solution for 300 days was measured.

The results indicate that rebar corrosion rates generally increase with temperature and boric acid concentration. The corrosion rate is low (~1 μm/yr or less) [~3.94×0^{-5} in/yr or less] when the solution pH is ~7.1 or higher. Below pH ~7.1, the corrosion rate increases with decreasing pH and can reach ~100 μm/yr [~3.94×10^{-3} in/yr] in solutions with pH less than ~6.7. The threshold pH for carbon steel corrosion in borated solution is between 6.8 and 7.3. The rebar corrosion rates determined in this study agree well with carbon steel corrosion rate data in published literature.

Petrographic examination of concrete cylinders that were immersed in boric acid solutions indicated that the cement paste affected by boric acid leaching is very soft, highly porous, and retains very little inherent strength. The affected paste exhibits a color change from grey to white in some specimens or to yellowish in others. Boric acid crystals also were observed to have deposited in near-surface voids of some specimens. The average depth affected by boric acid leaching increased with time, solution concentration, and temperature. The degradation depths due to boric acid leaching measured in this study are consistent with a square-root-of-time dependence similar to data from an EPRI study. However, the boric acid leaching rate determined in the EPRI study is significantly higher than the rates measured in the present study.

The measured compressive strength of concrete cylinders that were reacted with 2,400 ppm B solution for 300 days is higher than that of cylinders that were reacted with 1,200 ppm B

solution. This observation is consistent with literature data that showed higher compressive strength of concrete that was immersed in 25 wt% boric acid solution compared to concrete that was immersed in 1.2 wt% boric acid solution. Data from this study indicate that solution temperature has a significant effect on compressive strength. The measured compressive strength of concrete cylinders that were immersed in 2,400 ppm B solution at 60 °C [140 °F] is much lower than those of cylinders that were immersed in 2,400 ppm B solution at room temperature. Unfortunately, compressive strength measurements on concrete cylinders that were immersed in tap water or kept in a controlled temperature–relative humidity chamber for 300 days gave unexpectedly low values, which cannot be explained. Because of the unexpected results for the control and tap water samples, there is uncertainty in the measured compressive strengths of the concrete cylinders that were immersed in boric acid solutions.

1-D and 2-D reactive transport simulations were conducted to determine the degree of concrete dissolution and pH change that may occur as boric acid solution diffuses into the matrix or flows in the crack of a reinforced concrete structure. Simulations up to 100 years were performed using different boric acid concentrations, crack apertures, and solution flow rates. The depth of concrete leaching by boric acid solution derived from the 1-D model agrees relatively well with the Test 3 leaching depth data. The 1-D simulation results indicate that leaching by boric acid solution diffusing into concrete is mitigated by the acid-neutralizing capacity of the cement minerals such that reinforcement steel with a 5.1-cm [2-in] concrete cover is unlikely to undergo corrosion for at least 77 years. The 2-D simulation results indicate that concrete provides significant chemical reactivity to neutralize the acidic pH of borated water that may leak from an SFP, flow into a crack in the SFP concrete structure, and diffuse into the concrete matrix. However, reinforcement steel close to the crack inlet, whether exposed in the crack or covered by concrete, can become susceptible to corrosion depending on the crack aperture, solution flow rate and duration, and boric acid concentration.

7 RECOMMENDATIONS

The rebar corrosion rate measurements in this study were performed under aerated conditions. Under deaerated conditions, literature data indicate that carbon steel and low alloy steel corrosion rates in borated water are low (Nickell, 1988; EPRI, 2001). Based on the assumption that borated water present in SFP concrete joints will be deaerated and on the low corrosion rate in deaerated systems reported in the literature, Simons, et al. (2011) concluded that rebar corrosion in SFP concrete structures due to borated water leakage would be insignificant. The borated water in the SFP is saturated with respect to oxygen (EPRI, 2007). Simons, et al. (2011) explained that borated water that leaks from the SFP will become deaerated because oxygen will be quickly consumed in oxidation reactions with the carbon steel rebar, leakage channels, or other carbon steel surfaces in the SFP structure. However, the assumption of Simons, et al. (2011) about deaerated borated water is unsupported by comparison to empirical data. The degree to which borated water in SFP concrete joints or cracks becomes deaerated will depend on several factors, including the amount of steel material, borated water pH and flow rate, and steel corrosion (oxygen depletion) rate. Because it is impractical to measure the oxygen concentration of borated water in the leakage channels underneath the SFP liner and in the joints or cracks of SFP concrete structures, the reactive transport modeling discussed in Section 5 could be expanded to include oxygen consumption by carbon steel corrosion. Because even trace amounts of oxygen could significantly increase rebar corrosion rate, additional measurements would be useful to generate rebar corrosion rates in borated water as a function of oxygen concentration.

Experiments can complement and validate the reactive transport modeling presented in Section 5. The experimental design used in Test Method 2 can be improved to eliminate flow channeling of borated water in the simulated concrete crack. Microflow pH electrodes should be emplaced along the simulated crack, in addition to the coupled multielectrode array sensor and linear polarization resistance probes, such that both solution pH and corrosion rate can be monitored in real time. These experiments would provide information on the correlation between pH and corrosion rate and on the longevity of the alkaline pH buffering by the cementitious material.

The tests that measured the compressive strength of concrete cylinders that were immersed in boric acid solution should be repeated. A larger number of samples should be used such that measurements can be made on samples immersed for different time periods.

8 REFERENCES

Agarwala, V.S. and S. Ahmad. "Corrosion Detection and Monitoring—A Review." CORROSION/2000. Paper No. 271. Houston, Texas: NACE International. 2000.

Al-Madani, F., Z. Muhammad, P. Gaydecki, and G. Miller. "Signal Profiles and Images of Corroded Steel Bars in Concrete Generated by Inductive Scanning Technique Using Heterodyning Sensor." CORROSION/2010. Paper No. 10167. Houston, Texas: NACE International. 2010.

ASTM International. "Standard Practice for Petrographic Examination of Hardened Concrete." ASTM C856–11. West Conshohocken, Pennsylvania: ASTM International. 2011.

———. "Standard Practice for Preparing, Cleaning, and Evaluating Corrosion Test Specimens." ASTM G1–03. West Conshohocken, Pennsylvania: ASTM International. 2010.

———. "Standard Test Method for Conducting Potentiodynamic Polarization Resistance Measurements." ASTM G59–97. West Conshohocken, Pennsylvania: ASTM International. 2009a.

———. "Standard Test Method for Compressive Strength of Cylindrical Concrete Specimens." ASTM C39/C39M–09a. West Conshohocken, Pennsylvania: ASTM International. 2009b.

———. "Standard Guide for Online Monitoring of Corrosion in Plant Equipment (Electrical and Electrochemical Methods." ASTM G96–90. West Conshohocken, Pennsylvania: ASTM International. 2008.

———. "Standard Practice for Making and Curing Concrete Test Specimens in the Laboratory." ASTM C192/C192M–07. West Conshohocken, Pennsylvania: ASTM International. 2007.

———. "Standard Guide for Examination and Evaluation of Pitting Corrosion." ASTM G46–94. West Conshohocken, Pennsylvania: ASTM International. 2005.

———. "Standard Practice for Calculation of Corrosion Rates and Related Information from Electrochemical Measurements." ASTM G102–89. West Conshohocken, Pennsylvania: ASTM International. 2004.

Bajza, A., I. Rouseková, and M. Dubík. "Can Boric Acid Corrode Concrete?" V. Bilek and Z. Kersner, eds. International Symposium on Non-Traditional Cement and Concrete, Brno University of Technology, Brno, Czech Republic. pp. 447–456. 2002.

Barbarulo, R. "Modeling Chemical Degradation of Cement Pastes in Contact with Aggressive Solutions: Leaching and Carbonation." International RILEM Symposium on Concrete Modeling—CONMOD'08. May 26–28, 2008. Delft, The Netherlands. pp. 213–223. 2008.

Bertolini, L., B. Elsener, P. Pedeferri, and R. Polder, eds. *Corrosion of Steel in Concrete: Prevention, Diagnosis, Repair.* Weinheim, Germany: Wiley-VCH Verlag GmbH & Co. 2004.

Bethke, C.M. "Geochemical and Biogeochemical Reaction Modeling." New York City, New York: Cambridge University Press. 2008.

Blanc, P., X. Bourbon, A. Lassin, and E.C. Gaucher. "Chemical Model for Cement-Based Materials: Temperature Dependence of Thermodynamic Functions for Nanocrystalline and Crystalline C-S-H Phases." *Cement and Concrete Research.* Vol. 40. pp. 851–866. 2010.

Bothe, J.V. and P.W. Brown. "Kinetics of Tricalcium Aluminate Hydration in the Presence of Boric Acid and Calcium Hydroxide." *Journal of the American Ceramic Society.* Vol. 82. pp. 1,882–1,888. 1999.

Broomfield, J.O. "Corrosion Monitoring." Chapter 5. *Corrosion of Steel in Concrete– Understanding, Investigation and Repair.* 2nd Edition. New York City, New York: Taylor & Francis. pp. 103–111. 2007.

Brossia, C.S. "Electrical Resistance Techniques." Chapter 11. *Techniques for Corrosion Monitoring.* L. Yang, ed. Cambridge, England: Woodhead Publishing. pp. 277–292. 2008.

Carde, C. and R. Francois. "Modeling the Loss of Strength and Porosity Increase Due to the Leaching of Cement Pastes." *Cement and Concrete Composites.* Vol. 21. pp. 181–188. 1999.

———. "Effect of the Leaching of Calcium Hydroxide from Cement Paste on Mechanical and Physical Properties." *Cement and Concrete Research.* Vol. 27. pp. 539–550. 1997.

Cottis, R.A. "Electrochemical Noise for Corrosion Monitoring." Chapter 4. *Techniques for Corrosion Monitoring.* L. Yang, ed. Cambridge, England: Woodhead Publishing. pp. 86–110. 2008.

Davison, P.J. "Update to December 14, 2010 PSEG Nuclear, LLC Response to NRC Request for Additional Information Related to Structures Monitoring Associated with the Salem Nuclear Generating Station, Units 1 and 2 License Renewal Application." Letter (February 25) to U.S. Nuclear Regulatory Commission. Hancocks Bridge, New Jersey: PSEG Nuclear, LLC. 2011.

Dean, S.W. Jr. "Electrochemical Methods of Corrosion Testing." In *Electrochemical Techniques for Corrosion.* R. Baboian, ed. Houston, Texas: NACE International. pp. 52–60. 1977.

De Windt, L. and R. Badreddine. "Modelling of Long-Term Dynamic Leaching Tests Applied to Solidified/Stabilised Waste." *Waste Management.* Vol. 27. pp. 1,638–1,647. 2007.

Dillard, J.D. and J.O. Glanville. "Composition and Method for Combatting Chloride-Induced Corrosion in Steel in Reinforced Concrete." U.S. Patent Number 5,092,923. Issued March 3, 1992.

EPRI. "Pressurized Water Reactor Primary Water Chemistry Guidelines—Revision 6." Report No. 1014986. Palo Alto, California: Electric Power Research Institute. 2007.

———. "Boric Acid Corrosion Guidebook, Revision 1: Managing Boric Acid Corrosion Issues at PWR Power Stations." EPRI Report 1000975. Palo Alto, California: Electric Power Research Institute, Inc. 2001.

Fattuhi, N.I. and B.P. Hughes. "The Performance of Cement Paste and Concrete Subjected to Sulphuric Acid Attack." *Cement and Concrete Research.* Vol. 18. pp. 545–553. 1988.

Fei, Z., R.G. Kelly, and J.L. Hudson. "Spatiotemporal Patterns on Electrode Arrays." *Journal of Physical Chemistry.* Vol. 100. pp. 18,986–18,991. 1996.

Galíndez, J.M., J. Molinero, J. Samper, and C.B. Yang. "Simulating Concrete Degradation Processes by Reactive Transport Models." *Journal de Physique IV* (Proceedings). Vol. 136. pp. 177–188. 2006.

Grube, H. and W. Rechenberg. "Durability of Concrete Structures in Acidic Water." *Cement and Concrete Research.* Vol. 19. pp. 783–792. 1989.

Hearn, N. "Self-Sealing, Autogenous Healing and Continued Hydration: What Is the Difference?" *Materials and Structures.* Vol. 31. pp. 563–567. 1998.

Huang, P., Y. Bao, and Y. Yao. "Influence of HCl Corrosion on the Mechanical Properties of Concrete." *Cement and Concrete Research.* Vol. 35. pp. 584–589. 2005.

Ingri, N. "Equilibrium Studies of Polyanions. 8. On the First Equilibrium Steps in the Hydrolysis of Boric Acid, a Comparison Between Equilibria in 0.1 M and 3.0 M NaClO4." *Acta Chemica Scandinavica.* Vol. 16. pp. 439–448. 1962.

Ingri, N., G. Lagerström, M. Frydman, and L.G. Sillén. "Equilibrium Studies of Polyanions. II. Polyborates in $NaClO_4$ Medium." *Acta Chemica Scandinavica.* Vol. 11. pp. 1,034–1,058. 1957.

Jin, X., N. Jin, and Y. Tian. "Study on the Behavior and Durability of Reinforced Concrete in Boric Acid Environment." *Key Engineering Materials.* Vols. 400–402. pp. 441–446. 2009.

Kamali, S., M. Moranville, E. Garboczi, S. Prené, and B. Gérard. "Hydrate Dissolution Influence on the Young's Modulus of Cement Pastes." Fifth International Conference on Fracture Mechanics of Concrete and Concrete Structures, Vail, Colorado, April 12–16, 2004. Detroit, Michigan: American Concrete Institute. 2004.

Kosakowski, G., P. Blum, D. Kulik, W. Pfingsten, H., Shao, and A. Singh. "Evolution of a Generic Clay/Cement Interface: First Reactive Transport Calculations Utilizing a Gibbs Energy Minimization Based Approach for Geochemical Calculations." *Journal of Environmental Science for Sustainable Society.* Vol. 3. pp. 41–49. 2009.

Kulik, D. and M. Kersten. "Aqueous Solubility Diagrams for Cementitious Waste Stabilization Systems: II. End-Member Stoichiometries of Ideal Calcium Silicate Hydrate Solid Solutions." *Journal of American Ceramic Society.* Vol. 84. pp. 3,017–3,026. 2001.

Lagerblad, B. "Leaching Performance of Concrete Based on Studies of Samples from Old Concrete Constructions." TR–01–27. Stockholm, Sweden: Swedish Nuclear Fuel and Waste Management Company. 2001.

Law, D.W., S.G. Millard, and J.H. Bungery. "Effect of Electrode Orientation on Linear Polarization Measurements Using Sensor Controlled Guard Ring." *British Corrosion Journal.* Vol. 35. pp. 136–140. 2000.

Lichtner, P.C., C.I. Steefel, and E.H. Oelkers, eds. "Reactive Transport in Porous Media." *Reviews in Mineralogy.* Vol. 34. Washington, DC: Mineralogical Society of America. 1996.

Light, G. "Nondestructive Evaluation Technologies for Monitoring Corrosion." Chapter 12. *Techniques for Corrosion Monitoring.* L. Yang, ed. Cambridge, England: Woodhead Publishing. pp. 293–312. 2008.

Mansfeld, F. "The Polarization Resistance Technique for Measuring Corrosion Currents." *Advances in Corrosion Science and Technology.* Fontana, M.G. and R.W. Staehle, eds. New York City, New York: Plenum Publishing. Volume 6. pp.185–187. 1976.

MPR Associates, Inc. "Salem Generating Station Fuel Handling Building Assessment of Current Structural Adequacy." Presentation to Spent Fuel Pool Liner/Structural Leakage Issues Workshop, May 19, 2004. Alexandria, Virginia: MPR Associates, Inc. 2004.

Neville, A.M. *Properties of Concrete.* New York City, New York: John Wiley & Sons. 1996.

Nickell, R.E. "Degradation and Failure of Bolting in Nuclear Power Plants." Vol. 1. Palo Alto, California: Electric Power Research Institute. 1988.

NRC. Information Notice No. 2006-13, "Ground-Water Contamination Due to Undetected Leakage of Radioactive Water." ML060540038. Washington, DC: NRC. 2006.

———. Information Notice No. 2004-05, "Spent Fuel Pool Leakage to Onsite Groundwater." ML040580454. Washington, DC: NRC. 2004.

Oldham, K.B. and F. Mansfeld. "Corrosion Rates from Polarization Curves: A New Method." *Corrosion Science.* Vol. 13. pp. 813–819. 1973.

Pabalan, R.T., F.P. Glasser, D.A. Pickett, G.R. Walter, S. Biswas, M.R. Juckett, L.M. Sabido, and J.L. Myers. "Review of Literature and Assessment of Factors Relevant to Performance of Grouted Systems for Radioactive Waste Disposal." CNWRA 2009-001. San Antonio, Texas: CNWRA. 2009.

Pavlík, V. "Corrosion of Hardened Cement Paste by Acetic and Nitric Acids. Part III: Influence of Water/Cement Ratio." *Cement and Concrete Research.* Vol. 26. pp. 475–490. 1996.

Papavinasam, S. "Electrochemical Polarization Techniques for Corrosion Monitoring." Chapter 3. *Techniques for Corrosion Monitoring.* L. Yang, ed. Cambridge, England: Woodhead Publishing. pp. 49–85. 2008.

Pensado, O., D.S. Dunn, G.A. Cragnolino, and V. Jain. "Passive Dissolution of Container Materials—Modeling and Experiments." CNWRA Report 2003-01. San Antonio, Texas: Center for Nuclear Waste Regulatory Analyses. 2003.

Poursaee, A. and C. M. Hansson. "Reinforcing Steel Passivation in Mortar and Pore Solution." *Cement and Concrete Research.* Vol. 37. pp. 1,127–1,133. 2007.

Ramm, W. and M. Biscoping. "Autogenous Healing and Reinforcement Corrosion of Water-Penetrated Separation Cracks in Reinforced Concrete." *Nuclear Engineering and Design.* Vol. 179. pp. 191–200. 1998.

Rannou, G., D. Thierry, and N. LeBozec. "Ultrasonic Monitoring of Steel Corrosion During Accelerated Corrosion Testing and Outdoor Field Exposures." CORROSION/2010. Paper No. 10170. Houston, Texas: NACE International. 2010.

Raupach, M. "Models for the Propagation Phase of Reinforcement Corrosion—An Overview." *Materials and Corrosion*. Vol. 57. pp. 605–613. 2006.

Saling, J.H., A.W. Fentiman, and Y.S. Tang. *Radioactive Waste Management*. 2nd Edition. New York City, New York: Taylor & Francis. 2001.

Samson, E. and J. Marchand. "Modeling the Transport of Ions in Unsaturated Cement-Based Materials." *Computers and Structures*. Vol. 85. pp. 1,740–1,756. 2007.

Schiebl, P. and C. Dauberschmidt. "Corrosion Monitoring in Concrete." Chapter 16. *Techniques for Corrosion Monitoring*. L. Yang, ed. Cambridge, England: Woodhead Publishing. pp. 388–424. 2008.

Scully, J.R. "The Polarization Resistance Method for Determination of Instantaneous Corrosion Rates: A Review." CORROSION/1998. Paper No. 304. Houston, Texas: NACE International. 1998.

Shimada, T., A. Iizuka, K. Shiojiri, A. Yamasaki, and Y. Yanagisawa. "pH-Controlled Uphill Transport of Boric Acid Through a Poly(Vinyl Alcohol) (PVA) Membrane." *Journal of Applied Polymer Science*. Vol. 104. pp. 1,451–1,455. 2007.

Simons, J., C. Bagley, R.B. Leating, and J.E. Nestell, Jr. "Supplement to MPR–2613 Revision 3: Additional Discussion of Rebar Corrosion." Report 0108-0301-37. Rev. 0. Hancocks Bridge, New Jersey: PSEG Nuclear, LLC. 2011.

Simons, J., R. Keating, J. Nestell, and M. Frey. "Repair and Replacement Applications Center: Boric Acid Attack of Concrete and Reinforcing Steel in PWR Fuel Handling Buildings." Report 1019168. Palo Alto, California: Electric Power Research Institute. 2009.

Stern, M. and A.L. Geary. "Electrochemical Polarization." *Journal of Electrochemical Society*. Vol. 104. pp. 56–63. 1957.

Sun, X. "Online Monitoring of Corrosion Under Cathodic Protection Conditions Utilizing Coupled Multielectrode Sensors." CORROSION/2004. Paper No. 04094. Houston, Texas: NACE International. 2004.

Sugiyama, D. and T. Fujita. "A Thermodynamic Model of Dissolution and Precipitation of Calcium Silicate Hydrates." *Cement and Concrete Research*. Vol. 36. pp. 227–237. 2006.

Sun, X. and L. Yang. "Real-Time Monitoring of Localized and General Corrosion Rates in Drinking Water Utilizing Coupled Multielectrode Array Sensors." CORROSION/2006. Paper No. 06094. Houston, Texas: NACE International. 2006.

Tyrer, M., A. Atkinson, E. Ganjian, and P. Claisse. "Autogenous Crack Healing in Composite Cementitious Barriers Using Calcium Borate Binders." <http://www.mtyrer.net/resources/Meiringen_Poster2.pdf> (31 March 2010).

van der Lee, J., L. De Windt, and V. Lagneau. "Application of Reactive Transport Models in Cement-based Porous Media." International RILEM Symposium on Concrete Modeling—CONMOD'08, pp. 463–470. May 26–28, 2008. Delft, The Netherlands. 2008.

Wang, L. "Near-Field Chemistry of a HLW/SF Repository in Boom Clay—Scoping Calculations Relevant to the Supercontainer Design." SCK•CEN-ER-17. Mol, Belgium: SCK•CEN. 2009.

Yang, L. "Multielectrode Systems." Chapter 8. *Techniques for Corrosion Monitoring*. L. Yang, ed. Cambridge, England: Woodhead Publishing. pp. 187–243. 2008.

Yang, L., K.T. Chiang, P.K. Shukla, and N. Shiratori. "Internal Current Effects on Localized Corrosion Rate Measurements Using Coupled Multielectrode Array Sensors." *Corrosion*. Vol. 66. pp. 115,005–115,017. 2010a.

Yang, L., K.T. Chiang, and P.K. Shukla. "Distributed Node Electrodes for Corrosion Monitoring of Concrete Rebar and Buried Pipes." CORROSION/2010. Paper No. 10166. Houston, Texas: NACE International. 2010b.

Yang, L., N. Sridhar, C.S. Brossia, and D.S. Dunn. "Evaluation of the Coupled Multielectrode Array Sensor as a Real Time Corrosion Monitor." *Corrosion Science*. Vol. 47. pp. 1,794–1,809. 2005.

Yang, L., N. Sridhar, O. Pensado, and D. Dunn. "An *In-Situ* Galvanically Coupled Multi-Electrode Array Sensor for Localized Corrosion." *Corrosion*. Vol. 58. p. 1,004. 2002.

Zivica, V. "Acidic Attack of Cement Based Materials—A Review. Part 3: Research and Test Methods." *Construction and Building Materials*. Vol. 18. pp. 683–688. 2004.

Zivica, V. and A. Bajza. "Acidic Attack of Cement-Based Materials—A Review. Part 2: Factors of Rate of Acidic Attack and Protective Measures." *Construction and Building Materials*. Vol. 16. pp. 215–222. 2002.

———. "Acidic Attack of Cement Based Materials—A Review. Part 1: Principle of Acidic Attack." *Construction and Building Materials*. Vol. 15. pp. 331–340. 2001.

APPENDIX A

CONCRETE RESEARCH & TESTING, LLC REPORT NO 393:
PETROGRAPHIC EXAMINATION OF THREE CONCRETE CYLINDERS TO
DETERMINE THE EFFECTS OF EXPOSURE TO BORIC ACID SOLUTION

REPORT NO. P-393

ON

PETROGRAPHIC EXAMINATION OF THREE
CONCRETE CYLINDERS TO DETERMINE THE
EFFECTS OF EXPOSURE TO BORIC ACID SOLUTION
(SWRI PROJECT NO. 15555.01.013)

TO

SOUTHWEST RESEARCH INSTITUTE
SAN ANTONIO, TEXAS

MARCH 30, 2011

CRT

Concrete Research & Testing, LLC

REPORT NO. P-393

ON

PETROGRAPHIC EXAMINATION OF THREE
CONCRETE CYLINDERS TO DETERMINE THE
EFFECTS OF EXPOSURE TO BORIC ACID SOLUTION
(SWRI PROJECT NO. 15555.01.013)

INTRODUCTION

Southwest Research Institute (SWRI), San Antonio, Texas, is currently researching the effects of boric

acid solution on concrete. Concrete cylinder specimens were prepared and exposed to the three

following conditions:

- Immersed in 1200 ppm boric acid solution at room temperature
- Immersed in 2400 ppm boric acid solution at room temperature
- Immersed in 2400 ppm boric acid solution at $60^{o}C$

Cylinders will be exposed to the boric acid solutions for periods of 180 days, 240 days and 300 days.

Concrete Research & Testing (CRT) was requested by SWRI to perform petrographic examination on

the concrete cylinder specimens following each of the exposure periods. The objective of the

petrographic examinations is to determine to what extent the concrete is affected by the boric acid

solutions.

The concrete mix design used for the project is shown in Table 1 of Appendix A. The concrete was

produced by Ingram Ready Mix, Inc., located in New Braunfels, Texas.

Three concrete cylinder specimens were received at CRT from Ken Chiang of SWRI on February 28,

2011. The received cylinder specimens were immersed in the boric acid solutions for a period of 180

days.

GENERAL DESCRIPTION OF THE SPECIMENS

The received specimens were labeled 'ASP-10-180, 7-21, 021942, 18, NP'. Each specimen was additionally labeled No. 13, No. 19 or No. 31. Photographs of the as-received specimens are shown in Figure 1 through Figure 3 of Appendix B. The specimens are standard 4 in. by 8 in. molded cylinders. The top and bottom surfaces of each specimen have been covered with a layer of epoxy. The epoxy layers are generally 2 to 5 mm thick. The testing condition for each specimen is shown below.

Specimen	Boric Acid Concentration, ppm	Test Temperature
No. 13	1200	Room Temperature
No. 19	2400	Room Temperature
No. 31	2400	60°C

EXAMINATION METHODS

A portion of the circumference of each specimen was first coated with epoxy to protect and preserve features of the exterior surface during the specimen preparation. The concrete specimens were then saw-cut perpendicular to the long axis of each specimen.

The saw-cut sections were prepared for microscopic examination by lapping on a steel wheel with progressively-finer silicon carbide grit. The lapped sections were then examined under a stereo-microscope at magnifications of 7X to 100X. The examinations were performed following the guidelines in ASTM C 856, "Standard Practice for Petrographic Examination of Hardened Concrete."

The depth of the affected cement paste was measured in each of the concrete specimens. The measurements were performed at a magnification of 10X, using a micrometer located in the eyepiece of the microscope. The average depth of the affected cement paste was determined from 20 random measurements made around the circumference of each cylinder specimen.

EXAMINATION RESULTS

The affected cement paste is very soft, highly porous and retains very little inherent strength. The affected paste exhibits a color change from grey to white in Specimen No. 13. In Specimens No. 19 and No. 31, the affected paste is white or yellowish in color.   Cross-section photographs taken under the microscope showing the attacked cement paste are presented in Figure 4 through Figure 6 of Appendix B. Areas of the affected cement paste layer are occasionally lost from the lapped surface during specimen preparation. The depth of the severely affected paste for each cylinder specimen is shown below.

Specimen	Depth of Affected Cement Paste	
	Range, mm	Average, mm*
No. 13	0.5 to 1.1	0.75
No. 19	0.6 to 1.2	0.85
No. 31	0.8 to 2.6	1.27

*Average of 20 measurements

In specimen No. 13 and specimen No. 19, there is a distinct transition from the weak, porous, affected cement paste to the dense, unaffected cement paste. This transition is less defined in specimen No. 31. Also, in specimen No. 31, a very thin (~0.1 mm) line of weak cement paste is present at a depth ranging from 1½ to 2½ mm from the exterior cylinder surface. The thin line of altered cement paste is judged to be related to acid attack, although it is unclear how it formed beyond a layer of good quality cement paste. Photographs of this feature are shown in Figure 7.

pH testing was performed on the concrete to determine the depth of the affected cement paste based on the pH. Concrete has a typical pH of 13. Acid attack of concrete will lower the pH. The sawcut, lapped surfaces of the cylinder specimens were sprayed with a pH indicating solution (phenolphthalein). When the solution is applied to concrete, the cement paste will turn pink at a pH above 9, and will remain uncolored at pH values below 9. Therefore the depth of the uncolored cement paste will indicate the depth to which the acid has affected the pH of the cement paste. Photographs showing cross-section

views of Specimen No. 31 are shown in Figure 8. In Specimen No. 13 and No. 19, the reduced pH extends only about 0.1 mm past the degraded cement paste. In Specimen No. 31, the reduced pH extends up to 1.2 mm beyond the degraded cement paste (see Figure 8).

The coarse aggregate is comprised of a natural gravel. The gravel is comprised of roughly 90 percent limestone particles and 10 percent chert particles. In Specimen No. 31, limestone coarse aggregate particles within the degraded cement paste exhibit evidence of acid attack. The acid attack has affected the aggregate particles to a very shallow depth (see Figure 9).

Voids present on the exterior surface of specimen No. 31 are lined with boric acid crystals. Boric acid crystals were also observed in near-surface voids of the cross-sections of this specimen. Photographs of the boric acid crystals are shown in Figure 10 and Figure 11.

As previously mentioned, the surfaces of the concrete specimens were coated with epoxy to protect the attacked cement paste during the sample preparation. Due to the weak, porous nature of the attacked cement paste, the epoxy material has penetrated into the affected cement paste of Specimen No. 19 and Specimen No. 31 (see Figure 5 and Figure 6). In Specimen No. 19, the epoxy has penetrated to a typical depth of 0.2 mm, while in Specimen No. 31, the epoxy has penetrated to a typical depth of 0.3 to 0.5 mm. The greater depth of penetration in Specimen No. 31 indicates a weaker, more absorptive cement paste relative to Specimen No. 19. A different, more viscous epoxy was used in the preparation of Specimen No. 13 which did not penetrate into the affected cement paste.

Jason Cummins, Petrographer
Concrete Research & Testing, LLC

Nick Scaglione, President & Petrographer
Concrete Research & Testing, LLC

APPENDIX A

Table 1. Mix design for concrete specimens used to test the effects of long term exposure to boric acid solutions. The concrete was produced by Ingram Ready Mix, Inc.

Constituent	SSD Batch Weights, lb/yd^3	Specific Gravity	Volume, ft^3
Portland Cement	560	3.15	2.85
Coarse Aggregate	2200	2.57	13.72
Fine Aggregate	966	2.63	5.89
Water	258.5	1.00	4.14
Entrapped Air Void Content	---	---	0.41
Water Reducing/Retarding Admixture	3.0 oz/cwt	---	---
Totals	3984.5	---	27.00

Water-Cementitious Ratio: 0.46

Target Air Void Content: 1½% ± 1½%

Theoretical Unit Weight: 147.6 lb/ft^3

Theoretical Cement Paste Content: 32.7%

APPENDIX B

Figure 1. As-received photographs of Specimen No. 13 (upper) and Specimen No. 19 (lower).

Figure 2. As-received photographs of Specimen No. 31.

Figure 3.   Photographs taken under the microscope of the exterior surface of Specimen No. 31.

B-3

Figure 4. **Cross-section photographs taken under the microscope showing the acid attacked cement paste of Specimen No. 13. In the lower photograph, the epoxy has pulled away a portion of the attacked cement paste.**
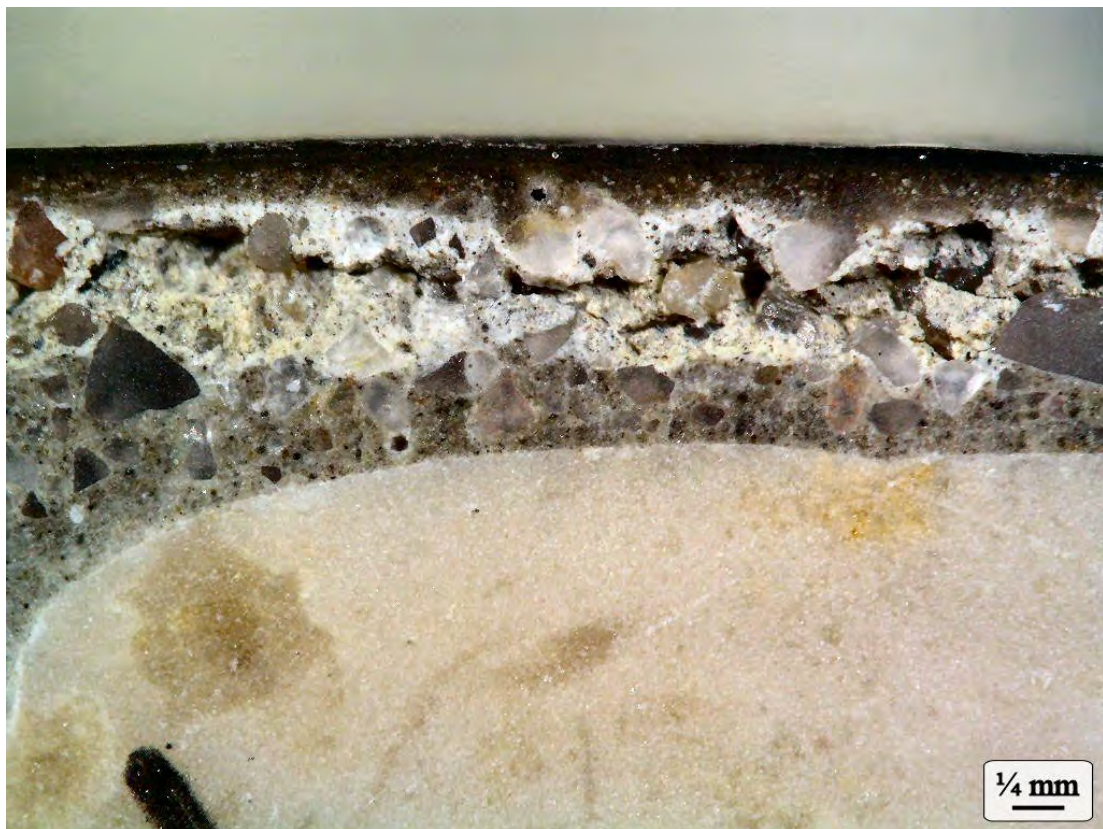
Figure 5. Cross-section photographs taken under the microscope showing the acid attacked cement paste of Specimen No. 19. The layers of penetrated epoxy can be seen in both photographs. In the lower photograph, some loss of material has occurred during the sample preparation.
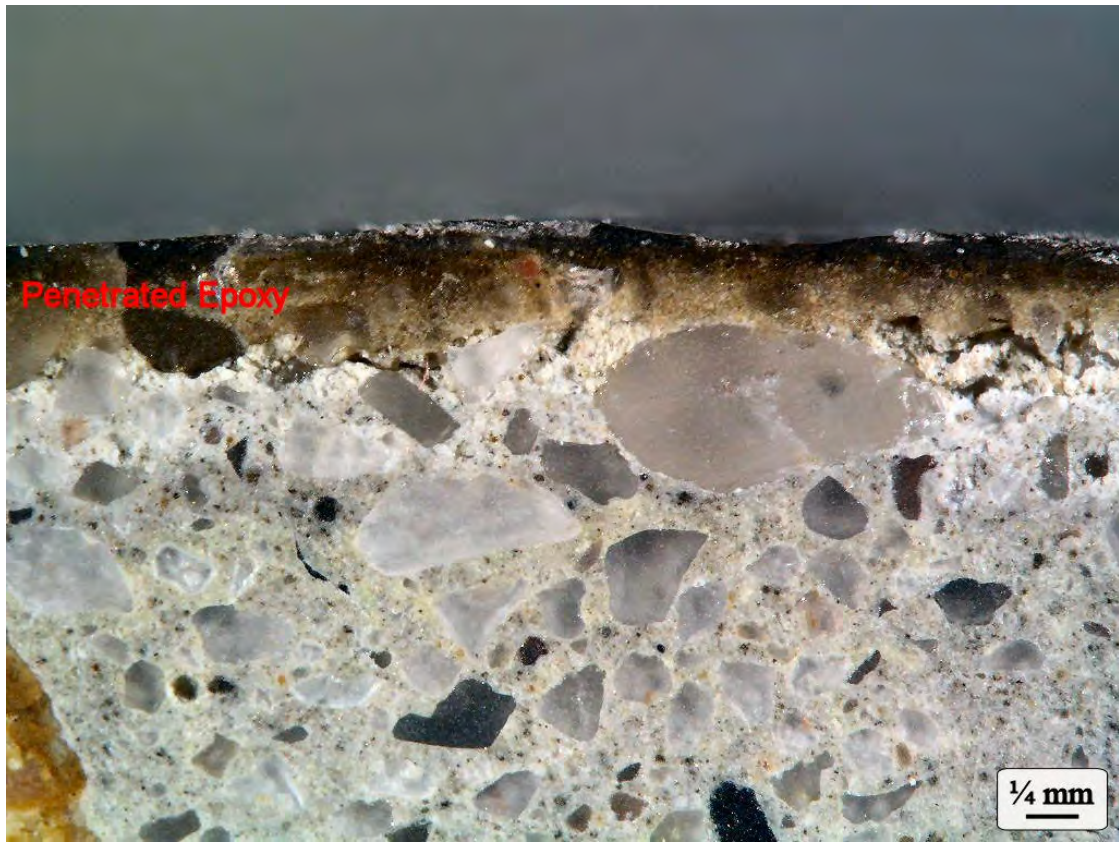
Figure 6. **Cross-section photographs taken under the microscope showing the acid attacked cement paste of Specimen No. 31.**
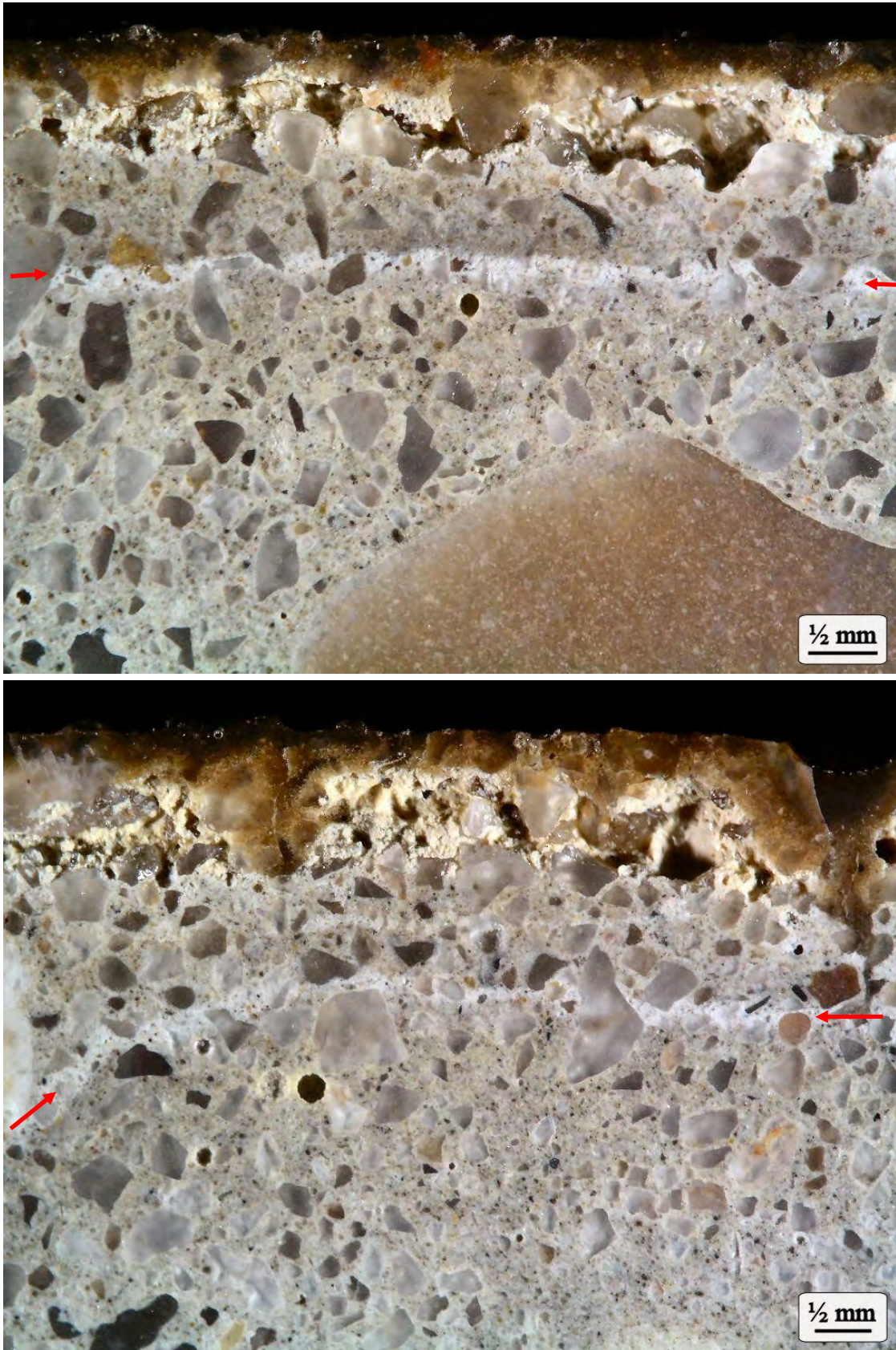
Figure 7. Cross-section photographs taken under the microscope showing the thin line of weak cement paste (arrows) present in the otherwise unaffected cement paste of Specimen No. 31.
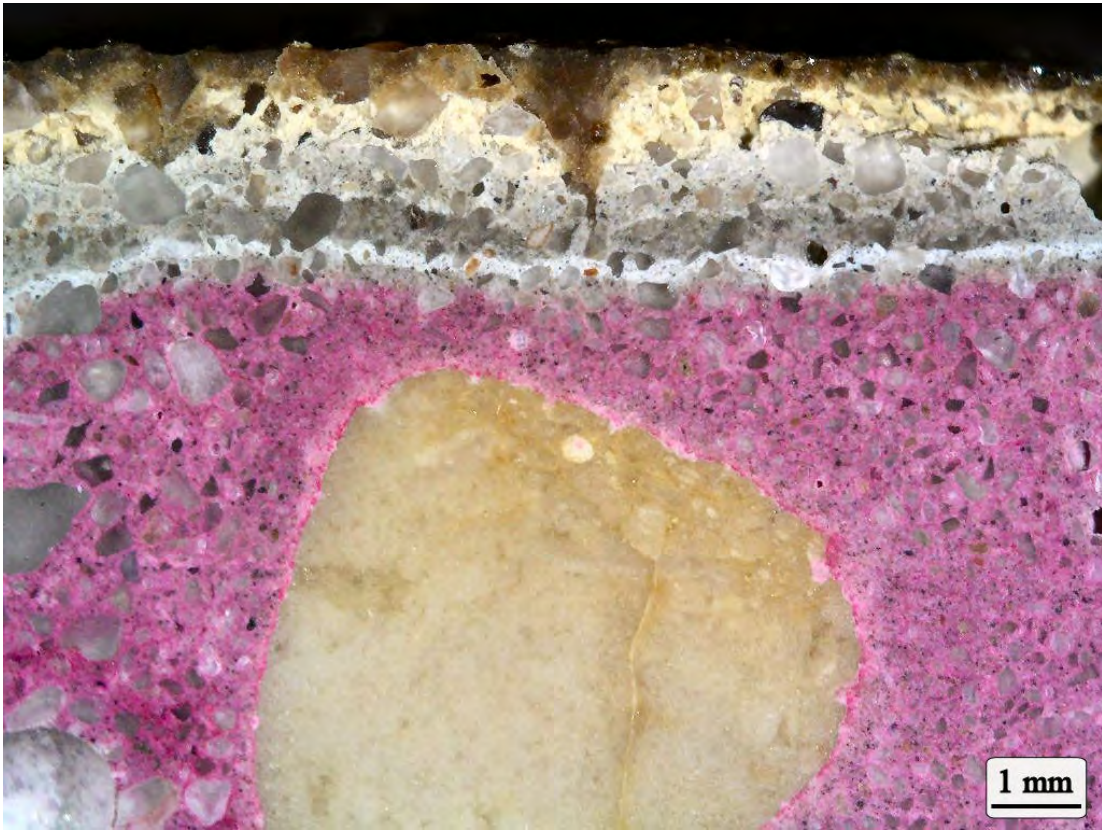
Figure 8. Cross-section photographs of Specimen No. 31 following the exposure to phenolphthalein solution. The depth to which the pH has been lowered by the acid exposure is represented by the uncolored cement paste.
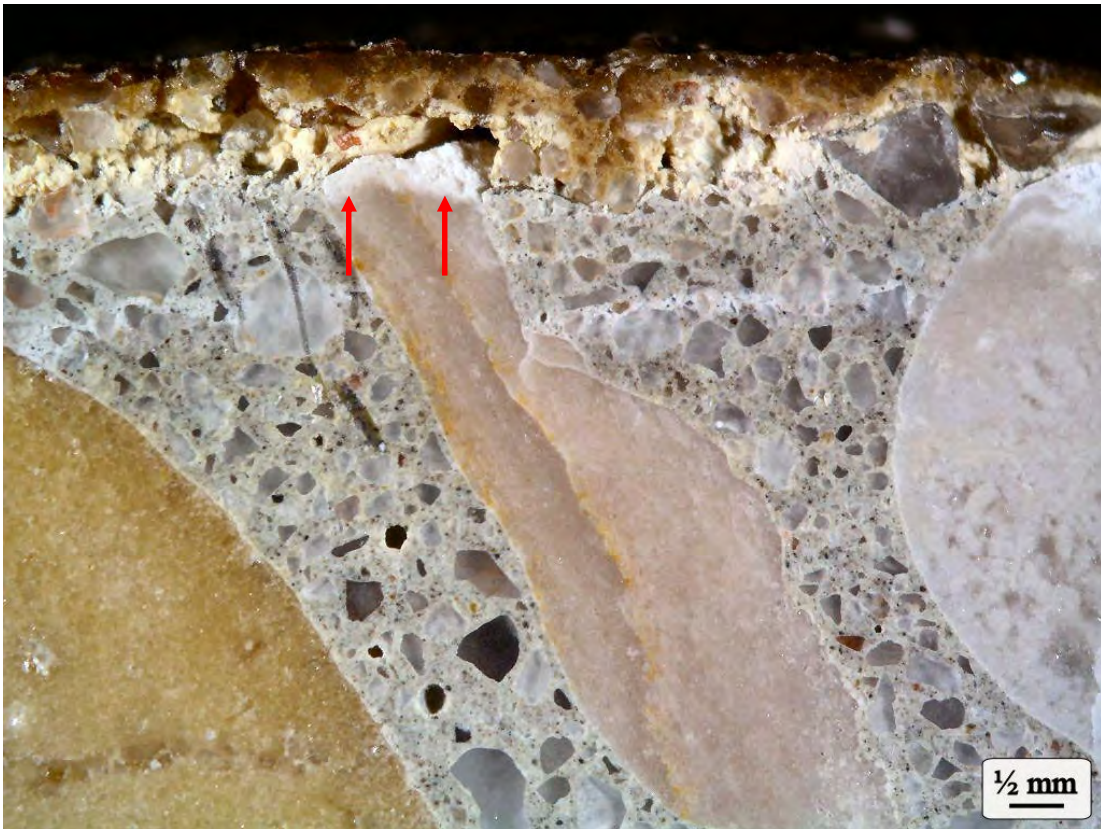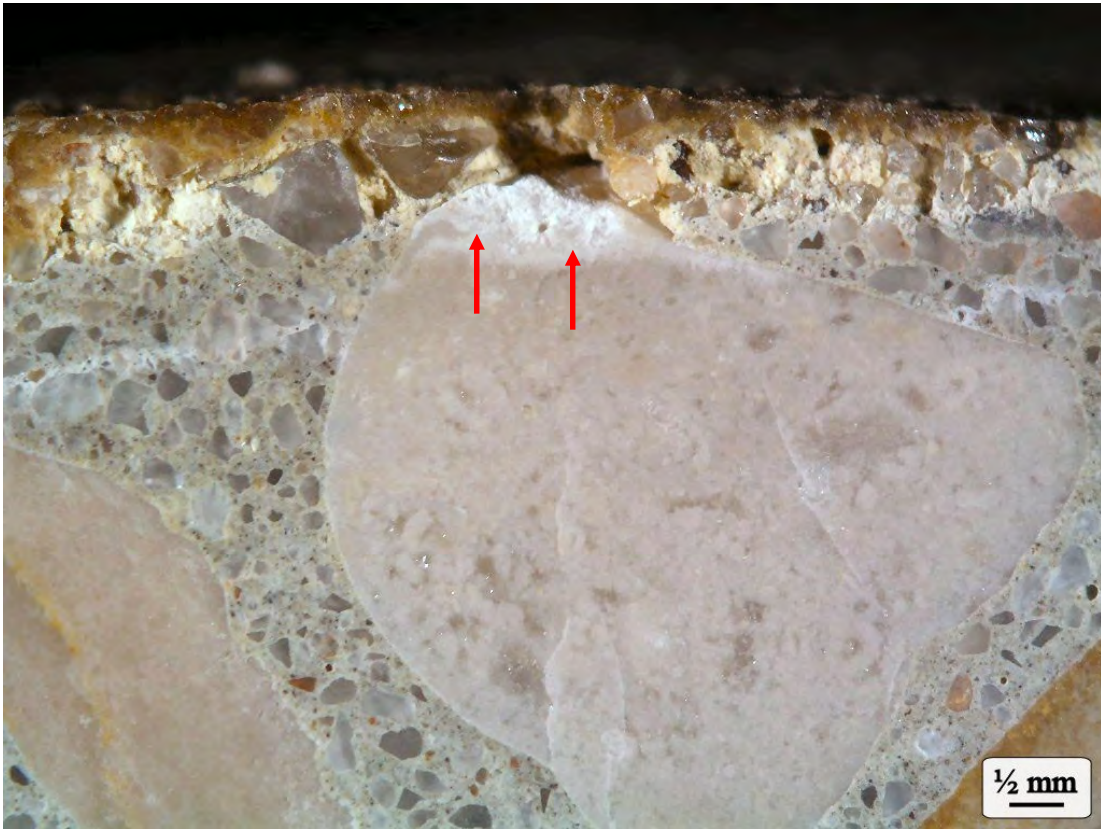
Figure 9. Cross-section photographs of Specimen No. 31 showing limestone coarse aggregate particles exhibiting acid attack.

Figure 10. Surface photographs taken under the microscope showing the boric acid crystals present within a surface void of Specimen No. 31.
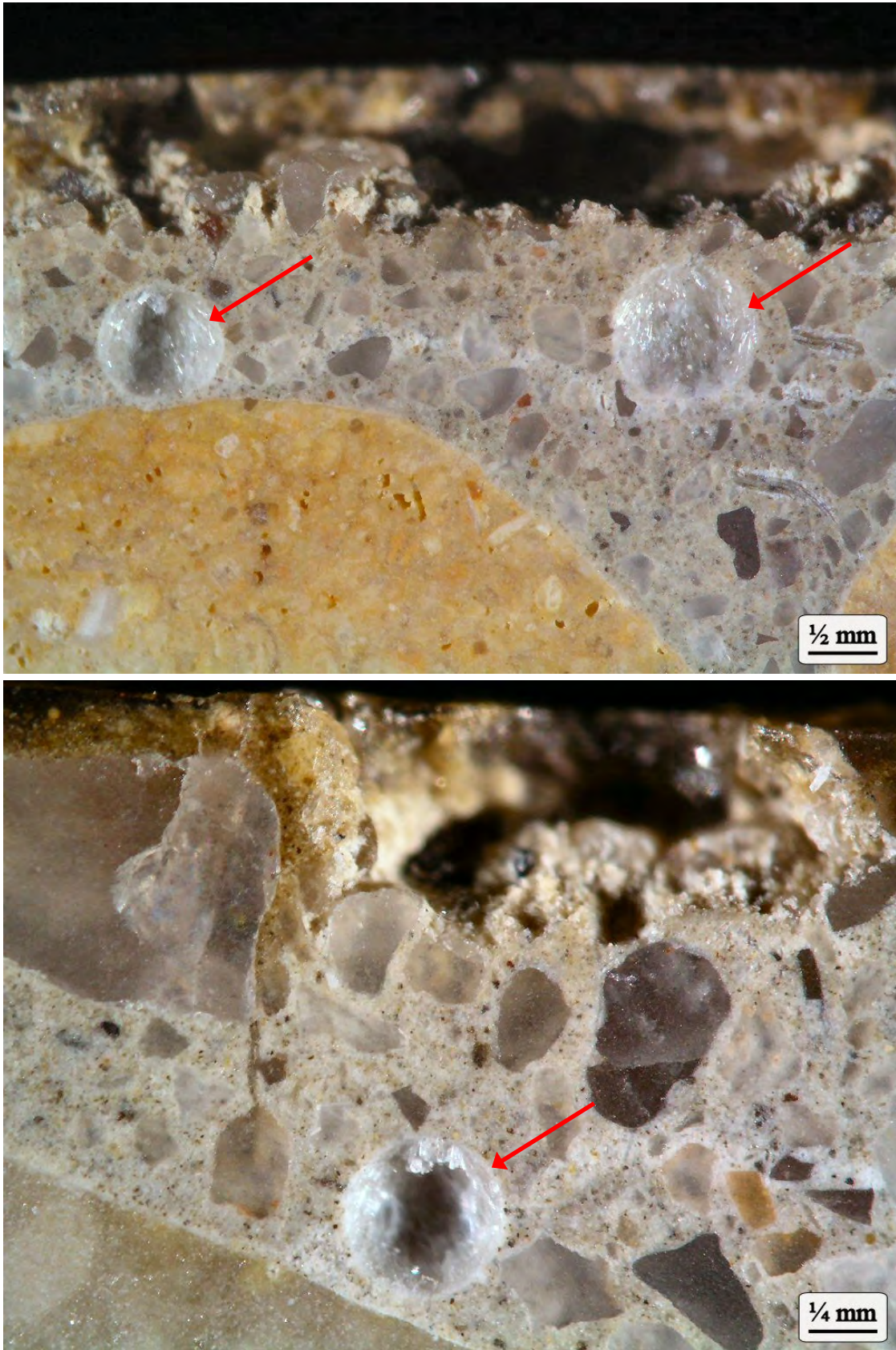
Figure 11. Cross-section photographs taken under the microscope showing the boric acid crystals present in the near-surface voids of Specimen No. 31.

APPENDIX C

Jason Cummins

Petrographer & Laboratory Manager, Concrete Research & Testing, LLC

Education

B.S. – Geology	*University of Massachusetts, Amherst*	**May 2000**

Employment

Concrete Research & Testing, LLC   *Columbus, Ohio*   **January 2001 to Present**

Concrete Petrographer   July 2006 to Present
- Perform petrographic examinations of concrete, aggregates and related materials
- Compose written reports providing the details and conclusions of petrographic examinations

Laboratory Manager   July 2004 to Present
- Calibrate and verify the operation of laboratory equipment and devices
- Supervise, train, and evaluate Laboratory Technicians
- Maintain and update company information and employee/equipment records
- Continue duties & responsibilities of a Laboratory Technician

Laboratory Technician   January 2001 to July 2004
- Prepare concrete, aggregates and related materials for petrographic examinations and testing
- Test concrete, aggregates and related materials according to standardized test procedures
- Produce written reports summarizing the results of the testing

Experience

Laboratory
- Petrographic examinations of concrete, aggregates and related materials
- Standardized (ASTM/AASHTO) testing of concrete, aggregates and related materials

Field
- Standardized (ASTM) testing of fresh concrete
- Specimen preparation for future laboratory testing

Certifications

American Concrete Institute
- Concrete Field Testing Technician – Grade I
- Concrete Strength Testing Technician
- Aggregate Testing Technician – Level 1
- Concrete Laboratory Testing Technician – Level 1

Ohio Ready Mixed Concrete Association
- Certified Concrete Technician

Professional Affiliations

American Concrete Institute (ACI) – Central Ohio Chapter
Society of Concrete Petrographers

Nick J. Scaglione
President, Concrete Research & Testing, LLC

Education

B.Sc., Geology – The Ohio State University, Columbus, Ohio	1987
Certified Concrete Technician – Ohio Ready Mix Concrete Association	1988
Concrete Field Testing Technician – American Concrete Institute	1988
Short Course in Refractory Concrete – Center for Professional Advancement	1991

Experience

Concrete Research & Testing, Columbus, Ohio President & Senior Petrographer	1996 - Present
Lankard Materials Laboratory, Columbus, Ohio Petrographer, Research Scientist & Technician	1986 - 1995

Affiliations

American Concrete Institute (ACI)
Central Ohio Chapter – Board Member (2008 – Present)

American Society for Testing and Materials (ASTM)
Committee C09 – Member
Subcommittees C09.65, C09.66, C09.26, C09.20 – Member
ASTM C457 Task Group – Chairman (2010)
Subcommittee C09.65 (Petrography) – Secretary (2010)

Society of Concrete Petrographers
Vice President (2010 – Present)
Treasurer (2007 – 2009)

Publications

Lankard, D.R., Bennett, J.E., Scaglione, N.S.; *Petrographic Examination of Reinforced Concrete from Cathodically Protected Structures*, Petrography of Cementitious Materials, ASTM STP 1215, 1994.

Presentations

Concrete under the Microscope. Presented to the Northeast Ohio Chapter of the American Concrete Institute, 2006.

Case Studies in Concrete Petrograhy, Presented at the Annual Meeting of Patriot Engineering and Environmental, Inc., July 2010

Professional Background

Twenty-four years of experience in the concrete analysis, research and testing field. Founded Concrete Research & Testing, LLC in 1996, following 10 years with Lankard Materials Laboratory as a Research Scientist and Concrete Petrographer. Overall area of expertise is in failure analysis, research, product development and testing of construction materials, including concrete, mortars, stucco, aggregates, cement, supplementary cementitious materials and chemical admixtures.

Concrete Petrography

Concrete petrography is the laboratory examination of hardened concrete using microscopes and various techniques. Petrographic examinations of concrete are typically performed due to a problem during construction or the premature failure of an existing concrete structure. In these instances, the petrographer is retained to determine the cause of the problem and oftentimes to determine the responsible party. Petrographic examinations are also performed as part of condition studies when older structures are being evaluated for rehabilitation or possible replacement.

Primary investigator in over 800 petrographic projects involving hardened concrete, mortar and stucco. Routinely perform petrographic examinations on concrete aggregate samples to determine suitability for use in portland-cement based construction materials. Equipment used for the petrographic work includes: stereomicroscopes, polarizing microscope, scanning electron microscope (SEM) and x-ray diffraction (XRD).

Experience with expert witness testimony for petrographic clients.

Petrographic examinations performed have covered the following problems:

- Alkali-Silica Reactions
- Alkali-Carbonate Reactions
- Low Strength Issues
- Freeze/Thaw Scaling Distress
- Freeze/Thaw Popout Distress
- Distress Due to Oxidation of Aggregates
- Delamination of Interior Floor Slabs
- Dusting of Interior Floor Slabs
- Curling of Interior Floor Slabs
- Cracking due to Corrosion of Reinforcing Steel
- Overdose of Supplementary Cementitious Materials
- Debonding of Floor Covering Materials
- Failure of Self-Leveling Underlayment Materials

- Drying Shrinkage Cracking
- Plastic Shrinkage Cracking
- Structural Cracking
- D-Cracking
- Sulfate Attack
- Chemical Attack
- Physical Salt Attack
- Improper Setting Time
- Contamination Issues
- Discoloration Problems
- Debonding of Stucco
- Cracking of Stucco

Research & Product Development

Experience working with many types of concrete and concrete materials including the following:

- High Strength Concrete
- Flowable Fills
- Ultra-High Strength Concrete
- Concrete Aggregates
- Steel Fiber Reinforced Concrete
- Pozzolanic Materials
- SIFCON (Slurry Infiltrated Fibrous Concrete)

- Gypsum Materials
- Refractory Concrete
- Cellular Concrete
- Lightweight Concrete
- Steel Slag Aggregate
- Heavyweight Concrete
- Wollastonite

Research projects have covered the following areas:

- Development and testing of concrete mix designs for the Security Industry, Fireplace Industry, Precast Concrete Industry, Ready Mix Concrete Industry and Heavyweight Concrete Applications.

- Development work on concrete anchor bolt system.

- Development work on the manufacture of nuclear waste storage containers using SIFCON.

- Study on Corrosion Inhibiting Admixtures in concrete.

- Study of D-Cracking in bridge deck structures.

- Study on the permeability of prestressed/precast concrete used for bridge components.

- Study on the use of wollastonite in portland cement products.

- Worked on startup operation for the manufacturing of aluminum impellers using plaster molds.

- Study on the long term affect of boric acid on concrete for the nuclear power industry.

- Development of innovative test methods for clients particular needs.

Testing

Experience with most ASTM specifications and tests involving concrete, concrete aggregates, mortars and cement.

APPENDIX B

CONCRETE RESEARCH & TESTING, LLC REPORT NO 393-2: PETROGRAPHIC EXAMINATION OF THREE CONCRETE CYLINDERS TO DETERMINE THE EFFECTS OF EXPOSURE TO BORIC ACID SOLUTION

REPORT NO. P-393-2

ON

**PETROGRAPHIC EXAMINATION OF THREE
CONCRETE CYLINDERS TO DETERMINE THE
EFFECTS OF EXPOSURE TO BORIC ACID SOLUTION
(SWRI PROJECT NO. 15555.01.013)**

TO

**SOUTHWEST RESEARCH INSTITUTE
SAN ANTONIO, TEXAS**

JUNE 8, 2011
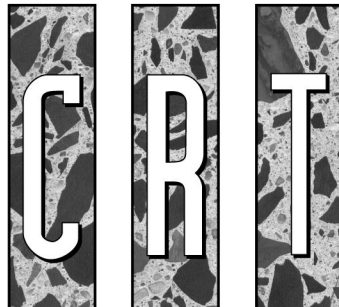
Concrete Research & Testing, LLC

REPORT NO. P-393-2

ON

PETROGRAPHIC EXAMINATION OF THREE
CONCRETE CYLINDERS TO DETERMINE THE
EFFECTS OF EXPOSURE TO BORIC ACID SOLUTION
(SWRI PROJECT NO. 15555.01.013)

INTRODUCTION

Southwest Research Institute (SWRI), San Antonio, Texas, is currently researching the effects of boric acid solution on concrete. Concrete cylinder specimens were prepared and exposed to the three following conditions:

- Immersed in 1200 ppm boric acid solution at room temperature
- Immersed in 2400 ppm boric acid solution at room temperature
- Immersed in 2400 ppm boric acid solution at $60^{\circ}C$

Cylinders will be exposed to the boric acid solutions for periods of 180 days, 240 days and 300 days.

Concrete Research & Testing (CRT) was requested by SWRI to perform petrographic examination on the concrete cylinder specimens following each of the exposure periods. The objective of the petrographic examinations is to determine to what extent the concrete is affected by the boric acid solutions.

The concrete mix design used for the project is shown in Table 1 of Appendix A. The concrete was produced by Ingram Ready Mix, Inc., located in New Braunfels, Texas.

Three concrete cylinder specimens were received at CRT from Ken Chiang of SWRI on April 28, 2011. The received cylinder specimens were immersed in the boric acid solutions for a period of 240 days.

GENERAL DESCRIPTION OF THE SPECIMENS

The received specimens were labeled 'ASP-10-180, 7-21, 021942, 18, NP'. Each specimen was additionally labeled No. 16, No. 20 or No. 34. Photographs of the as-received specimens are shown in Figure 1 of Appendix B. The specimens are standard 4 in. by 8 in. molded cylinders. The top and bottom surfaces of each specimen have been covered with a layer of epoxy. The epoxy layers are generally 2 to 5 mm thick. The testing condition for each specimen is shown below.

Specimen	Boric Acid Concentration, ppm	Test Temperature
No. 16	1200	Room Temperature
No. 20	2400	Room Temperature
No. 34	2400	60°C

EXAMINATION METHODS

A portion of the circumference of each specimen was first coated with epoxy to protect and preserve features of the exterior surface during the specimen preparation. The concrete specimens were then saw-cut perpendicular to the long axis of each specimen to produce a ~1 in. thick section. This section was then cut in half along the diameter to produce two, 1 in. thick, semi-circular halves. These halves were then saw-cut in half perpendicular to the original long axis of the cylinder to produce four, ½ in. thick semi-circular sections.

The final saw-cut surfaces of the ½ in. thick sections were prepared for microscopic examination by lapping on a steel wheel with progressively-finer silicon carbide grit. The lapped sections were then examined under a stereo-microscope at magnifications of 7X to 100X. The examinations were performed following the guidelines in ASTM C 856, "Standard Practice for Petrographic Examination of Hardened Concrete."

The depth of the affected cement paste was measured in each of the concrete specimens. The measurements were performed at a magnification of 10X, using a micrometer located in the eyepiece of the microscope. The average depth of the affected cement paste was determined from 20 random measurements made around the circumference of each cylinder specimen.

EXAMINATION RESULTS

The affected cement paste is very soft, highly porous and retains very little inherent strength. The affected paste typically exhibits a color change from grey to white in the examined specimens. However, in some areas of Specimen No. 34, the affected paste is yellowish in color. Cross-section photographs taken under the microscope showing the attacked cement paste are presented in Figure 2 through Figure 5 of Appendix B. Areas of the affected cement paste layer are occasionally lost from the lapped surface during specimen preparation. The depth of the affected cement paste for each cylinder specimen is shown below.

	Depth of Affected Cement Paste	
Specimen	**Range, mm**	**Average, mm***
No. 16	1.0 to 1.5	1.31
No. 20	1.2 to 1.7	1.42
No. 34	2.0 to 2.6	2.17

*Average of 20 measurements

In specimen No. 16 and specimen No. 20, there is a distinct transition from the weak, porous, affected cement paste to the dense, unaffected cement paste. This transition is less defined in specimen No. 34. In some areas of Specimen No. 34, the affected cement paste is similar to No. 16 and No. 20 (see Figure 4). In other areas, the severely affected cement paste is underlain by a dark colored, competent cement paste layer which is underlain by a thin white layer of weak cement paste (see Figure 5). Carbonation testing shows that the acid attack has affected the cement paste to the depth of the thin,

white layer of weakened cement paste (see Figure 6). The 'Depth of Affected Cement Paste' values for Specimen No. 34 shown in the above table, reflect measurements made to the thin white layer of weakened cement paste.

The coarse aggregate is comprised of a natural gravel. The gravel is comprised of roughly 90 percent limestone particles and 10 percent chert particles. In Specimen No. 34, near surface limestone coarse aggregate particles exhibit evidence of acid attack. Typically, the portion of the limestone particle within the layer of acid attacked cement paste exhibits evidence of acid attack (see Figure 7).

Jason Cummins, Petrographer
Concrete Research & Testing, LLC

Nick Scaglione, President & Petrographer
Concrete Research & Testing, LLC

APPENDIX A

Table 1. Mix design for concrete specimens used to test the effects of long term exposure to boric acid solutions. The concrete was produced by Ingram Ready Mix, Inc.

Constituent	SSD Batch Weights, lb/yd³	Specific Gravity	Volume, ft³
Portland Cement	560	3.15	2.85
Coarse Aggregate	2200	2.57	13.72
Fine Aggregate	966	2.63	5.89
Water	258.5	1.00	4.14
Entrapped Air Void Content	---	---	0.41
Water Reducing/Retarding Admixture	3.0 oz/cwt	---	---
Totals	3984.5	---	27.00

Water-Cementitious Ratio: 0.46

Target Air Void Content: 1½% ± 1½%

Theoretical Unit Weight: 147.6 lb/ft³

Theoretical Cement Paste Content: 32.7%

APPENDIX B

Figure 1. Photograph of the as-received specimens.

Figure 2. Cross-section photographs taken under the microscope showing the acid attacked cement paste of Specimen No. 16. The layer of penetrated epoxy can be seen in both photographs.
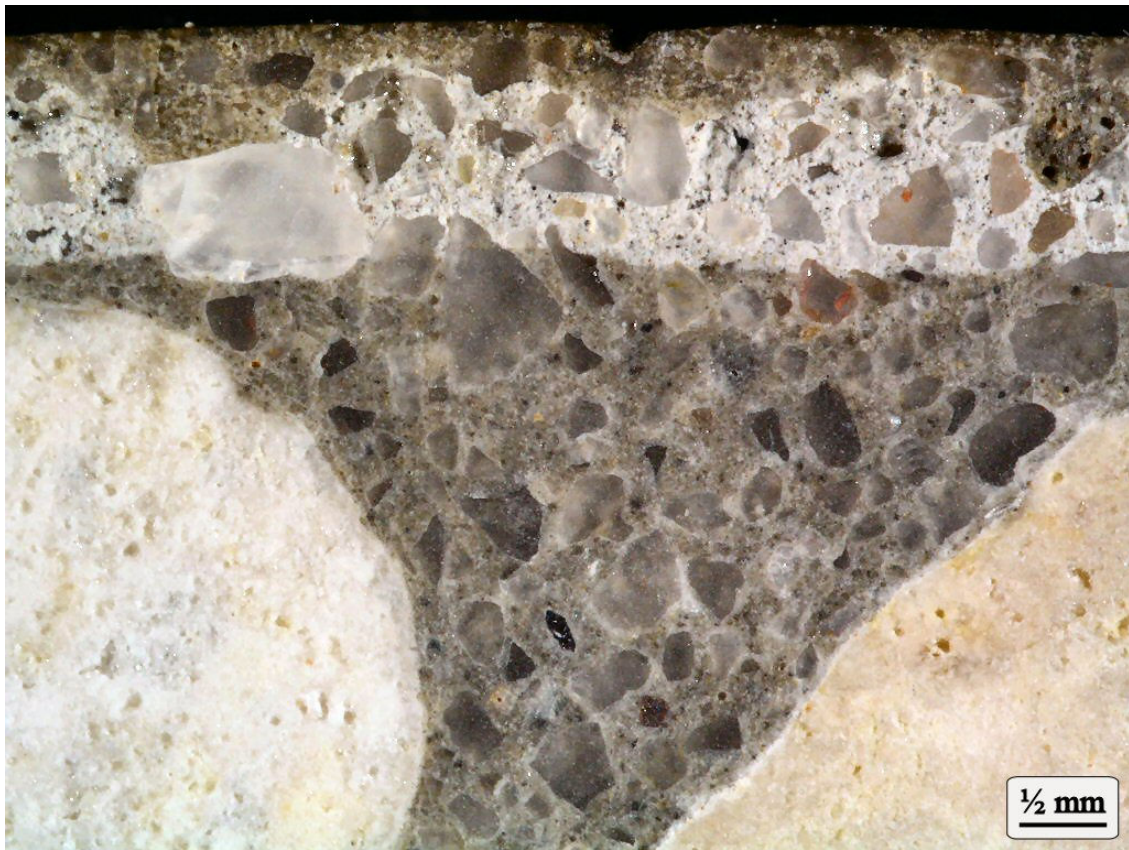
Figure 3. Cross-section photographs taken under the microscope showing the acid attacked cement paste of Specimen No. 20. The layer of penetrated epoxy can be seen in both photographs.

Figure 4. Cross-section photographs taken under the microscope showing the acid attacked cement paste of Specimen No. 34. The layer of penetrated epoxy can be seen in both photographs.
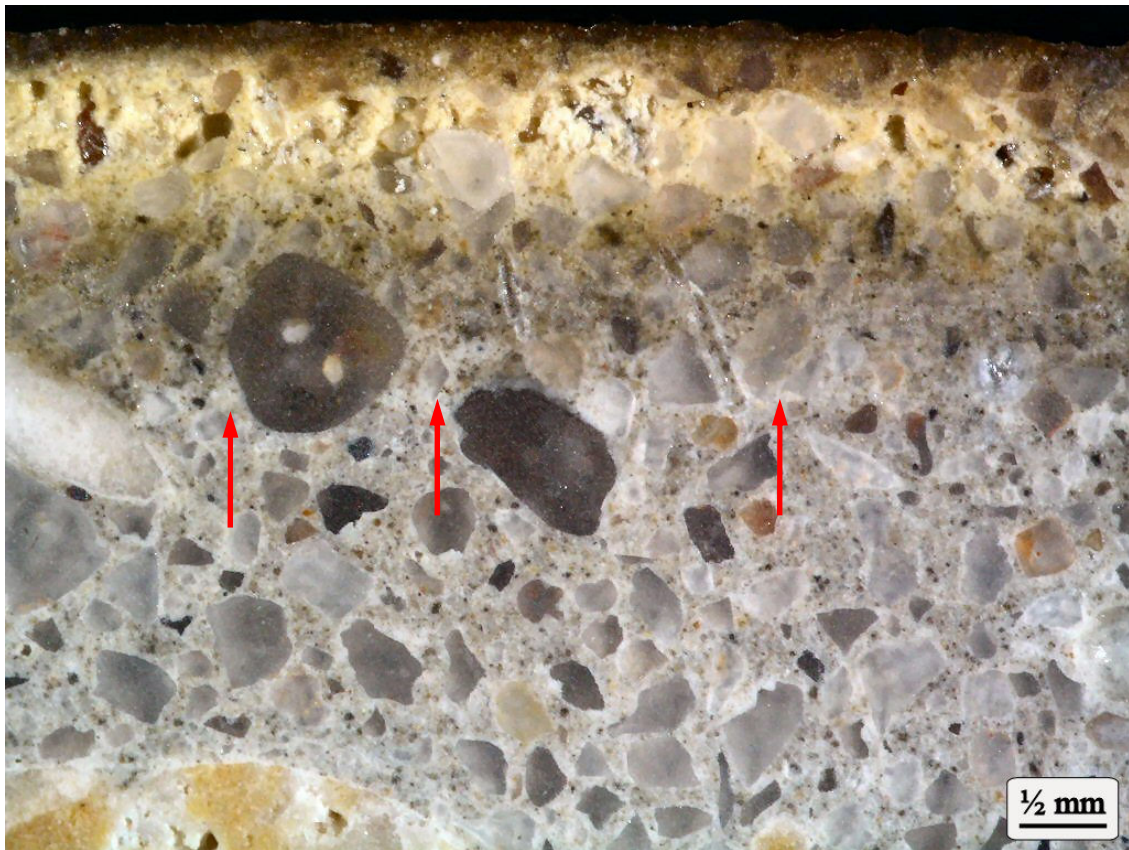
Figure 5. Cross-section photographs taken under the microscope showing the thin line of weak cement paste (arrows) present in the otherwise unaffected cement paste of Specimen No. 34.

Figure 6. Cross-section photographs of Specimen No. 34 following the exposure to phenolphthalein solution. The depth to which the pH has been lowered by the acid exposure is represented by the uncolored cement paste.
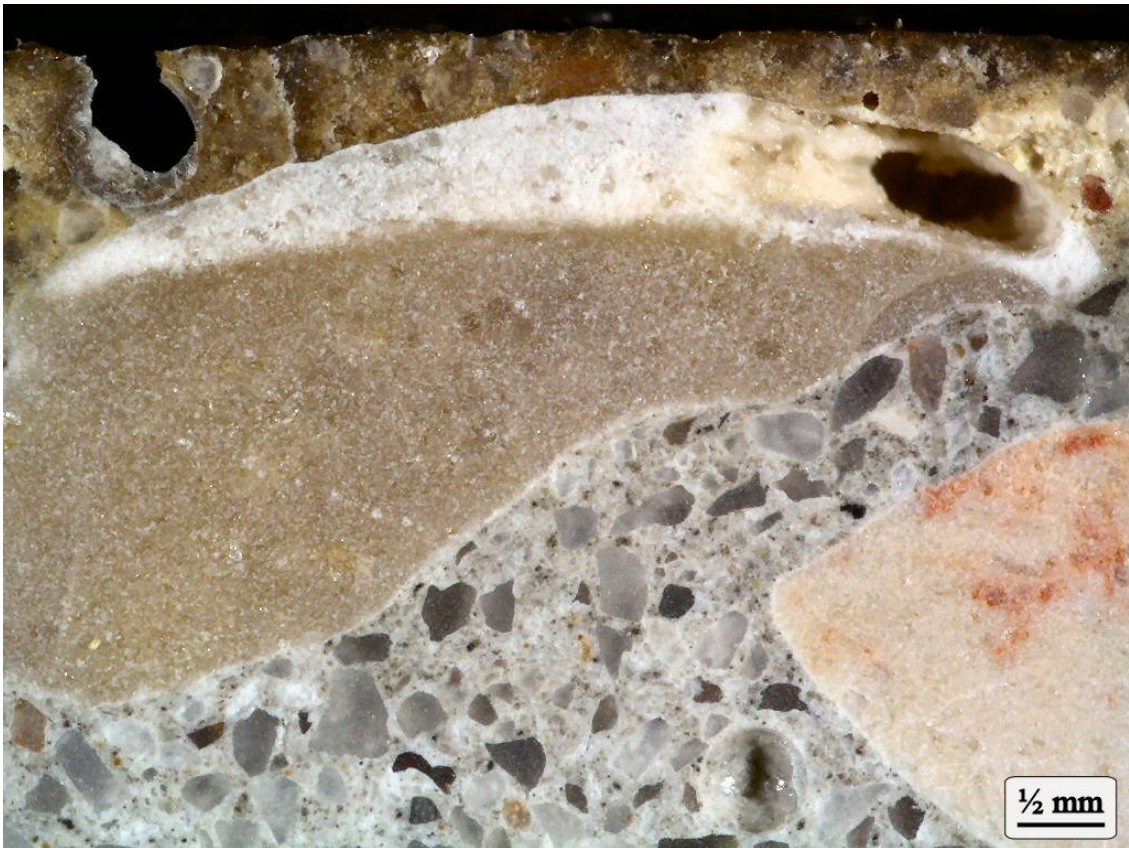
Figure 7. Cross-section photographs of Specimen No. 34 showing limestone coarse aggregate particles exhibiting acid attack.

APPENDIX C

Jason Cummins

Petrographer & Laboratory Manager, Concrete Research & Testing, LLC

Education

B.S. – Geology	*University of Massachusetts, Amherst*	**May 2000**

Employment

Concrete Research & Testing, LLC   *Columbus, Ohio*   **January 2001 to Present**

Concrete Petrographer   July 2006 to Present
- Perform petrographic examinations of concrete, aggregates and related materials
- Compose written reports providing the details and conclusions of petrographic examinations

Laboratory Manager   July 2004 to Present
- Calibrate and verify the operation of laboratory equipment and devices
- Supervise, train, and evaluate Laboratory Technicians
- Maintain and update company information and employee/equipment records
- Continue duties & responsibilities of a Laboratory Technician

Laboratory Technician   January 2001 to July 2004
- Prepare concrete, aggregates and related materials for petrographic examinations and testing
- Test concrete, aggregates and related materials according to standardized test procedures
- Produce written reports summarizing the results of the testing

Experience

Laboratory
- Petrographic examinations of concrete, aggregates and related materials
- Standardized (ASTM/AASHTO) testing of concrete, aggregates and related materials

Field
- Standardized (ASTM) testing of fresh concrete
- Specimen preparation for future laboratory testing

Certifications

American Concrete Institute
- Concrete Field Testing Technician – Grade I
- Concrete Strength Testing Technician
- Aggregate Testing Technician – Level 1
- Concrete Laboratory Testing Technician – Level 1

Ohio Ready Mixed Concrete Association
- Certified Concrete Technician

Professional Affiliations

American Concrete Institute (ACI) – Central Ohio Chapter
Society of Concrete Petrographers

Nick J. Scaglione
President, Concrete Research & Testing, LLC

Education

B.Sc., Geology – The Ohio State University, Columbus, Ohio	1987
Certified Concrete Technician – Ohio Ready Mix Concrete Association	1988
Concrete Field Testing Technician – American Concrete Institute	1988
Short Course in Refractory Concrete – Center for Professional Advancement	1991

Experience

Concrete Research & Testing, Columbus, Ohio	1996 - Present
President & Senior Petrographer	
Lankard Materials Laboratory, Columbus, Ohio	1986 - 1995
Petrographer, Research Scientist & Technician	

Affiliations

American Concrete Institute (ACI)
Central Ohio Chapter – Board Member (2008 – Present)

American Society for Testing and Materials (ASTM)
Committee C09 – Member
Subcommittees C09.65, C09.66, C09.26, C09.20 – Member
ASTM C457 Task Group – Chairman (2010)
Subcommittee C09.65 (Petrography) – Secretary (2010)

Society of Concrete Petrographers
Vice President (2010 – Present)
Treasurer (2007 – 2009)

Publications

Lankard, D.R., Bennett, J.E., Scaglione, N.S.; *Petrographic Examination of Reinforced Concrete from Cathodically Protected Structures*, Petrography of Cementitious Materials, ASTM STP 1215, 1994.

Presentations

Concrete under the Microscope. Presented to the Northeast Ohio Chapter of the American Concrete Institute, 2006.

Case Studies in Concrete Petrograhy, Presented at the Annual Meeting of Patriot Engineering and Environmental, Inc., July 2010

Professional Background

Twenty-four years of experience in the concrete analysis, research and testing field. Founded Concrete Research & Testing, LLC in 1996, following 10 years with Lankard Materials Laboratory as a Research Scientist and Concrete Petrographer. Overall area of expertise is in failure analysis, research, product development and testing of construction materials, including concrete, mortars, stucco, aggregates, cement, supplementary cementitious materials and chemical admixtures.

Concrete Petrography

Concrete petrography is the laboratory examination of hardened concrete using microscopes and various techniques. Petrographic examinations of concrete are typically performed due to a problem during construction or the premature failure of an existing concrete structure. In these instances, the petrographer is retained to determine the cause of the problem and oftentimes to determine the responsible party. Petrographic examinations are also performed as part of condition studies when older structures are being evaluated for rehabilitation or possible replacement.

Primary investigator in over 800 petrographic projects involving hardened concrete, mortar and stucco. Routinely perform petrographic examinations on concrete aggregate samples to determine suitability for use in portland-cement based construction materials. Equipment used for the petrographic work includes: stereomicroscopes, polarizing microscope, scanning electron microscope (SEM) and x-ray diffraction (XRD).

Experience with expert witness testimony for petrographic clients.

Petrographic examinations performed have covered the following problems:

- Alkali-Silica Reactions
- Alkali-Carbonate Reactions
- Low Strength Issues
- Freeze/Thaw Scaling Distress
- Freeze/Thaw Popout Distress
- Distress Due to Oxidation of Aggregates
- Delamination of Interior Floor Slabs
- Dusting of Interior Floor Slabs
- Curling of Interior Floor Slabs
- Cracking due to Corrosion of Reinforcing Steel
- Overdose of Supplementary Cementitious Materials
- Debonding of Floor Covering Materials
- Failure of Self-Leveling Underlayment Materials

- Drying Shrinkage Cracking
- Plastic Shrinkage Cracking
- Structural Cracking
- D-Cracking
- Sulfate Attack
- Chemical Attack
- Physical Salt Attack
- Improper Setting Time
- Contamination Issues
- Discoloration Problems
- Debonding of Stucco
- Cracking of Stucco

Research & Product Development

Experience working with many types of concrete and concrete materials including the following:

- High Strength Concrete
- Flowable Fills
- Ultra-High Strength Concrete
- Concrete Aggregates
- Steel Fiber Reinforced Concrete
- Pozzolanic Materials
- SIFCON (Slurry Infiltrated Fibrous Concrete)

- Gypsum Materials
- Refractory Concrete
- Cellular Concrete
- Lightweight Concrete
- Steel Slag Aggregate
- Heavyweight Concrete
- Wollastonite

Research projects have covered the following areas:

- Development and testing of concrete mix designs for the Security Industry, Fireplace Industry, Precast Concrete Industry, Ready Mix Concrete Industry and Heavyweight Concrete Applications.

- Development work on concrete anchor bolt system.

- Development work on the manufacture of nuclear waste storage containers using SIFCON.

- Study on Corrosion Inhibiting Admixtures in concrete.

- Study of D-Cracking in bridge deck structures.

- Study on the permeability of prestressed/precast concrete used for bridge components.

- Study on the use of wollastonite in portland cement products.

- Worked on startup operation for the manufacturing of aluminum impellers using plaster molds.

- Study on the long term affect of boric acid on concrete for the nuclear power industry.

- Development of innovative test methods for clients particular needs.

Testing

Experience with most ASTM specifications and tests involving concrete, concrete aggregates, mortars and cement.

APPENDIX C

**CONCRETE RESEARCH & TESTING, LLC REPORT NO 393-3:
PETROGRAPHIC EXAMINATION OF THREE CONCRETE CYLINDERS TO
DETERMINE THE EFFECTS OF EXPOSURE TO BORIC ACID SOLUTION**

REPORT NO. P-393-3

ON

PETROGRAPHIC EXAMINATION OF THREE
CONCRETE CYLINDERS TO DETERMINE THE
EFFECTS OF EXPOSURE TO BORIC ACID SOLUTION
(SWRI PROJECT NO. 15555.01.013)

TO

SOUTHWEST RESEARCH INSTITUTE
SAN ANTONIO, TEXAS

JULY 26, 2011

Concrete Research & Testing, LLC

REPORT NO. P-393-2

ON

PETROGRAPHIC EXAMINATION OF THREE
CONCRETE CYLINDERS TO DETERMINE THE
EFFECTS OF EXPOSURE TO BORIC ACID SOLUTION
(SWRI PROJECT NO. 15555.01.013)

INTRODUCTION

Southwest Research Institute (SWRI), San Antonio, Texas, is currently researching the effects of boric acid solution on concrete. Concrete cylinder specimens were prepared and exposed to the three following conditions:

- Immersed in 1200 ppm boric acid solution at room temperature
- Immersed in 2400 ppm boric acid solution at room temperature
- Immersed in 2400 ppm boric acid solution at 60°C

Cylinders will be exposed to the boric acid solutions for periods of 180 days, 240 days and 300 days.

Concrete Research & Testing (CRT) was requested by SWRI to perform petrographic examination on the concrete cylinder specimens following each of the exposure periods. The objective of the petrographic examinations is to determine to what extent the concrete is affected by the boric acid solutions.

The concrete mix design used for the project is shown in Table 1 of Appendix A. The concrete was produced by Ingram Ready Mix, Inc., located in New Braunfels, Texas.

Three concrete cylinder specimens were received at CRT from Ken Chiang of SWRI on June 29, 2011. The received cylinder specimens were immersed in the boric acid solutions for a period of 300 days.

GENERAL DESCRIPTION OF THE SPECIMENS

The received specimens were labeled 'ASP-10-180, 7-21, 021942, 18, NP'. Each specimen was

additionally labeled No. 18, No. 24 or No. 36. Photographs of the as-received specimens are shown in

Figure 1 of Appendix B. The specimens are standard 4 in. by 8 in. molded cylinders. The top and

bottom surfaces of each specimen have been covered with a layer of epoxy. The epoxy layers are

generally 2 to 5 mm thick.   The testing condition for each specimen is shown below.

Specimen	Boric Acid Concentration, ppm	Test Temperature
No. 18	1200	Room Temperature
No. 24	2400	Room Temperature
No. 36	2400	60°C

EXAMINATION METHODS

A portion of the circumference of each specimen was first coated with epoxy to protect and preserve

features of the exterior surface during the specimen preparation. The concrete specimens were then

saw-cut perpendicular to the long axis of each specimen to produce a ~1 in. thick section. This section

was then cut in half along the diameter to produce two, 1 in. thick, semi-circular halves. These halves

were then saw-cut in half perpendicular to the original long axis of the cylinder to produce four, ½ in.

thick semi-circular sections.

The final saw-cut surfaces of the ½ in. thick sections were prepared for microscopic examination by

lapping on a steel wheel with progressively-finer silicon carbide grit. The lapped sections were then

examined under a stereo-microscope at magnifications of 7X to 100X. The examinations were

performed following the guidelines in ASTM C 856, "Standard Practice for Petrographic Examination

of Hardened Concrete."

The depth of the affected cement paste was measured in each of the concrete specimens. The measurements were performed at a magnification of 10X, using a micrometer located in the eyepiece of the microscope. The average depth of the affected cement paste was determined from 20 random measurements made around the circumference of each cylinder specimen.

EXAMINATION RESULTS

The affected cement paste is very soft, highly porous and retains very little inherent strength. The affected paste typically exhibits a color change from grey to pale yellow in the examined specimens. Cross-section photographs taken under the microscope showing the attacked cement paste are presented in Figure 2 through Figure 5 of Appendix B. Areas of the weakened cement paste layer are occasionally lost from the lapped surface during specimen preparation. The depth of the affected cement paste for each cylinder specimen is shown below.

	Depth of Affected Cement Paste	
Specimen	**Range, mm**	**Average, mm***
No. 18	1.4 to 1.8	1.61
No. 24	1.4 to 1.8	1.60
No. 36	2.2 to 4.2	2.93

*Average of 20 measurements

In specimen No. 18 and specimen No. 24, there is a distinct transition from the weak, porous, affected cement paste to the dense, unaffected cement paste. This transition is less defined in specimen No. 36. In this specimen, the severely affected cement paste is underlain by a yellowish or gray colored, competent cement paste layer which is underlain by a thin white layer of weak cement paste (see Figures 4 and 5). Carbonation testing shows that the acid attack has affected the cement paste to the depth of the thin, white layer of weakened cement paste (see Figure 6). The 'Depth of Affected Cement Paste' values for Specimen No. 36 shown in the above table, reflect measurements made to the

3

thin white layer of weakened cement paste. The typical thickness of the severely affected cement paste in Specimen No. 36 is only 1.33 mm with a range of 0.9 to 2.2 mm. The carbonation testing of Specimen No. 16 and Specimen No. 24 show that the pH has been lowered in only the severely attacked cement paste.

The coarse aggregate is comprised of a natural gravel. The gravel is comprised of roughly 90 percent limestone particles and 10 percent chert particles. In Specimen No. 36, near surface limestone coarse aggregate particles exhibit evidence of acid attack. Typically, the portion of the limestone particle within the layer of acid attacked cement paste exhibits evidence of acid attack (see Figure 7). In Specimen No. 18 and Specimen No. 24, the coarse aggregate particles within the acid attacked cement paste do not appear affected by the chemical attack (see Figure 8).

Jason Cummins, Petrographer
Concrete Research & Testing, LLC

Nick Scaglione, President & Petrographer
Concrete Research & Testing, LLC

APPENDIX A

Table 1. Mix design for concrete specimens used to test the effects of long term exposure to boric acid solutions. The concrete was produced by Ingram Ready Mix, Inc.

Constituent	SSD Batch Weights, lb/yd^3	Specific Gravity	Volume, ft^3
Portland Cement	560	3.15	2.85
Coarse Aggregate	2200	2.57	13.72
Fine Aggregate	966	2.63	5.89
Water	258.5	1.00	4.14
Entrapped Air Void Content	---	---	0.41
Water Reducing/Retarding Admixture	3.0 oz/cwt	---	---
Totals	3984.5	---	27.00

Water-Cementitious Ratio: 0.46

Target Air Void Content: 1½% ± 1½%

Theoretical Unit Weight: 147.6 lb/ft^3

Theoretical Cement Paste Content: 32.7%

APPENDIX B

Figure 1. Photograph of the as-received cylinder specimens.

Figure 2. Cross-section photographs taken under the microscope showing the acid attacked cement paste of Specimen No. 18. The upper dark portion of the cement paste has been penetrated by the epoxy coating.
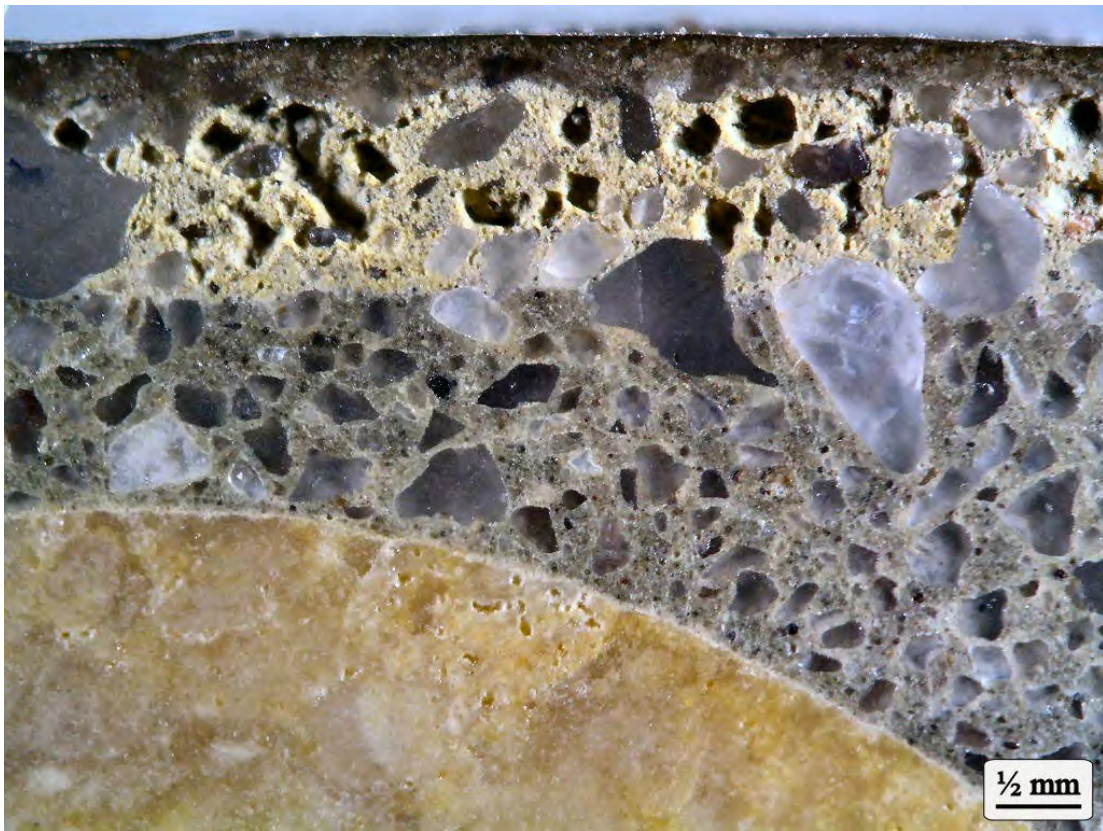
Figure 3. Cross-section photographs taken under the microscope showing the acid attacked cement paste of Specimen No. 24. The upper dark portion of the cement paste has been penetrated by the epoxy coating.
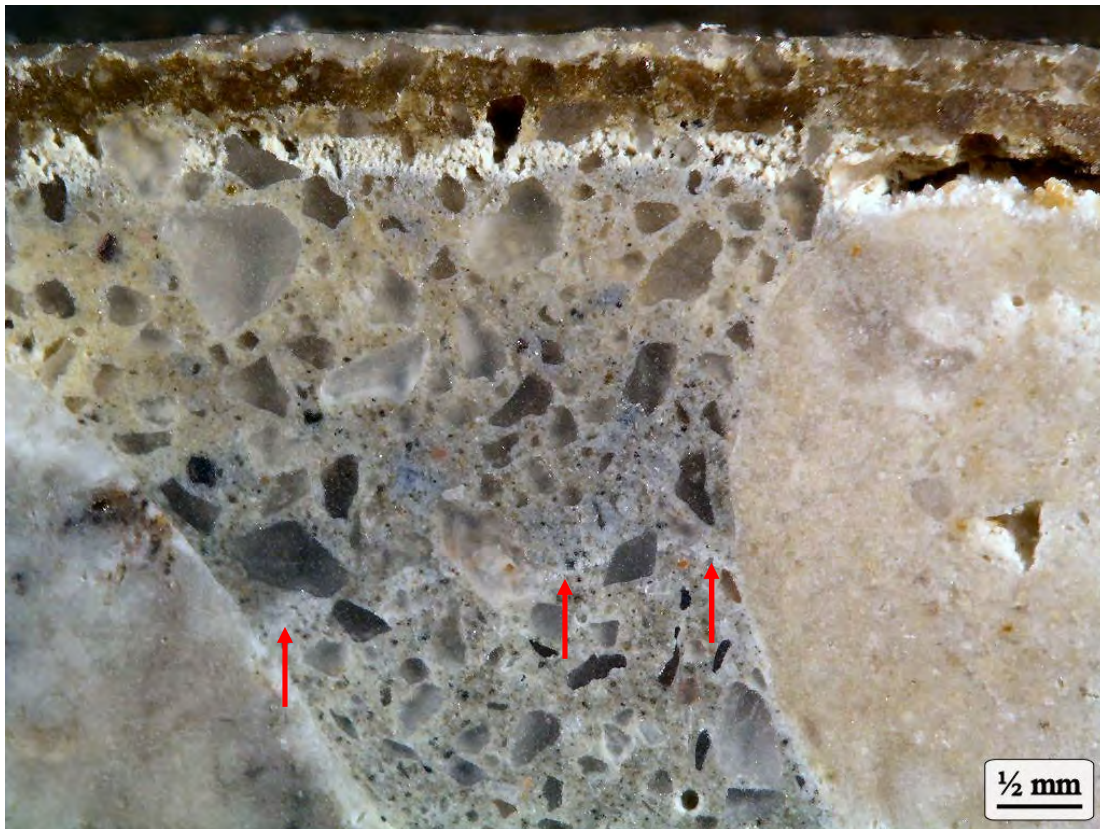
Figure 4. Cross-section photographs taken under the microscope showing the acid attacked cement paste of Specimen No. 36. The upper dark portion of the cement paste has been penetrated by the epoxy coating. The thin white layer of cement paste is shown by the arrows.
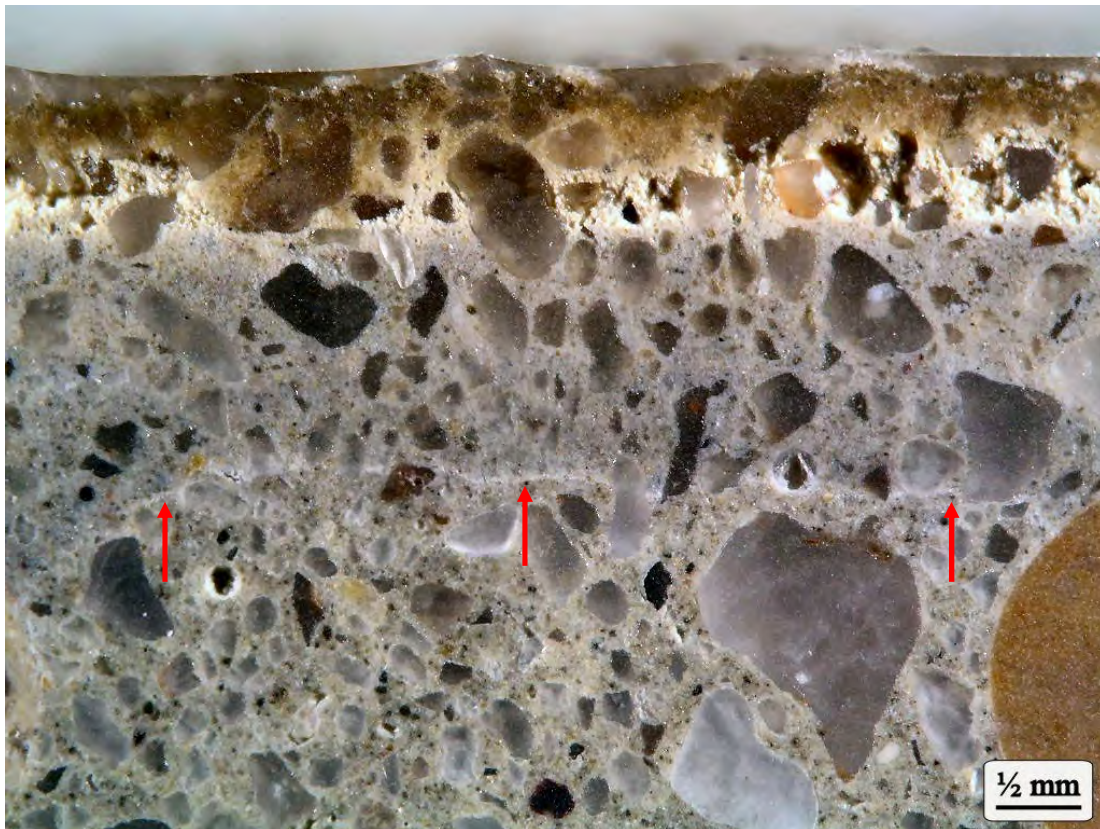
Figure 5. Cross-section photographs taken under the microscope showing the acid attacked cement paste of Specimen No. 36. The upper dark portion of the cement paste has been penetrated by the epoxy coating. The thin white layer of cement paste is shown by the arrows.

Figure 6. Cross-section photographs of Specimen No. 36 following the exposure to phenolphthalein solution. The depth to which the pH has been lowered by the acid exposure is represented by the uncolored cement paste.
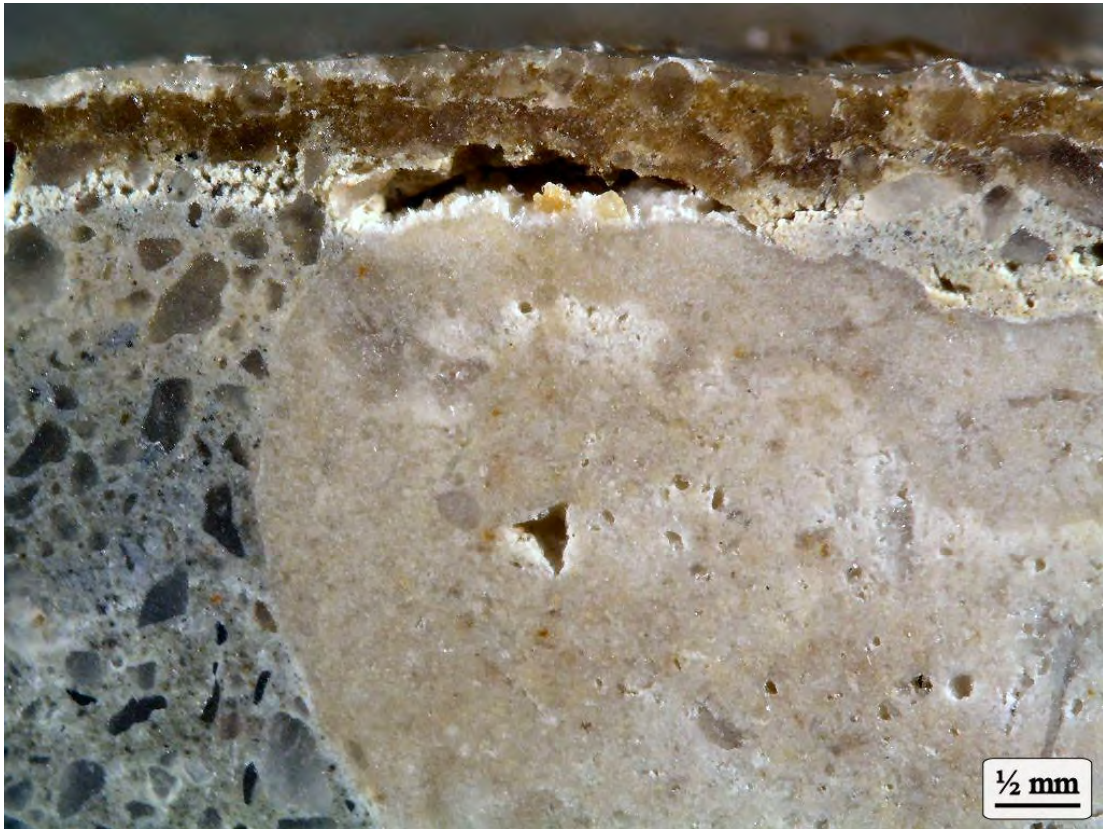
Figure 7.   Cross-section photographs of Specimen No. 36 showing limestone coarse aggregate particles exhibiting acid attack.
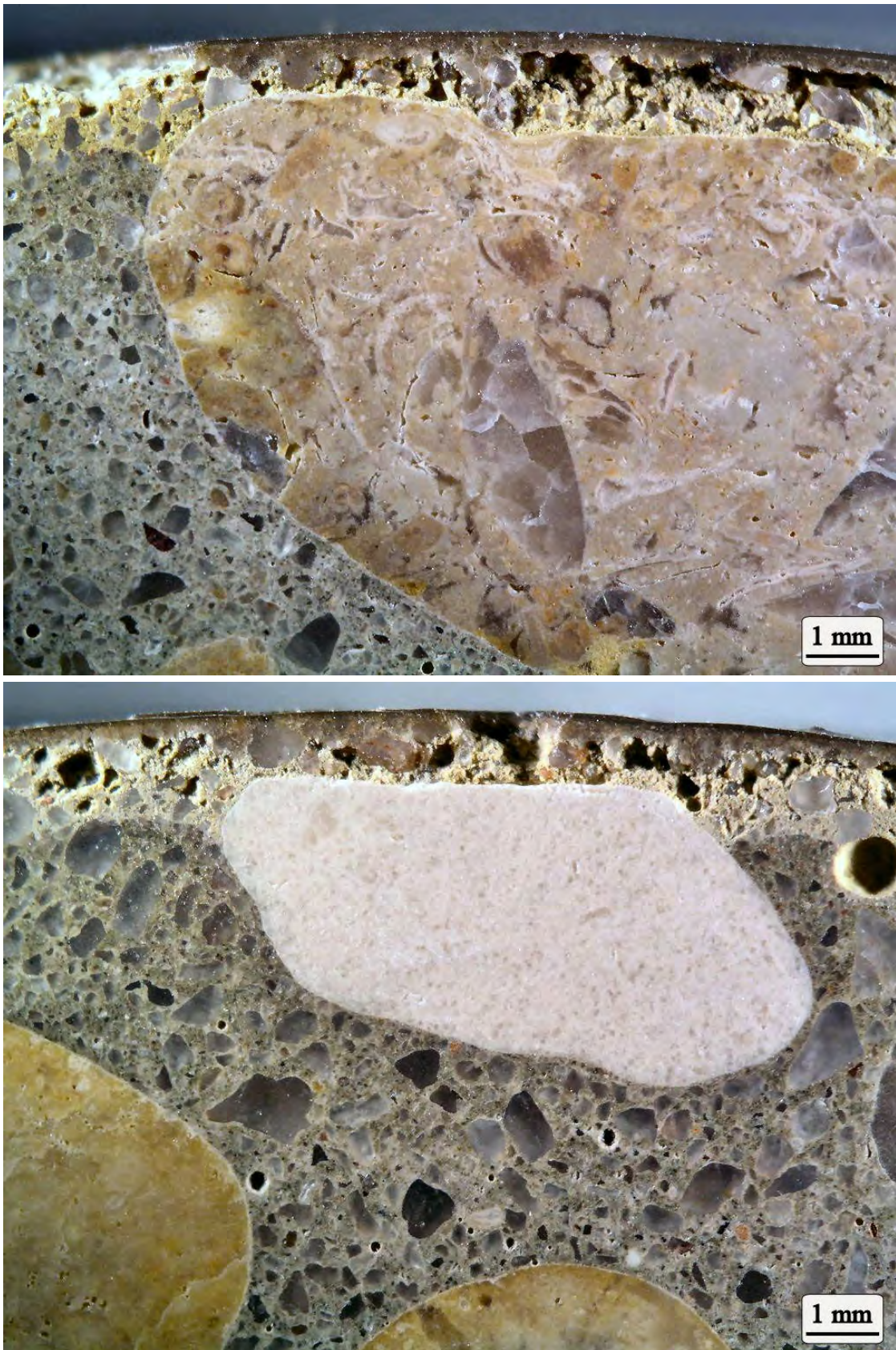
Figure 8. Cross-section photographs of Specimen No. 18 (upper) and Specimen No. 24 (lower) showing limestone coarse aggregate within the acid attacked cement paste. The limestone particles do not exhibit evidence of chemical attack.

APPENDIX C

Nick J. Scaglione
President, Concrete Research & Testing, LLC

Education

B.Sc., Geology – The Ohio State University, Columbus, Ohio	1987
Certified Concrete Technician – Ohio Ready Mix Concrete Association	1988
Concrete Field Testing Technician – American Concrete Institute	1988
Short Course in Refractory Concrete – Center for Professional Advancement	1991

Experience

Concrete Research & Testing, Columbus, Ohio President & Senior Petrographer	1996 - Present
Lankard Materials Laboratory, Columbus, Ohio Petrographer, Research Scientist & Technician	1986 - 1995

Affiliations

American Concrete Institute (ACI)
    Central Ohio Chapter – Board Member (2008 – Present)

American Society for Testing and Materials (ASTM)
    Committee C09 – Member
        Subcommittees C09.65, C09.66, C09.26, C09.20 – Member
    ASTM C457 Task Group – Chairman (2010)
    Subcommittee C09.65 (Petrography) – Secretary (2010)

Society of Concrete Petrographers
    Vice President (2010 – Present)
    Treasurer (2007 – 2009)

Publications

Scaglione, N, Simons, J., Keading, Nestell, J, Frey, M; Boric *Acid Attack of Concrete and Reinforcing Steel in PWR Fuel Handling Buildings,* Prepared for the Electric Power Research Institute, Palo Alto, CA, June 2009

Scaglione, N.S.; *Evaluation of Durability of ODOT Prestressed/Precast Concrete in Ohio,* Prepared for the Ohio Department of Transportation, September 2002.

Lankard, D.R., Bennett, J.E., Scaglione, N.S.; *Petrographic Examination of Reinforced Concrete from Cathodically Protected Structures*, Petrography of Cementitious Materials, ASTM STP 1215, 1994.

Presentations

Concrete under the Microscope. Presented to the Northeast Ohio Chapter of the American Concrete Institute, 2006.

Case Studies in Concrete Petrography, Presented at the Annual Meeting of Patriot Engineering and Environmental, Inc., July 2010

Professional Background

Twenty-five years of experience in the concrete analysis, research and testing field. Founded Concrete Research & Testing, LLC in 1996, following 10 years with Lankard Materials Laboratory as a Research Scientist and Concrete Petrographer. Overall area of expertise is in failure analysis, research, product development and testing of construction materials, including concrete, mortars, stucco, aggregates, cement, supplementary cementitious materials and chemical admixtures.

Concrete Petrography

Concrete petrography is the laboratory examination of hardened concrete using microscopes and various techniques. Petrographic examinations of concrete are typically performed due to a problem during construction or the premature failure of an existing concrete structure. In these instances, the petrographer is retained to determine the cause of the problem and oftentimes to determine the responsible party. Petrographic examinations are also performed as part of condition studies when older structures are being evaluated for rehabilitation or possible replacement.

Primary investigator in over 800 petrographic projects involving hardened concrete, mortar and stucco. Routinely perform petrographic examinations on concrete aggregate samples to determine suitability for use in portland-cement based construction materials. Equipment used for the petrographic work includes: stereomicroscopes, polarizing microscope, scanning electron microscope (SEM) and x-ray diffraction (XRD).

Experience with expert witness testimony for petrographic clients.

Petrographic examinations performed have covered the following problems:

- Alkali-Silica Reactions
- Alkali-Carbonate Reactions
- Low Strength Issues
- Freeze/Thaw Scaling Distress
- Freeze/Thaw Popout Distress
- Distress Due to Oxidation of Aggregates
- Delamination of Interior Floor Slabs
- Dusting of Interior Floor Slabs
- Curling of Interior Floor Slabs
- Cracking due to Corrosion of Reinforcing Steel
- Overdose of Supplementary Cementitious Materials
- Debonding of Floor Covering Materials
- Failure of Self-Leveling Underlayment Materials

- Drying Shrinkage Cracking
- Plastic Shrinkage Cracking
- Structural Cracking
- D-Cracking
- Sulfate Attack
- Chemical Attack
- Physical Salt Attack
- Improper Setting Time
- Contamination Issues
- Discoloration Problems
- Debonding of Stucco
- Cracking of Stucco

Research & Product Development

Experience working with many types of concrete and concrete materials including the following:

- High Strength Concrete
- Flowable Fills
- Ultra-High Strength Concrete
- Concrete Aggregates
- Steel Fiber Reinforced Concrete
- Pozzolanic Materials
- SIFCON (Slurry Infiltrated Fibrous Concrete)

- Gypsum Materials
- Refractory Concrete
- Cellular Concrete
- Lightweight Concrete
- Steel Slag Aggregate
- Heavyweight Concrete
- Wollastonite

Research projects have covered the following areas:

- Development and testing of concrete mix designs for the Security Industry, Fireplace Industry, Precast Concrete Industry, Ready Mix Concrete Industry and Heavyweight Concrete Applications.

- Development work on concrete anchor bolt system.

- Development work on the manufacture of nuclear waste storage containers using SIFCON.

- Study on Corrosion Inhibiting Admixtures in concrete.

- Study of D-Cracking in bridge deck structures.

- Study on the permeability of prestressed/precast concrete used for bridge components.

- Study on the use of wollastonite in portland cement products.

- Worked on startup operation for the manufacturing of aluminum impellers using plaster molds.

- Study on the long term affect of boric acid on concrete for the nuclear power industry.

- Development of innovative test methods for clients particular needs.

Testing

Experience with most ASTM specifications and tests involving concrete, concrete aggregates, mortars and cement.

Jason Cummins
Petrographer & Laboratory Manager, Concrete Research & Testing, LLC

Education

B.S. – Geology	*University of Massachusetts, Amherst*	**May 2000**

Employment

Concrete Research & Testing, LLC	*Columbus, Ohio*	**January 2001 to Present**

Concrete Petrographer   July 2006 to Present
- Perform petrographic examinations of concrete, aggregates and related materials
- Compose written reports providing the details and conclusions of petrographic examinations

Laboratory Manager   July 2004 to Present
- Calibrate and verify the operation of laboratory equipment and devices
- Supervise, train, and evaluate Laboratory Technicians
- Maintain and update company information and employee/equipment records
- Continue duties & responsibilities of a Laboratory Technician

Laboratory Technician   January 2001 to July 2004
- Prepare concrete, aggregates and related materials for petrographic examinations and testing
- Test concrete, aggregates and related materials according to standardized test procedures
- Produce written reports summarizing the results of the testing

Experience

Laboratory
- Petrographic examinations of concrete, aggregates and related materials
- Standardized (ASTM/AASHTO) testing of concrete, aggregates and related materials

Field
- Standardized (ASTM) testing of fresh concrete
- Specimen preparation for future laboratory testing

Certifications

American Concrete Institute
- Concrete Field Testing Technician – Grade I
- Concrete Strength Testing Technician
- Aggregate Testing Technician – Level 1
- Concrete Laboratory Testing Technician – Level 1

Ohio Ready Mixed Concrete Association
- Certified Concrete Technician

Professional Affiliations

American Concrete Institute (ACI) – Central Ohio Chapter
Society of Concrete Petrographers

FINAL

APPENDIX D

EXAMPLE GEOCHEMIST'S WORKBENCH X1T INPUT FOR ONE-DIMENSIONAL REACTIVE TRANSPORT SIMULATION OF CONCRETE LEACHING BY 2,400 PPM BORON SOLUTION

APPENDIX D

Example Geochemist's Workbench X1t Input for 1-D Reactive Transport Simulation of Concrete Leaching by 2,400 ppm Boron Solution[1]

```
# X1t script
data = "C:\Program Files\Gwb\Gtdata\thermo.com.v8.r6+.cement.dat" verify
time start = 0 years, end = 1 years
length = 1 cm
left = inlet
right = outlet
Nx = 50
discharge = 0 m/sec
porosity = .07
dispersivity = 0
decouple ALL
#
#Equation relating permeability, k, to porosity, phi, is
# log k(darcy) = intercept + porosity_coeff*porosity
# Note that "porosity_coeff" is defined in the script as "porosity"
#
permeability intercept = -7 porosity = 15
#
#Set diffusion coefficient to 1e-6 cm^2/s
#
diffusion_coef = 1.0e-6
#
#Inlet composition
#
scope = inlet
  H2O       = 1 free kg
  Na+       = 1.E-10 molar
  K+        = 1.E-10 molar
  Mg++      = 1.E-10 molar
  Ca++      = 1.E-10 molar
  Al+++     = 1.E-10 molar
  Fe+++     = 1.E-10 molar
  SiO2(aq) = 1.E-10 molar
  Cl-       = 1.E-10 molar
  HCO3-    = 1.E-10 molar
  SO4--     = 1.E-10 molar
  Ti(OH)4(aq) = 1.E-10 molar
  B(OH)3(aq)  = 0.222 molar
#
  balance on pH
#
#Initial condition – concrete and pore fluid composition
#
scope = initial
  swap Portlandite for Ca++
  swap Rutile for Ti(OH)4(aq)
```

---

[1]Reference: Bethke, C.M. and S. Yeakel. "The Geochemist's Workbench® Release 7.0 Reactive Transport Modeling Guide." University of Illinois, Urbana, Illinois. 2007.

```
   swap CSH_1.8 for SiO2(aq)
   swap Hydrogarnet for Al+++
   swap Hydrotalcite for Mg++
   swap Ettringite for SO4--
   swap Hematite for Fe+++
   1 kg H2O
#
#Mineralogy based on Table 6 of Wang (2009).
#Rutile is surrogate for concrete aggregate
#
  72 free volume% Rutile
  4.7 free volume% Portlandite
  8.3 free volume% CSH_1.8
  1.67 free volume% Hydrogarnet
  .46 free volume% Hydrotalcite
  3.2 free volume% Ettringite
  .33 free volume% Hematite
  .14 molarity Na+
  .37 molarity K+
  1e-10 molarity Cl-
  1e-10 molarity B(OH)3(aq)
  1e-10 molarity HCO3-
#
# Balance on OH-
#
   swap OH- for H+
   balance on OH-
#
suppress all
unsup Portlandite CSH_1.8 Ettringite Hydrogarnet
unsup Hydrotalcite Quartz Rutile Hematite
unsup CSH_1.1  CSH_0.8 Calcite
printout on
Xstable = .5
```

APPENDIX E

**EXAMPLE GEOCHEMIST'S WORKBENCH X2T INPUT FOR
TWO-DIMENSIONAL REACTIVE TRANSPORT SIMULATION OF
CONCRETE LEACHING BY 2,400 PPM BORON SOLUTION**

APPENDIX E

Example Geochemist's Workbench X2t Input for 2-D Reactive Transport Simulation of Concrete Leaching by 2,400 ppm Boron Solution[1]

X2t Script

```
#X2t script
data = "C:\Program Files\Gwb\Gtdata\thermo.com.v8.r6+.cement.dat" verify
time start = 0 years, end = 100 year
#
#crack half-width = 0.15 cm
#
deltay = {0.15|0.25|0.5|0.75|1|1.25|1.5|1.75} cm
Ny = 8
#
#Specify input file listing x-grid spacing
#
deltax = file my_table_deltax_20.txt cm
Nx = 20
#
discharge left  = .002 m/day
#
#Specify input file listing porosity in each node
#
porosity = file my_table_porosity_20x8_7%_porosity.txt
#
#Equation relating permeability, k, to porosity, phi, is
# log k(darcy) = intercept + porosity_coeff*porosity
#Note that "porosity_coeff" is defined in the script as "porosity"
#
permeability intercept = -7 porosity = 15
#
#Set diffusion coefficient to 1e-6 cm^2/s
#
diffusion_coef = 1.0e-6
#
decouple ALL
#
scope = inlet
  H2O       = 1 free kg
  Na+       = 1.E-10 molar
  K+        = 1.E-10 molar
  Mg++      = 1.E-10 molar
  Ca++      = 1.E-10 molar
  Al+++     = 1.E-10 molar
  Fe+++     = 1.E-10 molar
  SiO2(aq)  = 1.E-10 molar
  Cl-       = 1.E-10 molar
  HCO3-     = 1.E-10 molar
  SO4--     = 1.E-10 molar
```

---

[1]Reference: Bethke, C.M. and S. Yeakel. "The Geochemist's Workbench® Release 7.0 Reactive Transport Modeling Guide." University of Illinois, Urbana, Illinois. 2007.

```
   Ti(OH)4(aq) = 1.E-10 molar
   B(OH)3(aq)  = 0.222 molar
#
   balance on pH
#
#Initial condition – concrete and pore fluid composition
#
scope = initial
   swap Portlandite for Ca++
   swap Rutile for Ti(OH)4(aq)
   swap CSH_1.8 for SiO2(aq)
   swap Hydrogarnet for Al+++
   swap Hydrotalcite for Mg++
   swap Ettringite for SO4--
   swap Hematite for Fe+++
   1 kg H2O
   .14 molarity Na+
   .37 molarity K+
   1e-10 molarity Cl-
   1e-10 molarity B(OH)3(aq)
   1e-10 molarity HCO3-
#
#  Balance on OH-
#
   swap OH- for H+
   balance on OH-
#
#Mineralogy based on Table 6 of Wang (2009)
#Fracture has zero vol% of minerals
#Use Rutile as surrogate for Granite aggregate
#Set Rutile to 72 vol% at all node locations except in fracture
#
#Specify input files listing concrete mineralogy in each node
#
Rutile = my_table_Aggregate_20x8.txt vol%
Portlandite = my_table_Portlandite_20x8.txt vol%
CSH_1.8 = my_table_CSH_1.8_20x8.txt vol%
Ettringite = my_table_Ettringite_20x8.txt vol%
Hydrogarnet = my_table_Hydrogarnet_20x8.txt vol%
Hydrotalcite = my_table_Hydrotalcite_20x8.txt vol%
Hematite = my_table_Hematite_20x8.txt vol%
#
suppress all
unsup Portlandite CSH_1.8 Ettringite Hydrogarnet
unsup Hydrotalcite Quartz Rutile  Hematite
unsup CSH_1.1  CSH_0.8 Calcite
printout on
Xstable = .5
```

Input File my_table_deltax_20.txt

2.5 2.5 2.5 2.5 5 5 5 5 5 5 7.5 7.5 7.5 7.5 10 10 10 10 10 10

Input File my_table_porosity_20x8_7%_porosity.txt

1 1 1 1 1 1 1 1 1 1 1 1 1 1 1 1 1 1 1 1
0.07 0.07 0.07 0.07 0.07 0.07 0.07 0.07 0.07 0.07 0.07 0.07 0.07 0.07 0.07 0.07 0.07 0.07 0.07 0.07
0.07 0.07 0.07 0.07 0.07 0.07 0.07 0.07 0.07 0.07 0.07 0.07 0.07 0.07 0.07 0.07 0.07 0.07 0.07 0.07
0.07 0.07 0.07 0.07 0.07 0.07 0.07 0.07 0.07 0.07 0.07 0.07 0.07 0.07 0.07 0.07 0.07 0.07 0.07 0.07
0.07 0.07 0.07 0.07 0.07 0.07 0.07 0.07 0.07 0.07 0.07 0.07 0.07 0.07 0.07 0.07 0.07 0.07 0.07 0.07
0.07 0.07 0.07 0.07 0.07 0.07 0.07 0.07 0.07 0.07 0.07 0.07 0.07 0.07 0.07 0.07 0.07 0.07 0.07 0.07
0.07 0.07 0.07 0.07 0.07 0.07 0.07 0.07 0.07 0.07 0.07 0.07 0.07 0.07 0.07 0.07 0.07 0.07 0.07 0.07
0.07 0.07 0.07 0.07 0.07 0.07 0.07 0.07 0.07 0.07 0.07 0.07 0.07 0.07 0.07 0.07 0.07 0.07 0.07 0.07

Inpuf File my_table_Aggregate_20x8.txt

0 0 0 0 0 0 0 0 0 0 0 0 0 0 0 0 0 0 0 0
72 72 72 72 72 72 72 72 72 72 72 72 72 72 72 72 72 72 72 72
72 72 72 72 72 72 72 72 72 72 72 72 72 72 72 72 72 72 72 72
72 72 72 72 72 72 72 72 72 72 72 72 72 72 72 72 72 72 72 72
72 72 72 72 72 72 72 72 72 72 72 72 72 72 72 72 72 72 72 72
72 72 72 72 72 72 72 72 72 72 72 72 72 72 72 72 72 72 72 72
72 72 72 72 72 72 72 72 72 72 72 72 72 72 72 72 72 72 72 72
72 72 72 72 72 72 72 72 72 72 72 72 72 72 72 72 72 72 72 72

Input File my_table_Portlandite_20x8

0 0 0 0 0 0 0 0 0 0 0 0 0 0 0 0 0 0 0 0
4.7 4.7 4.7 4.7 4.7 4.7 4.7 4.7 4.7 4.7 4.7 4.7 4.7 4.7 4.7 4.7 4.7 4.7 4.7 4.7
4.7 4.7 4.7 4.7 4.7 4.7 4.7 4.7 4.7 4.7 4.7 4.7 4.7 4.7 4.7 4.7 4.7 4.7 4.7 4.7
4.7 4.7 4.7 4.7 4.7 4.7 4.7 4.7 4.7 4.7 4.7 4.7 4.7 4.7 4.7 4.7 4.7 4.7 4.7 4.7
4.7 4.7 4.7 4.7 4.7 4.7 4.7 4.7 4.7 4.7 4.7 4.7 4.7 4.7 4.7 4.7 4.7 4.7 4.7 4.7
4.7 4.7 4.7 4.7 4.7 4.7 4.7 4.7 4.7 4.7 4.7 4.7 4.7 4.7 4.7 4.7 4.7 4.7 4.7 4.7
4.7 4.7 4.7 4.7 4.7 4.7 4.7 4.7 4.7 4.7 4.7 4.7 4.7 4.7 4.7 4.7 4.7 4.7 4.7 4.7
4.7 4.7 4.7 4.7 4.7 4.7 4.7 4.7 4.7 4.7 4.7 4.7 4.7 4.7 4.7 4.7 4.7 4.7 4.7 4.7

Input File my_table_CSH_1.8_20x8.txt

0 0 0 0 0 0 0 0 0 0 0 0 0 0 0 0 0 0 0 0
8.3 8.3 8.3 8.3 8.3 8.3 8.3 8.3 8.3 8.3 8.3 8.3 8.3 8.3 8.3 8.3 8.3 8.3 8.3 8.3
8.3 8.3 8.3 8.3 8.3 8.3 8.3 8.3 8.3 8.3 8.3 8.3 8.3 8.3 8.3 8.3 8.3 8.3 8.3 8.3
8.3 8.3 8.3 8.3 8.3 8.3 8.3 8.3 8.3 8.3 8.3 8.3 8.3 8.3 8.3 8.3 8.3 8.3 8.3 8.3
8.3 8.3 8.3 8.3 8.3 8.3 8.3 8.3 8.3 8.3 8.3 8.3 8.3 8.3 8.3 8.3 8.3 8.3 8.3 8.3
8.3 8.3 8.3 8.3 8.3 8.3 8.3 8.3 8.3 8.3 8.3 8.3 8.3 8.3 8.3 8.3 8.3 8.3 8.3 8.3
8.3 8.3 8.3 8.3 8.3 8.3 8.3 8.3 8.3 8.3 8.3 8.3 8.3 8.3 8.3 8.3 8.3 8.3 8.3 8.3
8.3 8.3 8.3 8.3 8.3 8.3 8.3 8.3 8.3 8.3 8.3 8.3 8.3 8.3 8.3 8.3 8.3 8.3 8.3 8.3

Input File my_table_Ettringite_20x8.txt

0 0 0 0 0 0 0 0 0 0 0 0 0 0 0 0 0 0 0 0
3.2 3.2 3.2 3.2 3.2 3.2 3.2 3.2 3.2 3.2 3.2 3.2 3.2 3.2 3.2 3.2 3.2 3.2 3.2 3.2
3.2 3.2 3.2 3.2 3.2 3.2 3.2 3.2 3.2 3.2 3.2 3.2 3.2 3.2 3.2 3.2 3.2 3.2 3.2 3.2
3.2 3.2 3.2 3.2 3.2 3.2 3.2 3.2 3.2 3.2 3.2 3.2 3.2 3.2 3.2 3.2 3.2 3.2 3.2 3.2
3.2 3.2 3.2 3.2 3.2 3.2 3.2 3.2 3.2 3.2 3.2 3.2 3.2 3.2 3.2 3.2 3.2 3.2 3.2 3.2
3.2 3.2 3.2 3.2 3.2 3.2 3.2 3.2 3.2 3.2 3.2 3.2 3.2 3.2 3.2 3.2 3.2 3.2 3.2 3.2
3.2 3.2 3.2 3.2 3.2 3.2 3.2 3.2 3.2 3.2 3.2 3.2 3.2 3.2 3.2 3.2 3.2 3.2 3.2 3.2
3.2 3.2 3.2 3.2 3.2 3.2 3.2 3.2 3.2 3.2 3.2 3.2 3.2 3.2 3.2 3.2 3.2 3.2 3.2

Input File my_table_Hydrogarnet_20x8.txt

0 0 0 0 0 0 0 0 0 0 0 0 0 0 0 0 0 0 0 0
1.67 1.67 1.67 1.67 1.67 1.67 1.67 1.67 1.67 1.67 1.67 1.67 1.67 1.67 1.67 1.67 1.67 1.67 1.67 1.67
1.67 1.67 1.67 1.67 1.67 1.67 1.67 1.67 1.67 1.67 1.67 1.67 1.67 1.67 1.67 1.67 1.67 1.67 1.67 1.67
1.67 1.67 1.67 1.67 1.67 1.67 1.67 1.67 1.67 1.67 1.67 1.67 1.67 1.67 1.67 1.67 1.67 1.67 1.67 1.67
1.67 1.67 1.67 1.67 1.67 1.67 1.67 1.67 1.67 1.67 1.67 1.67 1.67 1.67 1.67 1.67 1.67 1.67 1.67 1.67
1.67 1.67 1.67 1.67 1.67 1.67 1.67 1.67 1.67 1.67 1.67 1.67 1.67 1.67 1.67 1.67 1.67 1.67 1.67 1.67
1.67 1.67 1.67 1.67 1.67 1.67 1.67 1.67 1.67 1.67 1.67 1.67 1.67 1.67 1.67 1.67 1.67 1.67 1.67 1.67
1.67 1.67 1.67 1.67 1.67 1.67 1.67 1.67 1.67 1.67 1.67 1.67 1.67 1.67 1.67 1.67 1.67 1.67 1.67 1.67

Input File my_table_Hydrotalcite_20x8.txt

0 0 0 0 0 0 0 0 0 0 0 0 0 0 0 0 0 0 0 0
0.46 0.46 0.46 0.46 0.46 0.46 0.46 0.46 0.46 0.46 0.46 0.46 0.46 0.46 0.46 0.46 0.46 0.46 0.46 0.46
0.46 0.46 0.46 0.46 0.46 0.46 0.46 0.46 0.46 0.46 0.46 0.46 0.46 0.46 0.46 0.46 0.46 0.46 0.46 0.46
0.46 0.46 0.46 0.46 0.46 0.46 0.46 0.46 0.46 0.46 0.46 0.46 0.46 0.46 0.46 0.46 0.46 0.46 0.46 0.46
0.46 0.46 0.46 0.46 0.46 0.46 0.46 0.46 0.46 0.46 0.46 0.46 0.46 0.46 0.46 0.46 0.46 0.46 0.46 0.46
0.46 0.46 0.46 0.46 0.46 0.46 0.46 0.46 0.46 0.46 0.46 0.46 0.46 0.46 0.46 0.46 0.46 0.46 0.46 0.46
0.46 0.46 0.46 0.46 0.46 0.46 0.46 0.46 0.46 0.46 0.46 0.46 0.46 0.46 0.46 0.46 0.46 0.46 0.46 0.46
0.46 0.46 0.46 0.46 0.46 0.46 0.46 0.46 0.46 0.46 0.46 0.46 0.46 0.46 0.46 0.46 0.46 0.46 0.46 0.46

Input File my_table_Hematite_20x8.txt

0 0 0 0 0 0 0 0 0 0 0 0 0 0 0 0 0 0 0 0
0.33 0.33 0.33 0.33 0.33 0.33 0.33 0.33 0.33 0.33 0.33 0.33 0.33 0.33 0.33 0.33 0.33 0.33 0.33 0.33
0.33 0.33 0.33 0.33 0.33 0.33 0.33 0.33 0.33 0.33 0.33 0.33 0.33 0.33 0.33 0.33 0.33 0.33 0.33 0.33
0.33 0.33 0.33 0.33 0.33 0.33 0.33 0.33 0.33 0.33 0.33 0.33 0.33 0.33 0.33 0.33 0.33 0.33 0.33 0.33
0.33 0.33 0.33 0.33 0.33 0.33 0.33 0.33 0.33 0.33 0.33 0.33 0.33 0.33 0.33 0.33 0.33 0.33 0.33 0.33
0.33 0.33 0.33 0.33 0.33 0.33 0.33 0.33 0.33 0.33 0.33 0.33 0.33 0.33 0.33 0.33 0.33 0.33 0.33 0.33
0.33 0.33 0.33 0.33 0.33 0.33 0.33 0.33 0.33 0.33 0.33 0.33 0.33 0.33 0.33 0.33 0.33 0.33 0.33 0.33
0.33 0.33 0.33 0.33 0.33 0.33 0.33 0.33 0.33 0.33 0.33 0.33 0.33 0.33 0.33 0.33 0.33 0.33 0.33 0.33